Selective Bivalent Reagents for the Study of Protein Kinases

Carrie M Gower

A dissertation
submitted in partial fulfillment of the
requirements for the degree of

Doctor of Philosophy

University of Washington
2014

Reading Committee:
Dustin Maly, Chair
Michael Heinekey
Champak Chatterjee

Program authorized to offer degree:
Chemistry

University of Washington

Selective Bivalent Reagents for the Study of Protein Kinases

Carrie M Gower

Chair of the Supervisory Committee:

Associate Professor Dustin J Maly
Department of Chemistry

Protein kinases are involved in the regulation of many intracellular processes. Misregulation of these enzymes has been implicated in a variety of diseases making protein kinases viable drug targets. Despite this interest in protein kinases, the cellular function of many members of this large enzyme family is not well understood. Chemical and genetic methods are currently in place for studying the function of protein kinases. However, these methods fall short in that chemical tools often have multiple off-targets within the highly conserved kinome, while genetic tools remove both catalytic and non-catalytic kinase function from the cell. Intracellular antibodies developed through phage and ribosomal display have been shown to bind potently and selectively to protein kinases of interest without affecting catalytic function. Seeking to develop selective and potent bivalent inhibitors of protein kinases for use in cellular studies, we have employed a chemical genetic method involving a self-labeling protein to tether a promiscuous kinase inhibitor with various intracellular antibodies. Kinome-wide selectivity profiling has enabled us to determine that these bivalent inhibitors are highly selective for their desired targets. Through this method, it is conceivable that potent and selective inhibitors of any protein kinase of interest might be developed for use in cells.

TABLE OF CONTENTS

List of Abbreviations

AAK1	AP2-associated protein kinase 1
Abl	Abelson tyrosine kinase
Abl3D	Abl 3 domain (SH1, SH2,SH3)
AblKD	Abl kinase domain
ACVR1	Activin receptor type-1
AdoC	adenosine-5'-carboxylic acid
ADP	adenosine diphosphate
AGT	O^6-alkylguanine-DNA alkyltransferase
Ala	alanine
AP4	adenosine tetraphosphate
aPP	avian pancreatic polypeptide
Arg	argenine
ASK1	apoptosis signal-regulating kinase 1
ATP	adenosine triphosphate
AurA	aurora kinase A
AURKA	aurora kinase A
BCR	breakpoint cluster region
BG	O^6-benzylguanine
Blk	B lymphoid tyrosine kinase
BMP2K	BMP2 inducible kinase
BTK	Bruton tyrosine kinase
C-terminus	carboxy terminus
C2	conserved domain 2
CaMKII	calcium/calmodulin-dependent protein kinase type II
cAMP	cyclic adenosine monophosphate
cd	catalytically dead
CDCP1	CUB domain-containing protein 1
CDK1	cyclin-dependent kinase 1
CHK2	checkpoint kinase 2
CK	casein kinase
CLK1	CDC-like kinase 1
CLP	4-(benzyloxy)-6- chloropyrimidin-2-amine
CPP	cell-penetrating peptide
CREB	cAMP-responsive element binding protein
Csk	C-Src kinase
Dap	2,3-diaminopropionic acid
DARPin	designed ankyrin repeat protein
DELFIA	dissociation-enhanced lanthanide fluorescent immunoassay
DMSO	dimethylsulfoxide
EGFR	epidermal growth factor receptor
ELBA	enzyme-linked ligand binding assay
ELISA	enzyme-linked immunosorbent assay
EphA5	ephrin type-A receptor 5
ERK	extracellular signal-regulated protein kinase

ESI	electrospray ionization
FHA	forkhead-associated
5’ FSBA	5'-[4-(fluorosulfonyl)benzoyl]adenosine
Grb2	growth factor receptor-bound protein 2
GSK3	glycogen synthase kinase 3
GST	glutathione S-transferase
HA	human influenza hemagglutinin
Hck	hematopoietic cell kinase
HDAC	histone deacetylase
HEK293T	human embryonic kidney cells with T antigen of SV40
HeLa	Henrietta Lacks epithelial cells
HIV-TAT	human immunodeficiency virus trans-activator of transcription
IC_{50}	half maximal inhibitory concentration
IL-3	interleukin-3
IRAK4	interleukin-1 receptor-associated kinase 4
IRK	insulin receptor protein tyrosine kinase
JIP1	c-Jun N-terminal kinase-interacting protein 1
JNK	c-Jun N-terminal kinase
K_d	dissociation constant
KI	kinase inhibitor
KPCB	protein kinase C beta type
Lck	leukocyte c-terminal Src kinase
Lyn	Lck/Yes-related novel protein tyrosine kinase
MAPK	mitogen-activated protein kinase
MAPK1	ERK2
MAPKAPK2	mitogen-activated protein kinase-activated protein kinase 2
MAPKK	mitogen-activated protein kinase kinase
MARCKS	myristoylated alanine-rich C-kinase substrate
MARCS	myristoylated alanine-rich C-kinase substrate
MARK4	MAP/microtubule affinity-regulating kinase 4
MAST3	microtubule-associated serine/threonine protein kinase 3
Mig6	mitogen-induced gene 6
Mnk2	MAPK-interacting serine/threonine kinase 2
N-terminus	amino terminus
NEK9	never in mitosis A-related kinase 9
NHS	N-Hydroxysuccinimide
PAK4	p21-activated kinase 4
PARP	poly ADP ribose polymerase
PDB ID	protein data bank identification
PEG	polyethylene glycol
PH	pleckstrin homology
Phe	phenylalanine
PI3	agonist-stimulated phosphoinositide 3
PKA	protein kinase A
PKB	protein kinase B
PKC	protein kinase C

PKG	protein kinase G
PKI	protein kinase inhibitor
PLK	polo-like kinase
PP	polyproline
PTK	protein tyrosine kinase
RB_{50}	half maximal residual binding
RNAi	RNA interference
SDS-PAGE	sodium dodecyl sulfate polyacrylamide gel electrophoresis
SEM	standard error of the mean
Ser	serine
SFK	Src family kinase
SH2	Src homology 2
SH3	Src homology 3
Src	avian sarcoma viral oncogene tyrosine kinase
STAT5	signal transducer and activator of transcription 5A
STK10	serine/threonine protein kinase 10
SYK	spleen tyrosine kinase
Thr	threonine
TYK2	non-receptor tyrosine kinase 2
Tyr	tyrosine
Yes	Yamaguchi sarcoma virus oncogene tyrosine kinase

Units

°	degree
Å	angstrom
C	celcius
g	gram
h	hour
kDa	kilodalton
L	liter
m	meter; milli
M	molar
Min	minute
mol	mole
n	nano
p	pico
s	second
µ	micro

NMR

d	doublet
dd	doublet of doublets
J	coupling constant in hertz
m	multiplet
MHz	megahertz
s	singlet
t	triplet
q	quartet
δ	chemical shift in parts per million

List of Figures

Chapter 1

Chapter 2

Chapter 3

List of Tables

Chapter 1

Acknowledgements

I would like to thank my advisor, Dusty, for the knowledge he has shared with me. His guidance has helped me to develop a valuable skill set and to complete a body of work that I am proud of. I am grateful to my friends and advisors at Novartis Institutes for Biomedical Research. Jason Thomas, Edmund Harrington, Markus Schirle and Rishi Jain; their time and dedication to my success are greatly appreciated. The people of the Maly Laboratory make this a supportive and fun place to work, and their encouragement has been instrumental to my completion of this degree. Lastly, I would like to thank my friends and family for the love and support they have shared with me. They have encouraged me to work hard, celebrated with me in my triumphs and comforted me when discouraged. I love you all, thank you.

Dedication

To sweet Joey Girl, my companion and my comfort. I love you.

Chapter 1*

Bivalent inhibitors of protein kinases

I. Introduction

Intra-cellular signaling pathways are utilized by eukaryotic organisms in order to regulate cellular behavior. Extra-cellular signals are received and propagated through tightly regulated intra-cellular signaling cascades that are mediated by spatially and temporally controlled intra-cellular interactions. A number of these interactions are regulated by protein phosphorylation, which is catalyzed by protein kinases. Protein kinases are a large subset of the human proteome, consisting of over 500 members (1). These enzymes catalyze the transfer of the γ-phosphate of adenosine triphosphate (ATP) to a protein substrate at a serine, threonine, or tyrosine residue. These phosphorylation events mediate important cellular processes such as development, differentiation, and transformation. Aberrant protein kinase activity has been implicated in a variety of diseases including diabetes, cancer, and chronic inflammation, making members of this enzyme family attractive drug targets (1-4). Despite widespread interest in this enzyme family, the cellular function of many protein kinases is not well understood. Chemical genetic tools can be used to better elucidate the function of protein kinases. In order to provide clear insight into kinase function, these tools must be selective for a particular kinase of interest, which is still a major challenge in kinase reagent development.

---

*This chapter is reprinted with permission from Gower CM, Chang MEK, Maly DJ (2014) Bivalent inhibitors of protein kinases. *Critical Reviews in Biochemistry and Molecular Biology* 49:102–115.

Current chemical methods for studying the function of protein kinases involve the use of ATP-competitive small molecule inhibitors (5). These reagents allow for high temporal control over kinase function in cells. There are, however, several disadvantages to the use of ATP-competitive molecules as functional probes of protein kinases. The active sites of protein kinases are highly conserved, which makes achieving specificity for a single kinase target difficult. Additionally, as these molecules can diffuse freely throughout the cell, spatial control cannot be readily achieved. Techniques such as RNAi and genetic knockouts can also provide the ability to study the cellular function of kinases. In contrast to small molecule inhibition of protein kinases, genetic methods remove the entire kinase of interest from the cell, and thus, the catalytic function of a kinase cannot be differentiated from its non-catalytic functions (6). Furthermore, these methods lack spatial and temporal control.

A pharmacological method that allows the rapid identification of potent and selective kinase inhibitors has the potential to overcome many of these problems. Bisubstrate and bivalent inhibitors are attractive in this regard because they can exploit the same interactions that kinases use for obtaining specificity in signaling (Figure 1-1). Bisubstrate and bivalent reagents are generated by linking an ATP-competitive small molecule to a ligand that targets a region outside of the ATP-binding cleft of a kinase of interest. By targeting two distinct binding sites on a particular kinase, the potency and selectivity of inhibition can be increased. Numerous reports of bisubstrate and bivalent inhibitors of protein kinases have emerged in the literature over the last two decades, providing insight into their design and functional properties. In this review, we highlight a number of signaling interactions that are used by kinases in signaling events and that

can be targeted by bisubstrate and bivalent inhibitors. Furthermore, this review provides an overview of efforts to develop and apply bisubstrate and bivalent inhibitors of protein kinases, highlighting the application of these reagents in a cellular setting.

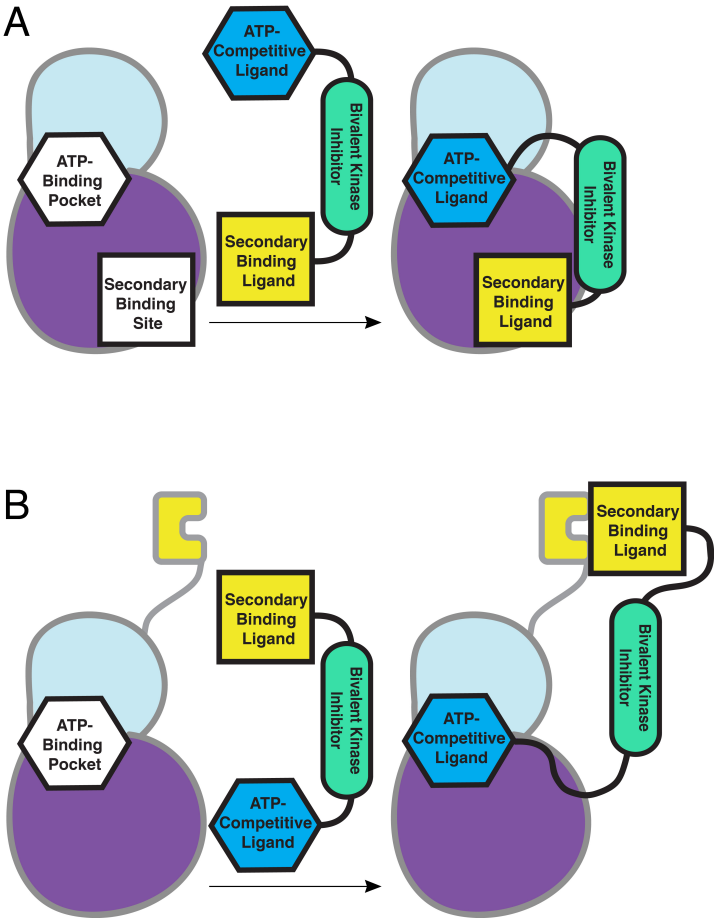

Figure 1-1. Bivalent inhibition of a protein kinase. **(A)** A single inhibitor is generated by fusing an ATP-competitive ligand to a secondary binding ligand. The ATP-competitive ligand interacts with the kinase active site, directing the bivalent inhibitor to the kinase. The secondary binding ligand introduces selectivity for a particular kinase. In the case of bisubstrate inhibitors, this ligand targets the protein substrate site of the protein kinase. **(B)** Regulatory domains of protein kinases present an avenue for bivalent inhibition where secondary-binding ligands can target domains distal to the kinase domain.

II. Protein kinases and substrate specificity

The conserved protein kinase fold consists of an N-terminal lobe composed mainly of β-strands and an α-helical C-terminal lobe (1, 7-10). At the junction of these two lobes lies the ATP-binding site. All protein kinases are bisubstrate enzymes that recognize both the cofactor ATP and specific protein substrates. Amidst the complex environment of the cell, kinases select specific substrates for phosphorylation, which is necessary for the proper alignment of signaling cascades. Various mechanisms play a role in the ability of a protein kinase to properly identify a specific substrate within the

cell. One of the major mechanisms is the interaction of the kinase with amino acid residues immediately surrounding the modified serine, threonine, or tyrosine (2-4, 9-11). The epitope displayed by the consensus phosphorylation sequence is complemented by the protein kinase active site. This recognition event conveys selectivity at the primary sequence level. Beyond the consensus sequence, protein kinases make interactions with the substrate that are distal to the site of phosphorylation (5, 11-14). These interactions can be mediated by distant binding sites on the catalytic domain or by modular binding domains.

A. Specificity determinants within the kinase domain

For most protein substrates, the four amino acids N-terminal and C-terminal to the phosphorylation site interact extensively with the kinase catalytic domain (9). The substrate preferences of kinases for residues surrounding the phosphorylation site have been mapped with a number of profiling techniques. One such method, described by Turk and coworkers, involves the radiometric analysis of biotinylated peptide substrates that have been treated with a purified kinase of interest (6, 12-14). With this method, libraries of peptides are analyzed where amino acids surrounding the phosphorylation site are systematically varied. From studies of this type, general trends regarding the preferences of protein kinases for substrates have been observed. While many kinases can generally be classified as acidophilic, basophilic, or proline-directed with respect to their phosphorylation sequence preference, the presence of particular residues at fixed positions plays a role in sequence selectivity as well (14). For some, determinants of this nature are one of the major mechanisms that are exploited to select substrates in the cell. However, for many protein kinases, protein substrate interactions are low-

affinity, which facilitates substrate turnover. Therefore, in most cases, the phosphorylation site consensus motif is not the main driver of substrate selection in the cell.

Distinct from the active site, protein kinases interact with substrates through other binding sites and modular domains. Within the kinase domain, certain serine/threonine kinases possess docking sites that are located outside of the active site (15). Docking sites interact with protein substrates through a binding motif that is distinct from the phosphoacceptor site, introducing an additional selectivity determinant for substrate interactions. In some cases, this site exhibits allosteric control over kinase function, either positively or negatively regulating kinase activity (9, 11, 16). The mitogen-activated protein kinases (MAPKs) are one example of a kinase family that utilizes a docking site to enhance substrate specificity. Interestingly, the three subfamilies of MAPKs, extracellular signal-regulated kinases (ERK), p38 MAPKs (p38) and c-Jun N-terminal kinases (JNK), display a striking lack of selectivity regarding their phosphorylation site consensus motif. Peptide library screening has shown that a necessary proline residue following the phosphoacceptor serine or threonine is the main factor dictating the phosphorylation consensus sequence for ERK2, p38α, p38δ, and JNK2 (16). This suggests that MAPKs likely use docking interactions to achieve proper phosphorylation of substrates within the cell. For example, a docking site for substrates that contain a DEF (docking site for ERK, FXF) motif, which recognizes an FX(F/Y)P sequence located approximately 6-20 amino acids C-terminal to the phosphoacceptor site, is a major determinant of ERK substrate selectivity (14, 16). While both ERK2 and p38α show a similar and strong preference for aromatic residues at positions one and

three of this motif, p38δ displays a striking preference for aliphatic residues at the first position. Binding determinants of this nature play a crucial role in the ability of MAPKs to successfully recognize and phosphorylate their proper targets in cells.

B. Obtaining specificity through modular domains

Through the interaction of protein substrates with recognition sites within the kinase domain, the efficiency and stringency of substrate phosphorylation is enhanced. This can occur through an increase in local substrate concentration or proper alignment of residues for phosphorylation (9, 17-19). Beyond the catalytic kinase domain, a number of kinases use separate modular binding domains to obtain substrate specificity. Modular binding domains have been shown to interact with unaltered substrate sequence motifs, as well as motifs that have been post-translationally modified (11). Modular binding domains not only deliver kinase catalytic domains to substrates in specific locations, but also serve a regulatory role. For example, the Src homology 3 (SH3) domains of Src-family kinases (SFKs) play a major role in the localization and regulation of the catalytic domains of these kinases. This domain regulates kinase function through both inter- and intra-molecular protein-protein interactions. SFK SH3 domains interact with substrate polyproline motifs inter-molecularly, facilitating substrate recognition, and intra-molecularly with sub-optimal linker sequences, to regulate kinase catalytic activity (20). SH3 domains are used by a number of additional non-receptor tyrosine kinases in a similar manner (21, 22).

A variety of modular domains are utilized by protein kinases to recognize post-translationally modified, mainly phosphorylated, recognition motifs within the cell. These binding events can serve both as substrate specificity determinants and regulatory

interactions. For example, the Src homology 2 (SH2) domains of SFKs recognize a phospho-tyrosine residue in their own C-terminal tail, which results in a closed, auto-inhibited kinase with low catalytic activity (22, 23). The same SFK SH2 domains also recognize substrates that contain phosphorylated tyrosine residues. Furthermore, the SH2 domains of other tyrosine kinases have been shown to recognize phospho-tyrosine residues in their substrates. This primed interaction facilitates multi-site phosphorylation of substrates, indicating further regulatory roles of the SH2 domain (24). Similarly, the polo-box domain of the mitotic serine/threonine polo-like kinase (PLK) family is a phospho-recognition domain that acts to both properly localize PLK during cell division and modulate PLK's kinase activity (17-19). These interactions not only provide greater phosphorylation fidelity, but also facilitate temporal control over signaling events.

Additional phospho-recognition domains include forkhead-associated (FHA) and conserved domain 2 (C2) domains. FHA domains are generally selective for phospho-threonine-containing motifs, and proteins containing these domains have been implicated in many cellular processes, such as DNA repair, signaling, transcription, and protein transport and degradation (25). The kinase CHK2 is involved in the DNA damage checkpoint response, and two tumor-associated mutations of this kinase have been mapped to the FHA domain, demonstrating its importance for proper cellular function of the kinase. The C2 domain of the kinase PKC was originally discovered as a modulator of catalytic activity through binding phospholipids and is found in a variety of human protein kinases (11). This domain has also been shown in the specific case of PKC, to bind a phosphotyrosine residue of the protein CDCP1, which has been primed by Src (26). Crystallographic data indicate that the sequence specificity of the C2

domain for a substrate peptide is determined by residues located both upstream and downstream of the phosphotyrosine residue, which may point toward a highly selective interaction (26).

Pleckstrin homology (PH) domains, like C2 domains, recognize phospholipids, which are often the products of agonist-stimulated phosphoinositide 3-kinases (PI3-kinases) (27). Additionally, a pathway has been described where the non-receptor tyrosine kinase BTK is recruited to PI3-kinase products in the plasma membrane through a PH domain. This allows BTK to act on substrates in a location-specific manner (23, 27). While BTK's PH domain does not interact with protein binding partners, it facilitates proper substrate selection by restricting the number of potential substrates available to this kinase. Therefore, this domain, like the protein-protein interaction motifs and modular domains described above, is an attractive target for the development of new and potentially selective inhibitors. While the affinities of the domains described above for their respective ligands are often weak, these interactions can, in many cases, be very selective. The exploitation of known substrate selection mechanisms of kinases represents an interesting avenue for the development of inhibitors with very high target specificity.

III. Overview of protein kinase inhibitors

Currently, most potent kinase inhibitors target the highly conserved ATP-binding site, which makes the generation of mono-selective pharmacological agents extremely challenging (28, 29). While it is possible to obtain ATP-competitive inhibitors with exquisite selectivity, this process requires iterative rounds of synthesis and testing and is quite laborious (5). As a result, there has been a high level of interest in the

development of inhibitors that disrupt the non-conserved binding interactions described above. Presumably, pharmacological tools that target these sites will have the same level of selectivity that kinases display in signaling cascades. However, most pharmacological agents that target sites outside of the ATP-binding pocket are of low affinity, with a majority of these ligands possessing dissociation constants in the micromolar to millimolar range. For this reason, bivalent ligands that target two distinct surfaces of a protein kinase have been pursued by a number of research groups. Many bivalent ligands are able to obtain selectivity by interacting with the low affinity, heterogeneous binding interfaces of protein kinases, while maintaining potency by engaging kinase active sites. If proper ligands and linkers are selected, bivalent reagents can possess incredibly high potency and selectivity. Bivalent inhibitors of protein kinases can be separated into two groups depending on the interactions that they make with their kinase target. Bisubstrate kinase inhibitors are composed of an ATP-competitive ligand covalently tethered through a linker to a pseudosubstrate peptide of the protein kinase of interest. On the other hand, bivalent kinase inhibitors display an active site-directed ligand tethered to a second ligand that targets a region outside of the active site. Both classes of inhibitors are described in this review.

A. Bisubstrate inhibitors of serine/threonine protein kinases

An early report of a bisubstrate protein kinase inhibitor was described in 1991, by Ricouart and coworkers (Table 1-1) (30). In this study, the serine/threonine protein kinase C (PKC) was targeted. In mammals, the PKC family is made up of over ten isozymes shown to be involved in numerous cellular processes (31). Elucidating the specific function of each PKC isoform has proven difficult due to high sequence

homology within the kinase domain and their largely overlapping substrate specificities. Probes that are able to differentiate between PKC family members would be highly valuable for achieving this goal. To this end, Ricouart and co-workers developed a PKC-directed bisubstrate inhibitor consisting of a pseudosubstrate peptide containing a single serine followed by six arginine residues, which targets the protein substrate site of PKC, linked to an ATP-competitive 5-isoquinolinylsulfonyl inhibitor, which targets the ATP-binding site. The 5-isoquinolinylsulfonyl inhibitor selected is a derivative of the known PKC inhibitor H7. The peptide and ATP-competitive ligands were covalently tethered through a 16 Å linker, a distance predicted to be optimal based on a crystal structure of phosphoglycerate kinase, which was the most similar kinase structure available at that time. To test the potency of this inhibitor, a PKC activity assay using histone as an *in vitro* substrate was developed. With this assay, it was observed that the bisubstrate inhibitor (IC_{50} = 0.3 μM) was 67-fold more potent against PKC activity than the 5-isoquinolinylsulfonyl ATP-competitive inhibitor alone (IC_{50} = 20 μM). Importantly, a bivalent effect was verified by testing kinase inhibition in the presence of a mixture of both unlinked monovalent ligands. Enhancement of potency was only observed when the two components of the bisubstrate inhibitor were covalently tethered together. Unfortunately, the potency of the bisubstrate inhibitor was 100-fold greater for closely-related PKA than for PKC, despite the pseudosubstrate peptide component of the bisubstrate inhibitor being selected for PKC specificity. Despite the lack of desired selectivity for PKC over PKA, this early example demonstrated that two distinct kinase ligands can be tethered together into a single bisubstrate molecule with enhanced potency.

Table 1-1. A summary of the bisubstrate and bivalent inhibitors of protein kinases described in this review.

Kinase	Specificity	Ligand A (active-site directed)	Fold Inc Over A	Ligand B	Fold Inc Over B	Linker	Reference
PKA/PKC	Ser/Thr	isoquinolinylsulfonyl	670/67	Ser-Arg_6 (substrate site)	N/A	-$NH[CH_2]_2NH[CH_2]_2CO$-	Ricouart *et al*. (1991)
PKCζ	Ser/Thr	bisindolyl maleimide	>43	CREB peptide (substrate site)	>43	alkylated Arg	van Ameijde *et al*. (2010)
PKCθ	Ser/Thr	bisindolyl maleimide	17	CREB peptide (substrate site)	>58	alkylated Arg	van Ameijde *et al*. (2010)
PKA	Ser/Thr	ATPγS	N/R	Kemptide (substrate site)	N/R	acetyl	Hines and Cole (2004)
PKA	Ser/Thr	indolocarbazole	0.038	PKA specificity epitope of PKI (substrate site)	32	-$NH[CH_2]_6NHCOCH_2$-	Schneider *et al.* (2005)
PKA	Ser/Thr	AdoC	1200	Arg_6 (substrate site)	>830	-$NH(CH_2)_5C(O)$-	Loog *et al.* (1999)
cIRK	Tyr	ATPγS	310	IRS727 peptide (substrate site)	N/R	acetyl	Parang *et al.* (2001)
CSK	Tyr	ATPγS	N/R	SRC (aa83-524) (substrate site)	> 17	-CONH-CQ-Aph-$NHCOCH_2S$-	Shen and Cole (2003)
JNK1	Ser/Thr	indazole	20000	JIP1-derived peptide (docking site)	> 70000	-$NH[CH_2]_3CONH$-GlyGly-	Stebbins *et al.* (2011)
JNK1	Ser/Thr	indazole	780	JIP1 TAT peptide (docking site)	> 2700	-$NH[CH_2]_3CONH$-GlyGly-	Stebbins *et al.* (2011)
PKA	Ser/Thr	staurosporine	93	cyclo(CTFRVFGC)G	22000	PEG_3	Meyer *et al.* (2007)
SRC	Tyr	EELL-(F_5)Phe-amide	230	coumarin-pYEEIE (SH2 domain)	N/R	Abu_8	Profit *et al.* (1999)
SRC	Tyr	(Ba)EEEIFGEFDap(Hna)	48	pYEEIE (SH2 domain)	50	$βAla_3$	Hah *et al.* (2006)

The upper panel shows bisubstrate inhibitors (categorized by kinase specificity), while the bottom panel shows bivalent inhibitors. Fold increase refers to the potency of kinase inhibition. (N/A = not applicable; N/R = not reported).

More recent efforts have been described to develop isozyme-selective PKC inhibitors. A PKC pseudosubstrate (EILSRRPAYRKIL), derived from the cAMP-responsive element binding protein (CREB), was tethered to a staurosporine mimetic to generate an isoform-selective PKC bisubstrate inhibitor (32). Tethering was achieved by modifying an arginine residue to present an azide moiety that was subsequently derivatized with an alkyne-displaying ATP-competitive small molecule using click chemistry. The resulting bisubstrate inhibitor was analyzed for its ability to prevent phosphorylation of substrates CREB1, KPCB, and MARCS by three clinically relevant and highly homologous PKC isoforms, PKCα, PKCζ, and PKCθ. The bisubstrate inhibitor exhibited modest potency against PKCζ (IC_{50} = 0.23-0.59 μM) and PKCθ (IC_{50} = 0.17-0.81 μM) but no inhibition of PKCα, while the staurosporine mimic only inhibited PKCα (IC_{50} = 1.8-2.9 μM) and PKCθ (IC_{50} = 2.3-2.9 μM). The pseudosubstrate alone was unable to inhibit any of the PKC isoforms, but microarray analysis of the parent peptide substrate showed that it is most strongly phosphorylated by PKCζ, followed by PKCθ and PKCα. Thus, the selectivity profile of the bisubstrate inhibitor tracks with that of the original substrate, suggesting that the secondary ligand acts to steer the affinity of this construct. Interestingly, a bisubstrate inhibitor previously studied by the same group which contained a neutral amino acid residue in place of the positively charged modified arginine, did not show inhibitory activity against PKCζ, but was selective for PKCθ (33). This could point to the importance of maintaining contacts made by the original substrate when generating a pseudosubstrate, as well as proper linkage of the ATP-competitive small molecule.

In addition to the unintended inhibition of PKA described above, bisubstrate inhibitors have been designed to specifically target this important serine/threonine protein kinase. The cAMP-dependent protein kinase A (PKA) is activated by a number of signaling pathways within the cell (34). Activated PKA then acts in a variety of distinct pathways, the differentiation of which is likely mediated through scaffolding complexes. Selective inhibition of PKA has the potential to illuminate the complex signaling networks that this kinase is involved in. One bisubstrate inhibitor of PKA that has been described used a pseudosubstrate peptide analog of the well-defined substrate kemptide fused through an acetyl linker to a non-hydrolyzable ATP derivative, ATPγS (35). By using kemptide as a selectivity determinant, this bisubstrate inhibitor showed a greater than 20-fold preference for PKA over closely-related PKC. Alternatively, Schneider and coworkers developed a bisubstrate inhibitor consisting of a PKA specificity epitope from the heat-stable Protein Kinase Inhibitor protein (PKI) linked to the high-affinity ATP-competitive inhibitor K252a (Figure 1-2 A) (36). Rather than using a linear peptide to display the PKI epitope, a designed miniature protein with the stable fold from avian pancreatic polypeptide (aPP) was employed as a scaffold. Miniature proteins based on this scaffold have been designed to present recognition epitopes from the α-helix of aPP and can often lead to potent binders of target proteins. Interestingly, the bisubstrate inhibitor displayed from the miniature protein was 60-fold more potent (IC_{50} = 3.7 nM) than a bisubstrate inhibitor consisting of K252a directly conjugated to PKI (IC_{50} = 220 nM). This may be due to differences in the binding modes between the two inhibitors or suboptimal linkage between K252a and PKI in the absence of the miniature protein. While the K252a-PKI (miniprotein) bisubstrate inhibitor

was 26-fold less potent than K252a (IC_{50} = 0.14 nM), a 32-fold increase in potency was observed compared to the PKI-displaying miniature protein (IC_{50} = 120 nM). Importantly, impressive selectivity was observed for PKA over closely related protein kinases. K252a and the bisubstrate inhibitor were assayed against AKT (PKB), PKCα, cGMP-dependent protein kinase (PKG), and Ca/calmodulin kinase II (CaMKII). While the small molecule K252a inhibits all of these kinases potently, the bivalent inhibitor was only observed to exhibit inhibition of PKA at concentrations up to 100 nM.

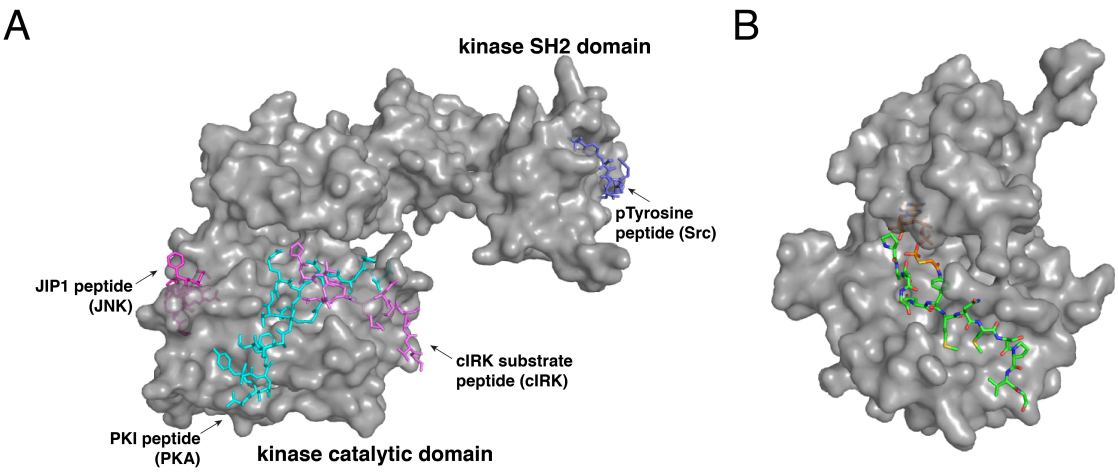

Figure 1-2. Reported bisubstrate/bivalent inhibitors of protein kinases. **(A)** Crystallographic representation of secondary binding ligands used in previously described bisubstrate/bivalent inhibitors superimposed on a protein kinase. [PDB IDs 1GAG, 2CPK, 1UKI, 1Y57]. **(B)** Crystal structure of cIRK in complex with a bisubstrate inhibitor. [PDB ID 1GAG].

Several earlier attempts at bisubstrate inhibition of PKA yielded modest inhibitors (37, 38). One approach, similar to that reported by Ricouart and coworkers, linked an Arg_6 peptide to adenosine-5'-carboxylic acid (AdoC) through a six carbon linker (38). This construct inhibited PKA, PKC, and cyclin-dependent protein kinase-1 (CDK1) with IC_{50} values of 0.12, 0.27, 1.2 μM, respectively. As expected, the inhibitor was inactive against casein kinases 1 (CK1) and 2 (CK2), which are acidophilic protein kinases. In a subsequent report, AdoC was linked to a poly-arginine peptide in order to develop bisubstrate inhibitors capable of selectively enriching PKA from lysate (39).

Medzihradszky and coworkers generated a bisubstrate inhibitor by directly linking adenosine diphosphate (ADP), ATP or adenosine tetraphosphate (AP4) to the PKA substrate, kemptide (37). It was seen that inhibitor potency, while modest, increased with the number of phosphates in the linker (IC_{50} = 935, 226, 68 μM for the ADP, ATP, and AP4 linkers, respectively). Inhibition was observed to be competitive with ATP but not with respect to kemptide, indicating that these inhibitors primarily interact with the ATP-binding site.

B. Bisubstrate inhibitors of tyrosine protein kinases

In an early report from Kruse and coworkers, a strategy for developing bisubstrate inhibitors of Abelson tyrosine kinase (Abl) was described (Table 1-1) (40). This method involves coupling a neutral ATP-mimetic, 5'-[4-(fluorosulfonyl)benzoyl]adenosine (5'-FSBA) to a tyrosine derivative. These assembled bisubstrate inhibitors were hypothesized to take advantage of the tyrosine substrate recognition preference exhibited by protein tyrosine kinases (PTKs). While modest inhibitors of Abl (IC_{50} = 19-120 μM) were developed by varying the tyrosine derivative and the linker to 5'-FSBA, the similarity of IC_{50} values displayed by the panel of compounds suggests that the inhibitors were binding only to the ATP-binding site. Further supporting this notion, these bisubstrate inhibitors possessed similar potencies against a non-tyrosine kinase, phosphorylase. These results highlight the importance of understanding substrate selectivity determinants for successful development of bisubstrate inhibitors. In a similar approach by Traxler and coworkers, sulfonylbenzoyl-nitrostyrene derivatives were synthesized as bisubstrate inhibitors of the epidermal growth factor receptor tyrosine kinase (EGFR) (41). The sulfonylbenzoyl moiety

represents the ATP-competitive portion of these molecules, while the nitrostyrene was selected to mimic the natural product Erbstatin, a peptide substrate-competitive PTK inhibitor (42). With this method, a potent (IC_{50} = 0.054 μM) EGFR inhibitor was developed that showed high selectivity with respect to Abl (IC_{50} = 27 μM) and PKC (IC_{50} = 500 μM). While a highly potent and seemingly selective inhibitor of EGFR was developed, studies were not carried out to verify that this bisubstrate inhibitor occupied both substrate-binding sites. A subsequent report from the same group described bisubstrate inhibitors that are composed of EGFR consensus sequence substrate motifs tethered to an adenosine moiety through a 2-hydroxy-4-sulfonylbenzoyl linker (43). This strategy resulted in the generation of a less potent (IC_{50} = 33 μM) bisubstrate inhibitor that demonstrated similar potency to the 2-hydroxy-4-sulfonylbenzoyl linker group. The low activity of this compound was hypothesized to be a result of weak interactions between EGFR and the substrate peptide.

Parang and Cole generated a bisubstrate inhibitor of the insulin receptor protein tyrosine kinase (IRK) by tethering a well characterized pseudosubstrate of this kinase, IRS727, to ATPγS (Figure 1-2 A and B) (44). This bisubstrate inhibitor was designed based on the principle that phosphate transfer in tyrosine kinases occurs through a dissociative mechanism. In a dissociative mechanism transition state, the bond between the attacked phosphorus and the leaving group (ADP) is largely broken before the bond between the nucleophile (the alcohol of Ser, Thr, or Tyr) and the phosphorus has fully formed (44, 45). For a bisubstrate inhibitor to accommodate such a transition state, the tether between peptide and the nucleotide must be at least 5 Å in length. An acetyl linker, which provides a distance between the Tyr oxygen surrogate of the peptide and

γ-phosphorus of ATP of 5.7 Å in an extended conformation, was envisioned as being optimal. Gratifyingly, the bisubstrate inhibitor was shown biochemically to have increased binding affinity compared to both ATPγS and the IRS727 peptide. Additionally, a crystal structure of IRK in complex with the bisubstrate inhibitor was solved. This confirmed that both the nucleotide and peptide binding sites of IRK were occupied by the bisubstrate inhibitor. Furthermore, the distance between the γ-phosphorus and the Tyr oxygen surrogate was found to be 5 Å, supporting the hypothesis of a dissociative mechanism of phosphate transfer. To further investigate the affinity contributions of this bisubstrate inhibitor, a series of changes were introduced into the linker, the amino acid sequence of the pseudosubstrate, and the identity of the Tyr oxygen surrogate (45). The parent bisubstrate IRK inhibitor displayed an anilino group where the tyrosine hydroxyl would appear in the native peptide substrate. This allowed the peptide moiety to be linked to ATPγS, while still retaining an important hydrogen bond. A hydrogen bond donor at this position can potentially interact with the carboxylate side chain of the catalytic Asp of IRK and was proposed to be important for the potency of the interaction between substrate and enzyme. As expected, replacement of the nitrogen with an ether linkage, which cannot make the same hydrogen bond, resulted in 80-fold weaker inhibition of IRK. Furthermore, when the acetyl linker was substituted with a longer propionyl group (~1.2 Å longer than acetyl), an 18-fold less potent bisubstrate IRK inhibitor resulted. In addition, replacement of ATP with ADP, shortening the distance between adenosine and the anilino nitrogen by ~4 Å, resulted in a 200-fold less potent inhibitor of IRK. These results further support the notion of a dissociative transition state for phosphate transfer.

Shen and Cole also generated a bisubstrate inhibitor of the protein tyrosine kinase Csk (46). Csk is responsible for the negative regulation of SFK activity through phosphorylation of their C-terminal tails (47). A bisubstrate inhibitor of Csk was assembled *in vitro* using expressed protein ligation to fuse a recombinant Src fragment (83-524) to a pseudosubstrate peptide/ATPγS conjugate. With this method, a bisubstrate inhibitor displaying an IC_{50} of 600 nM against Csk was generated, with the recombinant Src fragment alone showing no measureable inhibition at a concentration of 10 μM. The immobilized bisubstrate construct was also able to isolate Csk from Csk-enriched NIH3T3 cell lysate. The Src fragment alone showed no significant enrichment of Csk under the same conditions. This method presents a potential means to discover cellular actors of phosphorylation events through immobilization of a downstream protein.

C. Bivalent inhibitors of protein kinases

Several of the previously described bisubstrate kinase inhibitors represent excellent examples of potent kinase inhibition by targeting the ATP- and substrate-binding sites. The presence of domains and interaction sites distal to the site of phosphate transfer, however, presents an avenue for the development of numerous, potent bivalent inhibitors that are capable of selecting between closely-related kinases. Moving away from kinase active sites has given researchers the ability to target protein kinases of interest without dependence on the generally low-affinity substrate-binding site.

i. Bivalent inhibitors of serine/threonine protein kinases

In 2011, Stebbins and coworkers reported a bivalent inhibitor of the MAPK c-Jun N-terminal kinase 1 (JNK1) (Figure 1-2 A and Table 1-1) (48). This bivalent inhibitor was generated by linking an ATP-competitive inhibitor of the JNK family, an analog of SP600125, to a peptide that targets JNK1's docking groove. The peptide selected for this study was a minimal sequence derived from the D-domain of the JNK1 scaffolding protein, JIP1. While the minimal peptide selected does not inhibit JNK1 activity (IC_{50} > 50 μM), it is capable of displacing the inhibitory parent peptide, pepJIP1, in a dissociation enhanced lanthanide fluoro-immuno assay (DELFIA) platform. The bivalent inhibitor was linked through a glycine-glycine-diaminopropyl linkage and displayed sub-nanomolar (IC_{50} = 0.7 nM) JNK1 inhibition *in vitro*, a 20000-fold increase in JNK1 inhibition compared to the ATP-competitive inhibitor alone (IC_{50} = 14 μM). To confirm that this inhibitor interacts with both targeted sites *in vitro*, JNK1 was pre-incubated with an excess of the promiscuous kinase inhibitor staurosporine to eliminate one binding site prior to treatment with the bivalent inhibitor. This resulted in a 600-fold loss in the ability of the bivalent inhibitor to compete with pepJIP for the docking site of JNK1. Thus, a potent bivalent inhibitor of JNK1 was developed by linking a minimal peptide derived from the native interactor JIP1 to an ATP-competitive small molecule inhibitor of modest potency.

Meyer and coworkers took a different approach in developing a potent and selective bivalent inhibitor of PKA (49). An *in vitro* bivalent selection strategy was envisioned where small molecule targeting could be combined with biological selection so that no previous structural or peptide substrate data would be necessary for inhibitor

design. In this approach, a highly promiscuous staurosporine derivative of intermediate potency was used in a warhead-guided phage display selection strategy to yield cyclic peptide binders of PKA surfaces near the active site. The library and small molecule are tethered through a self-assembling heterodimer of Jun and Fos proteins. The small molecule tethered to Jun and cyclic peptide library displayed from Fos are brought within proximity of each other upon self-assembly of the Jun/Fos coiled coil. In this way, a PKA-binding cyclic peptide was selected and subsequently tethered to the staurosporine derivative to generate a bivalent inhibitor. The resulting inhibitor displayed an impressive increase in both potency and selectivity of inhibition. By introducing a bivalent interaction, potency increases of 93- and 21,000-fold were observed compared to the small molecule and cyclic peptide, respectively. Additionally, five kinases that share a similar staurosporine inhibition profile with PKA (ASK1, CaMKIIβ, cSrc, EphA5 and Mnk2) were assayed for activity in the presence of the bivalent inhibitor. Only PKA displayed a significant reduction in kinase activity in response to the inhibitor at a concentration of 100 nM. A bivalent inhibitor with an optimized linker between both monovalent ligands demonstrated even greater potency against PKA and showed remarkable selectivity for this kinase over an extended panel of 90 kinases (50). These reports not only demonstrate the utility of bivalent inhibitors for enhancing potency and selectivity but also present a model for the generation of bivalent inhibitors of kinases without a need for prior understanding of protein-protein interactions made by the kinase of interest. The generality of this strategy was demonstrated by the application of the same selection methodology to the serine/threonine kinase Aurora A (51). These

efforts resulted in the identification of cyclic peptides that target sites outside of the ATP- and substrate-binding clefts of Aurora A.

ii. Bivalent inhibitors of tyrosine protein kinases

In 1999, Profit and Lawrence reported a bivalent inhibitor targeting two distinct domains of Src tyrosine kinase (Figure 1-2 A and Table 1-1) (52). The phospho-recognition site of the Src SH2 domain was targeted with a peptidic derivative of the SH2 recognition sequence found in hamster polyomavirus middle-T antigen. This ligand was coupled to an active site-directed peptide displaying pentafluorophenylalanine as a non-phosphorylatable tyrosine analog. The optimal length for linking these two binding elements was determined empirically, with the most potent bivalent inhibitor exhibiting a 230-fold lower IC_{50} against Src (IC_{50} = 6.9 μM) than the active site-directed peptide alone (IC_{50} = 1,590 μM). While this report validated the concept of generating bivalent inhibitors that target two different domains in multi-domain tyrosine kinases, the highest affinity inhibitor only demonstrated modest potency against Src (IC_{50} = 6.9 ± 0.4 μM). Furthermore, the selectivity of this inhibitor was not examined. In a later report from the same group, the active site-directed peptide inhibitor of Src was optimized and nanomolar inhibition of this kinase was achieved (IC_{50} = 36 ± 2 nM) (53). Additionally, this inhibitor discriminated between the two SFK subgroups: Group A (Fyn, Fgr, Src, and Yes) and Group B (Blk, Hck, Lck, and Lyn). Inhibition selectivity from 13- to 1600-fold was observed between the two subgroups. The development of inhibitors that are selective for specific SFK members will prove useful in the quest to disentangle the overlapping roles of SFKs in the cell.

IV. Cellular applications of bivalent and bisubstrate inhibitors

Due to their high molecular weights and overall polar natures, bisubstrate and bivalent inhibitors are usually not cell permeable. This makes using these reagents in a cellular setting very challenging. The ability to study protein kinase function in a cellular environment with these reagents would be exceptionally valuable because the roles of many members of this enzyme family are not well understood, and there is a dearth of pharmacological tools that possess the necessary selectivity. However, several groups have pursued strategies that allow intra-cellular application of their bivalent reagents. Stebbins and coworkers reported a strategy for the intra-cellular targeting of their bivalent, sub-nanomolar JNK1 inhibitor (48). To do this, an all-D retro-inverso version of their bivalent inhibitor was fused to the cell penetrating HIV-TAT peptide sequence (GRKKRRQRRR). While the cell penetrant bivalent inhibitor was less active than the parent conjugate, this inhibitor still exhibited an IC_{50} of 18 nM against JNK1 *in vitro*, which is 780-fold lower than the monovalent ATP-competitive inhibitor alone. The cell penetrant bivalent inhibitor effectively inhibited JNK1-dependent processes in mammalian cells, while processes dependent on the closely related MAPK, p38α, were unaltered. Additionally, intraperitoneal injection of the inhibitor into glucose intolerant mice increased the ability of mice to process glucose compared to vehicle.

Ameijde and coworkers pursued a similar approach for conferring cellular penetrance to their bisubstrate PKC inhibitor. Two cell-penetrating peptides (CPPs), HIV-TAT and antennapedia homeodomain derived penetratin, were conjugated to their bisubstrate PKC inhibitor, either through linear synthesis onto the pseudosubstrate or via a disulfide linkage (54). HeLa cells incubated with fluorescently labeled constructs

showed cellular uptake by confocal microscopy and FACS for both CPPs and attachment methods. The intracellular activity of these bisubstrate inhibitors was assayed by ELISA using a phospho-specific antibody for the PKC substrate, MARCKS. The linear TAT-conjugate, linear penetratin-conjugate, and disulfide TAT-conjugate inhibited intra-cellular PKC phosphorylation of MARCKS, with IC_{50} values of 10, 19, and 17 μM, respectively. Interestingly, the disulfide penetratin-conjugate did not show significant inhibition in cells. This construct did exhibit a significantly shorter half-life compared to the other three constructs, perhaps explaining this result. Although these constructs showed decreased intra-cellular inhibition in comparison to the monovalent staurosporine analog (IC_{50} = 3.8 μM), microarray assays of HeLa lysate treated with either penetratin- or TAT-based bisubstrate inhibitors had diminished MARCKS phosphorylation, while the profile of other phosphorylation sites was similar to that of the control, which demonstrates selective on-target inhibition.

V. Bivalent inhibitors based on a SNAPtag protein scaffold

In order to provide a bivalent inhibition method that can be used in cells without the use of intra-cellular delivery methods, we developed a chemical genetic strategy based on a self-labeling protein called SNAPtag (or AGT). This allows one component of a bivalent inhibitor to be genetically encoded as a SNAPtag fusion protein and the other component to be assembled through a rapid and chemo-selective covalent reaction (55-57). This overall strategy is shown in Figure 1-3. A SNAPtag fusion protein, which contains a ligand that targets a region outside the ATP-binding site, is selectively labeled with an ATP-competitive small molecule inhibitor conjugate that contains a chemo-selective tag. This is a modular strategy that allows different combinations of

monovalent reagents to be assembled rapidly. This approach in generating bivalent kinase inhibitors with SNAPtag is unique from most reports in that, an entire, folded protein is used as a scaffold for ligand display. The labeled active site residue is located in a relatively shallow hydrophobic pocket, which allows favorable access to the ATP-competitive small molecule, while the secondary binding ligand can be displayed from either the N- or C-terminus of the protein scaffold. The N- and C-termini both sit on the same face of the active site of SNAPtag, which allows for favorable ligand display from the scaffold to the kinase target (Figure 1-4). Furthermore, the active site is only ~22 Å from the N-terminus and ~17 Å from the C-terminus.

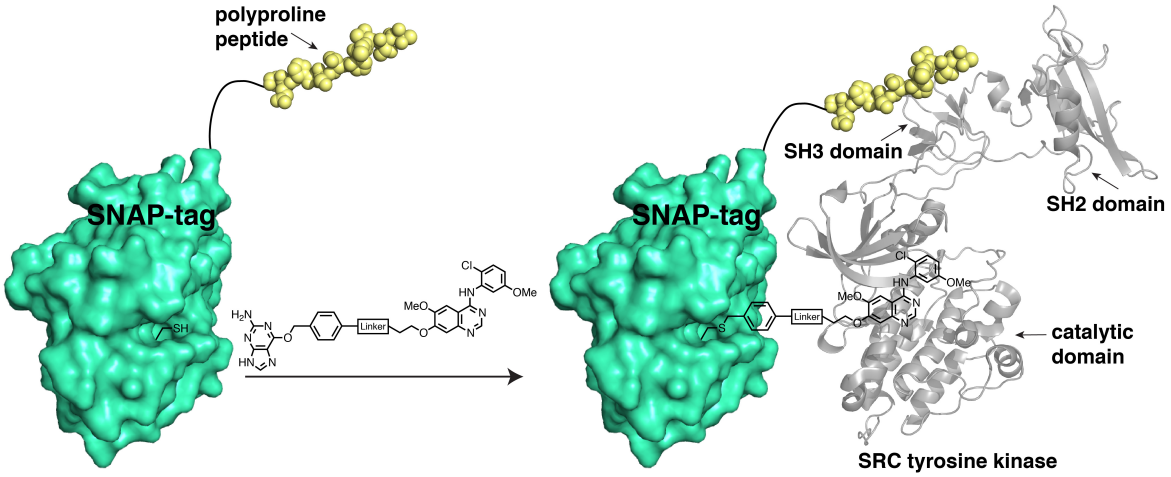

Figure 1-3. A SNAPtag-based bivalent inhibitor approach. Schematic depiction of a representative SNAPtag-based bivalent inhibitor. SNAPtag self-labels an active site cysteine with a quinazoline-based kinase inhibitor conjugated to a benzylguanine (BG) group. The genetically encoded SNAPtag fusion contains a polyproline peptide ligand, which recognizes the SH3 domain of Src. The two ligands of the bivalent inhibitor interact with distinct Src tyrosine kinase binding sites. [PDB IDs 3L00 and1Y57].

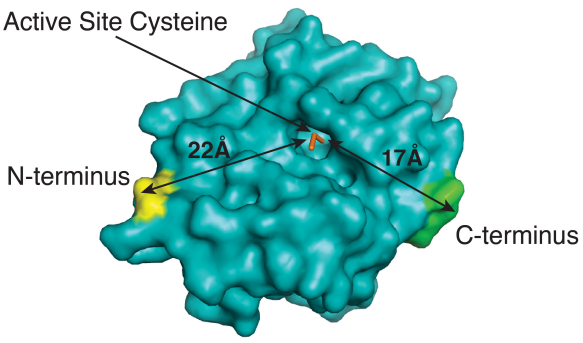

Figure 1-4. Crystallographic representation of the engineered protein SNAPtag. The N- and C-termini, as well as the active site cysteine, are shown. Lengths (in Å) represent the distances between the N-terminus and the active site or the C-terminus and the active site. [PDB ID 3L00].

The key to our bivalent inhibitor strategy is the unique reactivity of SNAPtag. SNAPtag is an engineered form of the DNA repair enzyme O^6-alkylguanine-DNA alkyltransferase (AGT). The normal function of AGT in the cell is to repair O^6-alkylated guanine bases in DNA by irreversibly transferring the alkyl group from the damaged base to its active site cysteine residue (58, 59). Johnsson and coworkers exploited the already relaxed substrate specificity of AGT to engineer variants that show significantly increased rates of reactivity with O^6-benzylguanine (BG) conjugates (60-63). To do this, a library of hAGT mutants were displayed on filamentous phage M13 as g3p fusions and selected for labeling by BG conjugates (61). After multiple rounds of enrichment, hAGT variants with greatly enhanced reactivity relative to the wild type protein were identified. Johnsson and coworkers have shown that optimized hAGT variants (referred to as SNAPtag) can be rapidly and specifically labeled *in vitro* and *in situ* with BG derivatives conjugated to fluorophores or affinity handles (60, 62, 64). Furthermore, New England Biolabs sells cloning vectors and BG conjugates that can be used to label a SNAPtag fusion protein of interest.

A. SNAPTAG-based bivalent inhibitors that target multi-domain protein kinases

Like Src, the tyrosine kinase Abl is a multi-domain tyrosine kinase that contains SH2 and SH3 domains. These domains modulate the catalytic activity and localization of Src and Abl. In addition, the catalytic domains of Src and Abl are very similar and most inhibitors have comparable affinities for their ATP-binding sites. Therefore, we felt that Src and Abl would be a good test for the ability of our bivalent inhibitor strategy to discriminate between two highly related kinases (Figure 1-5) (55). In order to target Src and Abl, bivalent inhibitors that contain an ATP-competitive inhibitor and a SH3 domain-

targeting ligand were generated. Two BG-derivatives based on a 4-anilinoquinazoline scaffold, and with differing linker lengths, were used as ATP-competitive small molecule inhibitors. *In vitro* activity assays showed that attaching BG through a linker had a minimal effect on the abilities of these conjugates to inhibit Abl and Src, relative to the parent 4-anilinoquinazoline compound. To target the SH3 domains of Src and Abl, SNAPtag fusion proteins that contain polyproline (PP)-containing peptides linked through a flexible serine-glycine spacer to the N- or C-terminus were expressed and purified. As the SH3 domain interaction was designed to be the selectivity determinant for these bivalent inhibitors, peptides that have previously been shown to have a preference for Src or Abl were used.

APTYSPPPPP — Abl

APPLPPRNRPRL — Src

SLPSYLNGVMPPTQSFAPDPKYVSS — EGFR

ARKRRRHPAGPPAA — PIM1

IKIKKIEDASNPLLLKRRKKARALEAAALAH — p38

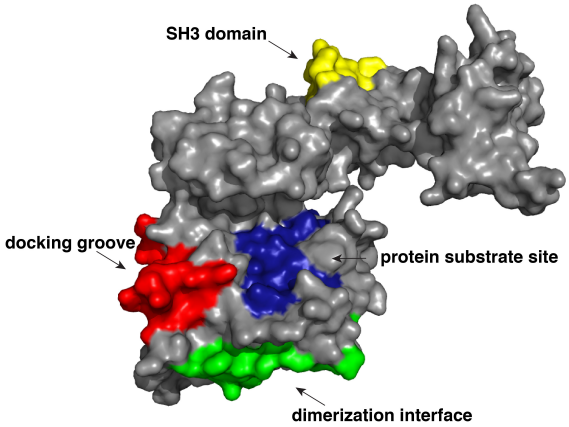

Figure 1-5. The sequences of peptide ligands that have been successfully used in SNAPtag-based bivalent/bisubstrate inhibitors and the kinases they target are shown. The binding sites that have been targeted with SNAPtag-based bivalent inhibitors are shown. These sites are superimposed on a crystal structure of Src tyrosine kinase. [PDB ID 1Y57].

The monovalent reagents described above were assembled into bivalent inhibitors and tested for their abilities to inhibit the catalytic activities of Src and Abl *in vitro* (Table 1-2). As expected, the 4-anilinoquinazoline ATP-competitive inhibitor was a less potent inhibitor of Src and Abl when displayed from the active site of wild type SNAPtag (SNAP(wt)). However, when this same inhibitor was displayed from a

SNAPtag fusion containing either an Abl- or Src-selective PP-containing peptide, a significant increase in potency for the targeted kinase was observed. Interestingly, increased potency was observed whether the SH3 ligand was displayed from the N- or C-terminus of SNAPtag, and the length of the serine-glycine linker had only a small effect on the IC_{50}. The most potent bivalent Src inhibitor (IC_{50} = 13 nM) displayed a >23-fold lower IC_{50} relative to the monovalent BG-derivative ATP-competitive inhibitor and a >380-fold lower IC_{50} relative to the SNAP(wt)-ATP-competitive inhibitor conjugate. Similar increases in potency against Abl using bivalent constructs that contain the Abl-selective PP peptide were observed, with the most potent inhibitor (IC_{50} <6 nM) demonstrating >85 fold more potent inhibition than the monovalent BG-derivative ATP-competitive inhibitor and >200 fold potency increase relative to SNAP(wt)-ATP-competitive inhibitor conjugate. Src-selective and Abl-selective bivalent inhibitors were assayed against a panel of 13 different kinases. As expected, all protein kinases in the panel lacking a SH3 domain were not significantly inhibited by either bivalent construct. The Src-selective PP bivalent construct showed >150-fold selectivity for Src (IC_{50} = 0.013 μM) over Abl (IC_{50} = 2.5 μM) and the SFK Lck (IC_{50} = 2.4 μM). Similarly, the Abl-selective bivalent construct used in this study had an IC_{50} for Abl of 0.018 μM, which was >30-fold lower than Src (IC_{50} = 0.640 μM) and >130-fold lower than Lck (IC_{50} >2.5 μM). Thus, targeting the SH3 domains of Src and Abl allowed highly selective inhibition to be achieved.

Table 1-2. Bisubstrate and bivalent inhibitors of protein kinases based on the SNAPtag protein scaffold.

Kinase	Specificity	Ligand A (active-site directed)	Fold Inc Over A	Ligand B	Fold Inc Over B	Linker	Reference
ABL	Tyr	4-anilinoquinazoline	>85	ABL-selective PP motif (SH3 domain)	N/A	$(GS)_2$	Hill *et al.* (2009)
SRC	Tyr	4-anilinoquinazoline	23	SRC-selective PP motif (SH3 domain)	N/A	$(SG)_2$	Hill *et al.* (2009)
EGFR	Tyr	Gefitinib	18	MIG6 peptide (dimer interface)	330	$(SG)_5$	Hill *et al.* (2012)
PIM1	Ser/Thr	SGI-1776	12	Pimtide pseudosubstrate (substrate site)	64	$(GS)_2$	Hill *et al.* (2012)
p38α	Ser/Thr	4-anilinoquinazoline	150	MAPKAPK2 (docking site)	>1600	$(SG)_5$	Hill *et al.* (2012)

Fold increase refers to the potency of kinase inhibition.

A more detailed analysis of the contributions of each monovalent component of the assembled bivalent inhibitors that target Src and Abl was undertaken (56). It had already been determined that the length of the linker and the fusion orientation (C- or N-terminal) of the SH3 ligand had only a small effect on bivalent inhibitor potency. However, varying the length of the linker between the 4-anilinoquinazoline ATP-competitive inhibitor and the SNAPtag fusion protein had a more pronounced effect on bivalent inhibitor potency. While tether length only had a small effect on the potencies of the Src-selective bivalent inhibitors, with the construct containing the longest linker possessing the lowest IC_{50}, there was a greater than 15-fold difference between Abl-selective bivalent inhibitors with variable ATP-competitive inhibitor linker lengths. Surprisingly, the bivalent construct with an intermediate linker length possessed the lowest IC_{50} for Abl activity. These results suggest that Abl may have a different relative orientation between its SH3 and catalytic domains compared to Src, which could potentially be exploited to further differentiate between these two kinases. In the same study, the contributions of the ATP-competitive inhibitor and PP-containing SH3 domain ligand were also probed. A small panel of BG-linked ATP-competitive inhibitors that displayed varying affinities for the active site of Abl and Src were tested. In all cases,

conjugating the BG-derivative inhibitors to a SNAPtag SH3 domain ligand fusion protein resulted in at least a small increase in potency against the kinase target. Furthermore, small differences in affinity between these monovalent ATP-competitive inhibitors had a direct and predictable effect on the potency of the corresponding bivalent inhibitor. This same trend was observed for the PP-containing SH3 domain ligand, where relative differences in the affinities of the peptide ligands for the SH3 domain of the kinase being targeted led to a predictable corresponding change in the potency of the assembled bivalent inhibitor. These studies further highlighted that the high selectivity exhibited by the Abl-selective and Src-selective bivalent inhibitors is due to the relative specificities of their corresponding SH3 domain ligands.

B. SNAPTAG-based bivalent inhibitors that target diverse protein kinases

SNAPtag-based bivalent inhibitors that are directed towards the diverse protein kinases PIM1, p38α, and EGFR have also been generated (Figure 1-5 and Table 1-2) (57). Importantly, these bivalent inhibitors all exploit diverse signaling interaction sites that are located in the catalytic domains of their kinase targets. To target PIM1, N- and C-terminal SNAPtag fusion proteins that contain a modified pseudosubstrate called Pimtide (ARKRRRHPSGPPTA), which is the peptide ligand corresponding to the consensus substrate motif of this kinase, were generated. A linkable analog of an imidazo[1,2-*b*]pyridazine inhibitor was used to target the ATP-binding site of Pim1. While the imidazo[1,2-*b*]pyridazine inhibitor exhibited a >9-fold loss in potency when displayed from the active site of SNAPtag(wt), its conjugation to SNAPtag fusions that contain Pimtide ligands led to an increase in potency relative to both monovalent components. For the bivalent inhibition of the MAPK p38α, its docking groove, which

interacts with a number of activators and substrates, was targeted using a 31-amino acid peptide derived from the mitogen activated protein kinase-activated protein kinase 2 (MAPKAPK2). This peptide is a ligand for a docking site on p38α and does not overlap with the kinase active site. Two different ATP-competitive inhibitors with variable affinities for the ATP-binding site of p38α were selected as the other monovalent components of the bivalent inhibitor. Consistent with the ability to simultaneously target p38α's ATP-binding site and docking groove, conjugation of either inhibitor to a SNAPtag-MAPKAPK2-peptide fusion protein led to more potent inhibition of p38α than either monovalent component alone. In contrast to PIM1 and p38α, a slightly different approach was needed for selecting a non-ATP-binding site ligand for EGFR because this kinase does not possess substrate interaction sites of sufficient binding affinity. Therefore, a 25-amino acid peptide from the mitogen-induced gene 6 (MIG6) protein, which binds to the hydrophobic dimer interface on the C-lobe of EGFR, was chosen as the genetically encodable ligand that was displayed as a SNAPtag fusion. Bivalent inhibitors were generated by conjugating the clinically approved drug gefitinib to SNAPtag fusions displaying the MIG6 peptide from their N-termini. Similar to p38α and PIM1, the assembled bivalent inhibitors were significantly more potent against their target, EGFR, than either individual monovalent component. These three examples demonstrate that SNAPtag-based bivalent inhibitors can target a number of different binding sites outside of the ATP-binding clefts of protein kinases.

Beyond showing increased potency for specific kinase targets, the SNAPtag-based bivalent inhibitors described above demonstrated increased overall selectivity. The most potent bivalent inhibitors of PIM1, p38α, and EGFR were assayed against a

panel of 27 kinases that were selected based on diversity and being known off-targets of the ATP-competitive inhibitor components used in the bivalent inhibitors. While the ATP-competitive inhibitor components of the EGFR- and p38α-targeting inhibitors were already fairly selective, the assembled bivalent conjugates were even more so. In both cases, the assembled bivalent inhibitors were >900-fold selective for their intended targets over the 26 other kinases tested. For the PIM1-targeting bivalent inhibitor, only PIM2 kinase showed any significant inhibition (IC_{50} = 1,700 nM) compared to PIM1 (IC_{50} = 45 nM). However, the assembled bivalent inhibitor showed enhanced selectivity between these two kinases relative to the monovalent substituents.

VI. Cellular applications of SNAPtag-based bivalent inhibitors

Like the bisubstrate inhibitors described above, the first cellular experiments with SNAPtag-based bivalent inhibitors involved the use of an intra-cellular delivery method (65). Specifically, a fully assembled bivalent inhibitor of Abl was encapsulated in dye-sensitized lipid nanocapsules, which were taken up by BCR-Abl-dependent Ba/F3 cells through endocytosis. Nanosecond laser pulses in the far red (645 nm) region allowed photothermal release of the bivalent inhibitor into the cytosol. As Ba/F3 cells are dependent on the activity of BCR-Abl for survival in the absence of interleukin-3 (IL-3), intra-cellular release of the bivalent Abl inhibitor led to rapid cell death. However, when a similar experiment was performed with Ba/F3 cells in the presence of IL-3, no cell death occurred, confirming that the phenotypic effect observed upon bivalent inhibitor release is through BCR-Abl.

While intra-cellular delivery methods allow bivalent SNAPtag-based inhibitors to be used in cells, the most general strategy for application of this methodology involves

the assembly of bivalent inhibitors in cells that are expressing SNAPtag fusion proteins (Figure 1-6). Johnsson and co-workers have demonstrated that BG derivatives conjugated to fluorophores or affinity handles are cell permeable and can undergo selective intra-cellular labeling of SNAPtag (60). We have found that, in general, BG-derivatized ATP-competitive inhibitors have low cell permeability. However, ATP-competitive inhibitors that are conjugated to an O^4-benzyl-2-chloro-6-aminopyrimidine (CLP) tag, which can also rapidly and selectivity label SNAPtag, are cell permeable and efficiently label intra-cellular SNAPtag. Four diverse CLP-conjugated ATP-competitive inhibitors of PIM1, p38α, and EGFR were able to label SNAPtag in a variety of cell lines (COS-7, HeLa, and HEK293) (57). These results set the stage for the intra-cellular assembly of potent and selective SNAPtag-based bivalent inhibitors in cells and their use in a number of cellular studies.

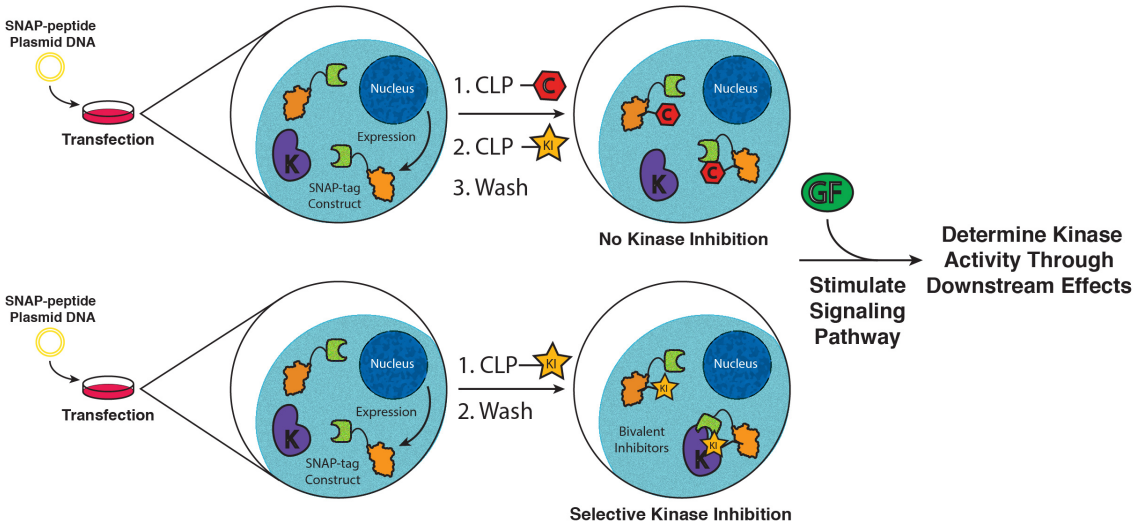

Figure 1-6. Schematic representation of the strategy for intra-cellular assembly and use of SNAPtag-based bivalent inhibitors. Mammalian cells express a genetically encoded SNAPtag fusion protein. A CLP-derivatized ATP-competitive kinase inhibitor (CLP-KI) passively diffuses into cells and labels the monovalent SNAPtag fusion. Excess monovalent CLP-KI is removed through several wash steps. Upon stimulation of the signaling pathway, kinase activity can be determined by monitoring downstream effects. As a control, a CLP-derivatized small molecule lacking inhibitory activity is used to label (block) the SNAPtag active site before addition of CLP-KI. Any effects observed are due to CLP-KI and not the SNAPtag-based bivalent inhibitor.

VII. Conclusion

Over the past two decades, there has been widespread interest in the use of bisubstrate and bivalent inhibitors to study protein kinases. Examples in the literature have shown that these tools, when built with appropriate linkage and ligand display, can be potent (nanomolar dissociation constants) inhibitors of target protein kinases. In order for bivalent inhibitors to be useful tools for the study of kinase function, they must also be highly selective. Early examples of bivalent inhibitors sought to differentiate between two or more closely related protein kinases, occasionally investigating selectivity over more diverse kinase family members (30, 35, 41). In certain instances, such as the work performed by Ricouart and coworkers, the observed selectivity was, regrettably, opposite of the authors' intentions. In general, all of these earlier studies only profiled a small panel of potential kinase off targets, and it is difficult to judge the true kinome selectivity of these reagents. More recent examples have included profiling against larger panels of protein kinases, ranging from 27 to 90 family members (50, 57). In these larger screens, the developed bivalent inhibitors were shown to be highly selective for the protein kinase of interest over both closely related family members and more distantly related kinases. With the recent advent of whole-kinome screening techniques (66-69), the ability to extensively profile bivalent reagents is now possible. With the application of these techniques to bisubstrate and bivalent inhibitors, it will be interesting to see if these reagents are truly as selective as theorized.

Another major challenge in the application of bisubstrate and bivalent inhibitors is in their use in a cellular environment. To date, there have been very few examples of the successful use of bivalent kinase inhibitors in cells. Where there has been success

is in the use of transport mechanisms to deliver these high molecular weight reagents to cells. For example, the attachment of a HIV-TAT peptide to a potent JNK1 inhibitor by Stebbins and coworkers, allowed the authors to achieve JNK1 inhibition both in cultured cells and in glucose-intolerant mice (48). Furthermore, we have shown that it is possible to photothermally release bivalent inhibitors that are encapsulated in dye-sensitized lipid nanocapsules (65). Examples of this type point to the likelihood of increased use of bisubstrate and bivalent inhibitors in cellular studies. However, the routine delivery of biomolecules of this kind is still a challenge. An alternative strategy is to assemble bivalent inhibitors inside the cell using the diversity of highly chemoselective conjugation methods that are currently available. This approach is actively being pursued (55-57).

Protein kinases represent a large and interesting family of proteins within the human proteome. Key players in diverse cellular signaling networks, these enzymes represent a large set of druggable targets. Despite this, the specific roles that many protein kinases play in both native signaling and disease states are not well understood. Likewise, selective and potent inhibitors of most protein kinases do not exist. The ability to develop powerful tools for the cellular study of a specific protein kinase is invaluable, and we feel that the development of cellular bivalent inhibitors is an excellent starting point in developing the necessary toolset for the cellular study of protein kinases.

VIII. References

1. Manning G, Whyte DB, Martinez R, Hunter T, Sudarsanam S (2002) The protein kinase complement of the human genome. *Science* 298:1912–1934.

2. Hunter T (2000) Signaling--2000 and beyond. *Cell* 100:113–127.

3. Blume-Jensen P, Hunter T (2001) Oncogenic kinase signalling. *Nature* 411:355–365.

4. Cohen P (2002) Protein kinases--the major drug targets of the twenty-first century? *Nat Rev Drug Discov* 1:309–315.

5. Knight ZA, Shokat KM (2005) Features of selective kinase inhibitors. *Chem Biol* 12:621–637.

6. Knight ZA, Shokat KM (2007) Chemical genetics: where genetics and pharmacology meet. *Cell* 128:425–430.

7. Taylor SS et al. (1988) CAMP-dependent protein kinase: prototype for a family of enzymes. *The FASEB Journal* 2:2677–2685.

8. Hanks SK, Hunter T (1995) Protein kinases 6. The eukaryotic protein kinase superfamily: kinase (catalytic) domain structure and classification. *The FASEB Journal* 9:576-596.

9. Ubersax JA, Ferrell JE Jr (2007) Mechanisms of specificity in protein phosphorylation. *Nat Rev Mol Cell Biol* 8:530–541.

10. Turk BE (2008) Understanding and exploiting substrate recognition by protein kinases. *Current Opinion in Chemical Biology* 12:4–10.

11. Bhattacharyya RP, Reményi A, Yeh BJ, Lim WA (2006) Domains, motifs, and scaffolds: the role of modular interactions in the evolution and wiring of cell signaling circuits. *Annu Rev Biochem* 75:655–680.

12. Hutti JE et al. (2004) A rapid method for determining protein kinase phosphorylation specificity. *Nat Chem Biol* 1:27–29.

13. Chen CC, Turk BEB (2010) Analysis of serine-threonine kinase specificity using arrayed positional scanning peptide libraries. *Curr Protoc Mol Biol* Chapter 18:Unit–14.

14. Mok J et al. (2010) Deciphering protein kinase specificity through large-scale analysis of yeast phosphorylation site motifs. *Science Signaling* 3:ra12–ra12.

15. Biondi RM, Nebreda AR (2003) Signalling specificity of Ser/Thr protein kinases through docking-site-mediated interactions. *Biochem J* 372:1.

16. Sheridan DL, Kong Y, Parker SA, Dalby KN, Turk BE (2008) Substrate discrimination among mitogen-activated protein kinases through distinct docking sequence motifs. *J Biol Chem* 283:19511–19520.

17. Barr FA, Silljé HHW, Nigg EA (2004) Polo-like kinases and the orchestration of cell division. *Nat Rev Mol Cell Biol* 5:429–440.

18. Lowery DM, Lim D, Yaffe MB (2005) Structure and function of Polo-like kinases. *Oncogene* 24:248–259.

19. Kothe M et al. (2007) Selectivity-determining residues in Plk1. *Chem Biol Drug Des* 70:540–546.

20. Qiu H, Miller WT (2003) Role of the Brk SH3 domain in substrate recognition. *Oncogene* 23:2216–2223.

21. Zarrinpar A, Bhattacharyya RP, Lim WA (2003) The structure and function of proline recognition domains. *Sci STKE* 2003:RE8.

22. Yadav SS, Miller WT (2008) The Evolutionarily Conserved Arrangement of Domains in Src Family Kinases Is Important for Substrate Recognition †. *Biochemistry* 47:10871–10880.

23. Schlessinger J, Lemmon MA (2003) SH2 and PTB domains in tyrosine kinase signaling. *Sci STKE* 2003:RE12.

24. Mayer BJ, Hirai H, Sakai R (1995) Evidence that SH2 domains promote processive phosphorylation by protein-tyrosine kinases. *Curr Biol* 5:296–305.

25. Durocher D, Jackson SP (2002) The FHA domain. *FEBS Lett* 513:58–66.

26. Benes CH et al. (2005) The C2 Domain of PKCδ Is a Phosphotyrosine Binding Domain. *Cell* 121:271–280.

27. Lemmon MA, Ferguson KM (2000) Signal-dependent membrane targeting by pleckstrin homology (PH) domains. *Biochem J* 350 Pt 1:1–18.

28. Krishnamurty R, Maly DJ (2007) Chemical genomic and proteomic methods for determining kinase inhibitor selectivity. *Comb Chem High Throughput Screen* 10:652–666.

29. Fedorov O et al. (2007) A systematic interaction map of validated kinase inhibitors with Ser/Thr kinases. *Proceedings of the National Academy of Sciences* 104:20523–20528.

30. Ricouart A, Gesquiere JC, Tartar A, Sergheraert C (1991) Design of potent protein kinase inhibitors using the bisubstrate approach. *J Med Chem* 34:73–78.

31. Rosse C et al. (2010) PKC and the control of localized signal dynamics. *Nature Reviews Molecular Cell Biology* 11:103–112.

32. van Ameijde J et al. (2010) Preparation of novel alkylated arginine derivatives suitable for click-cycloaddition chemistry and their incorporation into pseudosubstrate- and bisubstrate-based kinase inhibitors. *Org Biomol Chem* 8:1629–1639.

33. Poot AJ et al. (2009) Development of Selective Bisubstrate-Based Inhibitors Against Protein Kinase C (PKC) Isozymes By Using Dynamic Peptide Microarrays. *ChemBioChem* 10:2042–2051.

34. Carnegie GK, Means CK, Scott JD (2009) A-kinase anchoring proteins: from protein complexes to physiology and disease. *IUBMB Life* 61:394–406.

35. Hines AC, Cole PA (2004) Design, synthesis, and characterization of an ATP-peptide conjugate inhibitor of protein kinase A. *Bioorganic & Medicinal Chemistry Letters* 14:2951–2954.

36. Schneider TL et al. (2005) Increasing the Kinase Specificity of K252a by Protein Surface Recognition. *Org Lett* 7:1695–1698.

37. Medzihradszky D, Chen SL, Kenyon GL, Gibson BW (1994) Solid-phase synthesis of adenosine phosphopeptides as potential bisubstrate inhibitors of protein kinases. *J Am Chem Soc* 116:9413–9419.

38. Loog M, Uri A, Raidaru G, Järv J, Ek P (1999) Adenosine-5'-carboxylic acid peptidyl derivatives as inhibitors of protein kinases. *Bioorganic & Medicinal Chemistry Letters* 9:1447–1452.

39. Loog M, Uri A, Järv J, Ek P (2000) Bi-substrate analogue ligands for affinity chromatography of protein kinases. *FEBS Lett* 480:244–248.

40. Kruse CH et al. (1988) Synthesis and evaluation of multisubstrate inhibitors of an oncogene-encoded tyrosine-specific protein kinase. *J Med Chem* 31:1762–1767.

41. Traxler PM et al. (1991) Sulfonylbenzoyl-nitrostyrenes: potential bisubstrate type inhibitors of the EGF-receptor tyrosine protein kinase. *J Med Chem* 34:2328–2337.

42. Imoto M et al. (1987) Kinetic studies of tyrosine kinase inhibition by erbstatin. *Journal of antibiotics* 40:1471–1473.

43. Rossé G et al. (1997) Synthesis of Modified Tripeptides and Tetrapeptides as potential bisubstrate inhibitors of the epidermal growth factor receptor protein tyrosine kinase. *Helv Chim Acta* 80:653–670.

44. Parang K et al. (2001) Mechanism-based design of a protein kinase inhibitor. *Nat Struct Biol* 8:37–41.

45. Hines AC, Parang K, Kohanski RA, Hubbard SR, Cole PA (2005) Bisubstrate analog probes for the insulin receptor protein tyrosine kinase: Molecular yardsticks for analyzing catalytic mechanism and inhibitor design. *Bioorganic Chemistry* 33:285–297.

46. Shen K, Cole PA (2003) Conversion of a Tyrosine Kinase Protein Substrate to a High Affinity Ligand by ATP Linkage. *J Am Chem Soc* 125:16172–16173.

47. Levinson NM, Visperas PR, Kuriyan J (2009) The tyrosine kinase Csk dimerizes through Its SH3 domain. *PloS one* 4:e7683.

48. Stebbins JL et al. (2011) Design and Characterization of a Potent and Selective Dual ATP- and Substrate-Competitive Subnanomolar Bidentate c-Jun N-Terminal Kinase (JNK) Inhibitor. *J Med Chem* 54:6206–6214.

49. Meyer SC, Shomin CD, Gaj T, Ghosh I (2007) Tethering Small Molecules to a Phage Display Library: Discovery of a Selective Bivalent Inhibitor of Protein Kinase A. *J Am Chem Soc* 129:13812–13813.

50. Shomin CD, Meyer SC, Ghosh I (2009) Staurosporine tethered peptide ligands that target cAMP-dependent protein kinase (PKA): Optimization and selectivity profiling. *Bioorganic & Medicinal Chemistry* 17:6196–6202.

51. Shomin CD, Restituyo E, Cox KJ, Ghosh I (2011) Selection of cyclic-peptide inhibitors targeting Aurora kinase A: Problems and solutions. *Bioorganic & Medicinal Chemistry* 19:6743–6749.

52. Profit AA, Lee TR, Lawrence DS (1999) Bivalent Inhibitors of Protein Tyrosine Kinases. *J Am Chem Soc* 121:280–283.

53. Hah J-M, Sharma V, Li H, Lawrence DS (2006) Acquisition of a “Group A-”Selective Src Kinase Inhibitor via a Global Targeting Strategy. *J Am Chem Soc* 128:5996–5997.

54. van Wandelen LTM et al. (2013) Cell-Penetrating Bisubstrate-Based Protein Kinase C Inhibitors. *ACS Chem Biol*.

55. Hill ZB, Perera BGK, Maly DJ (2009) A Chemical Genetic Method for Generating Bivalent Inhibitors of Protein Kinases. *J Am Chem Soc* 131:6686–6688.

56. Hill ZB, Perera BGK, Maly DJ (2011) Bivalent inhibitors of the tyrosine kinases ABL and SRC: determinants of potency and selectivity. *Mol BioSyst* 7:447.

57. Hill ZB, Perera BGK, Andrews SS, Maly DJ (2012) Targeting Diverse Signaling Interaction Sites Allows the Rapid Generation of Bivalent Kinase Inhibitors. *ACS Chem Biol* 7:487–495.

58. Pegg AE (2000) Repair of O(6)-alkylguanine by alkyltransferases. *Mutat Res* 462:83–100.

59. Tubbs JL, Pegg AE, Tainer JA (2007) DNA binding, nucleotide flipping, and the helix-turn-helix motif in base repair by O6-alkylguanine-DNA alkyltransferase and its implications for cancer chemotherapy. *DNA Repair (Amst)* 6:1100–1115.

60. Keppler A et al. (2003) A general method for the covalent labeling of fusion proteins with small molecules in vivo. *Nat Biotechnol* 21:86–89.

61. Juillerat A et al. (2003) Directed evolution of O6-alkylguanine-DNA alkyltransferase for efficient labeling of fusion proteins with small molecules in vivo. *Chem Biol* 10:313–317.

62. Juillerat A et al. (2005) Engineering substrate specificity of O6-alkylguanine-DNA alkyltransferase for specific protein labeling in living cells. *ChemBioChem* 6:1263–1269.

63. Gronemeyer T, Chidley C, Juillerat A, Heinis C, Johnsson K (2006) Directed evolution of O6-alkylguanine-DNA alkyltransferase for applications in protein labeling. *Protein engineering, design & selection : PEDS* 19:309–316.

64. Corrêa IR et al. (2013) Substrates for improved live-cell fluorescence labeling of SNAP-tag. *Curr Pharm Des* 19:5414–5420.

65. Gregersen KAD et al. (2010) Intracellular Delivery of Bioactive Molecules using Light-Addressable Nanocapsules. *ACS Nano* 4:7603–7611.

66. Davis MI et al. (2011) Comprehensive analysis of kinase inhibitor selectivity. *Nat Biotechnol* 29:1046–1051.

67. Fabian MA et al. (2005) A small molecule-kinase interaction map for clinical kinase inhibitors. *Nat Biotechnol* 23:329–336.

68. Karaman MW et al. (2008) A quantitative analysis of kinase inhibitor selectivity. *Nat Biotechnol* 26:127–132.

69. Urbaniak MD et al. (2012) Chemical proteomic analysis reveals the drugability of the kinome of Trypanosoma brucei. *ACS Chem Biol* 7:1858–1865.

Chapter 2

Generation of bivalent kinase inhibitors starting from a single polypharmacological component for selective target modulation in cells

I. Introduction

Classical forward genetics has been a powerful technique for deconvoluting the cellular roles of proteins through loss of function studies, and is one of the principle means for discovering possible novel drug targets (1). Genetic methods that disrupt protein function prior to translation, like gene deletions and RNAi, are attractive for these studies due to their genome-wide scalability, high specificity and ease of implementation (2). Such methods of disrupting protein function do so by removing the entire protein from the cell, which for a multi-domain protein makes it difficult to attribute the observed phenotype to the inhibition of a specific function. For example, distinguishing between inhibition of catalytic activity and disruption of critical protein-protein interactions is not possible as both the catalytic and scaffolding functions have been inhibited simultaneously. Additionally, these methods introduce permanent changes, or slowly reversible in the case of RNAi, making it difficult to differentiate direct effects of inhibition of protein function from compensatory changes that occur due to chronic loss of protein function.

In some instances, small molecule inhibition of protein function, which occurs post-translationally, may be preferable for understanding the cellular function of proteins. This is especially true when validating putative drug targets because the mechanism of action is the same as that of a pharmacological agent; in many cases, pharmacological inhibition and RNAi do not lead to the same phenotype (2). The

challenge for small molecule inhibitors is achieving a sufficiently high degree of selectivity and proteome-wide scalability. Therefore, technologies that mimic the pharmacological consequences of post-translational protein target inhibition without requiring the extensive effort needed for the development a mono-selective inhibitor are valuable.

Protein kinases represent a large protein family (> 500 members) that are desirable drug targets, but the high degree of sequence identity and active site structural similarity makes the identification of selective inhibitors challenging (3, 4). The inherent plasticity and compensatory changes observed in protein kinase signaling cascades complicates the use of genetic-based methods to probe kinase function. Additionally, protein kinases participate in a number of protein-protein interactions and non-catalytic functions that are blocked by genetic reagents but not by small molecule inhibitors. Therefore, new tools that allow selective post-translational kinase inhibition would be useful reagents for exploring cell signaling and probing the suitability of particular kinases as drug targets.

In an attempt to identify selective and potent inhibitors of protein kinases, bivalent inhibition strategies have been employed wherein a small molecule targeting the highly conserved ATP-binding site is tethered to a second specificity ligand that binds to a unique interaction motif of a kinase of interest. If a potent and selective binder that can discriminate between closely related kinases is chosen as the second specificity ligand, and the linkage between the two monovalent components is favorable, potent and selective inhibitors can be generated (5, 6). We have developed a bivalent inhibitor strategy based on the self-labeling protein SNAPtag (7-9). By selectively labeling

SNAPtag fusion proteins, which display a secondary specificity ligand from their N- or C-termini, with an ATP-competitive inhibitor, potent and selective bivalent inhibitors of several kinases have been generated (10-12). Our previously described SNAPtag-based bivalent inhibitors relied on the use of genetically encoded, consensus-binding motifs as secondary specificity ligands. While this strategy led to impressive selectivity amongst closely related kinases, consensus-binding motif interactions are often not very selective, and, in general, exhibit modest affinities for their respective targets. Additionally, consensus-binding motifs for many kinases are not known or are poorly characterized, which limits the ability of this strategy to be generally applied throughout the kinome.

In a truly general approach for generating bivalent kinase inhibitors it would be highly desirable to identify specificity ligands with no prior knowledge of the kinase target; especially given the sheer number of poorly/uncharacterized protein kinases. To this end, new classes of non-immunoglobulin scaffolds have been identified that when coupled with *in vitro* display technologies allow for the rapid identification of potent and selective affinity capture reagents suitable for intracellular studies. In fact, intracellular antibodies based on two different protein scaffolds (called monobodies and DARPins) that selectively target several kinases have been identified (13-20). Unfortunately, the utility of intracellular antibodies for studying kinase function is often limited because many of these reagents target binding sites that do not overlap, or only partially overlap, with active site features. Thus, intracellular antibodies are potentially attractive candidates as second site specificity ligands of SNAPtag-based inhibitors.

Here, we show that intracellular antibodies can be used as highly effective secondary specificity ligands for SNAPtag-based bivalent kinase inhibitors (Figure 2-1 A). By linking a single pan ATP-competitive inhibitor to a SNAPtag intracellular antibody fusion, selective bivalent inhibitors for either BCR-Abl or phospho-ERK2 were obtained. These bivalent kinase inhibitors demonstrate increased potencies for their respective kinase targets and overall enhanced selectivity. For both bivalent inhibitors, the enhanced selectivities and affinities observed *in vitro* were rigorously tested in complex cell lysates. Applying competition-based quantitative chemical proteomics, both the BCR-Abl- and phospho-ERK2-targeted bivalent inhibitors exhibited significant increases in affinity and selectivity. Importantly, we show that a bivalent inhibitor of the protein tyrosine kinase Abl readily assembles in cells and inhibits the ability of BCR-Abl to phosphorylate a direct cellular target.

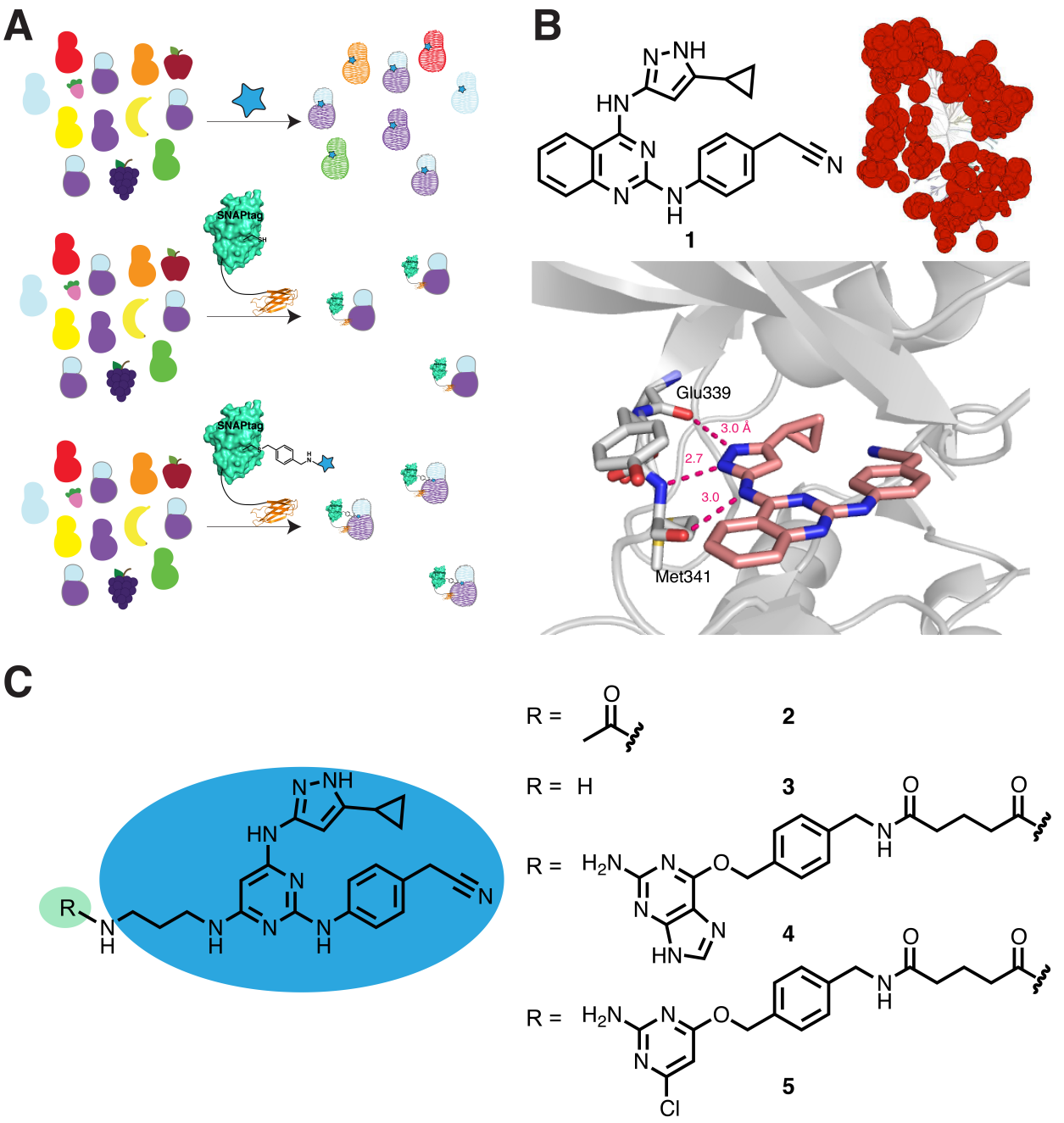

Figure 2-1. SNAPtag-based bivalent inhibitors of protein kinases using a pan-kinase pharmacophore where intracellular antibodies are used to direct selectivity. (A) A general strategy for the use of intracellular antibodies as specificity elements of SNAPtag-based bivalent kinase inhibitors. (Top panel) A promiscuous ATP-competitive inhibitor blocks the activity of the majority of the kinome. (Middle panel) A selective intracellular antibody-SNAPtag fusion selectivity interacts with its kinase target but does not block its activity. (Bottom panel) A bivalent inhibitor containing a non-selective ATP-competitive inhibitor and an intracellular antibody selectively interacts with its kinase target and blocks catalytic activity. (B) (Top panel) The pan-kinase inhibitor (**1**) used for the bivalent inhibitors in this study. (Bottom panel) A crystal structure of **1** bound to the kinase Src suggests a site of linker attachment. PDB ID 3F6X. (C) Reagents based on the pan-kinase inhibitor **1**.

II. Results and Discussion

To generate bivalent inhibitors based on SNAPtag, two components are necessary: (1) an ATP-competitive inhibitor linked to a chemoselective SNAPtag-labeling moiety and (2) a ligand that selectively interacts with unique regions of a kinase of interest. For the ATP-competitive inhibitor, we were particularly interested in a general ligand that could be used to target any kinase of interest. This would allow the rapid assembly of potent bivalent inhibitors of diverse kinases without the need to identify a target-specific pharmacophore. Furthermore, using a promiscuous kinase inhibitor would provide a true metric of the degree of selectivity that can be gained with an intracellular antibody-directed bivalent inhibitor. For these reasons, a previously reported 5-cyclopropyl-3-aminopyrazolo-based inhibitor (**1**) was of particular interest (21). This pharmacophore contains functional groups that are able to interact with active site features that are conserved in the ATP-binding sites of most kinases (22). Additionally, a co-crystal structure of **1** bound to the tyrosine kinase Src indicated a straightforward site of linker attachment that would likely not interfere with its interactions with kinase ATP-binding sites (Figure 2-1 B). Indeed, a derivative of **1** (**2**), which contains a linker that can be modified with diverse acylating agents, possesses a broad inhibitory profile as assessed with KINOMEscan™ (see Experimental Procedures).

Due to the linkable and modular nature of **2**, a single component kinase affinity matrix was readily generated by reacting an amine-containing version of this scaffold (**3**) with NHS-activated sepharose. With this tool, the ability of **2** to bind to a variety of full-length protein kinases in a complex cellular lysate was determined (Figure 2-2 A). K562

lysates were pre-incubated with varying concentrations of free **2** or DMSO control; after which, the lysates were incubated with the affinity matrix. The resin was washed and proteins were eluted under denaturing conditions before quantitative chemical proteomics were employed. In this way, the ability of **2** to self-compete for kinases bound to **2**-derivatized resin was assessed. Protein kinases enriched in the DMSO control sample represent those kinases capable of binding to **2** when attached to a solid support matrix. Those kinases exhibiting dose-dependent competition upon the addition of free **2** are those that exhibit the highest affinity for **2** when in solution (Figure 2-2 B).

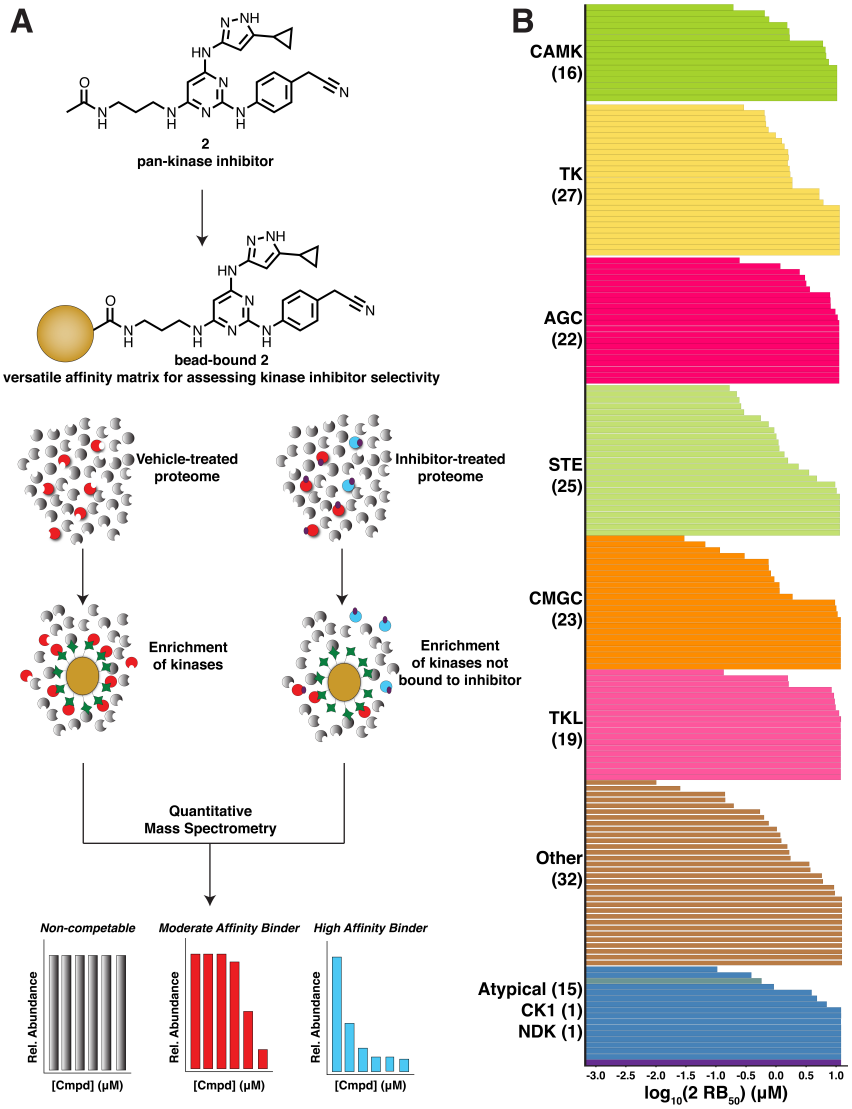

Figure 2-2. A single-component affinity matrix based on the pan-kinase inhibitor **2**. (A) Schematic of the quantitative chemical proteomics workflow. Lysates are pre-treated with free **2** or DMSO before enrichment with **2**-conjugated resin. Quantitative chemical proteomics are then employed to determine the affinity of cellular protein kinases for **2**. (B) Half-maximal residual binding (RB_{50}) is represented for members of various protein kinase families. Values are the average of two independent experiments.

From this analysis, >230 protein kinases were identified between replicate DMSO control samples, establishing the utility of **2** as single component kinase profiling tool compound. To our knowledge, this represents the largest swath of the kinome to be profiled by a single compound via chemical proteomics. For >180 protein kinases, an affinity for **2** could be estimated by calculating the concentration at which 50% of a given protein remained bound to the affinity matrix (residual binding (RB_{50}) value). As depicted in Figure 2-2 B, full-length protein kinases from the various branches of the kinome tree exhibit appreciable affinity for **2**. The number and diversity of kinase active sites targeted by **2** highlights the potential of this single compound to serve as both a versatile building block of bivalent inhibitors as well as a profiling tool for assessing bivalent inhibitor selectivity.

Derivatives of **2** that are capable of labeling SNAPtag (**4** and **5**) were generated by derivatizing its flexible linker with either O^6-benzylguanine (BG) or 4-(benzyloxy)-6-chloropyrimidin-2-amine (CLP) moieties (Figure 2-1 C). Compound **4** is ideally suited for *in vitro* labeling because of its ability to provide highly reproducible and nearly quantitative labeling of purified SNAPtag constructs. However, we have found that the benzylguanine moiety can drastically reduce the cell permeability of linked kinase inhibitors (12). To circumvent this issue, a CLP-derivatized analog (**5**) was also generated. While CLP derivatives provide incomplete SNAPtag labeling *in vitro* (Figure 2-3), we have found that inhibitors containing this group are able to efficiently label SNAPtag constructs in living cells, which is a requirement for *in situ* bivalent inhibitor assembly. As expected, derivatizing **2** with CLP or BG does not alter the broad kinase profile of the 5-cyclopropyl-3-aminopyrazolo pharmacophore (data not shown).

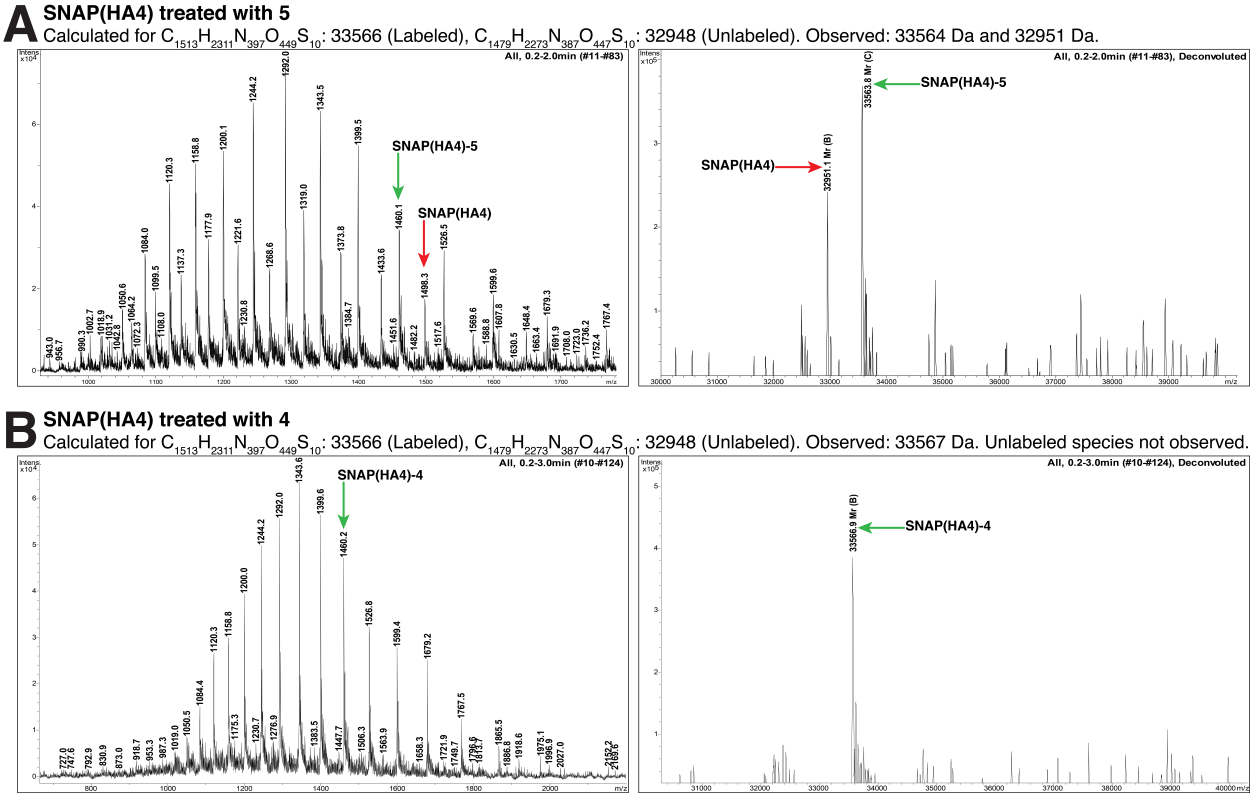

Figure 2-3. Mass spectra of a SNAPtag fusion protein treated with either (A) **5** or (B) **4**. Raw ESI spectra are seen on the left and deconvoluted mass spectra on the right.

The first kinase that we targeted with our bivalent reagents is the tyrosine kinase c-Abl. This multi-domain kinase interacts with cellular substrates through its Src homology 2 (SH2) and Src homology 3 (SH3) domains. The phosphotyrosine-binding SH2 domain is used by Abl to recognize primed substrates within a cell and facilitates processive phosphorylation (23). A potent (K_d = 7 nM) monobody-based intracellular antibody of Abl's SH2 domain has been identified (14). This eleven kDa reagent, called HA4, selectively interacts with the SH2 domains of Abl and Abl2 over other phosphotyrosine-binding proteins. The authors tested 84 SH2 domains on a protein microarray, and only one (the SH2 domain of the tyrosine kinase SYK) demonstrated comparable affinity to that of Abl and Abl2, while two others (Blk and Grb7) were within 10-fold. To test the suitability of the Abl monobody to serve as a component of a

bivalent inhibitor, a SNAPtag fusion (SNAP(HA4)) displaying HA4 from the C-terminus through a four amino acid linker was expressed and purified (Figure 2-4 A). Small molecule-labeled constructs were assembled by covalently labeling SNAPtag fusions with an excess of **4**. Size exclusion chromatography was then used to remove any excess **4** from labeled SNAPtag proteins. Complete removal of excess **4** was verified with an Abl activity assay, and mass spectrometry of the intact bivalent inhibitor was used to verify the degree of labeling with **4**. Constructs were found to be quantitatively labeled under these conditions (see Experimental Procedures).

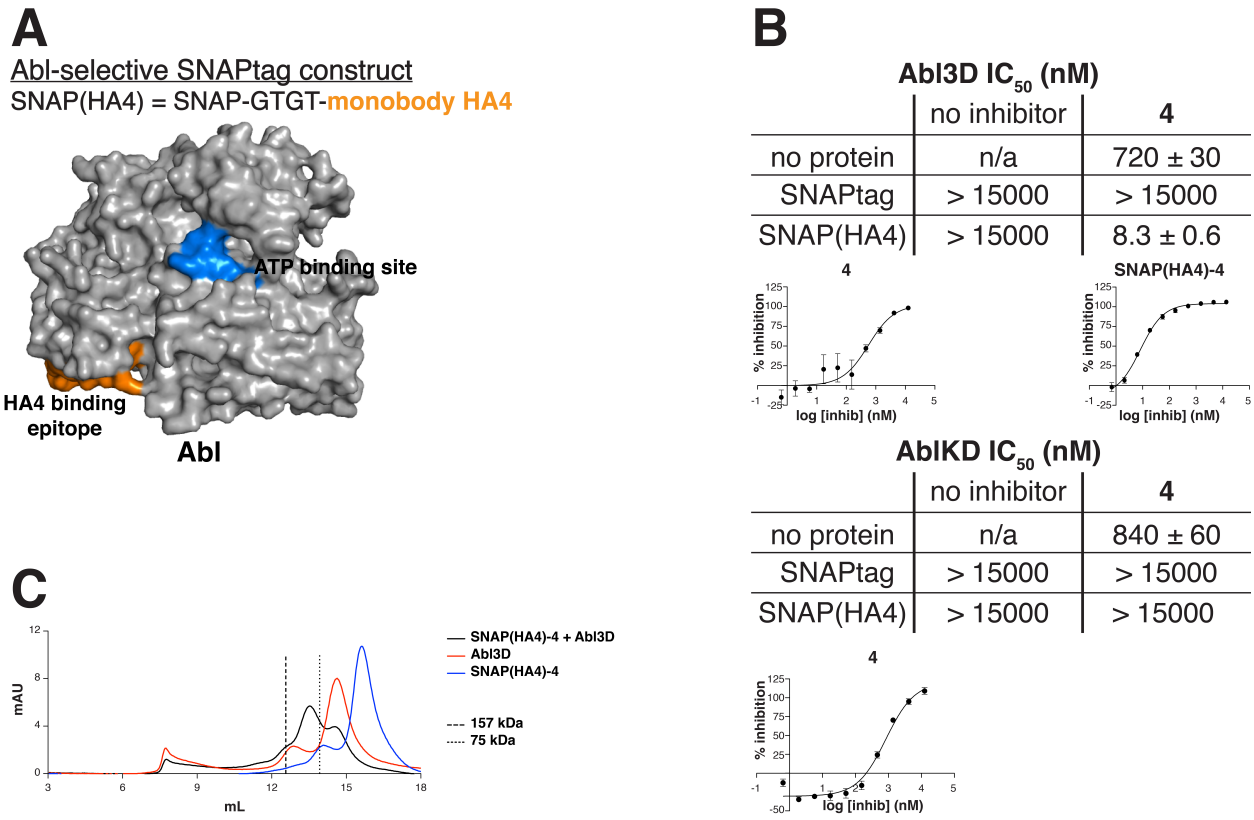

Figure 2-4. A bivalent inhibitor of Abl. (A) (Top panel) SNAPtag-HA4 fusion that was generated for this study. (Bottom panel) The binding sites for the two ligands of the bivalent inhibitor are superimposed on a crystal structure of Abl3D, PDB ID 2FO0. (B) *In vitro* activities of **4**, SNAPtag proteins and assembled SNAPtag-**4** conjugates against two different Abl constructs. Abl3D contains the kinase, SH2 and SH3 domains, while AblKD is the kinase domain alone. Values shown are the average of assays performed in triplicate ± SEM. (C) Size exclusion chromatograms of components are overlayed. Shown are the bivalent inhibitor-Abl3D complex (black), Abl3D (red) and the assembled bivalent inhibitor (blue) with molecular weight standards shown as dashed (157 kDa) and dotted (75 kDa) lines.

We next determined the ability of the bivalent inhibitor SNAP(HA4)-**4** and its constituent monovalent components to block the activity of a construct (Abl3D) that contains Abl's catalytic, SH2 and SH3 domains (Figure 2-4 B). Unconjugated **4** is only a modest inhibitor of Abl3D (IC_{50} = 720 nM). This potency is further diminished by conjugation to SNAPtag (SNAPtag-**4** IC_{50} = >15,000 nM), presumably due to unfavorable steric interactions. However, the assembled bivalent inhibitor (SNAP(HA4)-**4**) exhibits an IC_{50} of 8.3 nM against Abl3D, which is an 87-fold increase in potency relative to unconjugated **4** and a >1,800-fold increase in potency compared to the monovalent SNAPtag-**4**. While the observed increase in affinity is due to the conjugation of the pharmacophore to the HA4 monobody, SNAP(HA4) alone does not demonstrate any activity against Abl3D, even at the highest concentration tested (15,000 nM).

To further confirm that the observed increase in potency of bivalent SNAP(HA4)-**4** for Abl is due to its engagement of Abl's catalytic and SH2 domains, this construct was tested against AblKD, which only contains the catalytic domain of this kinase. While unconjugated **4** demonstrates an almost identical IC_{50} for AblKD and Abl3D, SNAP(HA4)-**4** shows almost no detectable inhibition of AblKD (Figure 2-4 B). Thus, in the absence of a SH2 domain to target, bivalent SNAP(HA4)-**4** behaves similarly to monovalent portions SNAPtag-**4** and SNAP(HA4). These results demonstrate that two separate interactions (**4**'s interaction with Abl's catalytic domain and HA4's interaction with Abl's SH2 domain) are necessary for potent inhibition of Abl.

Our working model for bivalent inhibition is that the SNAPtag-based bivalent inhibitor forms a 1:1 complex (heterodimer) with its target kinase. However, it is formally possible that inhibition could result from the formation of higher order kinase-bivalent

inhibitor complexes (heterotetramer or greater). To address this, equimolar portions of SNAP(HA4)-**4** and Abl3D were combined and equilibrated in buffered solution. The resulting complex was then analyzed using size exclusion chromatography (Figure 2-4 C). Consistent with our design strategy, only the molecular weight of the Abl3D-SNAP(HA4)-**4** heterodimer (theoretical = 88 kDa) was detected.

To further explore the generality of using intracellular antibodies as second site specificity ligands of bivalent inhibitors, we looked towards the mitogen-activated protein kinases (MAPKs), specifically, extracellular signal-regulated kinase (ERK). MAPKs are key components of numerous cellular signaling networks that are activated by the phosphorylation of a threonine and a tyrosine residue on their activation loops by upstream MAPK kinases (MAPKKs) (24). Recently, DARPin-based intracellular antibodies that selectively recognize activation loop-phosphorylated or unphosphorylated ERK2 have been reported (20). For this study, we explored the use of DARPins (pE57 and pE59) that recognize phosphorylated ERK2 because bivalent inhibitors based on these intracellular antibodies have the potential to be selective for the activated form of this MAPK. With this in mind, SNAPtag fusions (SNAP(pE57) and SNAP(pE59)) that contain pE57 or pE59 displayed from SNAPtag's C-terminus through an eight amino acid linker were generated (Figure 2-5 A). Monovalent and bivalent inhibitor complexes containing SNAP(pE57) and SNAP(pE59) were assembled and purified as described above. Furthermore, mass spectrometry was used to confirm that the labeling of these constructs was quantitative (see Experimental Procedures).

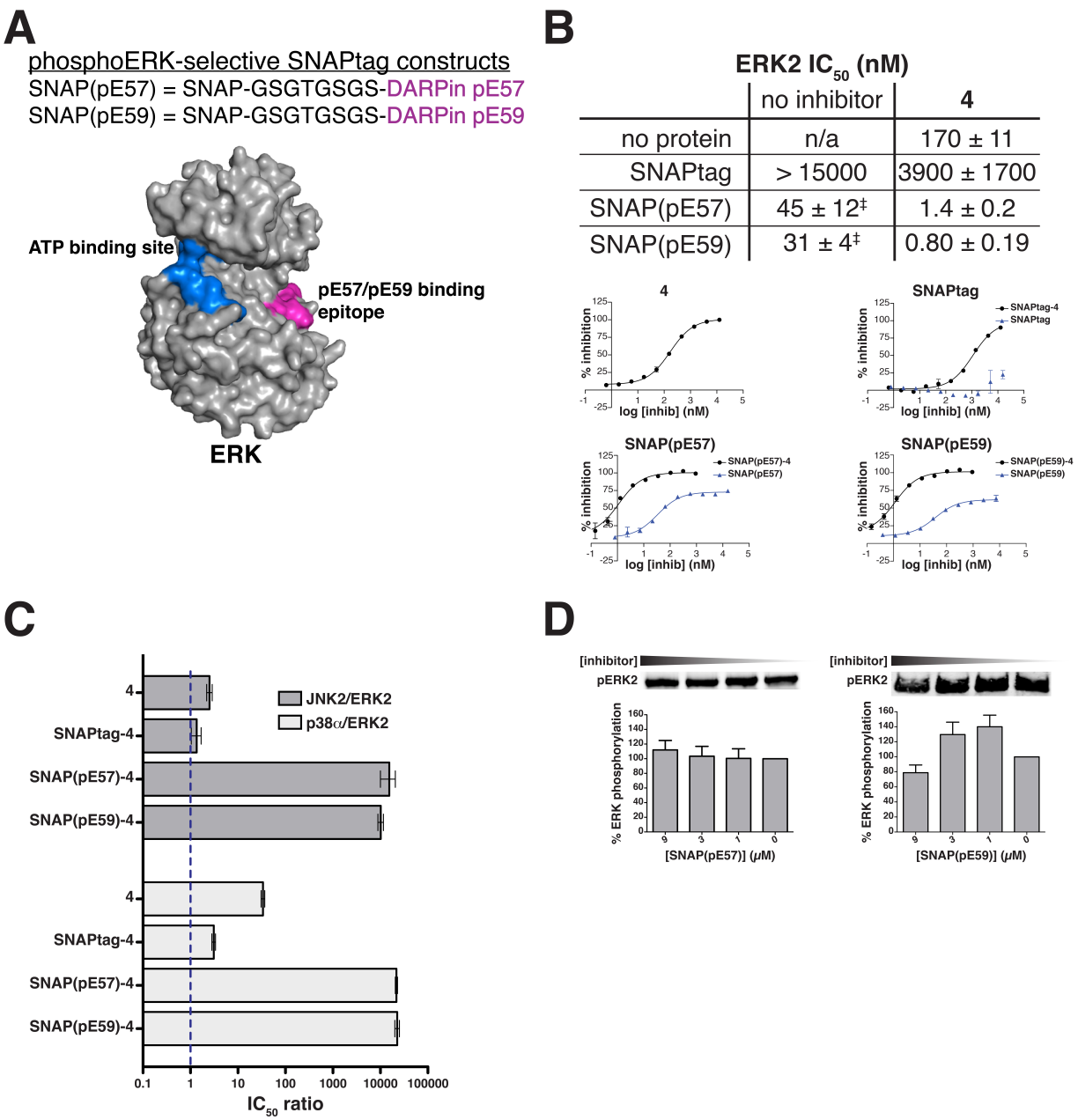

Figure 2-5. Phosphorylation state-dependent bivalent inhibitors of ERK2. (A) (Top panel) SNAPtag-DARPin fusions that were generated for this study. (Bottom panel) The binding sites for the ligands of the bivalent inhibitors are superimposed on a crystal structure of ERK2, PDB ID 3ZUV. (B) *In vitro* activities of **4**, SNAPtag proteins and assembled SNAPtag-**4** conjugates against doubly phosphorylated ERK2. Values shown are the average of assays performed in triplicate ± SEM. ‡ indicates that only partial inhibition of ERK2 was observed. (C) *In vitro* activity of **4** and assembled SNAPtag-**4** constructs against activated ERK2, JNK2 and p38α. IC_{50} values are shown as ratios and plotted on a log-based scale. A blue dashed line denotes an IC_{50} ratio of one, indicating equipotent inhibition of ERK2 and either JNK2 or p38α. (D) Levels of activated ERK2 in the presence of the constructs SNAP(pE57) and SNAP(pE59). ERK2 treated with MEK2 in the presence of various concentrations of the constructs was analyzed by immunoblot for doubly phosphorylated ERK2. Values shown are the average of assays performed in quadruplicate ± SEM.

The abilities of SNAP(pE57)-**4** and SNAP(pE59)-**4**, and their constituent monovalent components, to block ERK2 function were assessed with an activity assay using an activation loop-phosphorylated form of this kinase (Figure 2-5 B). Similar to Abl, unconjugated **4** is a moderately potent inhibitor (IC_{50} = 170 nM) of ERK2. Conjugation of the pharmacophore to SNAPtag also leads to reduced inhibition of ERK2, with SNAPtag-**4** demonstrating ~20-fold lower activity (IC_{50} = 3,900 nM). Gratifyingly, both bivalent inhibitors (SNAP(pE57)-**4** and SNAP(pE59)-**4**) exhibited significantly enhanced potency against ERK2. SNAP(pE57)-**4** showed an IC_{50} value of 1.4 nM for ERK2 activity, while SNAP(pE59)-**4** was slightly more potent (IC_{50} value of 0.8 nM). Conjugation of **4** to SNAP(pE57) or SNAP(pE59) leads to a 120-fold and 200-fold increase in potency against ERK2 relative to the unconjugated pharmacophore, respectively.

While it is important that a kinase inhibitor is potent against its target, it is also essential that these reagents are highly selective. As our ERK2-directed bivalent inhibitors rely on the use of intracellular antibodies that recognize phosphorylated activation loops in order to obtain selectivity, we wished to assess their effects amongst kinases that possess a similar phospho-motif. The closely-related MAPKs c-Jun N-terminal kinase 2 (JNK2) and p38α contain the same diphosphorylation motif (TXY) as ERK2 and are likely candidates for off-target inhibition (25). Therefore, we tested **4**, SNAPtag-**4**, SNAP(pE57)-**4** and SNAP(pE59)-**4** against phosphorylated JNK2 and p38α (Figure 2-5 C). The unconjugated pharmacophore is essentially an equipotent inhibitor of ERK2 and JNK2, whether as a free BG derivative or conjugated to SNAPtag. This is in striking contrast to conjugation of **4** to either SNAP(pE57) or SNAP(pE59) which

increases selectivity ~10,000-fold for ERK2 over JNK2. A similar trend is observed for p38α, despite a slight preference of **4** for ERK2 over p38α. Conjugation to SNAPtag slightly compresses the selectivity ratio, but SNAP(pE57)-**4** and SNAP(pE59)-**4** are >10,000-fold selective for ERK2 over p38α. Thus, phospho-specific intracellular antibodies are able to confer exquisite selectivity in the context of bivalent inhibitors, even amongst closely related kinase family members.

In an ideal situation, the genetically-encoded monovalent portion of a bivalent inhibitor would not perturb the function of its target until conjugated to an ATP-competitive inhibitor. We have found that monovalent SNAP(HA4) has a minimal effect on the catalytic activity of Abl (Figure 2-4 B) but were unsure of how the binding of SNAP(pE57) and SNAP(pE59) to the activation loop of ERK2 would affect its catalytic activity. Therefore, monovalent SNAP(pE57) and SNAP(pE59) were tested for their abilities to block ERK2's catalytic function in an *in vitro* activity assay (Figure 2-5 B). Both SNAPtag-intracellular antibody fusions affect phosphorylated ERK2's catalytic activity but the level of inhibition plateaus at ~60-75%. Conjugation of **4** to either SNAP(pE57) and SNAP(pE59) leads to complete suppression of ERK2 activity and increases potency by 30-40-fold. At this time, it is unclear how the partial inhibition observed *in vitro* would translate to the cellular activity of SNAP(pE57) and SNAP(pE59). As ERK2 exists in a predominantly unphosphorylated state in most cells that have not been stimulated with growth factors, we were curious whether SNAP(pE57) and SNAP(pE59) would affect the non-activated form of this kinase. Consistent with the reported selectivity of pE57 and pE59 for activation loop-phosphorylated ERK2 over the non-phosphorylated form, neither SNAP(pE57) nor

SNAP(pE59) interfere with the activation of ERK by the MAPKK MEK2 *in vitro* (Figure 2-5 D). Thus, both SNAPtag fusions would be expected to minimally affect the function of the predominant form of ERK2 in cells when not conjugated to **4**.

Detailed biochemical experiments have enabled the characterization of bivalent inhibitors of Abl and phosphorylated ERK2. As anticipated, each bivalent inhibitor exhibits a dramatic increase in potency for their respective targets. By profiling a small panel of ERK2-related family members, it appears that tethering a non-specific ATP-competitive inhibitor to an intracellular antibody can confer a marked increase in selectivity. However, the question remains as to how such selectivity profiles would hold up across the expressed kinome. To address this, the relative potencies and selectivities of the bivalent inhibitors SNAP(HA4)-**4**, SNAP(pE57)-**4** and SNAP(pE59)-**4**, and a monovalent SNAPtag-**4** control, were assessed using the quantitative competition-based chemical proteomics method shown in Figure 2-2. Dose-response competition experiments were performed with each assembled inhibitor in K562 lysates, from which RB_{50} values were calculated (Figure 2-6).

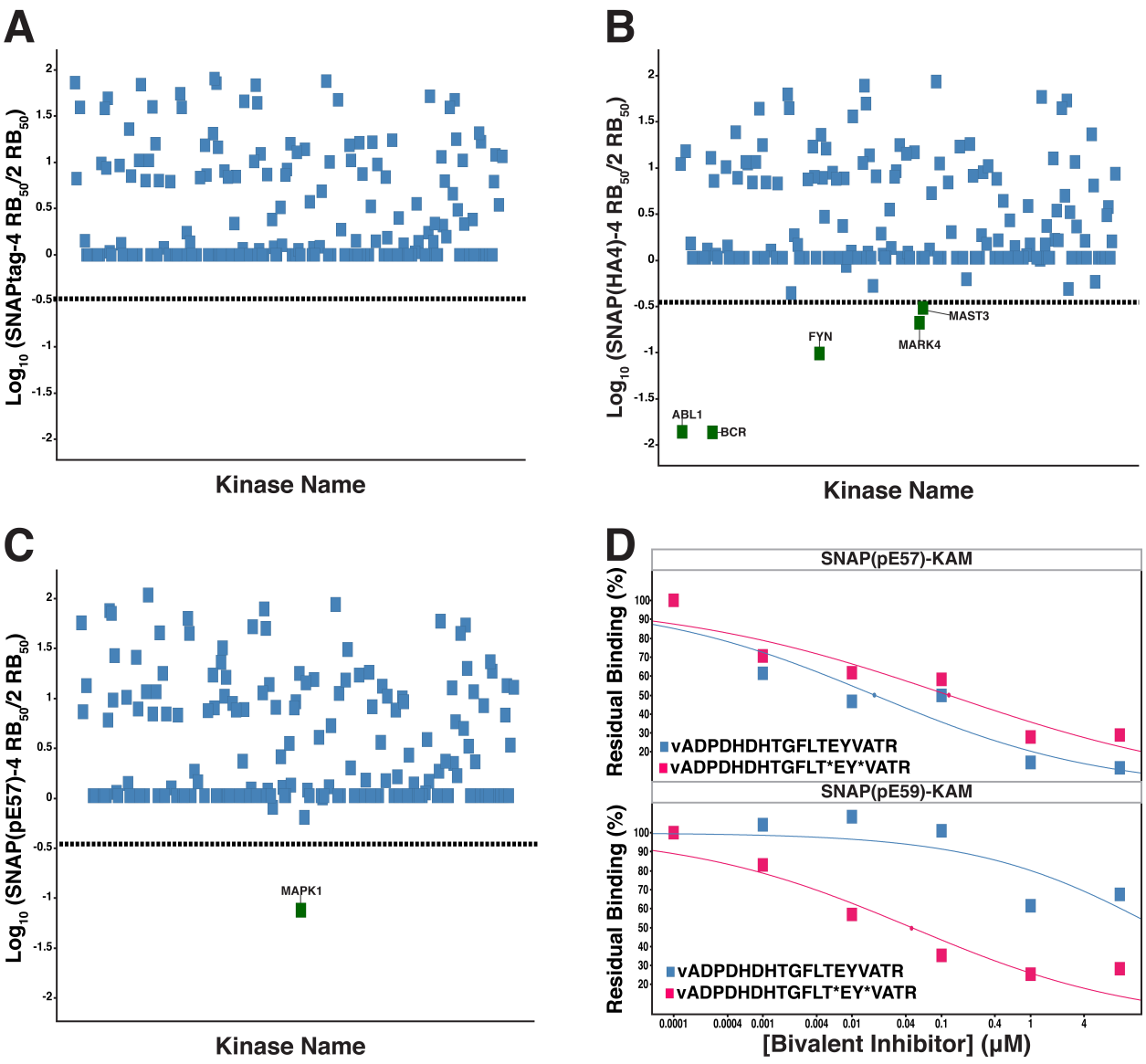

Figure 2-6. Quantitative competition-based chemical proteomics. In each case, the dotted line represents ≥3-fold increase in potency for the assembled bivalent inhibitor. (A) Relative RB_{50} values (average of 2 independent experiments) of kinases for SNAPtag-**4** compared to **2**. (B) Relative RB_{50} values (average of 2 independent experiments) of kinases for SNAP(HA4)-**4** compared to **2**. (C) Relative RB_{50} values (average of 2 independent experiments) of kinases for SNAP(pE57)-**4** compared to **2**. MAPK1 is ERK2. (D) Dose-response curves of the ERK activation loop peptide when treated with (top panel) SNAP(pE57)-**4** or (bottom panel) SNAP(pE59)-**4**. Curves are shown in pink for the phosphorylated peptide and blue for the nonphosphorylated peptide.

Comparison of the relative RB_{50} values for acetylated molecule **2** versus SNAPtag-**4** reveals that conjugation of this pharmacophore to SNAPtag is generally detrimental to potency, consistent with the *in vitro* activity assay results for Abl (Figure 2-4 B) and Erk2 (Figure 2-5 B). For kinases in which an RB_{50} could be calculated, an

average of a 14-fold loss in potency was observed for SNAPtag-**4** relative to **2** alone (Figure 2-6 A). Notably, no kinases showed enhanced affinity for SNAPtag-**4** relative to **2**.

Similar to SNAPtag-**4**, SNAP(HA4)-**4** exhibited a markedly reduced potency for the majority of protein kinases in which an RB_{50} value could be calculated. However, unlike SNAPtag-**4**, SNAP(HA4)-**4** exhibited increased potency for four protein kinases (Figure 2-6 B). Gratifyingly, BCR-Abl exhibited the strongest level of competition of any of the protein kinases identified with an RB_{50} of 0.021 μM, which is a 71-fold increase in potency relative to **2** alone (RB_{50} = 1.5 μM) and a > 470-fold increase in potency relative to SNAPtag-**4** (RB_{50} > 10 μM). Interestingly, SYK, which contains a SH2 domain that is recognized by HA4, demonstrated only a 2-fold increase in overall potency relative to **2**; Blk, which also contains a SH2 domain recognized by HA4, was not identified in the proteomics experiments. Other protein kinases showing increased potency for SNAP(HA4)-**4** relative to **2** include Fyn (RB_{50} = 0.94 μM; 10-fold increase), MAST3 (RB_{50} = 0.93 μM; 3.5-fold increase) and MARK4 (RB_{50} = 0.54 μM; 5.0-fold increase). It is worth noting that in the original characterization of the HA4 monobody, this reagent was shown to enrich Fyn from HEK293T and K562 lysates. Based on the lack of observed binding of HA4 to the SH2 domain of Fyn, the authors concluded that Fyn enrichment was likely due to its interaction with BCR-Abl rather than direct binding to the monobody itself (14). It is quite likely that the apparent increased affinity for SNAP(HA4)-**4** displayed by Fyn could be attributed to forming a protein complex with BCR-Abl. It is also tempting to speculate that the lower RB_{50}s observed for MAST3 and

MARK4 are due to their interaction with BCR-Abl, as neither kinase possesses a SH2 domain.

Profiling of SNAP(pE57)-**4** and SNAP(pE59)-**4** proved slightly more problematic. At first glance, ERK2 is the only protein kinase that exhibited increased affinity for SNAP(pE57)-**4** over **2** (RB_{50} = 0.74 μM; 13-fold increase) (Figure 2-6 C); similar results were obtained for SNAP(pE59)-**4** (data not shown). While these results highlight the relative specificity for ERK2 over other protein kinases, the context specificity (phosphorylated versus unphosphorylated ERK2) was more difficult to evaluate. Efforts to identify activated ERK2 in the K562 lysate were unsuccessful; both mass spectrometry- and western blot-based methods failed to detect the presence of phosphorylated ERK2 in the K562 lysates used (data not shown). To circumvent this issue, competition-based quantitative chemical proteomics experiments were performed with SNAP(pE57)-**4** and SNAP(pE59)-**4** in K562 lysates spiked with exogenous activation loop-phosphorylated ERK2 (phospho-ERK2). The relative affinities of both bivalent inhibitors for unphosphorylated and phosphorylated ERK2 were monitored by quantification of an activation loop tryptic peptide that contains the TXY motif. Upon addition of phospho-ERK2, SNAP(pE59)-**4** shows potent and robust competition of phospho-ERK2 (RB_{50} = 0.05 μM) and little affinity for unphosphorylated ERK2 (RB_{50} = >10 μM) resulting in >200-fold selectivity (Figure 2-6 D). Curiously, SNAP(pE57)-**4** shows little preference (~5-fold) for either activated or inactivated ERK2. These results highlight that bivalent inhibition has the potential to extend beyond just the inhibition of a single kinase, but allows selective inhibition of specific kinase activation states.

It is important to emphasize that while the increased affinities are impressive, the bivalent inhibitors in this study are not yet to the point of single kinase inhibition. The specificity component alone cannot overcome some of the challenges imposed by utilizing a kinase inhibitor with such inherent broad specificity. Quantitative chemical proteomics profiling of **2** demonstrates that 46 kinases exhibit RB_{50} values ≤1 μM. Profiling of the BCR-Abl specific bivalent inhibitor shows that this bivalent inhibitor exhibits the greatest affinity for BCR-Abl (RB_{50} = 0.021 μM) with an additional 11 kinases with RB_{50} values ≤1 μM; the BCR-Abl specific bivalent inhibitor has 4-fold greater affinity for BCR-Abl over the next potently bound kinase. A similar observation can be made regarding the phospho-ERK2 specific bivalent inhibitor, SNAP(pE59)-**4**, if one extrapolates the enhanced potency observed in the presence of phospho-ERK2 with the selectivity observed in whole cell lysates where no detectable level of phospho-ERK2 is present. The phospho-ERK2 specific bivalent inhibitor exhibits the greatest affinity for phospho-ERK2 (RB_{50} = 0.05 μM) with only 4 additional kinases with RB_{50} values ≤1 μM; the phospho-ERK2 specific bivalent inhibitor has 8-fold greater affinity over the next potently bound kinase. If one wanted to achieve the goal of single kinase inhibition, then it is likely that a more selective compound other than **2** would be needed.

The competition experiments verified that intracellular antibody-containing bivalent inhibitors are highly selective for their target kinases. For this method to be truly useful, it is important that bivalent inhibitors can be readily assembled inside cells and capable of inhibiting the activities of their kinase targets. Prior to performing cellular experiments, we verified that molecule **5** is cell permeable and able to label SNAPtag in K562 cells. To test these parameters, K562 cells transiently transfected with

SNAP(HA4) were subjected to an intracellular blocking assay. In this assay, cells were first incubated with varying concentrations (2.5 μM, 5 μM and 10 μM) of **5**. After one hour, cells were treated with the cell permeable SNAPtag-labeling reagent, TMR-star. Under this regime, any SNAPtag that is not labeled by **5** will be conjugated to rhodamine. The extent of SNAPtag labeling by **5** can then be determined by lysing cells, subjecting the lysate to SDS-PAGE and quantifying the loss in fluorescent signal (Figure 2-7 A). The marked dose-dependent decrease in rhodamine-SNAPtag signal at all three concentrations of **5** tested shows that this molecule is cell permeable and able to label its target (Figure 2-7 B).

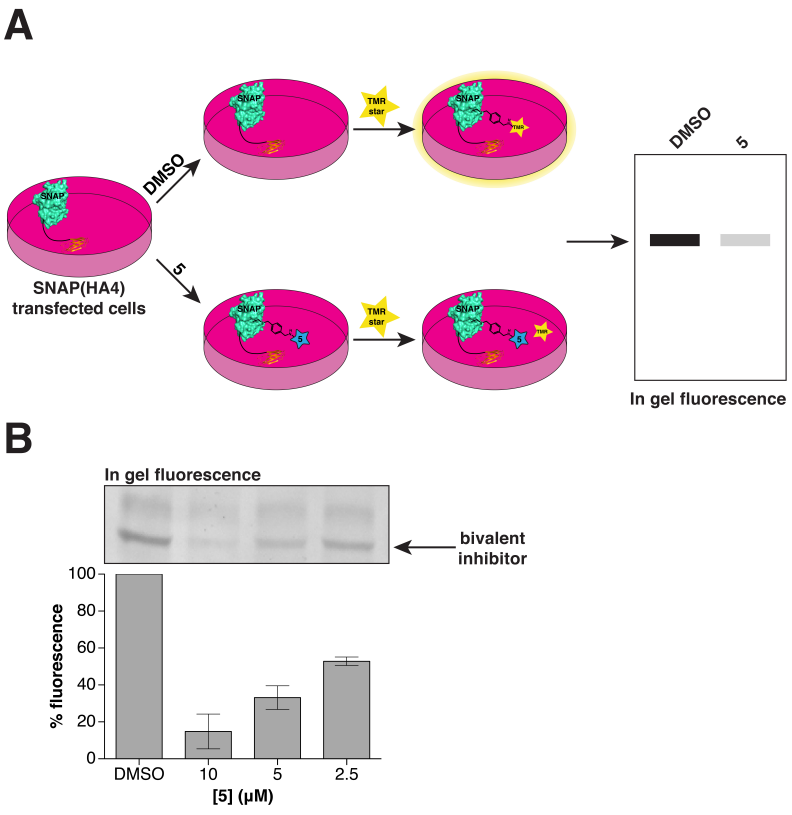

Figure 2-7. Cell permeability of **5** in K562 cells. (A) Schematic of the cell permeability assay used to study **5**. K562 cells transfected with the construct SNAP(HA4) are first pre-treated with DMSO or varying concentrations of **5**. Cells are then incubated with the cell permeable fluorophore TMR-star. Cells are lysed and proteins analyzed by in-gel fluorescence after SDS-PAGE. (B) Fluorophore labeling of SNAPtag is blocked by conjugation to **5**. % fluorescence is relative to the DMSO control. Values shown are averages of duplicate treatments ± SEM.

Next, we determined whether our Abl-selective bivalent inhibitor (SNAP(HA4)-**5**) is capable of inhibiting BCR-Abl activity in cells. In K562 cells, the protein STAT5 is a direct substrate of the constitutively active BCR-Abl fusion and provides a convenient read-out for monitoring BCR-Abl activity. By measuring phospho-STAT5 levels in the presence of SNAP(HA4)-**5** and its individual monovalent components, the efficacy of bivalent intracellular inhibition was determined. K562 cells were transfected with SNAP(HA4) and treated with varying concentrations of **5**. Flow cytometry was used to sort transfected from non-transfected cells, and phospho-STAT5 levels were determined with a phospho-specific antibody. Gratifyingly, cells expressing SNAP(HA4) demonstrated a dose-dependent decrease in phospho-STAT5 in the presence of **5** (Figure 2-8 A). Consistent with phospho-STAT5 inhibition occurring through bivalent inhibition, subjecting cells to the same concentrations of **5** in the absence of SNAP(HA4) does not show a dose-dependent decrease in phospho-STAT5 levels (Figure 2-8 B and C). Thus, **5** alone is not capable of inhibiting BCR-Abl. Cells expressing monovalent SNAP(HA4) do show some level of BCR-Abl inhibition (Figure 2-8 A), but the magnitude of phospho-STAT5 suppression is significantly enhanced in the presence of **5**. Furthermore, **5** must be conjugated to SNAP(HA4) in order for robust phospho-STAT5 inhibition to be observed, as incubating 5 μM **5** with a catalytically dead SNAPtag-monobody fusion construct (*cd*SNAP(HA4)) does not lead to reduced phospho-STAT5 levels beyond *cd*SNAP(HA4) alone (Figure 2-8 D). Therefore, assembly of both components into a bivalent inhibitor is necessary in order to obtain robust BCR-Abl inhibition in K562 cells.

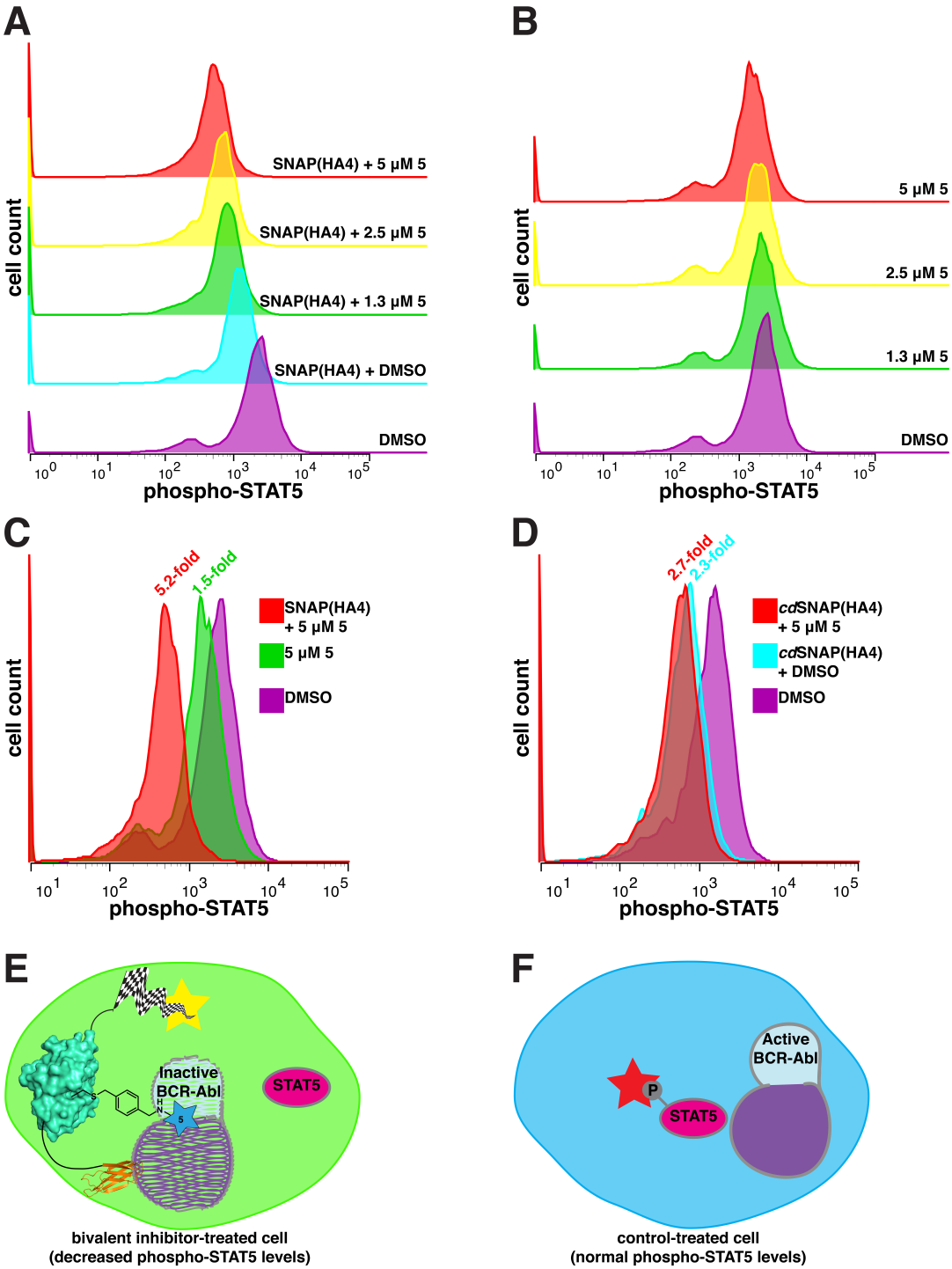

Figure 2-8. BCR-Abl activity in K562 cells as assessed by phosphorylated STAT5 levels after 1 hour of treatment with varying concentrations of **5**. (A) Flag-SNAP(HA4)-transfected cells were treated with varying concentrations of **5** and sorted using a flag-FITC antibody and compared to vehicle-treated cells. (B) Vehicle-transfected cells were treated with varying concentrations of **5** and compared to vehicle-treated cells. (C) An overlay of curves from (A) and (B). Fold-change values are with respect to vehicle-treated cells. (D) An overlay of curves for cells transfected with the catalytically dead mutant, *cd*flag-SNAP(HA4) or vehicle. Transfected cells were treated with DMSO or 5 μM **5**. Fold-change values are with respect to vehicle-treated cells. (E and F) Schematics of BCR-Abl activity assessment in K562 cells. (E) Bivalent inhibitor-treated cells are compared to (F) control-treated cells.

III. Conclusion

The data presented here take several critical steps toward applying modular bivalent inhibitor systems; moving from a biochemical concept to suitable strategy for interrogating biology. Starting from a single pan ATP-competitive inhibitor, selective bivalent inhibitors for either BCR-Abl or phospho-ERK2 could be obtained with dramatically increased potencies for their target kinases (87-fold and 210-fold, respectively) and overall enhanced selectivity, as assessed by kinase activity assays. For both bivalent inhibitors, the enhanced selectivities and affinities observed *in vitro* were rigorously tested in complex cell lysates. Applying competition-based quantitative chemical proteomics, both the BCR-Abl and phospho-ERK2 bivalent inhibitors exhibited increased affinities and enhanced selectivity profiles. Equally important is that in each case, the most potently bound and competed protein was the intended target.

One of the key steps in the evaluation of the SNAPtag-based bivalent inhibitor strategy was the discovery and characterization of a general kinase inhibitor scaffold, **2**. The enabling feature of **2** is its very broad specificity, which allows it to serve as a potential starting point in the development of next-generation bivalent inhibitors. We envision that **4** and **5** could be thought of as off-the-shelf building blocks in the continued development of SNAPtag-based bivalent inhibitors. The ability to access a single compound that can be efficiently transformed into a selective inhibitor for kinases irrespective of their degree of homology enables a significantly simplified strategy. For example, BCR-Abl and ERK2 differ significantly in their respective ATP binding pockets, and few compounds are able to engage both binding pockets (26). Because of the versatility of **2**, we were able to use this single reagent to generate potent and selective

bivalent inhibitors for either BCR-Abl or ERK2. Importantly, because of the ability of **2** to access such diverse kinase active sites, the utility of **2** is not limited to just these examples.

Additionally, the broad specificity of **2** can be leveraged to create a general selectivity-profiling tool for hundreds of endogenously expressed kinases. While many different scaffolds already exist for profiling the kinome via chemical proteomics, the ability of a single compound covering a large swath of the kinome offers some technical advantages. For example, generally reduced synthetic burden/cost and the inherent simplicity of making one affinity matrix versus making multiple affinity matrices and combining the various matrices into a cocktail for profiling. Furthermore, due to the conservation of general pharmacological characteristics of kinase inhibition across organisms, a **2**-based affinity matrix can be expected to be applicable across the kinome of any organism under investigation (27).

Perhaps the most critical step towards the application of SNAPtag-based bivalent inhibitors is the demonstration that these reagents can be used to modulate cellular signaling pathways. Treating K562 cells expressing SNAP(HA4) with **5** led to a significant and dose-dependent decrease in phospho-STAT5 levels. Collectively these results demonstrate that SNAPtag-based bivalent inhibitors can self-assemble in cells and engage the intended target protein to modulate signaling pathways.

One of the distinguishing features of the bivalent inhibitor approach presented here, as compared to more traditional bivalent inhibitor approaches, which rely solely on small molecules, is the ability to achieve activation state specific inhibition. The ability to select and evolve a specificity component to recognize subtle molecular or

conformational differences in the target, as exemplified by the activation state-dependent phosphorylation of ERK, has tremendous implications for cellular assays, where within an entire population of a given protein numerous subpopulations may exist that differ in PTMs, activation and/or conformational state. With the proper selection strategy it should be possible to survey the molecular function of a precise subset of a protein population using the bivalent inhibitor strategy described here.

Another point of contrast to more traditional bivalent inhibitor strategies is that the SNAPtag-based bivalent strategy potentially overcomes one of the key bottlenecks of purely small molecule-based approaches in the development of chemical tools, namely intracellular delivery. Penetrating through the membrane is often difficult for small molecule-based bivalent inhibitors because of their inevitably large size. The advantage of SNAPtag-based bivalent inhibitors is that one component is expressed in the cell line of interest, thus reducing the size of the small molecule portion of the bivalent inhibitor and hence increasing membrane permeability. It should be noted that expressing the specificity component intracellularly means that the levels of SNAPtag protein can influence the extent of observable inhibition, and expression levels might need to be further optimized for inhibiting e.g. highly expressed proteins. In the described proof-of-concept studies, the BCR-Abl bivalent inhibitor is only modestly potent when expressed and assembled in cells, despite being a potent inhibitor (8 nM) *in vitro*. This is in part due to the incomplete assembly of the bivalent inhibitor (Figure 2-7 B) and in part due to high endogenous levels of BCR-Abl expression in K562 cells, which is expressed at 100 times greater levels than in cellular settings where BCR-Abl is not the driver. However,

despite this additional layer of complexity, this work clearly demonstrates the potential of SNAPtag-based bivalent inhibitors as powerful tools for cellular applications.

While the focus of this manuscript has been kinase-centric, the approach described has applications beyond just kinases. As mentioned previously, the identification of a suitable small molecule with pan inhibitory properties for a large class of targets is a distinct advantage. Through the efforts aimed at profiling large swaths of protein families by chemoproteomic and other approaches, high quality probes have been developed for several target classes including PARPs, HDACs, and Bromodomain containing proteins (28-30). Additionally, the increasing number of available nonimmunoglobulin protein scaffolds including DARPins and monobodies as well as continuous advances in high-throughput selection will greatly facilitate the tailoring of specific and selective bivalent inhibitors to dissect complex biological phenotypes.

The resurgence of phenotypic-based screening has brought along with it a renewed interest in targeted and *de novo* target deconvolution technologies. However, the stark reality is that it is not uncommon for such experiments to identify multiple proteins capable of binding a compound of interest; any one of which could be the efficacy target (assuming that indeed only one protein is responsible for the observed phenotype). This can be in part rationalized by the fact that while compounds coming from phenotypic-based screens can be optimized for potency in a particular cellular assay, it is not until a comprehensive binding profile is obtained that the full spectrum of potential on- and off-targets can be appreciated. This is particularly true for ATP-competitive kinase inhibitors due to high similarity of the ATP-binding pocket across the kinome. In some instances a firm understanding of the biological pathway can guide

and (de)prioritize proteins for follow-up efforts. However, this can be a misleading approach, especially if the pharmacology of the compound is simply ahead of the current biological understanding. In these instances it would be ideal to have a modular method for enhancing the potency and selectivity of a compound for each of the possible target hypotheses, allowing one to determine to what extent, if any, each protein contributes to the overall phenotype. To this end, the design and application of bivalent inhibitors is an attractive approach for selectively enhancing the potency and selectivity for a desired protein target. We believe that the advances presented in this work will help enable the field to develop increasingly potent and selective tools for tackling the key question of target validation in drug discovery.

IV. Experimental Procedures

A. Chemical synthesis

GENERAL METHODS. Unless otherwise stated, all reagents were obtained from commercial suppliers and used without further purification. Analytical LC/ESI-MS data were recorded using a Waters LCT Premier mass spectrometer with dual electrospray ionization source and Agilent 1100 liquid chromatograph. HPLC separation was performed using 1.0 mL/min flow rate with a gradient from 5% to 95% MeCN over 10 min, 0.1% formic acid used as the modifier additive in the aqueous phase. 3.0 x 100 mm 3 μm C_{18} column. ^{1}H-NMR and ^{13}C-NMR spectra were recorded on Bruker Advance instruments. Data are reported as follows: chemical shift in ppm, multiplicity (s = singlet, br s = broad singlet, d = doublet, t = triplet, q = quartet, m = multiplet, dd = doublet of doublets), coupling constants *J* in Hz, and signals were referenced against solvent peaks. Preparative reverse-phase HPLC was performed on a Waters system

equipped with Sunfire 5 µm 30 x 50 mm column with a gradient using 0.1% TFA in acetonitrile and water or an X-bridge 5 µm 30 x 50 mm column, 5 mM NH_4OH in acetonitrile and water with a flow rate of 75 mL/min with 1.5 mL for the injection volume. UPLC-MS measurements were conducted on a Waters Acquity UPLC-UV-ELSDMS/Waters SQD mass spectrometer system using a BEH column 1.7 µm 2.1 x 50 mm at 50 °C with a gradient comprised of the following eluents: [Eluent A: water + 0.05% formic acid + 3.75 mM ammonium acetate], [Eluent B: acetonitrile + 0.04% formic acid]; 2-98% Eluent A ➔ B in 4.4 min, 1 mL/min flow rate. LC-UV/HRMS was measured on an Waters Acquity G2 Xevo QTof, using a CSH column 1.7 µm 2.1 x 50 mm at 50 °C, with a gradient comprised of the following eluents: [Eluent A = water + 0.1% formic acid + 3.75 mM ammonium acetate], [Eluent B: acetonitrile + 0.08% Formic Acid]. A gradient of Eluent A ➔ B starting from 1-30% in 3.2 min and then to 98% in another 1.95 min with a 1.0 mL/min flow rate was used.

Scheme 1.

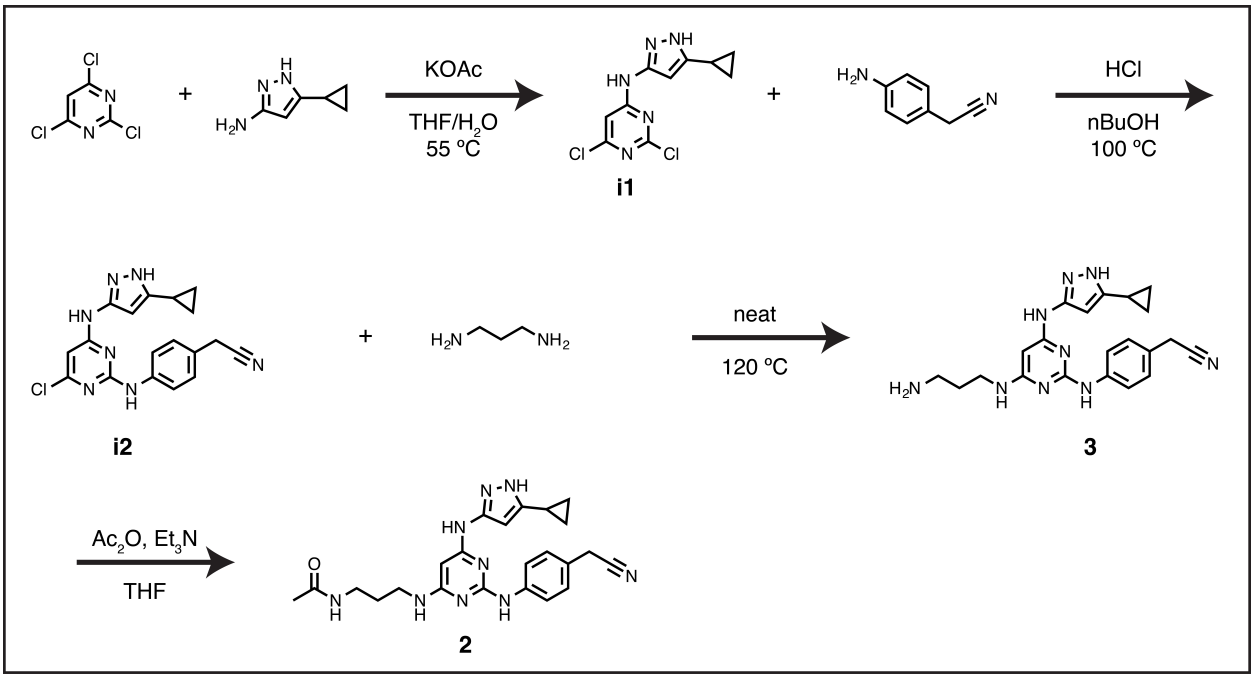

Synthesis of intermediate i1: To a stirred solution of 2,4,6-trichloropyrimidine (1.921 g, 10.47 mmol) and 5-cyclopropyl-1H-pyrazol-3-amine (1.29 g, 10.47 mmol) in THF/H_2O (100 mL) was added potassium acetate (30.8 g, 314 mmol). The reaction was stirred at 55 °C overnight then cooled to RT. The organics were separated off and stripped down *in vacuo*. The crude product was purified by silica column (10% MeOH:$CHCl_3$, isocratic elution) giving the desired product **i1** as on off-white solid (1.5 g, 53% yield).

^{1}H-NMR (400 MHz, CHLOROFORM-d) ppm 0.66 - 0.88 (m, 2 H) 1.05 (dd, J = 8.53, 2.01 Hz, 2 H) 1.78 - 1.98 (m, 1 H) 5.88 (br s, 1 H) 7.28 (s,1 H) 8.48 (br s, 1 H).

^{13}C-NMR (101 MHz, CHLOROFORM-d) ppm 6.88 (s, 1 C) 7.89 (s, 1 C) 93.69 (s, 1 C) 102.81 (s, 1 C) 146.71 (s, 1 C) 148.02 (s, 1 C) 159.56 (s, 1 C) 161.19 (s, 1 C) 161.56 (s, 1 C).

HRMS: *m/z*: calculated for $C_{10}H_9Cl_2N_5$ is 270.0313, measured mass was 270.0310 for the [M+H]+ ion.

Synthesis of intermediate i2: To solution of 2,6-dichloro pyrimidine **i1** (250 mg, 0.93 mmol) and 4-aminophenylacetonitrile (122 mg, 0.93 mmol) in n-Butanol (9 mL) was added concentrated HCl (0.1 mL) and the reaction was heated at 100 °C overnight resulting in the formation of an off-white precipitate. The reaction was cooled to room temperature and filtered. The resulting precipitate was washed with cold n-Butanol and dried under vacuum. The crude product was dissolved in DMSO (1 mL) and purified by reverse phase preparative HPLC (gradient 10-90% MeCN:H_2O; 0.1% TFA) giving desired product **i2** as a white solid (158 mg, 57% yield).

^{1}H-NMR (400 MHz, METHANOL-d_4) ppm 1.13 (d, J = 6.06 Hz, 2 H) 2.00 (d, J = 9.09 Hz, 1 H) 3.85 (s, 2 H) 5.94 (s, 1 H) 6.32 (s, 1 H) 7.30 (m, J = 8.08 Hz, 2 H) 7.66 (m, J = 8.59 Hz, 2 H).

^{13}C-NMR (101 MHz, METHANOL-d_4) ppm 8.01 (s, 1 C) 9.26 (s, 1 C) 22.94 (s, 1 C) 91.99 (s, 1 C) 97.51 (s, 1 C) 119.83 (s, 1 C) 121.10 (s, 1 C) 126.21 (s, 1 C) 129.55 (s, 1 C) 140.51 (s, 1 C) 146.26 (s, 1 C) 152.77 (s, 1 C) 160.24 (s, 1 C) 161.17 (s, 1 C) 161.94 (s, 1 C).

HRMS: *m/z*: calculated for $C_{18}H_{16}ClN_7$ is 366.1234, measured mass was 366.1232 for the [M+H]+ ion.

Synthesis of compound 3: To round bottom flask containing chloropyrimidine **i2** (100 mg, 0.3 mmol) was added 1,3-propanediamine (1.9 mL, 22.55 mmol) and the reaction was heated neat at 120 °C overnight. The reaction was cooled to room temperature, partitioned between ethyl acetate, saturated ammonium chloride and extracted. The organics were washed with brine, dried over Na_2SO_4 and stripped down *in vacuo*. The crude product was dissolved in DMSO (1 mL) and purified by reverse phase preparative HPLC (gradient 0-70% MeCN:H_2O; 0.1% TFA) giving desired product **3** as a clear oil (74 mg, 47% yield).

^{1}H-NMR (400 MHz, METHANOL-d_4) ppm 0.52 - 0.84 (m, 2 H) 1.02 (q, J = 6.53 Hz, 1 H) 1.73 - 2.14 (m, 3 H) 3.00 (t, J = 7.53 Hz, 2 H) 3.49 (br s, 2 H) 5.63 (br s, 1 H) 7.40 (d, J = 8.53 Hz, 2 H) 7.62 (d, J = 8.03 Hz, 2 H).

^{13}C-NMR (101 MHz, METHANOL-d_4) ppm 7.49 (s, 1 C) 8.67 (s, 1 C) 23.06 (s, 1 C) 28.48 (s, 1 C) 38.45 (s, 1 C) 39.35 (s, 1 C) 76.78 (br s, 1 C) 91.29 (s, 1 C) 119.66 (s, 1

C) 123.49 (s, 1 C) 128.82 (s, 1 C) 129.92 (s, 1 C) 138.26 (s, 1 C) 149.42 (s, 1 C) 149.93 (s, 1 C) 151.91 (s, 1 C).

HRMS*: m*/z: calculated for $C_{21}H_{25}ClN_9$ is 404.2311, measured mass was 404.2303 for the [M+H]+ ion**.**

Synthesis of compound 2: To a solution of amine **3** (25 mg, 0.063 mmol) in THF was added a 1 M solution of acetic anhydride (68 µL, 0.068 mmol) in THF. After 1 hour the reaction was partitioned between ethyl acetate, saturated ammonium chloride and extracted. The organics were washed with brine, dried over Na_2SO_4 and stripped down *in vacuo*. The crude product was purified by reverse phase HPLC (gradient 15-45% MeCN:H_2O; 5 mM NH_4OH) giving compound **2** as a white solid (15.3 mg, 55% yield).

^{1}H-NMR (400 MHz, METHANOL-d_4) ppm 0.69 (br s, 2 H) 0.92 (br s, 2 H) 1.78 (m, 2 H) 1.83 (m, 1H) 1.96 (s, 3 H) 3.25 (m, 2 H) 3.34 (m., 2 H) 3.82 (s, 2 H) 5.28 (br d, 1 H) 5.77 (br d, 1 H) 7.24 (br s, 2 H) 7.71 (s, 2 H).

^{13}C-NMR (101 MHz, METHANOL-d_4) ppm 7.71 (br s, 1 C) 8.23 (s, 1 C) 10.15 (br s, 1 C) 22.58 (s, 1 C) 22.89 (s, 1 C) 30.41 (s, 1 C) 38.13 (s, 1 C) 39.50 (s, 1 C) 77.89 (br s, 1 C) 86.82 (br s, 1 C) 93.96 (br s, 1 C) 120.04 (s, 1 C) 120.51 (s, 1 C) 124.32 (s, 1 C) 129.35 (s, 1 C) 142.31 (s, 1 C) 160.85 (s, 1 C) 165.53 (s, 1 C) 173.42 (s, 1 C).

HRMS*: m*/z: calculated for $C_{23}H_{27}N_9O$ is 446.2417, measured mass was 446.2421 for the [M+H]+ ion.

Scheme 2.

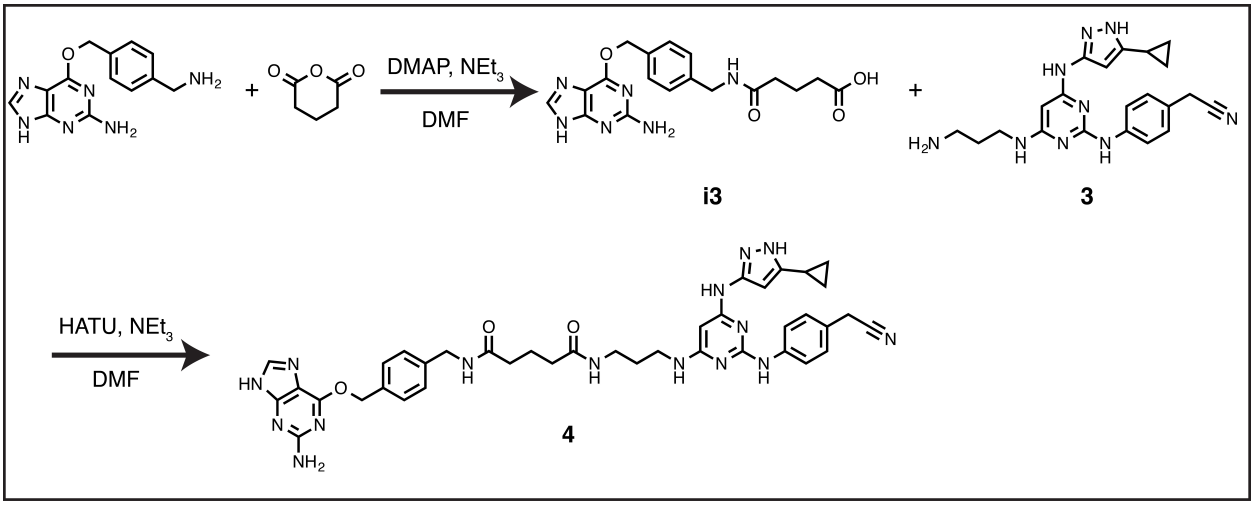

Synthesis of intermediate i3: To a solution of O-benzylguanine-4-methylamine (100 mg, 0.370 mmol), glutaric anhydride (42.2 mg, 0.370 mmol), DMAP (2.7 mg, 0.022 mmol) in anhydrous dimethylformamide (0.5 mL) was added triethylamine (103 µL, 0.740 mmol) and the reaction was stirred at room temperature overnight resulting in conversion to product by LC/MS. The reaction was stripped down *in vacuo* and the crude product was purified by reverse phase HPLC (gradient 35-60% MeCN:H_2O; 0.1% TFA) giving the desired product **i3** as a white solid (129 mg, 91% yield).

^{1}H-NMR (400 MHz, METHANOL-d_4) ppm 1.90 (t, J = 7.40 Hz, 2 H) 2.31 (dt, J = 11.86, 7.50 Hz, 4 H) 4.37 (s, 2 H) 5.64 (s, 2 H) 7.33 (d, J = 8.03 Hz, 2 H) 7.51 (d, J = 8.03 Hz, 2 H) 8.35 (s, 1 H).

^{13}C-NMR (101 MHz, METHANOL-d_4) ppm 22.33 (s, 1 C) 34.08 (s, 1 C) 36.08 (s, 1 C) 43.74 (s, 1 C) 71.02 (s, 1 C) 107.87 (s, 1 C) 128.83 (s, 1 C) 130.32 (s, 1 C) 135.28 (s, 1 C) 141.10 (s, 1 C) 143.85 (s, 1 C) 153.51 (s, 1 C) 158.06 (s, 1 C) 161.13 (s, 1 C) 175.36 (s, 1 C) 176.80 (s, 1 C).

Synthesis of compound 4: A solution of carboxylic acid **i3** (31.2 mg, 0.081 mmol), amine **3** (42 mg, 0.081 mmol), HATU (33.9 mg,0.089 mmol) and triethylamine 34 µL, 0.242 mmol) in DMF was stirred at room temperature overnight resulting in conversion to desired product by LC/MS. The reaction was stripped down *in vacuo* and the crude product was dissolved in DMSO and purified by reverse phase HPLC (gradient 15-40% MeCN:H_2O; 5 mM NH_4OH) giving the desired product **4** as a brown solid (21.6 mg, 35% yield).

^{1}H-NMR (400 MHz, METHANOL-d_4) ppm 0.71 (br s, 2 H) 1.02 (br s, 2 H) 1.81 (s, 2 H) 1.90 (br s, 3 H) 2.20 (br s, 2 H) 2.25 (s, 2 H) 3.23 (br s, 2 H) 3.43 (br s, 2 H) 3.91 (s, 2 H) 4.36 (s, 2 H) 5.53 - 5.73 (m, 3 H) 7.31 (s, 2 H) 7.39 (s, 2 H) 7.49 (s, 2 H) 7.64 (s, 2 H) 8.37 (s, 1 H).

^{13}C-NMR (101 MHz, METHANOL-d_4) ppm 7.45 (s, 1 C) 8.60 (s, 1 C) 23.02 (s, 1 C) 23.34 (s, 1 C) 30.11 (s, 1 C) 36.25 (s, 1 C) 36.32 (s, 1 C) 37.82 (s, 1 C) 39.87 (s, 1 C) 43.73 (s, 1 C) 71.02 (s, 1 C) 90.95 (s, 1 C) 107.74 (s, 1 C) 119.66 (s, 1 C) 123.34 (s, 1 C) 128.80 (s, 1 C) 129.94 (s, 1 C) 130.29 (s, 1 C) 135.23 (s, 1 C) 138.35 (s, 1 C) 141.01 (s, 1 C) 143.88 (s, 1 C) 149.81 (s, 1 C) 153.37 (s, 1 C) 157.95 (s, 1 C) 161.09 (s, 1 C) 175.28 (s, 1 C) 175.57 (s, 1 C).

HRMS: m/z: calculated for $C_{17}H_{19}ClN_4O_4$ is 446.2339, measured mass was 446.2386 for the [M+H]+ ion.

Scheme 3.

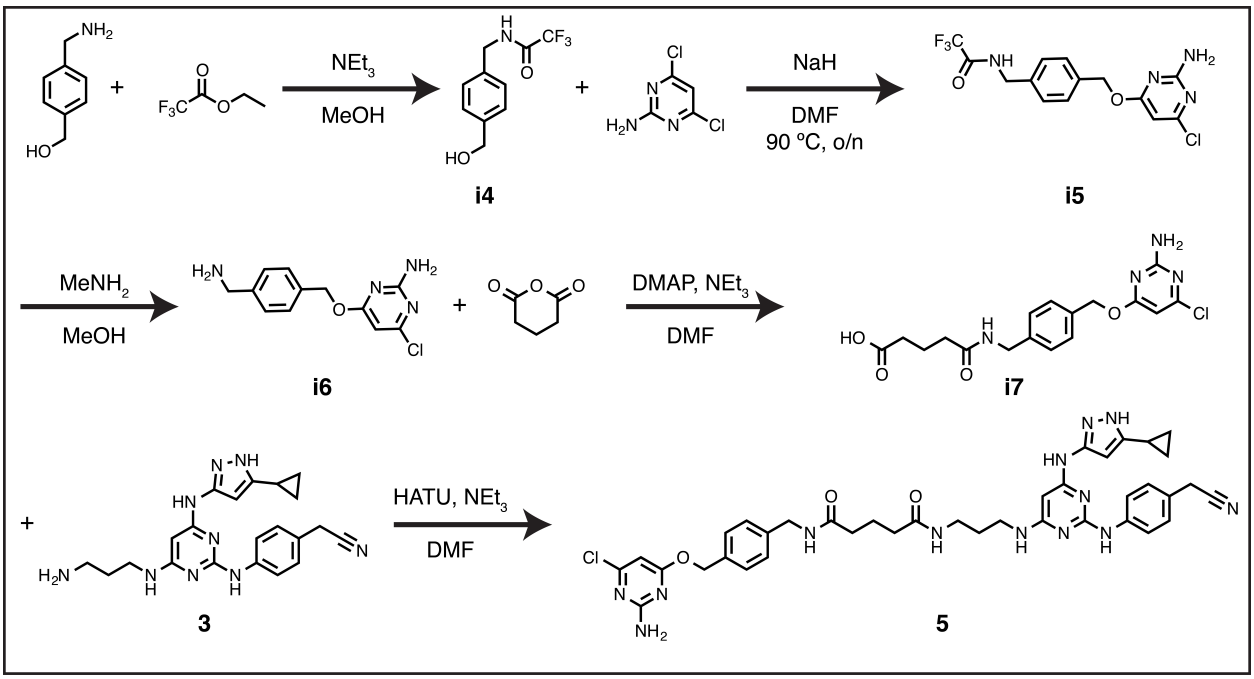

Synthesis of intermediate i4: To a solution of (4-(aminomethyl)phenyl)methanol (250 mg, 1.44 mmol) in MeOH (7.5 mL) was added triethylamine (0.4 mL, 2.88 mmol) followed by ethyl 2,2,2-trifluoroacetate (206 µL, 1.73 mmol). The reaction was stirred at room temperature for 1 hour resulting in conversion to product by LCMS (negative ion mass only observed). The reaction was partitioned between EtOAc/H_2O and extracted. The organics were washed with brine, dried over Na_2SO_4 and stripped down *in vacuo* giving compound **i4** as a white solid (264 mg, 79% yield).

^{1}H-NMR (400 MHz, DMSO-d_6) d 4.36 (d, J = 5.77 Hz, 2 H) 4.47 (d, J = 5.52 Hz, 2 H) 5.18 (t, J = 5.65 Hz, 1 H) 7.29 (d, J = 8.2 Hz, 1H), 7.22 (d, J = 8.2 Hz, 1H), 10.01 (br s, 1 H).

^{13}C-NMR (101 MHz, DMSO-d_6) ppm 42.27 (s, 1 C) 62.48 (s, 1 C) 109.97 - 121.09 (m, 1 C) 126.49 (s, 2 C) 127.08 (s, 2 C) 135.69 (s, 1 C) 141.59 (s, 1 C) 154.48 - 157.35 (m, 1 C).

LCMS: m/z: calculated for $C_{10}H_{10}F_3NO_2$ is 233.07, measured mass was 232.0 for the [M-H]- ion.

Synthesis of intermediate i5: To a solution of benzyl alcohol **i4** (250 mg, 1.07 mmol) in 3 mL dry dimethylformamide under nitrogen atmosphere was added 60% NaH in mineral oil (90 mg , 2.25 mmol) portion-wise. After 5 minutes, 2-amino-4,6-dichloropyrimidine (193 mg, 1.18 mmol) was added and the solution stirred at 90 °C overnight. 1 mL water was added dropwise to quench any excess NaH and the mixture poured into 50 mL 0.5 N HCl. The crude product was extracted with ethyl acetate, the combined organics washed with brine, dried over Na_2SO_4 and stripped down *in vacuo*. The product was purified by reverse phase HPLC (gradient 35-60% MeCN:H_2O; 0.1% TFA) giving desired product **i5** as a white solid (100 mg, 26% yield).

^{1}H-NMR (400 MHz, DMSO-d_6) ppm 4.39 (d, J = 5.77 Hz, 2 H) 5.30 (s, 2 H) 6.14 (s, 1 H) 7.13 (br s, 2 H) 7.29 (d, J = 8.03 Hz, 2 H) 7.42 (d, J = 7.78 Hz, 2 H) 10.03 (t, J = 5.65 Hz, 1 H).

^{13}C-NMR (101 MHz, DMSO-d_6) ppm 42.22 (s, 1 C) 67.03 (s, 1 C) 94.28 (s, 1 C) 113.46 - 118.31 (m, 1 C) 127.37 (s, 2 C) 128.48 (s, 2 C) 135.22 (s, 1 C) 137.30 (s, 1 C) 156.05 (m, 1 C) 159.89 (s, 1 C) 162.66 (s, 1 C) 170.15 (s, 1 C).

HRMS: m/z: calculated for $C_{14}H_{12}ClF_3N_4O_2$ is 360.0601, measured mass was 361.0631 for the [M+H]+ ion.

Synthesis of intermediate i6: 16.5 mg (0.046 mmol) of trifluoroacetamide **i5** was dissolved in 1 mL methanol and treated with 2 mL 33% methylamine in ethanol. The reaction was stirred at room temperature overnight and all volatiles were removed *in vacuo*. The product was purified by reverse phase HPLC (gradient 35-60% MeCN:H_2O;

0.1% TFA) giving desired product **i6** as a clear oil (Yield: 12.3 mg, 71% of the TFA salt).

^{1}H-NMR (400 MHz, DMSO-d_6) ppm 3.98 - 4.13 (m, 2 H) 5.33 (s, 2 H) 6.15 (s, 1 H) 7.14 (br s, 2 H) 7.48 (q, J = 8.45 Hz, 4 H) 8.17 (br s, 3 H).

^{13}C-NMR (101 MHz, DMSO-d_6) ppm 41.89 (s, 1 C) 66.84 (s, 1 C) 94.29 (s, 1 C) 111.5-122.2 (m, 1 C) 128.48 (s, 2 C) 128.85 (s, 2 C) 133.72 (s, 1 C) 136.50 (s, 1 C) 157.90 (s, 1 C) 159.94 (m, 1 C) 162.64 (s, 1 C) 170.10 (s, 1 C).

HRMS: m/z: calculated for $C_{12}H_{13}ClN_4O$ is 265.0778, measured mass was 265.0859 for the [M+H]+ ion.

Synthesis of intermediate i7: To a solution of amine **i6** (59 mg, 0.223 mmol), glutaric anhydride (24.5 mg, 0.223 mmol), DMAP (2.7 mg, 0.022 mmol) in anhydrous dimethylformamide (1.5 mL) was added triethylamine (62 µL, 0.446 mmol) and the reaction was stirred at room temperature overnight resulting in conversion to product by LC/MS. The reaction was stripped down *in vacuo* and the crude product was purified by reverse phase HPLC (gradient 35-60% MeCN:H_2O; 0.1% TFA) giving the desired product **i7** as a white solid (13 mg, 15% yield).

^{1}H-NMR (400 MHz, DMSO-d_6) ppm 1.73 (quin, J = 7.40 Hz, 2 H) 2.11 - 2.28 (m, 4 H) 4.25 (d, J = 5.77 Hz, 2 H) 5.28 (s, 2 H) 6.14 (s, 1 H) 7.13 (br s, 2 H) 7.24 (d, J = 8.03 Hz, 2 H) 7.38 (d, J = 8.03 Hz, 2 H) 8.35 (t, J = 5.90 Hz, 1 H) 12.07 (s, 1 H).

^{13}C-NMR (101 MHz, METHANOL-d_4) ppm 22.33 (s, 1 C) 34.08 (s, 1 C) 36.08 (s, 1 C) 43.74 (s, 1 C) 71.02 (s, 1 C) 107.87 (s, 1 C) 128.83 (s, 1 C) 130.32 (s, 1 C) 135.28 (s, 1 C) 141.10 (s, 1 C) 143.85 (s, 1 C) 153.51 (s, 1 C) 158.06 (s, 1 C) 161.13 (s, 1 C) 175.36 (s, 1 C) 176.80 (s, 1 C).

HRMS: m/z: calculated for $C_{17}H_{19}ClN_4O_4$ is 379.1095, measured mass was 379.1192 for the [M+H]+ ion.

Synthesis of compound 5: A solution of carboxylic acid **i7** (10.0 mg, 0.019 mmol), amine **3** (8.05 mg, 0.021 mmol), HATU (8.1 mg, 0.021 mmol) and triethylamine (0.058 mmol, 8,1 µL) in DMF was stirred at room temperature overnight resulting in conversion to desired product by LC/MS. The reaction was stripped down *in vacuo* and the crude product was dissolved in DMSO and purified by reverse phase HPLC (gradient 25-50% MeCN:H_2O; 5 mM NH_4OH) giving desired product **5** as an off-white solid (6.8 mg, 46% yield).

^{1}H-NMR (400 MHz, METHANOL-d_4) ppm 0.68 (br s, 2 H) 0.90 (br s, 2 H) 1.78 (br s, 2 H) 1.89 (m, 3 H) 2.21 (m, 4 H) 3.26 (m, 2 H) 3.34 (br s, 2 H) 3.81 (s, 2 H) 4.33 (s, 2 H) 5.30 (m, 3 H) 5.62-5.94 (br d, 1 H) 6.08 (s, 1 H) 7.24 (s, 4 H) 7.36 (s, 2 H) 7.68 (s, 2 H).

^{13}C-NMR (101 MHz, METHANOL-d_4) ppm 8.23 (s, 1 C) 22.90 (s, 1 C) 23.24 (s, 1 C) 30.44 (s, 1 C) 36.11 (s, 1 C) 36.24 (s, 1 C) 37.96 (s, 1 C) 39.44 (s, 1 C) 43.82 (s, 1 C) 68.97 (s, 1 C) 96.58 (s, 1 C) 120.05 (s, 1 C) 120.52 (s, 1 C) 128.68 (s, 1 C) 129.36 (s, 1 C) 129.59 (s, 1 C) 136.72 (s, 1 C) 140.04 (s, 1 C) 142.30 (s, 1 C) 161.74 (s, 1 C) 164.45 (s, 1 C) 165.48 (s, 1 C) 172.35 (s, 1 C) 175.22 (s, 1 C) 175.45 (s, 1 C).

HRMS: m/z: calculated for $C_{17}H_{19}ClN_4O_4$ is 764.3222, measured mass was 764.3284 for the [M+H]+ ion.

B. ^{1}H- and ^{13}C-NMR spectra of compounds

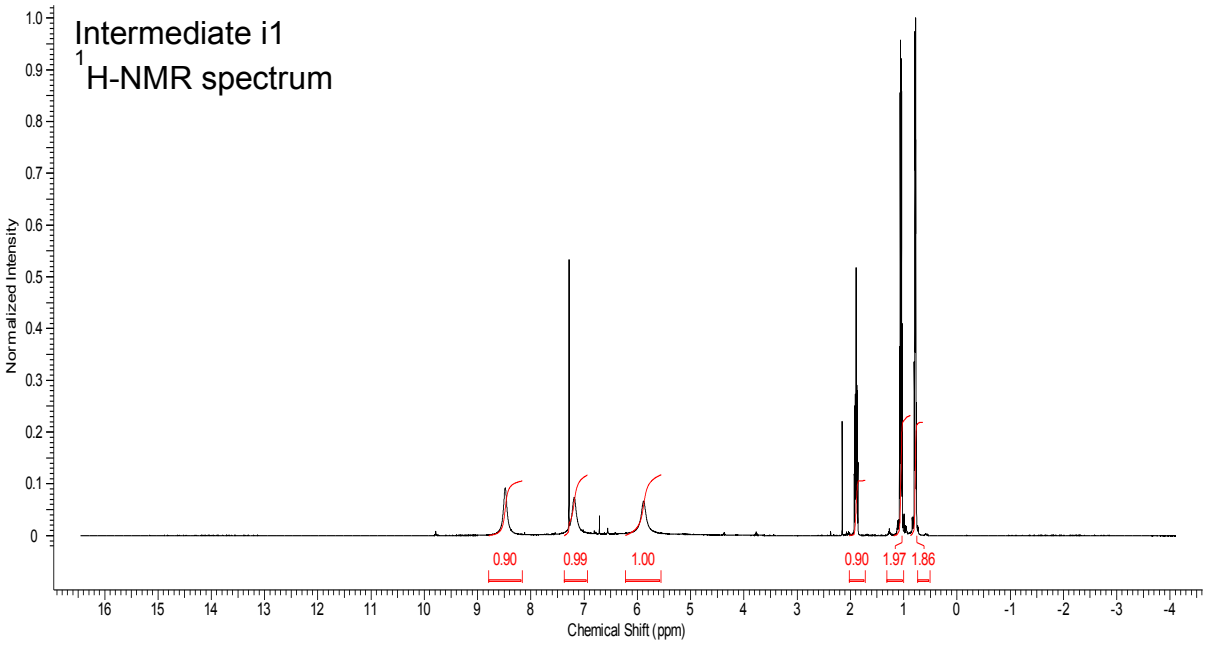

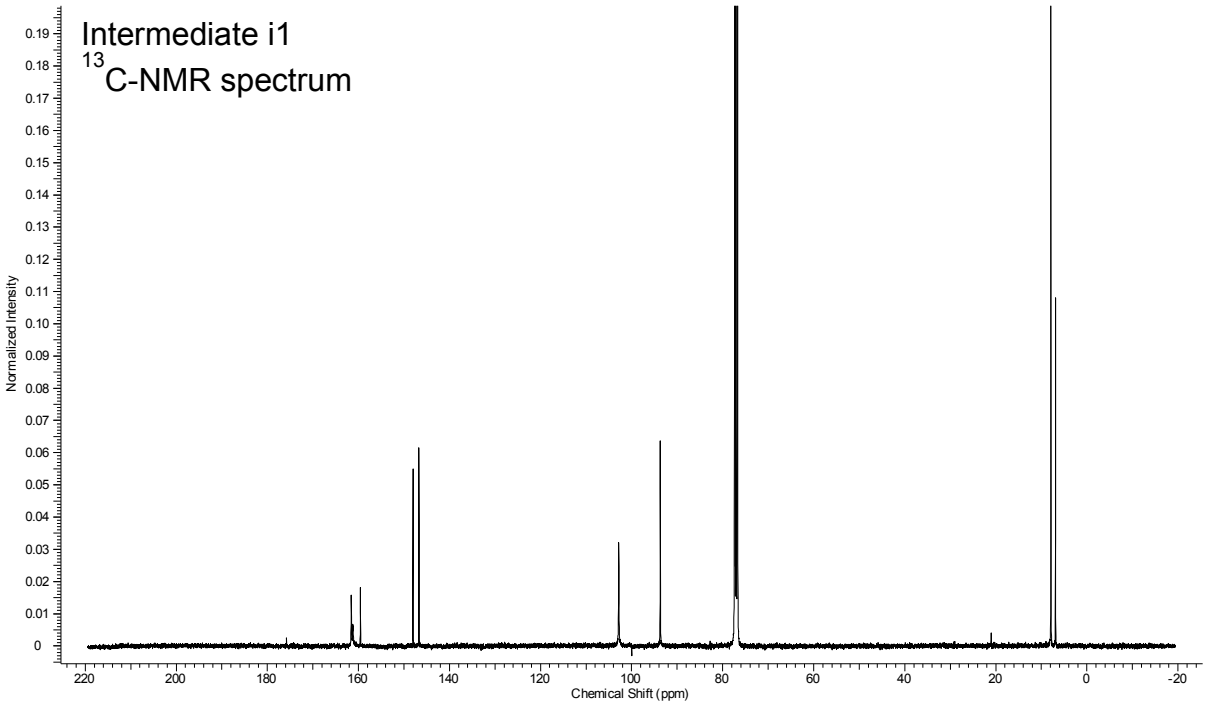

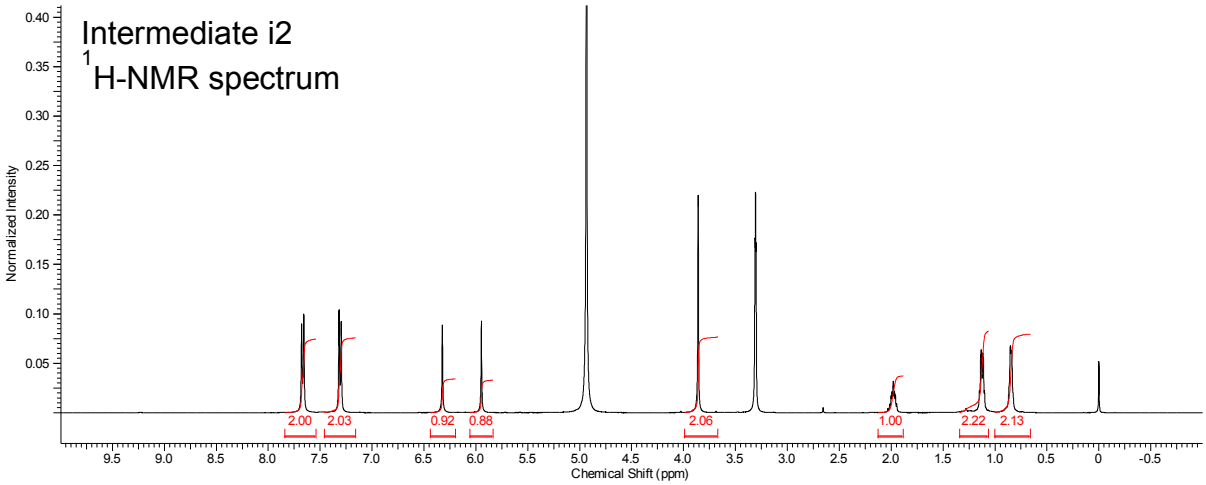
Intermediate i2
1H-NMR spectrum
Normalized Intensity
Chemical Shift (ppm)
2.00
2.03
0.92
0.88
2.06
1.00
2.22
2.13

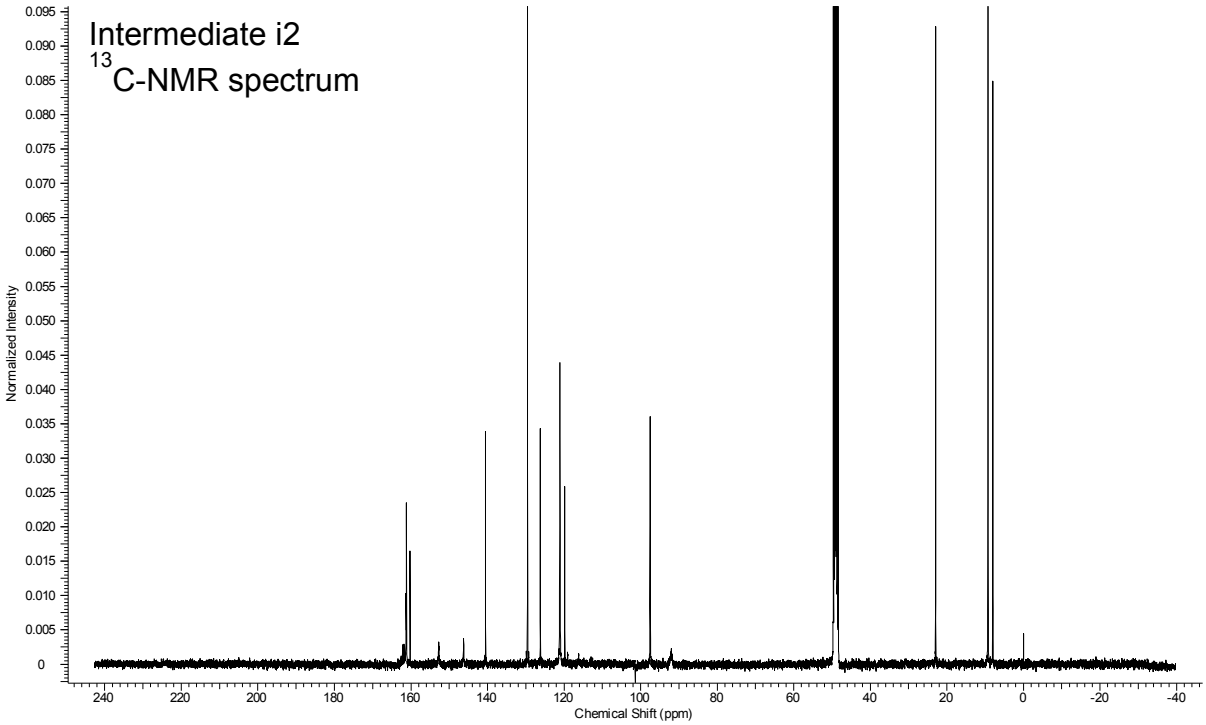
Intermediate i2
13C-NMR spectrum
Normalized Intensity
Chemical Shift (ppm)

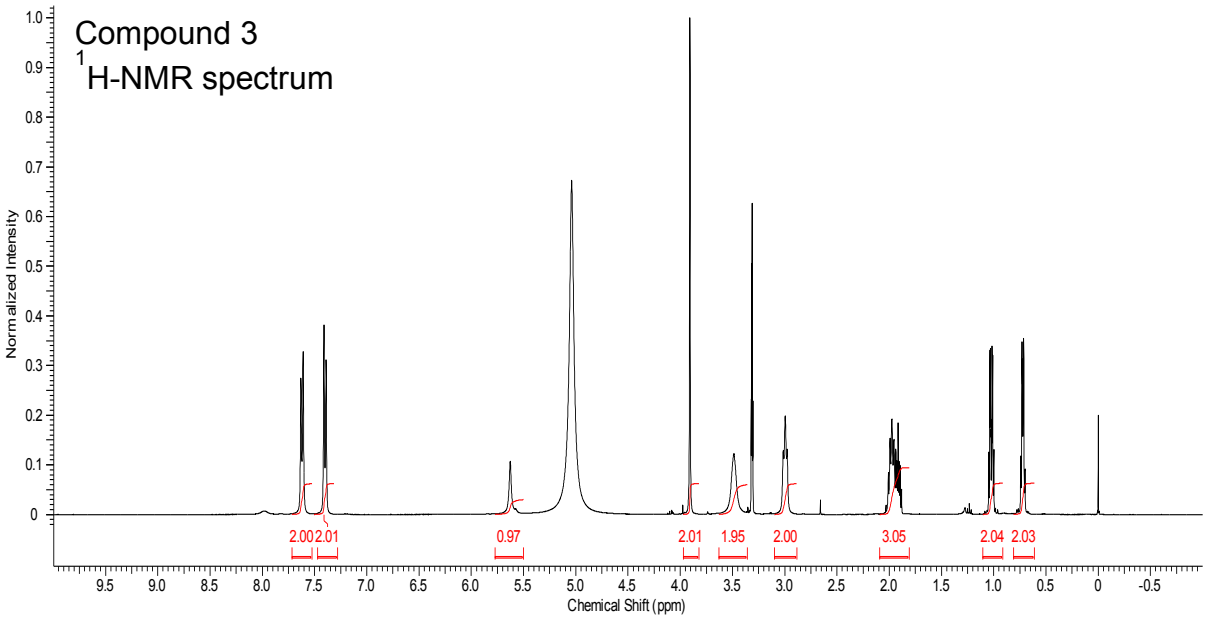
Compound 3
1H-NMR spectrum
Normalized Intensity
Chemical Shift (ppm)
2.00
2.01
0.97
2.01
1.95
2.00
3.05
2.04
2.03

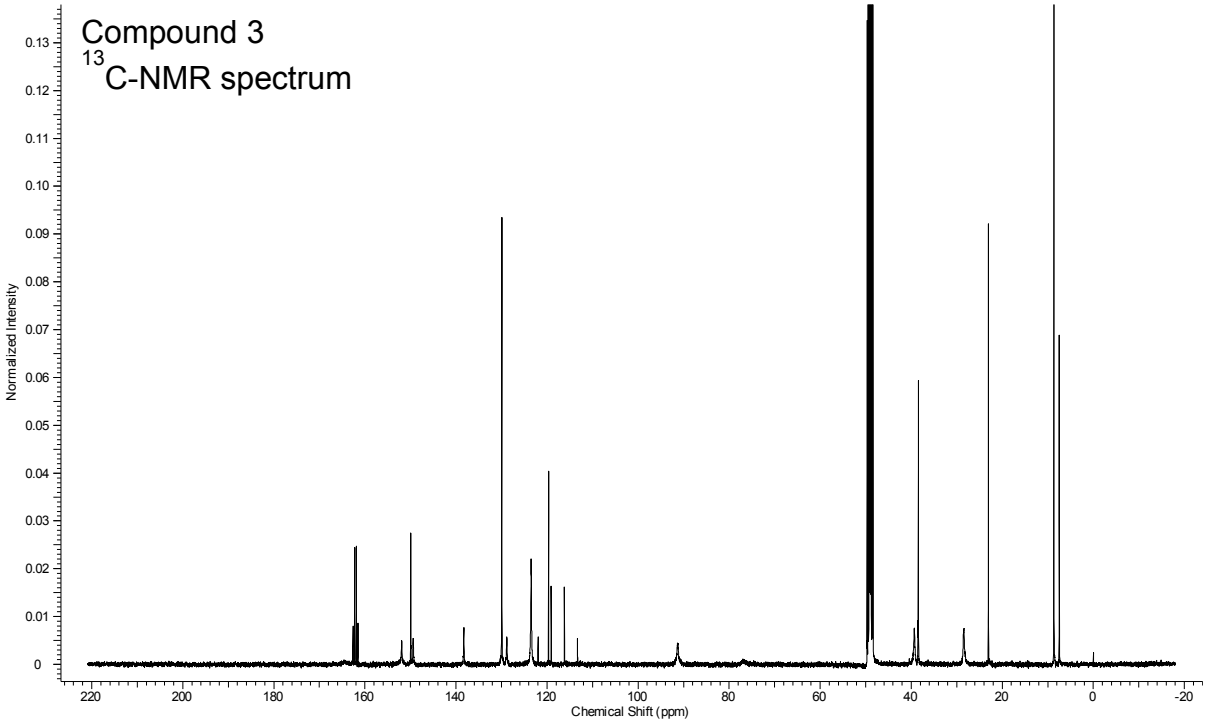
Compound 3
13C-NMR spectrum
Normalized Intensity
Chemical Shift (ppm)

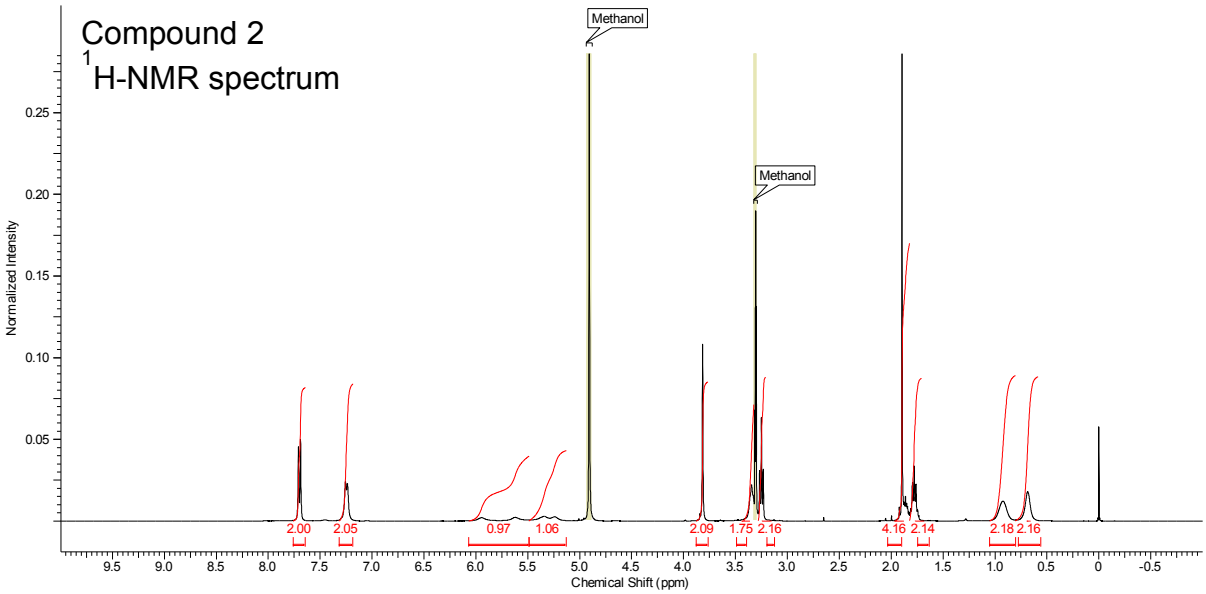
Compound 2
1H-NMR spectrum
Methanol
Methanol
Normalized Intensity
0.25
0.20
0.15
0.10
0.05
2.00
2.05
0.97
1.06
2.09
1.75
2.16
4.16
2.14
2.18
2.16
9.5 9.0 8.5 8.0 7.5 7.0 6.5 6.0 5.5 5.0 4.5 4.0 3.5 3.0 2.5 2.0 1.5 1.0 0.5 0 -0.5
Chemical Shift (ppm)

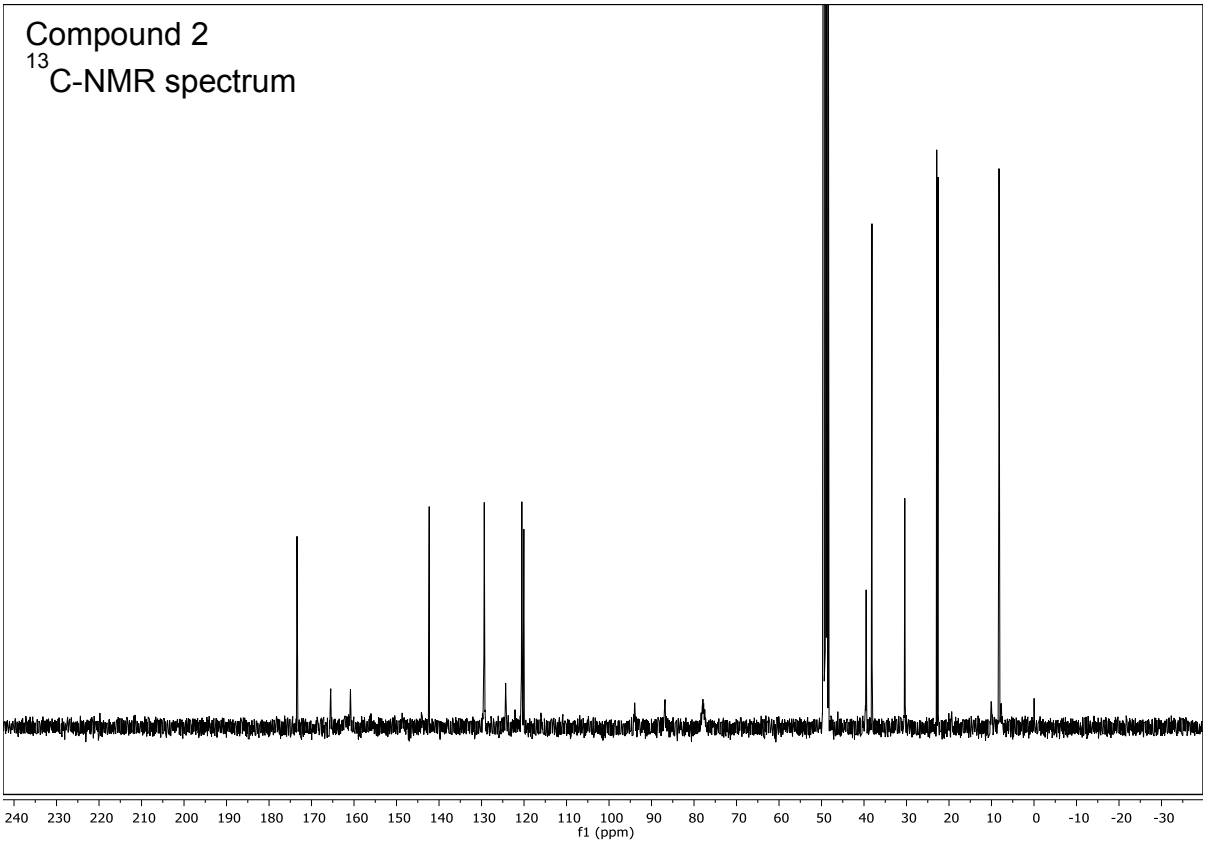
Compound 2
13C-NMR spectrum
240 230 220 210 200 190 180 170 160 150 140 130 120 110 100 90 80 70 60 50 40 30 20 10 0 -10 -20 -30
f1 (ppm)

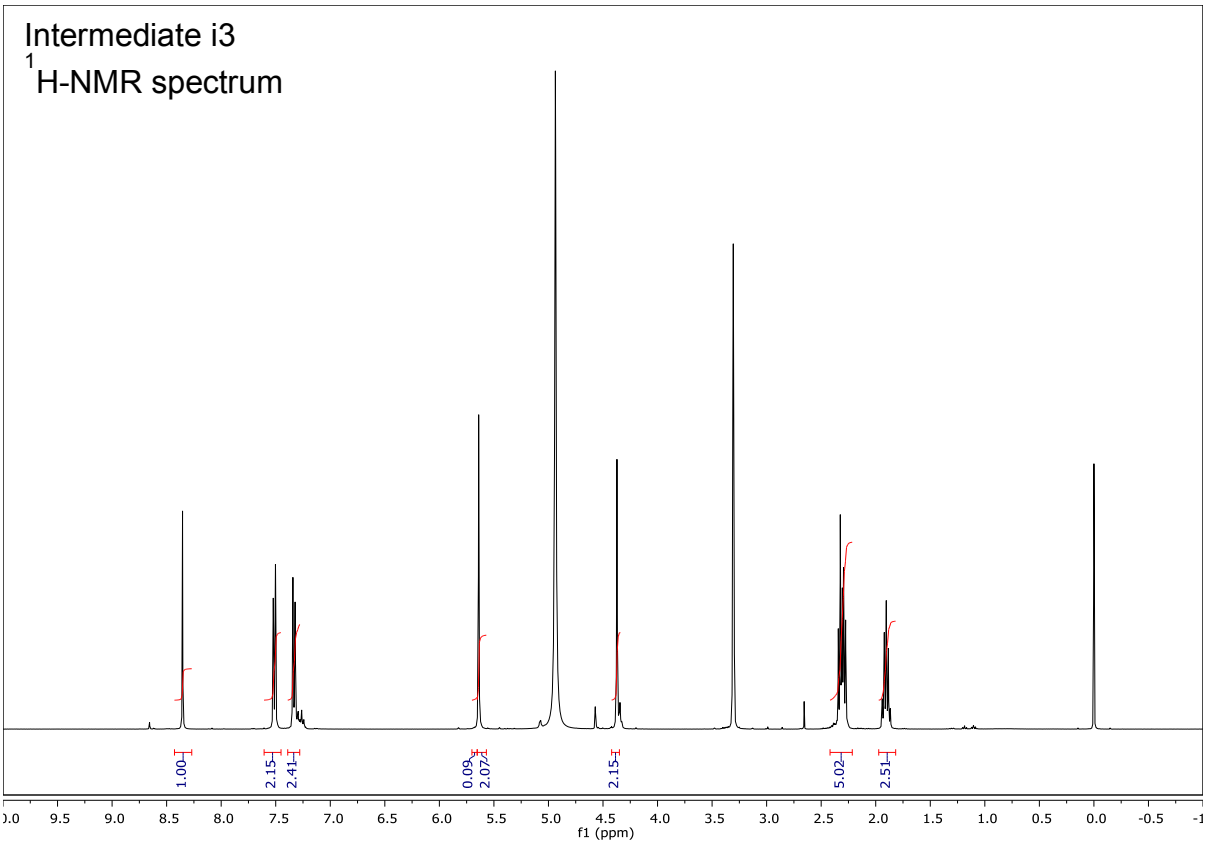
Intermediate i3
1H-NMR spectrum
1.00
2.15
2.41
0.09
2.07
2.15
5.02
2.51
f1 (ppm)

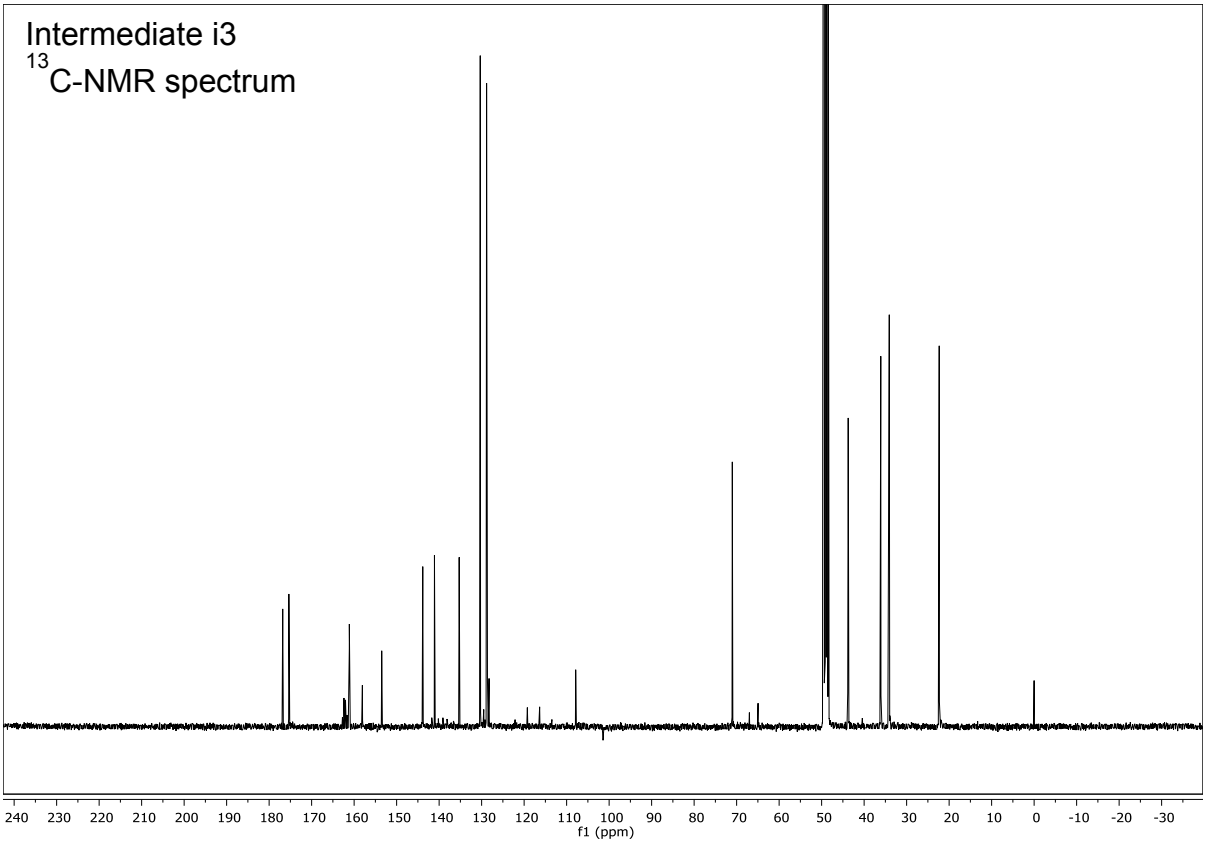
Intermediate i3
13C-NMR spectrum
f1 (ppm)

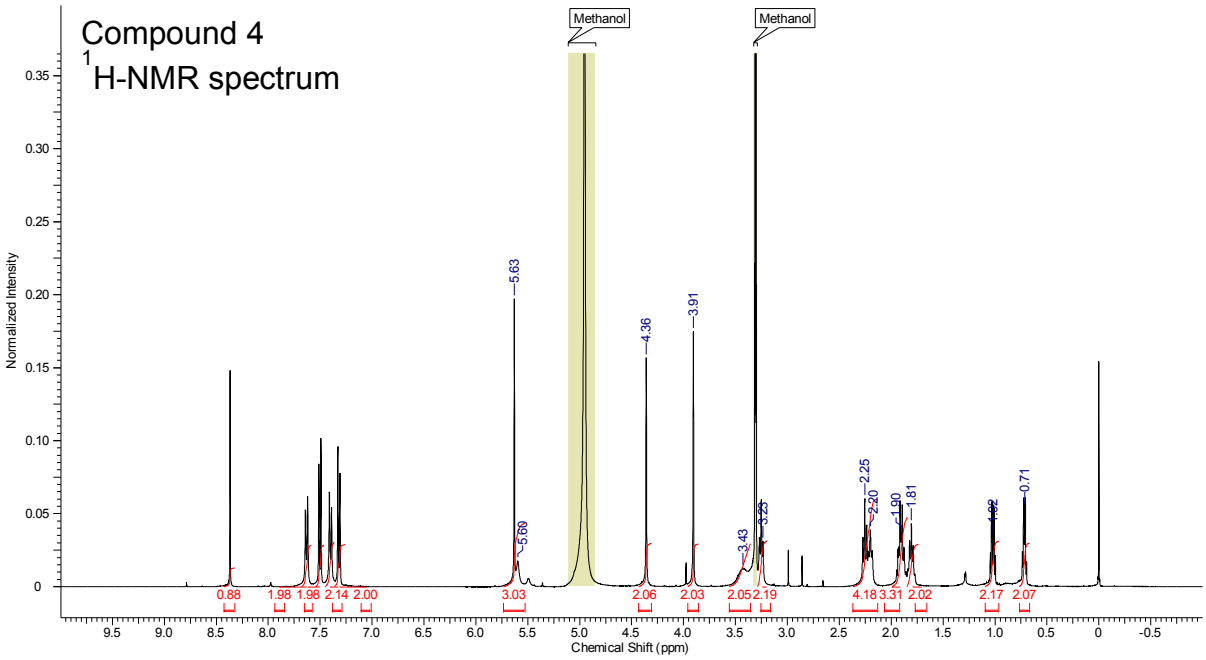
Compound 4
1H-NMR spectrum
Methanol
Methanol
Normalized Intensity
Chemical Shift (ppm)
5.63
5.60
4.36
3.91
3.43
3.25
2.25
2.20
1.90
1.81
1.62
0.71
0.88
1.98
1.98
2.14
2.00
3.03
2.06
2.03
2.05
2.19
4.18
3.31
2.02
2.17
2.07

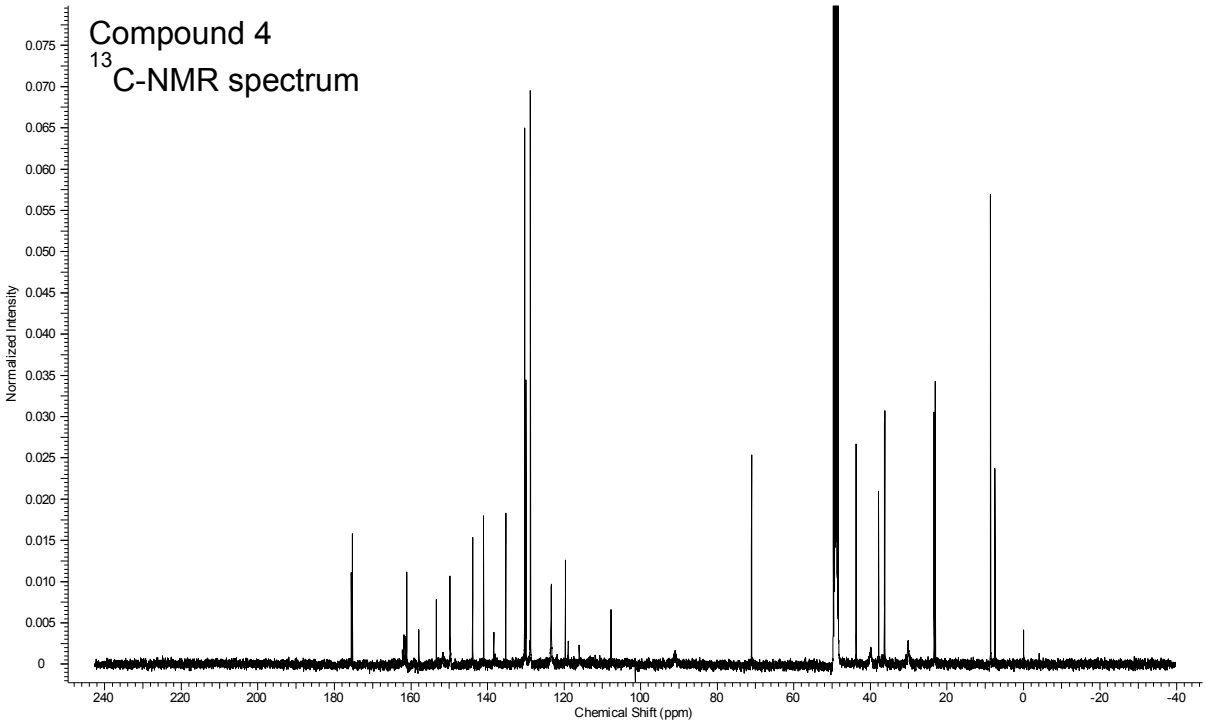
Compound 4
13C-NMR spectrum
Normalized Intensity
Chemical Shift (ppm)

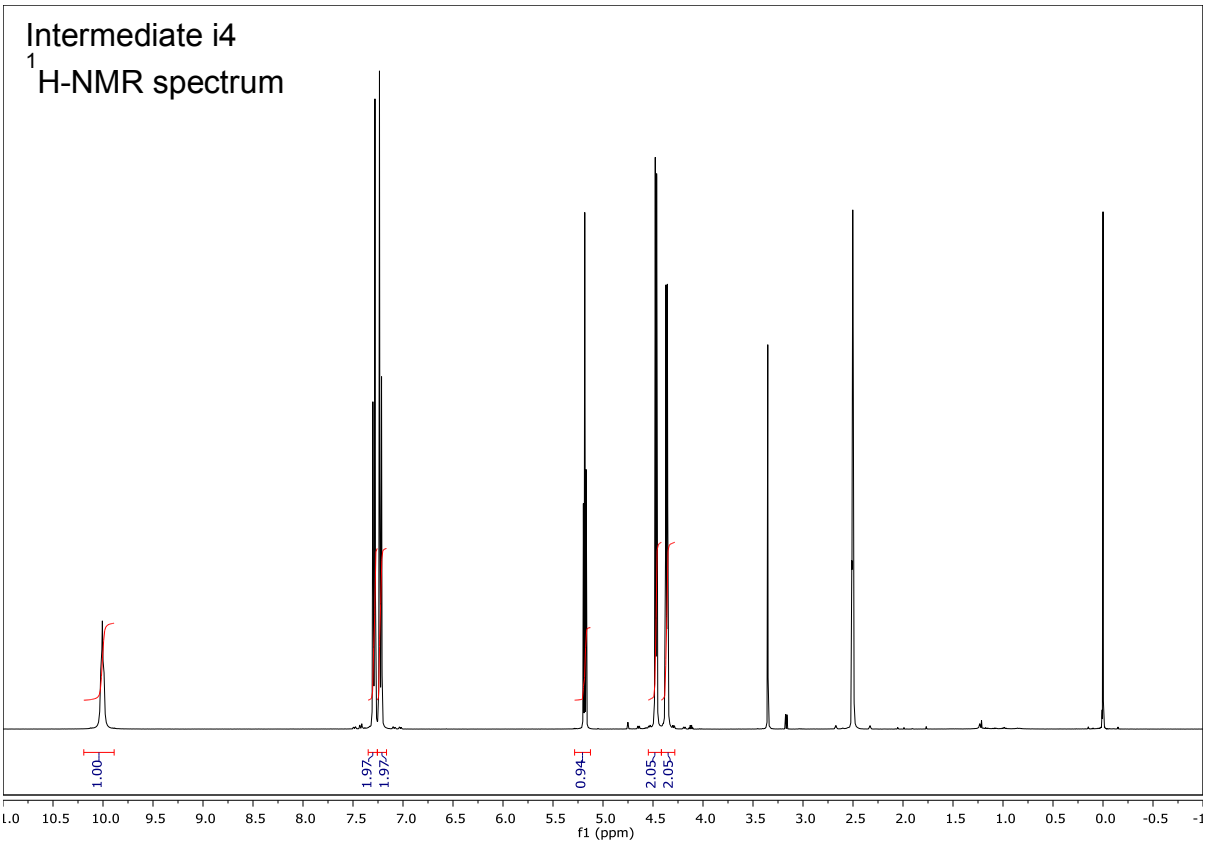
Intermediate i4
1H-NMR spectrum
1.00
1.97
1.97
0.94
2.05
2.05
f1 (ppm)

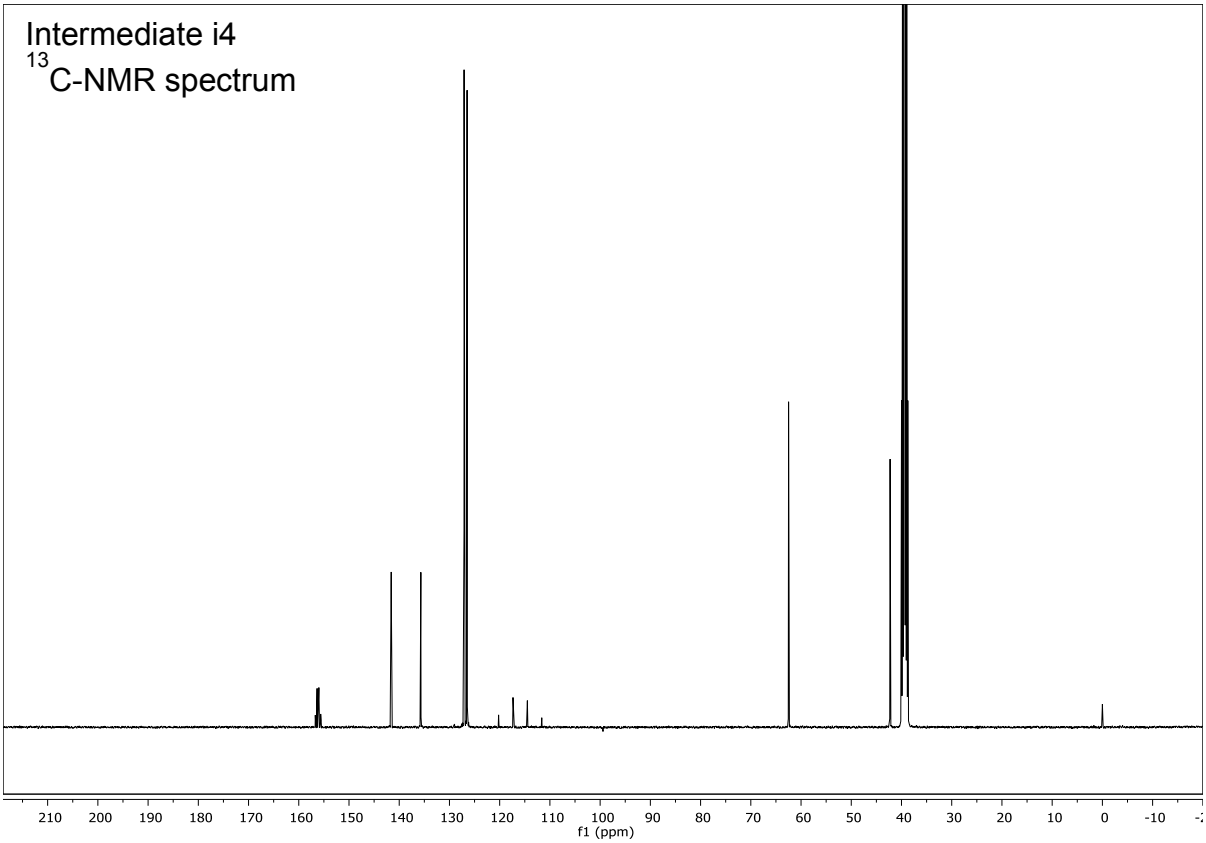
Intermediate i4
13C-NMR spectrum
f1 (ppm)

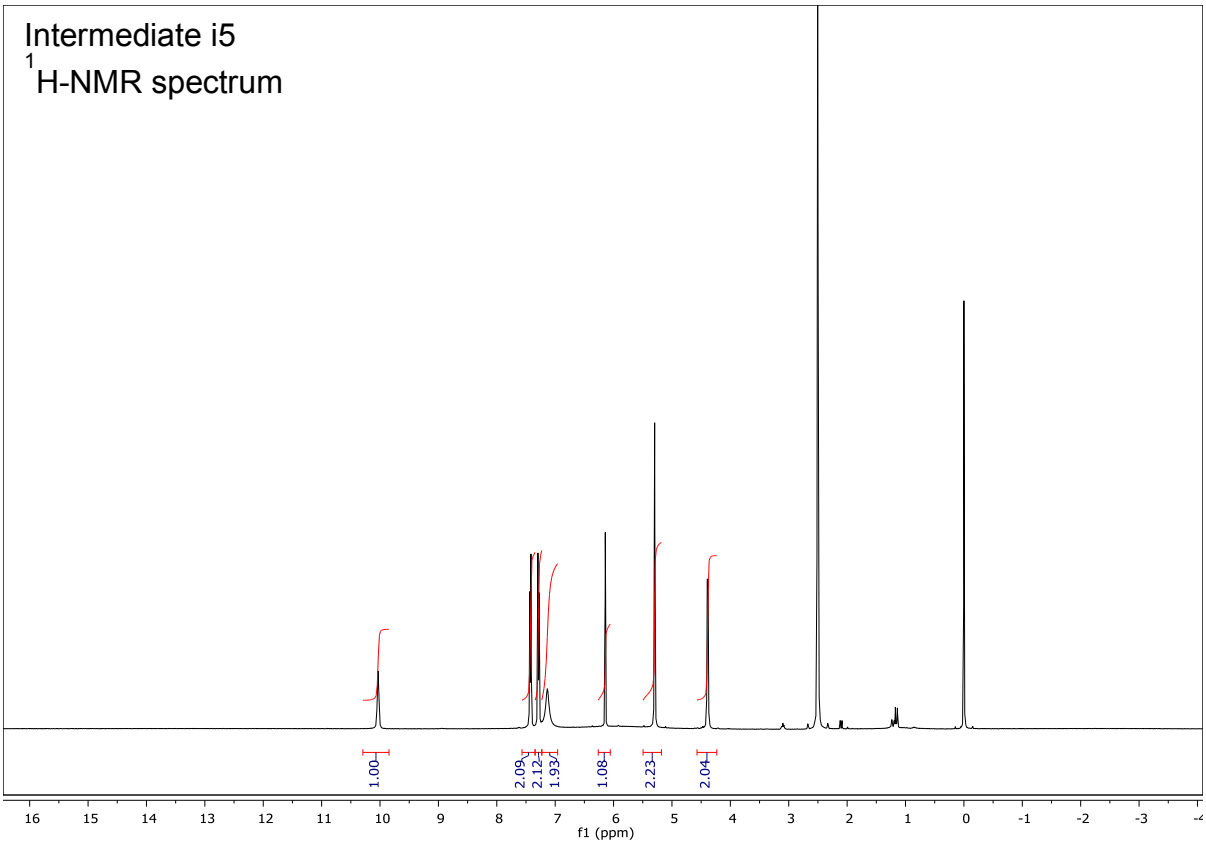
Intermediate i5
1H-NMR spectrum
1.00
2.09
2.12
1.93
1.08
2.23
2.04
f1 (ppm)

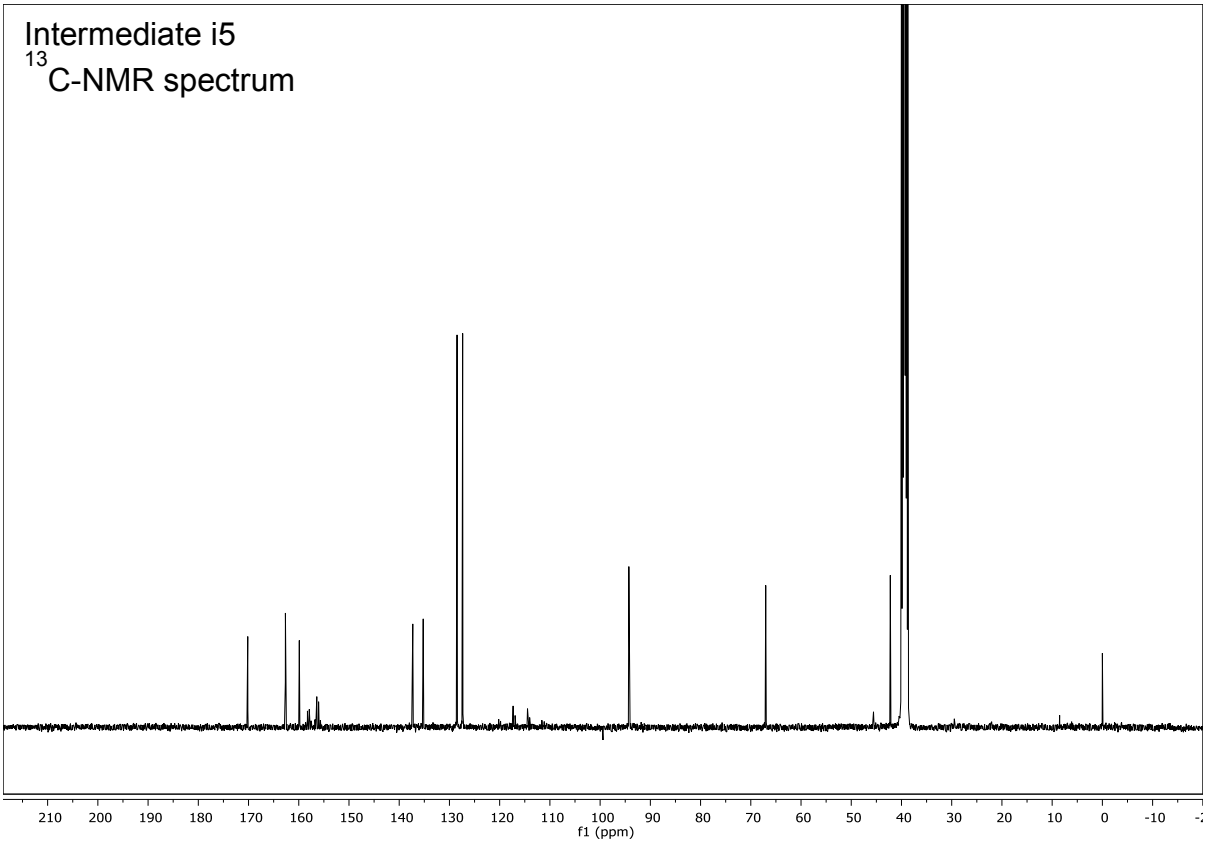
Intermediate i5
13C-NMR spectrum
f1 (ppm)

Intermediate i6

^{1}H-NMR spectrum

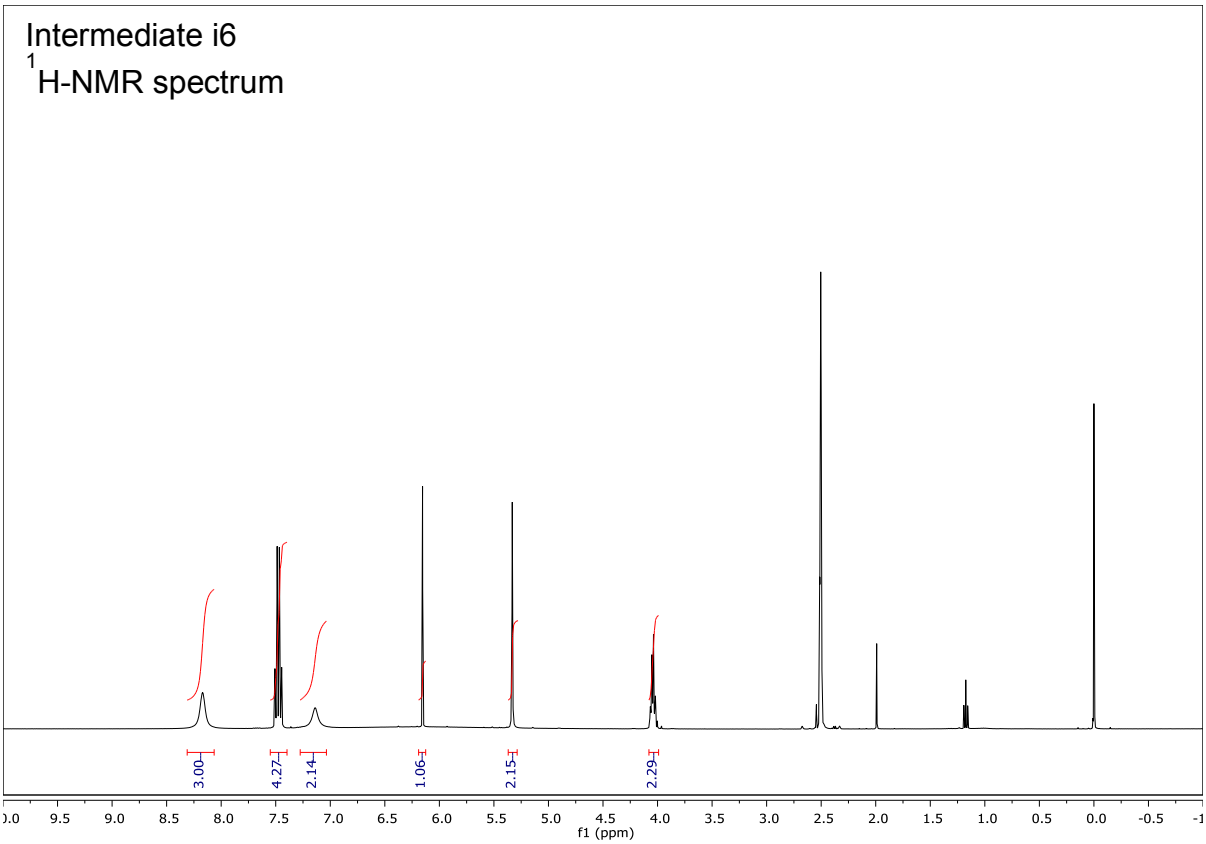

Intermediate i6

^{13}C-NMR spectrum

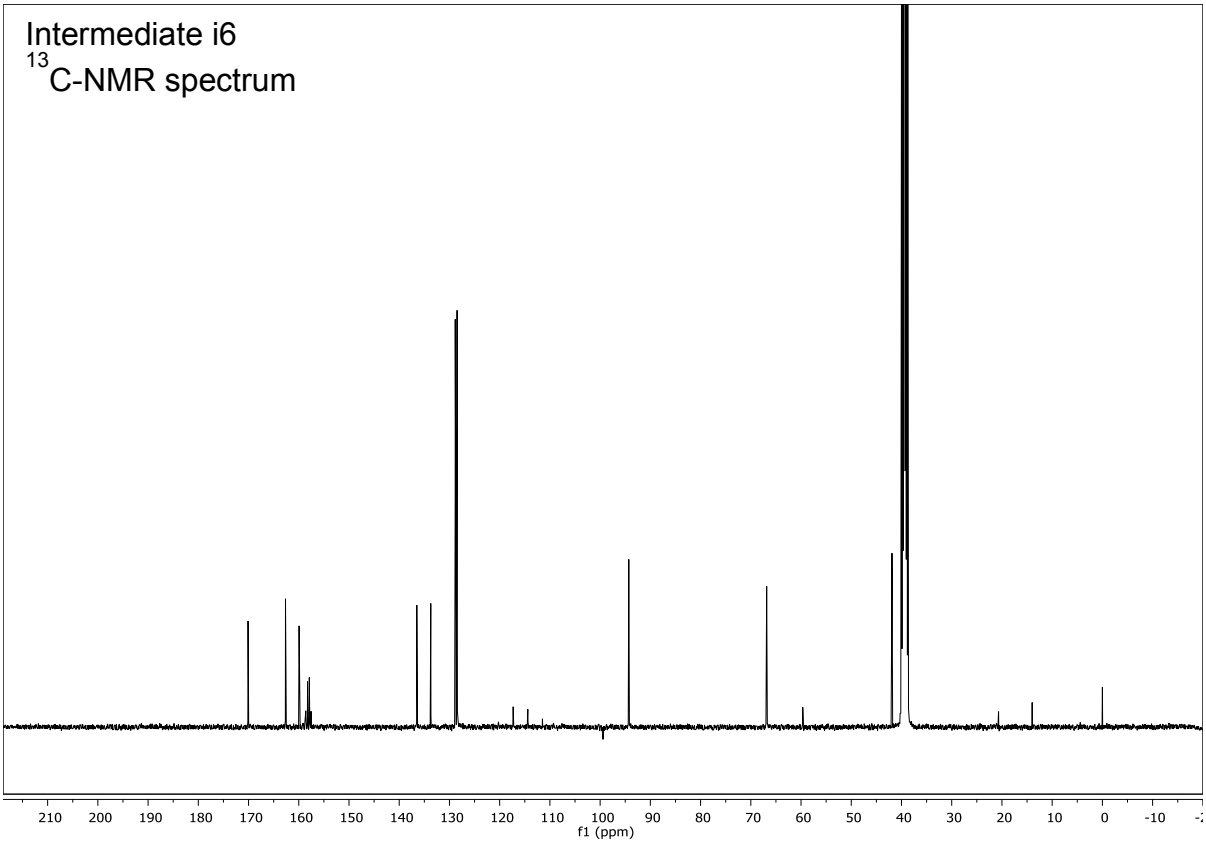

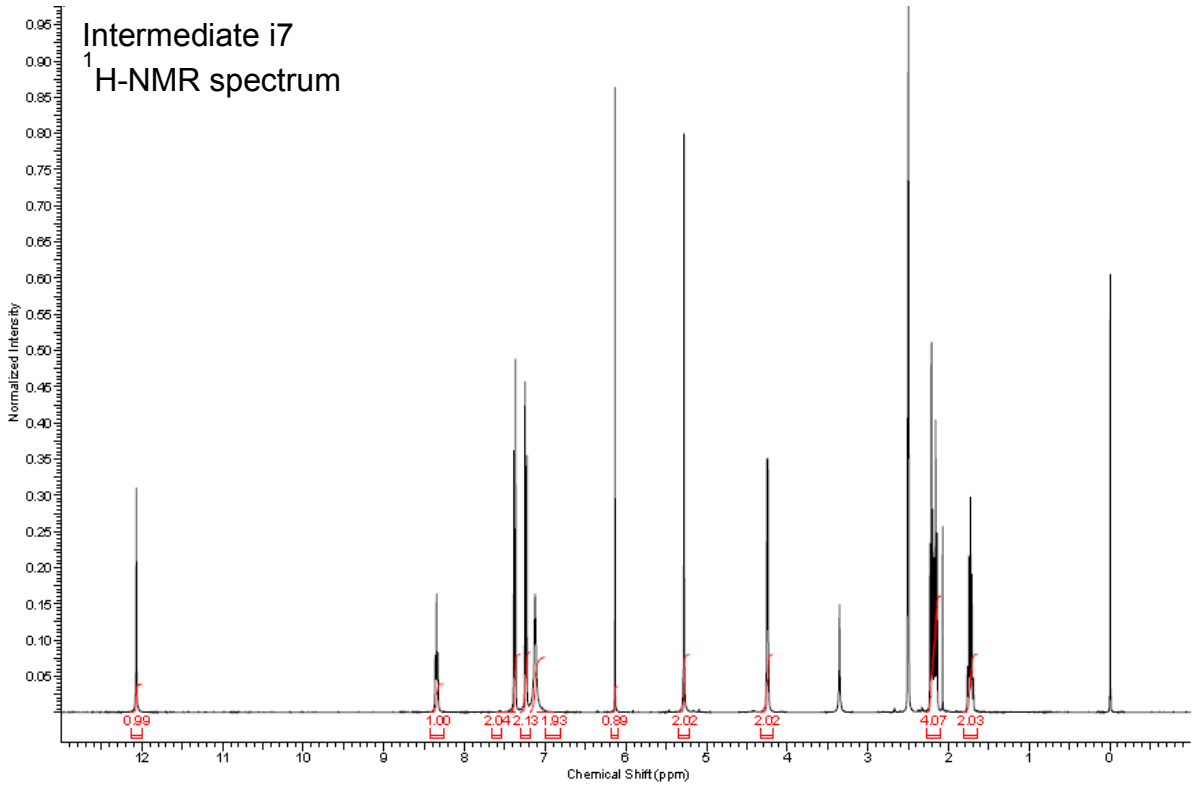
Intermediate i7
1H-NMR spectrum
Normalized Intensity
Chemical Shift (ppm)
0.99
1.00
2.04
2.13
1.93
0.89
2.02
2.02
4.07
2.03

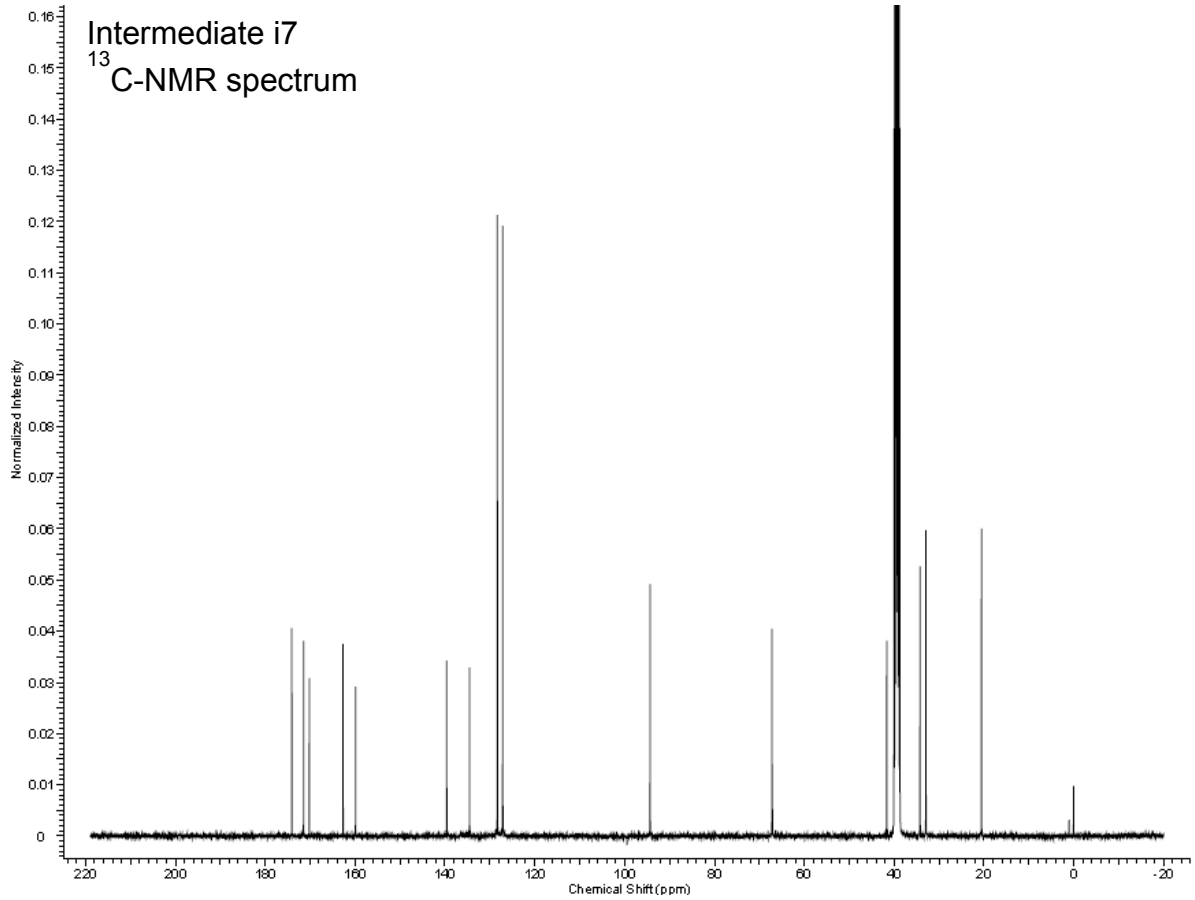
Intermediate i7
13C-NMR spectrum
Normalized Intensity
Chemical Shift (ppm)

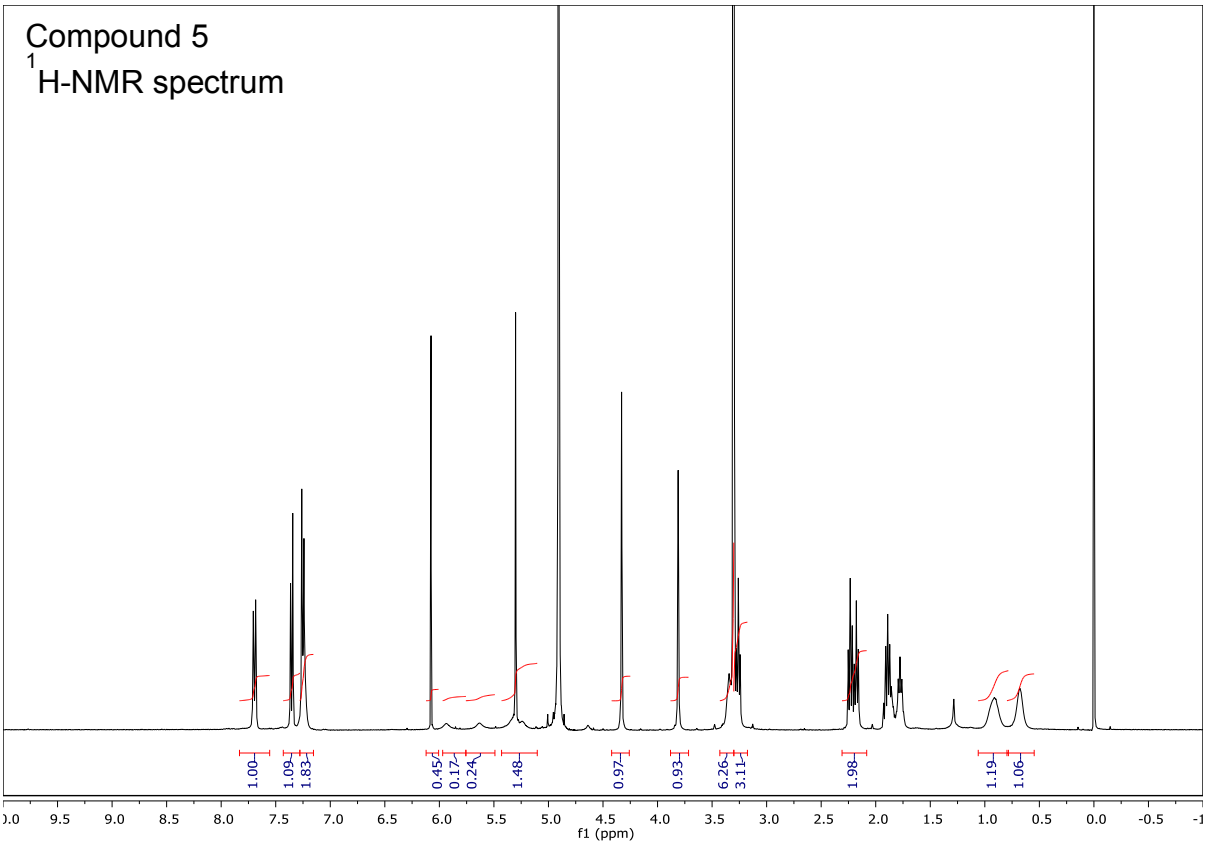
Compound 5
1H-NMR spectrum
1.00
1.09
1.83
0.45
0.17
0.24
1.48
0.97
0.93
6.26
3.11
1.98
1.19
1.06
f1 (ppm)

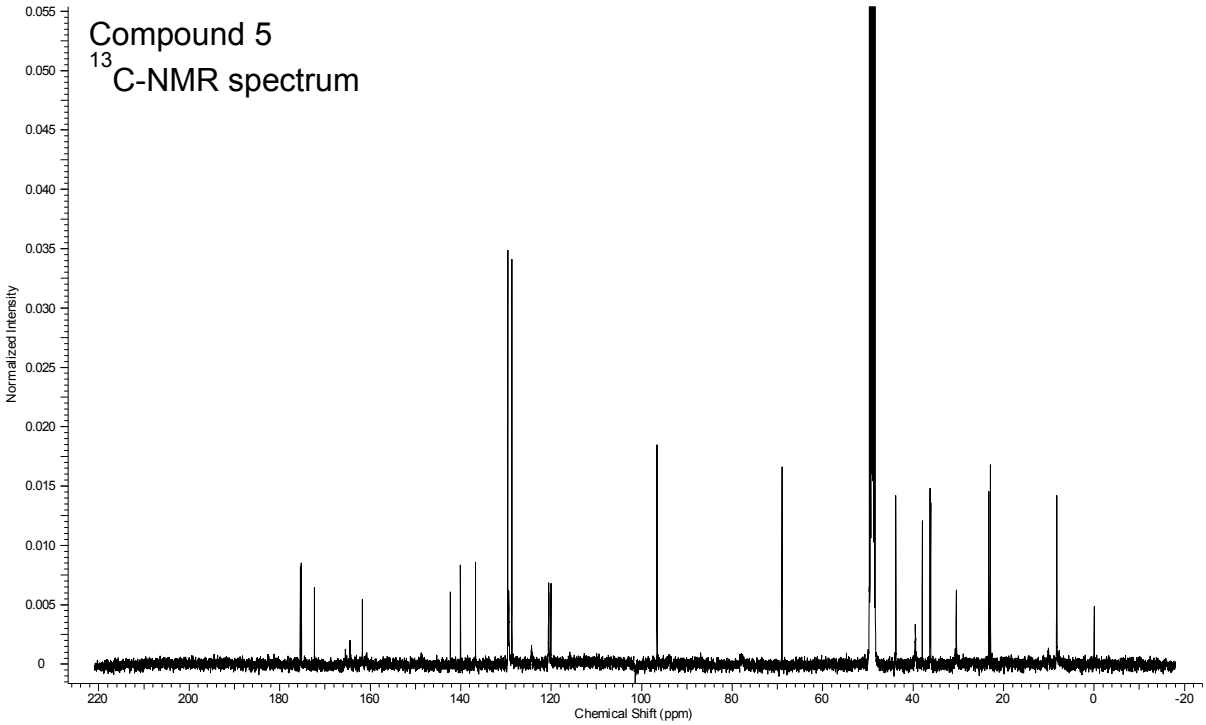
Compound 5
13C-NMR spectrum
Normalized Intensity
Chemical Shift (ppm)

C. Design of fusion constructs, protein expression and purification

i. SNAPtag fusion protein design

GENE DESIGN OF ABL-RECOGNIZING FUSION CONSTRUCTS. A fusion construct was designed to display the monobody HA4 from the C-terminus of SNAPtag.

GENE DESIGN OF ERK-RECOGNIZING FUSION CONSTRUCTS. Fusion constructs were designed to display the desired DARPin from the C-terminus of SNAPtag.

GENE SYNTHESIS. GENERAL METHODS. The monobody or DARPin genes were amplified from the pUC57 plasmid (Genscript) using the primers listed for the monobody or DARPin fragments. A mutant form of the human gene O^6-alkylguanine-DNA-alkyltransferase was amplified from the pSS26(b) plasmid (Covalys) using primers listed for the SNAPtag fragment. To obtain the fusion constructs, overlap extension PCR of the two fragments was performed using the primers listed for the fusion steps.

CLONING. GENERAL METHODS. Linear PCR fragments were cloned into the designated plasmids using ligation independent cloning (31).

ii. Primers used to generate the Abl-targeting construct

SNAPTAG-FUSION CONSTRUCT SEQUENCES:

SNAP(mA) = His6-SNAPtag-GTGT-monobody

SNAPTAG SEQUENCE:

DKDCEMKRTTLDSPLGKLELSGCEQGLHEIKLLGKGTSAADAVEVPAPAAVLGGPEPL
MQATAWLNAYFHQPEAIEEFPVPALHHPVFQQESFTRQVLWKLLKVVKFGEVISYQQL
AALAGNPAATAAVKTALSGNPVPILIPCHRVVSSSGAVGGYEGGLAVKEWLLAHEGHR
LGKPGLG

MONOBODY SEQUENCE:

GSSVSSVPTKLEVVAATPTSLLISWDAPMSSSSVYYYRITYGETGGNSPVQEFTVPYS

SSTATISGLSPGVDYTITVYAWGEDSAGYMFMYSPISINYRTC

SEQUENCE ENCODED BY PMCSG7:

MHHHHHHSSGVDLGTENLYFQSN

MONOBODY FRAGMENT:

Step 1:

Fwd: 5’ - AAA CCG GGT CTG GGA GGT ACG GGC ACC GGC TCT TCT GTT TCA - 3’

Rev: 5’ - TTAT CCA CTT CCA ATG CTA GCA AGT GCG ATA GTT - 3’

SNAPTAG FRAGMENT:

Step 2:

Fwd: 5’ - TAC TTC CAA TCC AAT GAC AAA GAT TGC GAA - 3’

Rev: 5’ - TGA AAC AGA AGA GCC GGT GCC CGT ACC TCC CAG ACC CGG TTT - 3’

FUSION PCR:

Step 3:

Fwd: 5’ - TAC TTC CAA TCC AAT GAC AAA GAT TGC GAA - 3’

Rev: 5’ - TTAT CCA CTT CCA ATG CTA GCA AGT GCG ATA GTT - 3’

iii. Primers used to generate pERK-targeting constructs

SNAPTAG-FUSION CONSTRUCT SEQUENCES:

SNAP(dpE57) = His6-SNAPtag-GSGTGSGS-DARPin pE57

SNAP(dpE59) = His6-SNAPtag-GSGTGSGS-DARPin pE59

SNAPTAG SEQUENCE:

DKDCEMKRTTLDSPLGKLELSGCEQGLHEIKLLGKGTSAADAVEVPAPAAVLGGPEPL

MQATAWLNAYFHQPEAIEEFPVPALHHPVFQQESFTRQVLWKLLKVVKFGEVISYQQL

AALAGNPAATAAVKTALSGNPVPILIPCHRVVSSSGAVGGYEGGLAVKEWLLAHEGHR

LGKPGLG

DARPIN PE57 SEQUENCE:

DLGKKLLEAARAGQDDEVRILVANGADVNALDEEGLTPLHLAAQMGHLEIVEVLLKNG

ADVNANDSYGITPLHLAATRGHLEIVEVLLKYGADVNAQDKFGKTAFDISIDNGNEDLA

EILQKLN

DARPIN PE59 SEQUENCE:

DLGKKLLEAARAGQDDEVRILMANGADVNALDEDGLTPLHLAAQLGHLEIVEVLLKYGA

DVNAEDNFGITPLHLAAIRGHLEIVEVLLKHGADVNAQDKFGKTAFDISIDNGNEDLAEIL

QKLN

SEQUENCE ENCODED BY PMCSG7:

MHHHHHHSSGVDLGTENLYFQSN

PE57 DARPIN FRAGMENT:

Step 1 (pE57):

Fwd: 5’ - GTA AAC CGG GTC TGG GAG GCA GCG GTA CGG GCT CGG GTT CCG

ATC TGG GGA AGA AAC TGC - 3’

Rev: 5’ - TTAT CCA CTT CCA ATG CTA GTT CAG TTT CTG GAG GAT TTC - 3’

PE59 DARPIN FRAGMENT:

Step 1 (pE59):

Fwd: 5’ - GGT AAA CCG GGT CTG GGA GGC AGC GGT ACG GGC TCG GGT TCC

GAT CTG GGT AAA AAA CTG CTG - 3’

Rev: 5’ - TTAT CCA CTT CCA ATG CTA GTT CAG TTT CTG GAG GAT TTC - 3’

SNAPTAG FRAGMENT:

Step 2 (pE57):

Fwd: 5’ - TAC TTC CAA TCC AAT GAC AAA GAT TGC GAA ATG AAA C - 3’

Rev: 5’ - GCA GTT TCT TCC CCA GAT CGG AAC CCG AGC CCG TAC CGC TGC CTC CCA GAC CCG GTT TAC - 3’

Step 2 (pE59):

Fwd: 5’ - TAC TTC CAA TCC AAT GAC AAA GAT TGC GAA ATG AAA C - 3’

Rev: 5’ - CAG CAG TTT TTT ACC CAG ATC GGA ACC CGA GCC CGT ACC GCT GCC TCC CAG ACC CGG TTT ACC - 3’

FUSION PCR:

Step 3 (pE57):

Fwd: 5’ - TAC TTC CAA TCC AAT GAC AAA GAT TGC GAA ATG AAA C - 3’

Rev: 5’ - TTAT CCA CTT CCA ATG CTA GTT CAG TTT CTG GAG GAT TTC - 3’

Step 3 (pE59):

Fwd: 5’ - TAC TTC CAA TCC AAT GAC AAA GAT TGC GAA ATG AAA C - 3’

Rev: 5’ - TTAT CCA CTT CCA ATG CTA GTT CAG TTT CTG GAG GAT TTC - 3’

iv. Site-directed mutagenesis to make *cd*SNAPtag mutants

Change of SNAPtag residue Cys144 to alanine was made using QuikChange mutagenesis and the following primers:

Fwd: 5’ - GCCGATTCTGATTCCG GC CCATCGTGTGGTTAGCTC - 3’

Rev: 5’ - GAGCTAACCACACGATGG GC CGGAATCAGAATCGGC - 3’

v. Protein expression and purification

SNAPtag protein plasmids were transformed into BL21(DE3) *e. coli* cells and three colonies were used to inoculate 250 mL of LB broth with ampicillin (100 µg/mL). Cultures were grown at 37 °C to an OD_{600} of 1.0, cooled to 18 °C and induced with 0.5 mM IPTG. Proteins were expressed at 18 °C overnight. Cells were harvested by centrifugation, and the pellets were stored at -80 °C. For protein purification, the pellets were thawed at 0 °C and resuspended in 8 mL of His6 lysis buffer (50 mM HEPES pH 7.5, 100 mM NaCl, 20 mM imidazole) supplemented with PMSF (1 mM) and a Pierce™ Protease Inhibitor Mini Tablet (EDTA-free) (Pierce #88666). The cells were lysed using sonication, and the lysate was cleared by centrifugation at 4 °C. The cleared lysate was added to 250 µL of 5 PRIME® PerfectPro Ni-NTA Agarose and rotated at 4 °C for 1 h. The resin was washed with His6 lysis buffer (15 × 1 mL) and eluted with His6 elution buffer (50 mM HEPES pH 7.5, 100 mM NaCl, 300 mM imidazole). The most concentrated fractions were pooled and exchanged into storage buffer (50 mM Tris, pH 7.5, 100 mM NaCl, 5 mM DTT). Proteins were analyzed by SDS-PAGE and found to be >95% pure by Coomassie stain. The proteins were separated into aliquots, snap-frozen and stored at -80 °C.

D. Bivalent inhibitor assembly and purification

(Protocol adapted from Mollwitz, *et al*.) (32) SNAPtag or the SNAPtag-intracellular antibody constructs were labeled with **4** using the following conditions. Purified SNAPtag protein (50 µM) was incubated with **4** (75 µM; 1.5-fold excess) in labeling buffer (20 mM Tris buffer, pH 8, 200 mM NaCl, and 4 mM DTT) for 2 h at 25 °C. The final reaction volume was 2.5 mL. The protein-small molecule conjugates were then

purified using GE Healthcare PD-10 Desalting Columns equilibrated with 50 mM HEPES pH 7.5, 150 mM NaCl, 1.5 mM $MgCl_2$, 5% glycerol and 1 mM DTT. Labeling reactions were purified twice using two PD-10 Desalting Columns according to the manufacturer's procedure. The concentration of the eluted protein was determined using Coomassie® Plus Protein Assay Reagent Kit. Constructs were snap-frozen and stored at -80 °C.

Thawed inhibitors were analyzed by LC-MS on a Bruker Esquire Ion Trap MS instrument and deconvoluted species compared to verify quantitative labeling.

E. Mass spectra of bivalent inhibitors assembled using 4.

Raw ESI spectra are seen on the left and deconvoluted mass spectra on the right.

SNAPtag-4 Calculated for $C_{1015}H_{1566}N_{280}O_{285}S_6$: 22443 Da. Observed: 22473 Da. Unlabeled species not observed.

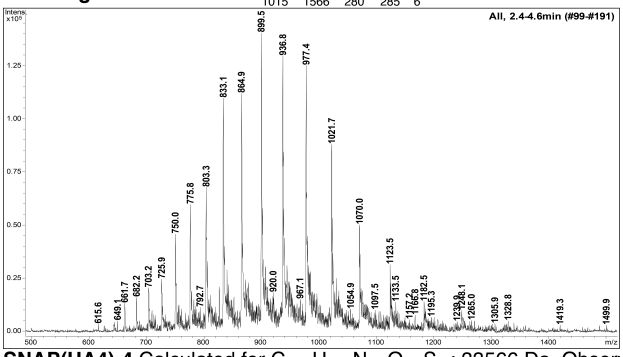

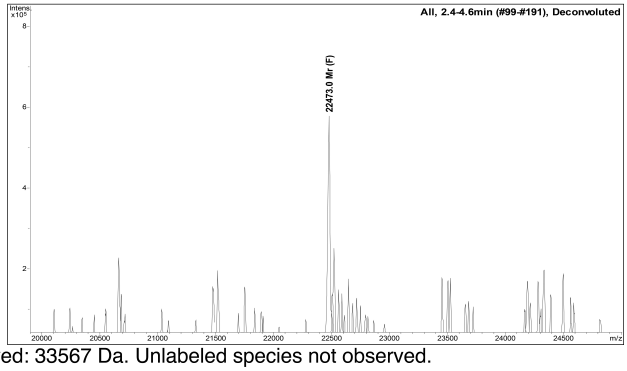

SNAP(HA4)-4 Calculated for $C_{1513}H_{2311}N_{397}O_{449}S_{10}$: 33566 Da. Observed: 33567 Da. Unlabeled species not observed.

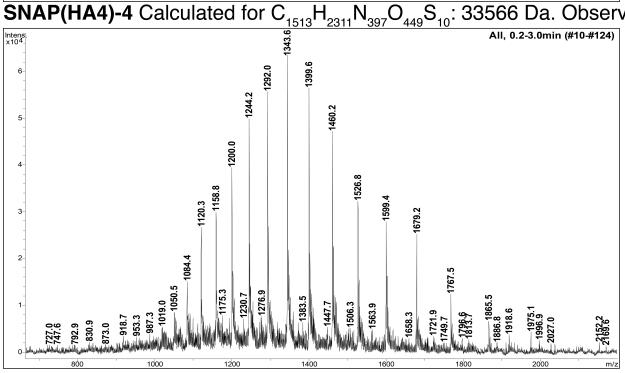

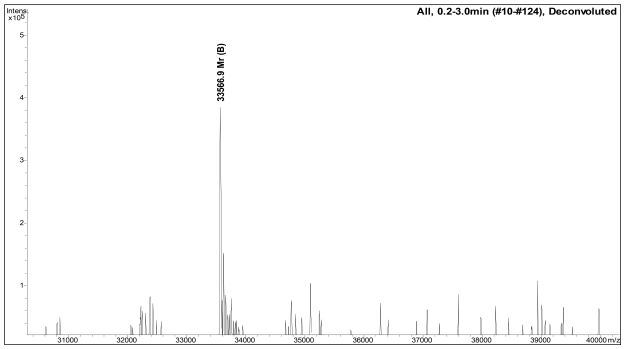

SNAP(pE57)-4 Calculated for $C_{1618}H_{2541}N_{449}O_{486}S_7$: 36283 Da. Observed: 36291 Da. Unlabeled species not observed.

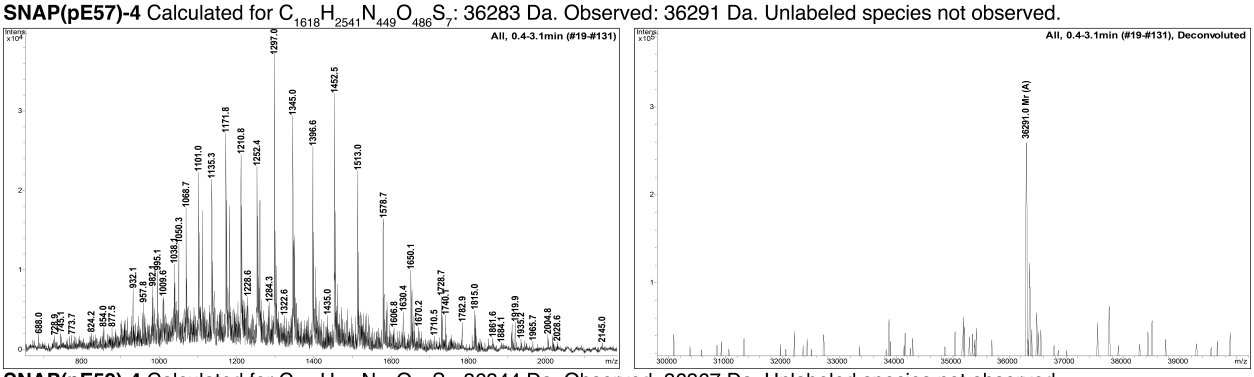

SNAP(pE59)-4 Calculated for $C_{1624}H_{2548}N_{450}O_{484}S_7$: 36344 Da. Observed: 36367 Da. Unlabeled species not observed.

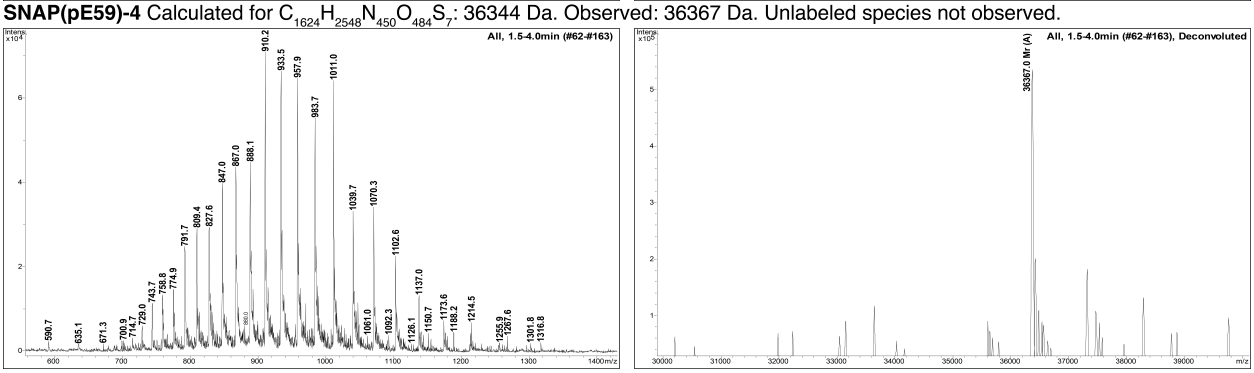

F. *In vitro* activity assay conditions

i. Assay conditions for Abl3D

ASSAY CONDITIONS FOR **4** AGAINST ABL3D. **4** (initial concentration in DMSO = 12.5 μM, 3-fold serial dilutions, 10 data points) was assayed in triplicate against Abl3D (final concentration = 0.8 nM) in assay buffer containing 75 mM HEPES, pH = 7.5, 150 mM NaCl, 15 mM $MgCl_2$, 3.75 mM EGTA, 0.2 mg/mL BSA, 3.75 mM DTT, 0.75 mM Na_3VO_4, 5% DMSO, γ^{32}P ATP (0.2 μCi/well) and an optimized Abl peptide substrate of the sequence Ac-EAIYAAPFAKKK (final concentration = 100 μM). The final volume of each assay well was 30 μL. The enzymatic reaction was run at room temperature for 2 hours and terminated by spotting 4.6 μL of the reaction mixture onto a phosphocellulose membrane. Membranes were washed with 0.5% phosphoric acid (4 × 10 minutes each wash), dried, and the radioactivity was determined by phosphorimaging with a GE Typhoon FLA 9000 phosphor scanner. The scanned membranes were quantified with

ImageQuant software and converted to percent inhibition. Data was analyzed using Prism Graphpad software and IC_{50} values were determined using non-linear regression analysis.

ASSAY CONDITIONS FOR SNAPTAG, SNAP(HA4) AND **4** CONJUGATES AGAINST ABL3D. SNAPtag proteins (initial concentration = 15-30 μM, 3-fold serial dilutions, 10 data points) were assayed in triplicate against Abl3D (final concentration = 0.8 nM) in assay buffer containing 75 mM HEPES, pH = 7.5, 150 mM NaCl, 15 mM $MgCl_2$, 3.75 mM EGTA, 0.2 mg/mL BSA, 3.75 mM DTT, 0.75 mM Na_3VO_4, $\gamma^{32}P$ ATP (0.2 μCi/well) and an optimized Abl peptide substrate of the sequence Ac-EAIYAAPFAKKK (final concentration = 100 μM). The final volume of each assay well was 30 μL. The enzymatic reaction was run at room temperature for 2 hours and terminated by spotting 4.6 μL of the reaction mixture onto a phosphocellulose membrane. Membranes were washed with 0.5% phosphoric acid (4 × 10 minutes each wash), dried, and the radioactivity was determined by phosphorimaging with a GE Typhoon FLA 9000 phosphor scanner. The scanned membranes were quantified with ImageQuant software and converted to percent inhibition. Data was analyzed using Prism Graphpad software and IC_{50} values were determined using non-linear regression analysis.

ii. Assay conditions for AblKD

ASSAY CONDITIONS FOR **4** AGAINST ABLKD. **4** (initial concentration in DMSO = 12.5 μM, 3-fold serial dilutions, 10 data points) was assayed in triplicate against AblKD (final concentration = 1 nM) in assay buffer containing 75 mM HEPES, pH = 7.5, 150 mM NaCl, 15 mM $MgCl_2$, 3.75 mM EGTA, 0.2 mg/mL BSA, 3.75 mM DTT, 0.75 mM Na_3VO_4, 5% DMSO, $\gamma^{32}P$ ATP (0.2 μCi/well) and an optimized Abl peptide substrate of

the sequence Ac-EAIYAAPFAKKK (final concentration = 100 μM). The final volume of each assay well was 30 μL. The enzymatic reaction was run at room temperature for 2 hours and terminated by spotting 4.6 μL of the reaction mixture onto a phosphocellulose membrane. Membranes were washed with 0.5% phosphoric acid (4 × 10 minutes each wash), dried, and the radioactivity was determined by phosphorimaging with a GE Typhoon FLA 9000 phosphor scanner. The scanned membranes were quantified with ImageQuant software and converted to percent inhibition. Data was analyzed using Prism Graphpad software and IC_{50} values were determined using non-linear regression analysis.

ASSAY CONDITIONS FOR SNAPTAG, SNAP(HA4) AND **4** CONJUGATES AGAINST ABLKD. SNAPtag proteins (initial concentration = 15-30 μM, 3-fold serial dilutions, 10 data points) were assayed in triplicate against Abl3D (final concentration = 1 nM) in assay buffer containing 75 mM HEPES, pH = 7.5, 150 mM NaCl, 15 mM $MgCl_2$, 3.75 mM EGTA, 0.2 mg/mL BSA, 3.75 mM DTT, 0.75 mM Na_3VO_4, $\gamma^{32}P$ ATP (0.2 μCi/well) and an optimized Abl peptide substrate of the sequence Ac-EAIYAAPFAKKK (final concentration = 100 μM). The final volume of each assay well was 30 μL. The enzymatic reaction was run at room temperature for 2 hours and terminated by spotting 4.6 μL of the reaction mixture onto a phosphocellulose membrane. Membranes were washed with 0.5% phosphoric acid (4 × 10 minutes each wash), dried, and the radioactivity was determined by phosphorimaging with a GE Typhoon FLA 9000 phosphor scanner. The scanned membranes were quantified with ImageQuant software and converted to percent inhibition. Data was analyzed using Prism Graphpad software and IC_{50} values were determined using non-linear regression analysis.

iii. Assay conditions for ERK2

ASSAY CONDITIONS FOR **4** AGAINST ERK2. **4** (initial concentration in DMSO = 12.5 μM, 3-fold serial dilutions, 10 data points) was assayed in triplicate against *in vitro* activated ERK2 (final concentration = 50 pM) in assay buffer containing 45 mM HEPES, pH = 7.5, 15 mM $MgCl_2$, 0.9 mM EGTA, 0.2 mg/mL BSA, 3.75 mM DTT, 2.5 mM β-glycerophosphate, 5% DMSO, $\gamma^{32}P$ ATP (0.2 μCi/well) and 0.2 mg/mL myelin basic protein. The final volume of each assay well was 30 μL. The enzymatic reaction was run at room temperature for 1 hour and terminated by spotting 4.6 μL of the reaction mixture onto a phosphocellulose membrane. Membranes were washed with 0.5% phosphoric acid (4 × 10 minutes each wash), dried, and the radioactivity was determined by phosphorimaging with a GE Typhoon FLA 9000 phosphor scanner. The scanned membranes were quantified with ImageQuant software and converted to percent inhibition. Data was analyzed using Prism Graphpad software and IC_{50} values were determined using non-linear regression analysis.

ASSAY CONDITIONS FOR SNAPTAG, SNAP(PE57), SNAP(PE59) AND **4** CONJUGATES AGAINST ERK2. SNAPtag proteins (initial concentration = 2-30 μM, 3-fold serial dilutions, 10 data points) were assayed in triplicate against *in vitro* activated ERK2 (final concentration = 50 pM) in assay buffer containing 45 mM HEPES, pH = 7.5, 15 mM $MgCl_2$, 0.9 mM EGTA, 0.2 mg/mL BSA, 3.75 mM DTT, 2.5 mM β-glycerophosphate, 5% DMSO, $\gamma^{32}P$ ATP (0.2 μCi/well) and 0.2 mg/mL myelin basic protein. The final volume of each assay well was 30 μL. The enzymatic reaction was run at room temperature for 1 hour and terminated by spotting 4.6 μL of the reaction mixture onto a phosphocellulose membrane. Membranes were washed with 0.5% phosphoric

acid (4 × 10 minutes each wash), dried, and the radioactivity was determined by phosphorimaging with a GE Typhoon FLA 9000 phosphor scanner. The scanned membranes were quantified with ImageQuant software and converted to percent inhibition. Data was analyzed using Prism Graphpad software and IC_{50} values were determined using non-linear regression analysis.

iv. Assay conditions for JNK2

ASSAY CONDITIONS FOR **4** AGAINST JNK2. **4** (initial concentration in DMSO = 12.5 μM, 3-fold serial dilutions, 10 data points) was assayed in triplicate against *in vitro* activated JNK2 (final concentration = 2 nM) in assay buffer containing 45 mM HEPES, pH = 7.5, 15 mM $MgCl_2$, 0.9 mM EGTA, 0.2 mg/mL BSA, 3.75 mM DTT, 2.5 mM β-glycerophosphate, 5% DMSO, $\gamma^{32}P$ ATP (0.2 μCi/well) and 0.2 mg/mL myelin basic protein. The final volume of each assay well was 30 μL. The enzymatic reaction was run at room temperature for 4 hours and terminated by spotting 4.6 μL of the reaction mixture onto a phosphocellulose membrane. Membranes were washed with 0.5% phosphoric acid (4 × 10 minutes each wash), dried, and the radioactivity was determined by phosphorimaging with a GE Typhoon FLA 9000 phosphor scanner. The scanned membranes were quantified with ImageQuant software and converted to percent inhibition. Data was analyzed using Prism Graphpad software and IC_{50} values were determined using non-linear regression analysis.

ASSAY CONDITIONS FOR SNAPTAG-**4**, SNAP(PE57)-**4** AND SNAP(PE59)-**4** AGAINST JNK2. SNAPtag proteins (initial concentration = 10 μM, 3-fold serial dilutions, 10 data points) were assayed in triplicate against *in vitro* activated JNK2 (final concentration = 2 nM) in assay buffer containing 45 mM HEPES, pH = 7.5, 15 mM

$MgCl_2$, 0.9 mM EGTA, 0.2 mg/mL BSA, 3.75 mM DTT, 2.5 mM β-glycerophosphate, 5% DMSO, $\gamma^{32}P$ ATP (0.2 μCi/well) and 0.2 mg/mL myelin basic protein. The final volume of each assay well was 30 μL. The enzymatic reaction was run at room temperature for 4 hours and terminated by spotting 4.6 μL of the reaction mixture onto a phosphocellulose membrane. Membranes were washed with 0.5% phosphoric acid (4 × 10 minutes each wash), dried, and the radioactivity was determined by phosphorimaging with a GE Typhoon FLA 9000 phosphor scanner. The scanned membranes were quantified with ImageQuant software and converted to percent inhibition. Data was analyzed using Prism Graphpad software and IC_{50} values were determined using non-linear regression analysis.

v. Assay conditions for p38α

ASSAY CONDITIONS FOR **4** AGAINST P38α. **4** (initial concentration in DMSO = 12.5 μM, 3-fold serial dilutions, 10 data points) was assayed in triplicate against *in vitro* activated p38α (final concentration = 2 nM) in assay buffer containing 45 mM HEPES, pH = 7.5, 15 mM $MgCl_2$, 0.9 mM EGTA, 0.2 mg/mL BSA, 3.75 mM DTT, 2.5 mM β-glycerophosphate, 5% DMSO, $\gamma^{32}P$ ATP (0.2 μCi/well) and 0.2 mg/mL myelin basic protein. The final volume of each assay well was 30 μL. The enzymatic reaction was run at room temperature for 3 hours and terminated by spotting 4.6 μL of the reaction mixture onto a phosphocellulose membrane. Membranes were washed with 0.5% phosphoric acid (4 × 10 minutes each wash), dried, and the radioactivity was determined by phosphorimaging with a GE Typhoon FLA 9000 phosphor scanner. The scanned membranes were quantified with ImageQuant software and converted to

percent inhibition. Data was analyzed using Prism Graphpad software and IC_{50} values were determined using non-linear regression analysis.

ASSAY CONDITIONS FOR SNAPTAG-**4**, SNAP(PE57)-**4** AND SNAP(PE59)-**4** AGAINST P38α. SNAPtag proteins (initial concentration = 10 μM, 3-fold serial dilutions, 10 data points) were assayed in triplicate against *in vitro* activated p38α (final concentration = 2 nM) in assay buffer containing 45 mM HEPES, pH = 7.5, 15 mM $MgCl_2$, 0.9 mM EGTA, 0.2 mg/mL BSA, 3.75 mM DTT, 2.5 mM β-glycerophosphate, 5% DMSO, γ^{32}P ATP (0.2 μCi/well) and 0.2 mg/mL myelin basic protein. The final volume of each assay well was 30 μL. The enzymatic reaction was run at room temperature for 3 hours and terminated by spotting 4.6 μL of the reaction mixture onto a phosphocellulose membrane. Membranes were washed with 0.5% phosphoric acid (4 × 10 minutes each wash), dried, and the radioactivity was determined by phosphorimaging with a GE Typhoon FLA 9000 phosphor scanner. The scanned membranes were quantified with ImageQuant software and converted to percent inhibition. Data was analyzed using Prism Graphpad software and IC_{50} values were determined using non-linear regression analysis.

G. Size exclusion chromatographic analysis of SNAP(HA4)-4

Purified SNAP(HA4)-**4** (110 μg) or Abl3D (80 μg) were subjected to analytical gel filtration using a Superdex 200 10/300 GL column (GE Healthcare) equilibrated in 50 mM HEPES pH 7.5, 300 mM NaCl. The Abl3D/SNAP(HA4)-**4** complex was prepared by combining a 1:1 mixture of the two purified proteins at 10 μM in equilibration buffer at a final volume of 100 μL. Column calibration was performed using molecular weight

standards conalbumin (GE Healthcare) and aldolase (Worthington Biochemical Corporation).

H. *In vitro* effects of SNAP(pE57) and SNAP(pE59) on ERK2 phosphorylation by MEK

SNAPtag proteins (1-9 μM) were pre-incubated in quadruplicate with unphosphorylated ERK2 (final concentration = 40 nM) in assay buffer containing 50 mM MOPS, pH = 7.5, 10 mM $MgCl_2$, 1 mM DTT and 0.001% Tween-20. The initial volume of each assay well was 40 μL and the proteins were pre-incubated at room temperature for 2 hours. His6-MEK2 was added (final concentration = 3.1 nM) to the mixture in buffer containing 50 mM HEPES pH 7.5, 300 mM NaCl and 0.1 mg/mL BSA. ATP was added (final concentration = 5 mM) and the final volume in each assay well was 50 μL. The enzymatic reaction was run at room temperature for 2 hours and terminated by adding 25 μL 3X SDS loading buffer (240 mM Tris-Cl pH 6.8, 6% (w/v) SDS, 0.06% (w/v) bromophenol blue, 30% glycerol and 16 % β-mercaptoethanol). Phosphorylated proteins were separated by SDS-PAGE, transferred to nitrocellulose using a Trans-Blot®Turbo™ Instrument (Bio-Rad) and detected by immunoblot for phosphorylated ERK (Cell Signaling Technology #4370) and total ERK (Cell Signaling Technology #9107). Secondary detection was achieved using IRDye secondary antibodies (Li-Cor #926-32211 and #926-68070). The scanned blots were quantified with Li-Cor Odyssey software to determine percentage of phosphorylated ERK relative to a control.

I. Cellular assays

i. General methods

MAMMALIAN CELL CULTURE. GENERAL METHODS. K562 cells were cultured in RPMI media supplemented with 10% fetal bovine serum and penicillin/streptomycin. Cells were incubated at 37 °C in a humidified atmosphere containing 5% CO_2.

ii. Cellular blocking assays

CELLULAR BLOCKING ASSAYS. K562 cells (2 x 10^5) were transfected with SNAP(HA4) (1 µg) using Lipofectamine 2000 (Invitrogen) in 1 mL antibiotic-free RPMI for 24 hours. Transfected cells were incubated with **5** (2.5-10 µM) or DMSO in 1050 µL serum-free growth medium (RPMI) with a final DMSO content of 0.2%. After incubation at 37°C (5% CO_2) for 1 h, cells were incubated in serum-free growth medium containing SNAP-Cell® TMR-star (New England Biolabs, final concentration = 3 µM, 0.4% DMSO). Cells were incubated with the fluorophore for 30 min at 37 °C (5% CO_2). Cells were pelleted and washed with DPBS (1 x 1 mL) and lysed using 50 µL 1X SDS sample buffer. Lysed samples were boiled for 30 min before being subjected to SDS-PAGE. Fluorescence was measured with a GE Typhoon FLA 9000 scanner and quantified using ImageQuant software. Proteins were transferred to nitrocellulose and probed with Anti-SNAPtag® Antibody (Polyclonal, New England Biolabs #P9310). Secondary detection was achieved using IRDye secondary antibody (Li-Cor #926-32211). The scanned blots were quantified with Li-Cor Odyssey software and fluorescent signal was corrected for well-to-well transfection variations. All data points were performed in duplicate.

iii. Flow cytometry

FLOW CYTOMETRY. GENERAL METHODS. For phosphoflow analyses, K562 cells were transfected with the following SNAPtag plasmids. *cd*SNAPtag (Cys144Ala) in a pcDNA5 flag-tagged vector. SNAP(HA4) in pcFlagLIC. *cd*SNAP(HA4) (Cys144Ala) in pcFlagLIC. SNAPtag in pcDNA3.2V5. Flow cytometry was performed with a LSR II (BD Biosciences) using standard methods.

PHOSPHOFLOW ANALYSES. (Protocol adapted from Shah et al.) (33) K562 cells (5 x 10^5) were transfected with desired SNAPtag construct (2 µg) using Lipofectamine 2000 (Invitrogen) in 2 mL antibiotic-free RPMI for 24 hours. Transfected cells were incubated with **5** (1.25-5 µM) or DMSO in 2300 µL serum-free growth medium (RPMI) with a final DMSO content of 0.2%. After incubation at 37°C (5% CO_2) for 1 h, cells were fixed using 4% paraformaldehyde in DPBS for 20 min at room temperature. Following centrifugation cell pellets were aspirated and resuspended in 90% methanol and stored overnight at −20 °C. Cells were rehydrated by resuspending in 5 mg/mL BSA in DPBS and blocked in this buffer for 10 min at room temperature. Cells were stained with 100 µL of an antibody mix containing 10 µL phospho-STAT5 Alexa Fluor® 647 antibody (BD Biosciences #612599) and a 1:200 dilution of Flag-FITC antibody (Sigma #F4049) in blocking buffer; staining proceeded for 30 min at room temperature in darkness. Cells were washed with DPBS (2 x 3 mL), aspirated, and resuspended in 300 µL DPBS + 1 µg/mL DNAseI. Approximately 5000 Flag-positive events were collected for each sample on a LSR II (BD Biosciences) and analyzed using FlowJo software (Tree Star, Inc.). All analyses were performed at least in triplicate and yielded similar results. The SNAPtag pcDNA3.2V5 was used as a no-Flag control. The *cd*SNAPtag pcDNA5 flag-

tagged vector was used as a vehicle for experiments without the HA4 portion of the bivalent inhibitor.

J. Quantitative Chemical Proteomics

i. Synthesis of 3-based affinity matrix

For synthesis of **3**-derivatized resin, 2 mL packed resin volume of NHS-activated sepharose 4 fast flow (GE Healthcare) was washed 3X with 10 mL anhydrous DMSO (Sigma-Aldrich). To the washed NHS-activated sepharose resin 8 mL of 0.5 mM amine **3** in anhydrous DMSO (2 µmol compound/mL of resin) was then added and 30 µL triethylamine (Sigma-Aldrich). The reaction mixture was vortexed to mix and spun at 100 x g for 2 min. A 50 µL aliquot of the supernatant was saved for LC/MS analysis. The reaction mixture was allowed incubate overnight at room temp with end-over-end rotating agitation. The following day, the reaction mixture was spun at 100 x g for 2 min. A 50 µL aliquot of the supernatant was saved for LC/MS analysis. Completion of coupling was inferred by loss of starting material following LC/MS analysis. 100 µL ethanolamine (Sigma-Aldrich) was added to the reaction mixture, vortexed, and allowed to incubate overnight at room temp with end-over-end agitation. After which, the **3**-derivatized resin was washed 3X with 10 mL anhydrous DMSO and 3X with 95% EtOH.

ii. K562 lysate generation

K562 cell pellets were thawed on ice and resuspended in 2X cell pellet volume with cold Lysis buffer (50 mM HEPES (pH 7.4), 150 mM NaCl, 1.5 mM $MgCl_2$, 1 mM DTT, 0.8% NP-40, 1X HALT protease inhibitor (Peirce Biotechnology)). The resuspended cell pellet was lysed by dounce homogenization (10 strokes with tight fitting pestle), then spun at 800 x g for 10 min at 4°C. The resulting supernatant (S0.8) was saved, while the pellet

(P0.8) was processed further. The P0.8 pellet was first resuspended with cold 0.5X pellet volume Low Salt Buffer (20 mM HEPES (pH7.4), 25% glycerol, 1.5 mM $MgCl_2$, 0.2 mM EDTA, 1 mM DTT, 1X HALT protease inhibitor), then cold 0.5X pellet volume of High Salt Buffer (Low Salt Buffer + 2.4 M NaCl) was added dropwise. The resuspended P0.8 pellets were further lysed via pressure cycling (Barocycler NEP2320, Pressure Biosciences Inc.) with 5 cycles of 35,000 PSI for 20 sec followed by atmospheric pressure for 20 sec at 4 °C, treated with benzonase (Sigma) at a final concentration of 90 units/mL overnight at 4 °C; after which the P0.8 lysate was centrifuged at 14,000 x g for 20 min at 4 °C. The S0.8 and P0.8 lysates were combined at a ratio of 9:1 and this combined lysate was used as input material for affinity enrichment experiments.

iii. Affinity enrichment and compound competition experiments in K562 lysates

For each affinity enrichment condition, 1 mL of K562 lysate (5 mg) was preincubated with either varying concentration of competition compound or DMSO control for 1 hr at 4 °C. During this pre-incubation, the **3**-derivatized sepharose beads (35 µL per sample) were washed 3X with 3 mL Wash Buffer 2 (50 mM HEPES (pH 7.4), 150 mM NaCl, 1.5 mM MgCl2, 1 mM DTT, 0.4% NP-40). Preincubated lysates were then incubated with **3**-derivatized resin for 4 hrs at 4 °C with end-over-end agitation. The beads were transferred to individual columns (MoBiTec), washed with 3 mL Wash Buffer 2 then 1.5 mL Wash Buffer 1 (50 mM HEPES (pH 7.4), 150 mM NaCl, 1.5 mM $MgCl_2$, 1 mM DTT). To elute bound proteins, 50 µL 2X LDS sample buffer (NuPAGE) + 10 mM DTT was added to each sample, which were incubated at 55 °C for 30 min. Eluted proteins were separated from resin by centrifugation (14,000 x g for 2 min at room temp). Proteins were alkylated with 200 mg/mL iodoacetamide for 30 min**.**

iv. Sample preparation and mass spectrometry data acquisition and analysis

Proteins were subjected to in-solution trypsinization over night at 37 °C followed by isobaric labeling using TMT 6plex reagents (Thermo Fisher) using the labels 126-130 for varying concentrations of competitor compound and 131 for the DMSO-treated control sample. Samples were mixed and separated using high pH reverse phase chromatography (Dionex Ultimate 3000 HPLC, Waters Xbridge column (1 mm x15 cm), mobile phase A: 100% H_2O; mobile phase B: 100% MeCN; mobile phase C (modifier, constant at 10%): 200 mM ammonium formate, pH 10; flow rate: 250 µl/min, 60 min effective gradient). Fractions were pooled to 16 samples which were analyzed by nanocapillary liquid chromatography-tandem mass spectrometry on an Easy-nLC 1000 HPLC system coupled to a Q-Exactive mass spectrometer (Thermo Scientific), using an in-house fabricated 75 µm ID spraying capillary packed with ReproSil-Pur 120 C_{18}-AQ, 3 µm material (Dr. Maisch GmbH; 150 mm bed length) with a vented trapping column set-up (1 cm Michrom Magic C_{18}AQ, 5 µm). The peptides were eluted with a gradient of 3% Buffer B (70% acetonitrile in 0.1% formic acid) to 45% B in 80 min (0.5% B/min) delivered at a flow rate of 300 nL/min and using a top 12 HCD data-dependent acquisition method. Peptide mass and fragmentation data were searched against a combined forward-reverse UniProt canonical human protein sequence database (version Jan 9 2013) supplemented with typical lab contaminants using Mascot (Matrix Science). Precursor and fragment ion tolerances were set to 10 ppm and 0.1 Da, respectively, allowing for 2 missed tryptic cleavages. Carbamidomethyl (C) was selected as fixed modification and TMT6 (K), TMT6 (N-term), Oxidation (M) as variable modifications. Peptide and protein validation was done using Transproteomic pipeline

v3.3sqall (Institute for Systems Biology; http://tools.proteomecenter.org/software.php) using a false positive threshold of <1% for protein identifications. For each peptide sequence and modification state, reporter ion signal intensities from all spectral matches were summed for each reporter ion type and corrected according to the isotope correction factors given by the manufacturer. Only peptides unique to a given protein within the total dataset of identified proteins were used for relative protein quantification. Peptide fold changes were calculated (treatment over DMSO control) and subsequently renormalized within each replicate analysis using the median fold change of all quantified peptides to compensate for differences in total protein yield for each affinity purification. Protein fold changes were calculated as median peptide fold change and p-values were calculated using a one-way T-test (arbitrarily set to 1 for non-significant single peptide quantitations) and adjusted using the Benjamini-Hochberg False Discovery Rate (FDR). Data were visualized for further analysis using Spotfire DXP. For calculating residual binding 50 values resulting from competitor competition, for each protein the percent residual binding at each concentration was calculated (100*10^(protein fold change)). XLfit was used for curve fitting and determination of RB_{50} values using a constrained 4 parameter single-site dose-response model (eq 200): (A+(B/(1+((x/C)^D)))); where A is the low end of the curve fit (set = 0% residual binding), B is the high end of curve fit (set = 100% residual binding), and D is the Hill slope (set = 1). For detection and quantitation of phosphorylated ERK2, targeted MS analysis was performed using Accurate Inclusion Mass Spectrometry as described (34). Briefly, a peptide list was generated by *in silico* trypsinization of ERK2 using the ProteinProspector software (http://prospector.ucsf.edu) and corresponding peptides with

and without phosphorylation on Serine and Threonine were selected for an inclusion list. This list was used for targeted re-analysis of samples on an Orbitrap Elite mass spectrometer (Thermo Scientific) using the same nanoLC-MS configuration as described above for the Q-Exactive-based system.

K. KINOMEscan^{TM} of 2.

KINOMEscan is a competition-based binding assay that measures the ability of test compounds to compete with an immobilized, active-site binding ligand. Compound **2** was screened at 10 μM and the binding interaction is reported as "% Ctrl" by the following calculation: [(test compound signal-positive control signal)/(negative control signal-positive control signal)]*100. Negative control = DMSO (set to 100% Ctrl) and positive control = control compound (set to 0% Ctrl).

Ambit Gene Symbol	%Ctrl @ 10000nM
AAK1	0.05
ABL1(E255K)-phosphorylated	0
ABL1(F317I)-nonphosphorylated	6.4
ABL1(F317I)-phosphorylated	0
ABL1(F317L)-nonphosphorylated	3.7
ABL1(F317L)-phosphorylated	0.05
ABL1(H396P)-nonphosphorylated	0
ABL1(H396P)-phosphorylated	0
ABL1(M351T)-phosphorylated	0
ABL1(Q252H)-nonphosphorylated	0
ABL1(Q252H)-phosphorylated	0
ABL1(T315I)-nonphosphorylated	1.6
ABL1(T315I)-phosphorylated	0
ABL1(Y253F)-phosphorylated	0
ABL1-nonphosphorylated	0
ABL1-phosphorylated	0
ABL2	0
ACVR1	0
ACVR1B	3.4
ACVR2A	0.25
ACVR2B	0.35
ACVRL1	0
ADCK3	67
ADCK4	35
AKT1	100
AKT2	100
AKT3	100
ALK	0
AMPK-alpha1	0
AMPK-alpha2	0.05
ANKK1	0
ARK5	0.05
ASK1	11
ASK2	48
AURKA	0
AURKB	0
AURKC	0.35
AXL	0
BIKE	1.4

0 ≤ x ≤1
1 ≤ x ≤10
10 ≤ x ≤35
<35

Ambit Gene Symbol	%Ctrl @ 10000nM
BLK	0
BMPR1A	0.45
BMPR1B	0
BMPR2	0
BMX	1.2
BRAF	27
BRAF(V600E)	25
BRK	4.2
BRSK1	19
BRSK2	8.6
BTK	0.15
CAMK1	0.05
CAMK1D	0.2
CAMK1G	43
CAMK2A	1.9
CAMK2B	5.8
CAMK2D	2.4
CAMK2G	5
CAMK4	100
CAMKK1	0.15
CAMKK2	0.15
CASK	8.8
CDC2L1	48
CDC2L2	44
CDC2L5	0
CDK11	92
CDK2	0
CDK3	0
CDK4-cyclinD1	0
CDK4-cyclinD3	0
CDK5	0.15
CDK7	0.15
CDK8	85
CDK9	1.4
CDKL1	0
CDKL2	0.05
CDKL3	0
CDKL5	0
CHEK1	0.55
CHEK2	0
CIT	0.05
CLK1	0.15
CLK2	0.4

Ambit Gene Symbol	%Ctrl @ 10000nM
CLK3	0.75
CLK4	0
CSF1R	0.1
CSK	2.4
CSNK1A1	18
CSNK1A1L	42
CSNK1D	99
CSNK1E	28
CSNK1G1	77
CSNK1G2	51
CSNK1G3	54
CSNK2A1	0
CSNK2A2	0
CTK	17
DAPK1	0.2
DAPK2	1.8
DAPK3	0.75
DCAMKL1	0
DCAMKL2	1.6
DCAMKL3	0.05
DDR1	0
DDR2	0
DLK	0
DMPK	0.55
DMPK2	3.8
DRAK1	0
DRAK2	0.15
DYRK1A	0
DYRK1B	0.2
DYRK2	0
EGFR	14
EGFR(E746-A750del)	2.7
EGFR(G719C)	24
EGFR(G719S)	33
EGFR(L747-E749del,	A750P)
EGFR(L747-S752del,	P753S)
EGFR(L747-T751del,Sins)	5.5
EGFR(L858R)	2.9
EGFR(L858R,T790M)	0
EGFR(L861Q)	22
EGFR(S752-I759del)	9.5
EGFR(T790M)	2
EIF2AK1	37

Ambit Gene Symbol	%Ctrl @ 10000nM
EPHA1	0.15
EPHA2	0.2
EPHA3	0.05
EPHA4	0.4
EPHA5	0
EPHA6	0
EPHA7	0
EPHA8	0.55
EPHB1	0
EPHB2	0
EPHB3	1.4
EPHB4	0
EPHB6	0
ERBB2	76
ERBB3	6.4
ERBB4	32
ERK1	5.8
ERK2	7.1
ERK3	0.1
ERK4	0.9
ERK5	14
ERK8	0.05
ERN1	1.8
FAK	0
FER	0.15
FES	1.3
FGFR1	0.1
FGFR2	0.25
FGFR3	0
FGFR3(G697C)	0
FGFR4	0.2
FGR	0.1
FLT1	0
FLT3	0.05
FLT3(D835H)	0
FLT3(D835Y)	0
FLT3(ITD)	0
FLT3(K663Q)	0
FLT3(N841I)	0.05
FLT3(R834Q)	0.45
FLT4	0
FRK	1.2
FYN	0.1

Ambit Gene Symbol	%Ctrl @ 10000nM
GAK	1.1
GCN2(Kin.Dom.2,S808G)	0.15
GRK1	2.7
GRK4	0.6
GRK7	0
GSK3A	0
GSK3B	0
HCK	0
HIPK1	0
HIPK2	0
HIPK3	0
HIPK4	0
HPK1	0
HUNK	5.3
ICK	0
IGF1R	0.05
IKK-alpha	0
IKK-beta	4.5
IKK-epsilon	1.2
INSR	0
INSRR	0
IRAK1	0
IRAK3	0.15
IRAK4	0
ITK	0
JAK1(JH1domain-catalytic)	0.1
JAK1(JH2domain-pseudokinase)	0
JAK2(JH1domain-catalytic)	0
JAK3(JH1domain-catalytic)	0
JNK1	0.85
JNK2	0.05
JNK3	0
KIT	0
KIT(A829P)	0.85
KIT(D816H)	0.05
KIT(D816V)	0.05
KIT(L576P)	0.1
KIT(V559D)	0
KIT(V559D,T670I)	0.4
KIT(V559D,V654A)	1.1
LATS1	0.35
LATS2	0
LCK	0

Ambit Gene Symbol	%Ctrl @ 10000nM
LIMK1	1
LIMK2	7.6
LKB1	0.55
LOK	0
LRRK2	0
LRRK2(G2019S)	0.1
LTK	0.85
LYN	1.1
LZK	4
MAK	1.4
MAP3K1	0
MAP3K15	35
MAP3K2	0
MAP3K3	0
MAP3K4	10
MAP4K2	0
MAP4K3	0.1
MAP4K4	0
MAP4K5	0.05
MAPKAPK2	100
MAPKAPK5	0
MARK1	2.7
MARK2	0.75
MARK3	3
MARK4	0.65
MAST1	0
MEK1	0
MEK2	0
MEK3	0
MEK4	0.9
MEK5	0
MEK6	1
MELK	0
MERTK	0
MET	0
MET(M1250T)	0
MET(Y1235D)	0
MINK	0.35
MKK7	24
MKNK1	55
MKNK2	0
MLCK	0
MLK1	0

Ambit Gene Symbol	%Ctrl @ 10000nM
MLK2	0
MLK3	0
MRCKA	14
MRCKB	3
MST1	0
MST1R	5.2
MST2	2.4
MST3	0
MST4	0.65
MTOR	97
MUSK	0.15
MYLK	10
MYLK2	0.1
MYLK4	0
MYO3A	0.4
MYO3B	0
NDR1	0.15
NDR2	0.95
NEK1	5
NEK11	49
NEK2	1.6
NEK3	0
NEK4	43
NEK5	0.1
NEK6	0
NEK7	0
NEK9	0.15
NIM1	30
NLK	45
OSR1	4.6
p38-alpha	100
p38-beta	100
p38-delta	22
p38-gamma	38
PAK1	1.2
PAK2	24
PAK3	0.45
PAK4	0.45
PAK6	0.05
PAK7	0
PCTK1	0.05
PCTK2	0.6
PCTK3	0.95

Ambit Gene Symbol	%Ctrl @ 10000nM
PDGFRA	0.2
PDGFRB	0
PDPK1	18
PFCDPK1(P.falciparum)	0.25
PFPK5(P.falciparum)	66
PFTAIRE2	1.6
PFTK1	2.4
PHKG1	1.2
PHKG2	1
PIK3C2B	100
PIK3C2G	100
PIK3CA	100
PIK3CA(C420R)	100
PIK3CA(E542K)	100
PIK3CA(E545A)	100
PIK3CA(E545K)	100
PIK3CA(H1047L)	93
PIK3CA(H1047Y)	89
PIK3CA(I800L)	100
PIK3CA(M1043I)	100
PIK3CA(Q546K)	100
PIK3CB	100
PIK3CD	100
PIK3CG	99
PIK4CB	74
PIM1	70
PIM2	100
PIM3	76
PIP5K1A	1
PIP5K1C	0
PIP5K2B	0.1
PIP5K2C	32
PKAC-alpha	15
PKAC-beta	5
PKMYT1	68
PKN1	0
PKN2	3.4
PKNB(M.tuberculosis)	0.2
PLK1	0.55
PLK2	1
PLK3	5.2
PLK4	0
PRKCD	4.8

Ambit Gene Symbol	%Ctrl @ 10000nM
PRKCE	0
PRKCH	1.8
PRKCI	41
PRKCQ	0
PRKD1	0.3
PRKD2	0
PRKD3	0.4
PRKG1	1.1
PRKG2	1.8
PRKR	0.8
PRKX	46
PRP4	0
PYK2	0.15
QSK	0.45
RAF1	100
RET	0
RET(M918T)	0
RET(V804L)	0
RET(V804M)	0
RIOK1	0.4
RIOK2	0
RIOK3	0
RIPK1	0
RIPK2	9.9
RIPK4	0.05
RIPK5	6
ROCK1	14
ROCK2	15
ROS1	0.05
RPS6KA4(Kin.Dom.1-N-terminal)	0.4
RPS6KA4(Kin.Dom.2-C-terminal)	0.15
RPS6KA5(Kin.Dom.1-N-terminal)	0.85
RPS6KA5(Kin.Dom.2-C-terminal)	4.4
RSK1(Kin.Dom.1-N-terminal)	0.2
RSK1(Kin.Dom.2-C-terminal)	9
RSK2(Kin.Dom.1-N-terminal)	0
RSK3(Kin.Dom.1-N-terminal)	0
RSK3(Kin.Dom.2-C-terminal)	0.5
RSK4(Kin.Dom.1-N-terminal)	0
RSK4(Kin.Dom.2-C-terminal)	7.8

Ambit Gene Symbol	%Ctrl @ 10000nM
S6K1	0.8
SBK1	1.7
SgK110	0
SGK3	0.3
SIK	0.1
SIK2	3
SLK	0
SNARK	11
SNRK	29
SRC	0
SRMS	0.1
SRPK1	0
SRPK2	0.25
SRPK3	0.15
STK16	0
STK33	0
STK35	1
STK36	21
STK39	3.9
SYK	0
TAK1	0.05
TAOK1	0.45
TAOK2	0.45
TAOK3	0
TBK1	0.35
TEC	4.2
TESK1	23
TGFBR1	0.85
TGFBR2	0
TIE1	0.65
TIE2	0.4
TLK1	0.05
TLK2	0
TNIK	0
TNK1	0.15
TNK2	0.25
TNNI3K	13
TRKA	0
TRKB	0.45
TRKC	0.05
TRPM6	81
TSSK1B	1.6
TTK	0.3

Ambit Gene Symbol	%Ctrl @ 10000nM
TXK	0.25
TYK2(JH1domain-catalytic)	0.05
TYK2(JH2domain-pseudokinase)	0
TYRO3	15
ULK1	0
ULK2	0
ULK3	0
VEGFR2	0
VRK2	42
WEE1	1.4
WEE2	0.1
YANK1	10
YANK2	2
YANK3	33
YES	0
YSK1	1.4
YSK4	0.45
ZAK	0.45
ZAP70	0

L. Gene sequences

Affinity tag/vector sequence = red
SNAPtag = orange
Flexible linker = green
Intracellular antibody = blue

SNAP(HA4)
ATGCACCATCATCATCATCATTCTTCTGGTGTAGATCTGGGTACCGAGAACCTGTA
CTTCCAATCCAATGACAAAGATTGCGAAATGAAACGTACCACCCTGGATAGCCCGC
TGGGCAAACTGGAACTGAGCGGCTGCGAACAGGGCCTGCATGAAATTAAACTGCT
GGGTAAAGGCACCAGCGCGGCCGATGCGGTTGAAGTTCCGGCCCCGGCCGCCGT
GCTGGGTGGTCCGGAACCGCTGATGCAGGCGACCGCGTGGCTGAACGCGTATTT
TCATCAGCCGGAAGCGATTGAAGAATTTCCGGTTCCGGCGCTGCATCATCCGGTG
TTTCAGCAGGAGAGCTTTACCCGTCAGGTGCTGTGGAAACTGCTGAAAGTGGTTAA
ATTTGGCGAAGTGATTAGCTATCAGCAGCTGGCGGCCCTGGCGGGTAATCCGGCG
GCCACCGCCGCCGTTAAAACCGCGCTGAGCGGTAACCCGGTGCCGATTCTGATTC
CGTGCCATCGTGTGGTTAGCTCTAGCGGTGCGGTTGGCGGTTATGAAGGTGGTCT
GGCGGTGAAAGAGTGGCTGCTGGCCCATGAAGGTCATCGTCTGGGTAAACCGGG
TCTGGGAGGTACGGGCACCGGCTCTTCTGTTTCAAGCGTTCCGACCAAGCTGGAG
GTTGTTGCTGCCACACCGACAAGTCTGCTGATTTCATGGGATGCCCCGATGAGCT
CCTCTAGTGTTTATTACTATCGCATTACATACGGCGAAACCGGCGGTAACAGCCCG
GTGCAGGAGTTTACCGTTCCCTATTCAAGCTCCACCGCCACAATTTCTGGGCTGAG

CCCGGGAGTCGATTACACTATCACCGTGTATGCGTGGGGTGAAGACTCAGCAGGG
TATATGTTTATGTATTCTCCCATCTCCATCAACTATCGCACTTGCTAG

SNAP(pE57)
ATGCACCATCATCATCATCATTCTTCTGGTGTAGATCTGGGTACCGAGAACCTGTA
CTTCCAATCCAATGACAAAGATTGCGAAATGAAACGTACCACCCTGGATAGCCCGC
TGGGCAAACTGGAACTGAGCGGCTGCGAACAGGGCCTGCATGAAATTAAACTGCT
GGGTAAAGGCACCAGCGCGGCCGATGCGGTTGAAGTTCCGGCCCCGGCCGCCGT
GCTGGGTGGTCCGGAACCGCTGATGCAGGCGACCGCGTGGCTGAACGCGTATTT
TCATCAGCCGGAAGCGATTGAAGAATTTCCGGTTCCGGCGCTGCATCATCCGGTG
TTTCAGCAGGAGAGCTTTACCCGTCAGGTGCTGTGGAAACTGCTGAAAGTGGTTAA
ATTTGGCGAAGTGATTAGCTATCAGCAGCTGGCGGCCCTGGCGGGTAATCCGGCG
GCCACCGCCGCCGTTAAAACCGCGCTGAGCGGTAACCCGGTGCCGATTCTGATTC
CGTGCCATCGTGTGGTTAGCTCTAGCGGTGCGGTTGGCGGTTATGAAGGTGGTCT
GGCGGTGAAAGAGTGGCTGCTGGCCCATGAAGGTCATCGTCTGGGTAAACCGGG
TCTGGGAGGCAGCGGTACGGGCTCGGGTTCCGATCTGGGGAAGAAACTGCTGGA
GGCGGCTCGGGCTGGACAGGACGACGAAGTTCGCATTCTGGTCGCCAACGGCGC
GGATGTGAATGCCCTGGACGAAGAGGGTCTGACTCCACTGCACCTGGCAGCACA
GATGGGACATCTGGAAATCGTGGAGGTTCTGCTGAAAAACGGGGCAGATGTTAAC
GCTAATGACAGCTATGGAATTACCCCCCTGCACCTGGCAGCTACACGTGGTCATCT
GGAAATCGTCGAGGTGCTGCTGAAGTACGGCGCCGATGTGAATGCGCAGGACAA
ATTTGGCAAGACCGCATTTGACATTAGCATTGATAACGGGAACGAAGACCTGGCG
GAAATCCTCCAGAAACTGAACTAG

SNAP(pE59)
ATGCACCATCATCATCATCATTCTTCTGGTGTAGATCTGGGTACCGAGAACCTGTA
CTTCCAATCCAATGACAAAGATTGCGAAATGAAACGTACCACCCTGGATAGCCCGC
TGGGCAAACTGGAACTGAGCGGCTGCGAACAGGGCCTGCATGAAATTAAACTGCT
GGGTAAAGGCACCAGCGCGGCCGATGCGGTTGAAGTTCCGGCCCCGGCCGCCGT
GCTGGGTGGTCCGGAACCGCTGATGCAGGCGACCGCGTGGCTGAACGCGTATTT
TCATCAGCCGGAAGCGATTGAAGAATTTCCGGTTCCGGCGCTGCATCATCCGGTG
TTTCAGCAGGAGAGCTTTACCCGTCAGGTGCTGTGGAAACTGCTGAAAGTGGTTAA
ATTTGGCGAAGTGATTAGCTATCAGCAGCTGGCGGCCCTGGCGGGTAATCCGGCG
GCCACCGCCGCCGTTAAAACCGCGCTGAGCGGTAACCCGGTGCCGATTCTGATTC
CGTGCCATCGTGTGGTTAGCTCTAGCGGTGCGGTTGGCGGTTATGAAGGTGGTCT
GGCGGTGAAAGAGTGGCTGCTGGCCCATGAAGGTCATCGTCTGGGTAAACCGGG
TCTGGGAGGCAGCGGTACGGGCTCGGGTTCCGATCTGGGTAAAAAACTGCTGGA
AGCGGCACGGGCGGGACAGGACGACGAAGTTCGCATTCTGATGGCCAACGGCGC
GGATGTCAATGCCCTGGATGAAGACGGTCTGACCCCACTGCACCTGGCAGCACAG
CTGGGACATCTGGAAATTGTGGAGGTTCTGCTGAAATATGGGGCAGATGTGAACG
CTGAGGACAATTTTGGAATCACACCCCTGCACCTGGCAGCTATTCGTGGTCATCTG
GAAATCGTCGAGGTGCTGCTGAAGCACGGCGCCGATGTTAACGCGCAGGACAAAT
TCGGCAAGACCGCATTTGACATCTCCATTGACAACGGAAACGAAGACCTGGCTGA
AATCCTCCAGAAACTGAACTAG

flag-SNAP(HA4)

ATGGATTACAAGGATGACGATGACAAGGGAATTCTGTACTTCCAATCCAATGACAA
AGATTGCGAAATGAAACGTACCACCCTGGATAGCCCGCTGGGCAAACTGGAACTG
AGCGGCTGCGAACAGGGCCTGCATGAAATTAAACTGCTGGGTAAAGGCACCAGCG
CGGCCGATGCGGTTGAAGTTCCGGCCCCGGCCGCCGTGCTGGGTGGTCCGGAAC
CGCTGATGCAGGCGACCGCGTGGCTGAACGCGTATTTTCATCAGCCGGAAGCGAT
TGAAGAATTTCCGGTTCCGGCGCTGCATCATCCGGTGTTTCAGCAGGAGAGCTTTA
CCCGTCAGGTGCTGTGGAAACTGCTGAAAGTGGTTAAATTTGGCGAAGTGATTAG
CTATCAGCAGCTGGCGGCCCTGGCGGGTAATCCGGCGGCCACCGCCGCCGTTAA
AACCGCGCTGAGCGGTAACCCGGTGCCGATTCTGATTCCGTGCCATCGTGTGGTT
AGCTCTAGCGGTGCGGTTGGCGGTTATGAAGGTGGTCTGGCGGTGAAAGAGTGG
CTGCTGGCCCATGAAGGTCATCGTCTGGGTAAACCGGGTCTGGGAGGTACGGGC
ACCGGCTCTTCTGTTTCAAGCGTTCCGACCAAGCTGGAGGTTGTTGCTGCCACAC
CGACAAGTCTGCTGATTTCATGGGATGCCCCGATGAGCTCCTCTAGTGTTTATTAC
TATCGCATTACATACGGCGAAACCGGCGGTAACAGCCCGGTGCAGGAGTTTACCG
TTCCCTATTCAAGCTCCACCGCCACAATTTCTGGGCTGAGCCCGGGAGTCGATTAC
ACTATCACCGTGTATGCGTGGGGTGAAGACTCAGCAGGGTATATGTTTATGTATTC
TCCCATCTCCATCAACTATCGCACTTGCTAG

flag-*cd*SNAPtag

ATGGACTACAAGGACGACGATGACAAGGGCAGCGACAAAGATTGCGAAATGAAAC
GTACCACCCTGGATAGCCCGCTGGGCAAACTGGAACTGAGCGGCTGCGAACAGG
GCCTGCATGAAATTAAACTGCTGGGTAAAGGCACCAGCGCGGCCGATGCGGTTGA
AGTTCCGGCCCCGGCCGCCGTGCTGGGTGGTCCGGAACCGCTGATGCAGGCGAC
CGCGTGGCTGAACGCGTATTTTCATCAGCCGGAAGCGATTGAAGAATTTCCGGTTC
CGGCGCTGCATCATCCGGTGTTTCAGCAGGAGAGCTTTACCCGTCAGGTGCTGTG
GAAACTGCTGAAAGTGGTTAAATTTGGCGAAGTGATTAGCTATCAGCAGCTGGCG
GCCCTGGCGGGTAATCCGGCGGCCACCGCCGCCGTTAAAACCGCGCTGAGCGGT
AACCCGGTGCCGATTCTGATTCCGGCCCATCGTGTGGTTAGCTCTAGCGGTGCGG
TTGGCGGTTATGAAGGTGGTCTGGCGGTGAAAGAGTGGCTGCTGGCCCATGAAG
GTCATCGTCTGGGTAAACCGGGTCTGGGATAG

flag-*cd*SNAP(HA4)

ATGGATTACAAGGATGACGATGACAAGGGAATTCTGTACTTCCAATCCAATGACAA
AGATTGCGAAATGAAACGTACCACCCTGGATAGCCCGCTGGGCAAACTGGAACTG
AGCGGCTGCGAACAGGGCCTGCATGAAATTAAACTGCTGGGTAAAGGCACCAGCG
CGGCCGATGCGGTTGAAGTTCCGGCCCCGGCCGCCGTGCTGGGTGGTCCGGAAC
CGCTGATGCAGGCGACCGCGTGGCTGAACGCGTATTTTCATCAGCCGGAAGCGAT
TGAAGAATTTCCGGTTCCGGCGCTGCATCATCCGGTGTTTCAGCAGGAGAGCTTTA
CCCGTCAGGTGCTGTGGAAACTGCTGAAAGTGGTTAAATTTGGCGAAGTGATTAG
CTATCAGCAGCTGGCGGCCCTGGCGGGTAATCCGGCGGCCACCGCCGCCGTTAA
AACCGCGCTGAGCGGTAACCCGGTGCCGATTCTGATTCCGGCCCATCGTGTGGTT
AGCTCTAGCGGTGCGGTTGGCGGTTATGAAGGTGGTCTGGCGGTGAAAGAGTGG
CTGCTGGCCCATGAAGGTCATCGTCTGGGTAAACCGGGTCTGGGAGGTACGGGC
ACCGGCTCTTCTGTTTCAAGCGTTCCGACCAAGCTGGAGGTTGTTGCTGCCACAC
CGACAAGTCTGCTGATTTCATGGGATGCCCCGATGAGCTCCTCTAGTGTTTATTAC

TATCGCATTACATACGGCGAAACCGGCGGTAACAGCCCGGTGCAGGAGTTTACCG
TTCCCTATTCAAGCTCCACCGCCACAATTTCTGGGCTGAGCCCGGGAGTCGATTAC
ACTATCACCGTGTATGCGTGGGGTGAAGACTCAGCAGGGTATATGTTTATGTATTC
TCCCATCTCCATCAACTATCGCACTTGCTAG

V. References

1. Knight ZA, Shokat KM (2007) Chemical genetics: where genetics and pharmacology meet. *Cell* 128:425–430.

2. Weiss WA, Taylor SS, Shokat KM (2007) Recognizing and exploiting differences between RNAi and small-molecule inhibitors. *Nat Chem Biol* 3:739–744.

3. Cohen P (2002) Protein kinases--the major drug targets of the twenty-first century? *Nat Rev Drug Discov* 1:309–315.

4. Manning G, Whyte DB, Martinez R, Hunter T, Sudarsanam S (2002) The protein kinase complement of the human genome. *Science* 298:1912–1934.

5. Profit AA, Lee TR, Lawrence DS (1999) Bivalent Inhibitors of Protein Tyrosine Kinases. *J Am Chem Soc* 121:280–283.

6. Gower CM, Chang MEK, Maly DJ (2014) Bivalent inhibitors of protein kinases. *Critical Reviews in Biochemistry and Molecular Biology* 49:102–115.

7. Gronemeyer T, Chidley C, Juillerat A, Heinis C, Johnsson K (2006) Directed evolution of O6-alkylguanine-DNA alkyltransferase for applications in protein labeling. *Protein engineering, design & selection : PEDS* 19:309–316.

8. Juillerat A et al. (2003) Directed evolution of O6-alkylguanine-DNA alkyltransferase for efficient labeling of fusion proteins with small molecules in vivo. *Chem Biol* 10:313–317.

9. Juillerat A et al. (2005) Engineering substrate specificity of O6-alkylguanine-DNA alkyltransferase for specific protein labeling in living cells. *ChemBioChem* 6:1263–1269.

10. Hill ZB, Perera BGK, Maly DJ (2009) A Chemical Genetic Method for Generating Bivalent Inhibitors of Protein Kinases. *J Am Chem Soc* 131:6686–6688.

11. Hill ZB, Perera BGK, Maly DJ (2011) Bivalent inhibitors of the tyrosine kinases ABL and SRC: determinants of potency and selectivity. *Mol BioSyst* 7:447.

12. Hill ZB, Perera BGK, Andrews SS, Maly DJ (2012) Targeting Diverse Signaling Interaction Sites Allows the Rapid Generation of Bivalent Kinase Inhibitors. *ACS Chem Biol* 7:487–495.

13. Karatan E et al. (2004) Molecular recognition properties of FN3 monobodies that bind the Src SH3 domain. *Chem Biol* 11:835–844.

14. Wojcik J et al. (2010) A potent and highly specific FN3 monobody inhibitor of the Abl SH2 domain. *Nature Structural & Molecular Biology* 17:519–527.

15. Gulyani A et al. (2011) A biosensor generated via high-throughput screening quantifies cell edge Src dynamics. *Nat Chem Biol* 7:437–444.

16. Huang R, Fang P, Kay BK (2012) Isolation of monobodies that bind specifically to the SH3 domain of the Fyn tyrosine protein kinase. *New Biotechnology* 29:526–533.

17. Amstutz P, Koch H, Binz HK, Deuber SA, Plückthun A (2006) Rapid selection of specific MAP kinase-binders from designed ankyrin repeat protein libraries. *Protein engineering, design & selection : PEDS* 19:219–229.

18. Bandeiras TM et al. (2008) Structure of wild-type Plk-1 kinase domain in complex with a selective DARPin. *Acta crystallographica Section D, Biological crystallography* 64:339–353.

19. Kummer L et al. (2013) Knowledge-based design of a biosensor to quantify localized ERK activation in living cells. *Chem Biol* 20:847–856.

20. Kummer L et al. (2012) Structural and functional analysis of phosphorylation-specific binders of the kinase ERK from designed ankyrin repeat protein libraries. *Proceedings of the National Academy of Sciences* 109:E2248–57.

21. Statsuk AV et al. (2008) Tuning a Three-Component Reaction For Trapping Kinase Substrate Complexes. *J Am Chem Soc* 130:17568–17574.

22. Aronov AM, Murcko MA (2004) Toward a pharmacophore for kinase frequent hitters. *J Med Chem* 47:5616–5619.

23. Mayer BJ, Hirai H, Sakai R (1995) Evidence that SH2 domains promote processive phosphorylation by protein-tyrosine kinases. *Curr Biol* 5:296–305.

24. Pearson G et al. (2001) Mitogen-Activated Protein (MAP) Kinase Pathways: Regulation and Physiological Functions 1. *Endocrine Reviews* 22:153–183.

25. Chen Z et al. (2001) MAP kinases. *Chem Rev* 101:2449–2476.

26. Davis MI et al. (2011) Comprehensive analysis of kinase inhibitor selectivity. *Nat Biotechnol* 29:1046–1051.

27. Urbaniak MD et al. (2012) Chemical proteomic analysis reveals the drugability of the kinome of Trypanosoma brucei. *ACS Chem Biol* 7:1858–1865.

28. Wahlberg E et al. (2012) Family-wide chemical profiling and structural analysis of PARP and tankyrase inhibitors. *Nat Biotechnol* 30:283–288.

29. Bantscheff M et al. (2011) Chemoproteomics profiling of HDAC inhibitors reveals selective targeting of HDAC complexes. *Nat Biotechnol* 29:255–265.

30. Gallenkamp D, Gelato KA, Haendler B, Weinmann H (2014) Bromodomains and Their Pharmacological Inhibitors. *ChemMedChem* 9:438–464.

31. Stols L et al. (2002) A new vector for high-throughput, ligation-independent cloning encoding a tobacco etch virus protease cleavage site. *Protein Expr Purif* 25:8–15.

32. Mollwitz B et al. (2012) Directed evolution of the suicide protein O^6-alkylguanine-DNA alkyltransferase for increased reactivity results in an alkylated protein with exceptional stability. *Biochemistry* 51:986–994.

33. Shah NP et al. (2008) Transient potent BCR-ABL inhibition is sufficient to commit chronic myeloid leukemia cells irreversibly to apoptosis. *Cancer Cell* 14:485–493.

34. Jaffe JD et al. (2008) Accurate inclusion mass screening: a bridge from unbiased discovery to targeted assay development for biomarker verification. *Mol Cell Proteomics* 7:1952–1962.

Chapter 3

Intracellular antibody-based bivalent inhibitors of protein kinases: exploring the roles and generality of these ligands

I. Introduction

Recently, we described a bivalent method of protein kinase inhibition utilizing an ATP-competitive pan-kinase inhibitor tethered to selective intracellular antibodies of the kinases Abl and ERK (Chapter 2). These non-immunoglobulin scaffolds, termed monobodies and DARPins, have been identified using *in vitro* display technologies to potently bind to kinases of interest (1-5). The intracellular antibody is displayed from the N- or C-terminus of the protein SNAPtag, which readily labels its active site with ATP-competitive small molecules bearing benzylguanine derivatives (6, 7) (Figure 3-1 A). These bivalent reagents potently inhibited target kinase activity *in vitro* and displayed impressive selectivity within mammalian cell lysate. By tethering selective intracellular antibodies, the selectivity of a promiscuous small molecule inhibitor was steered towards kinases of interest.

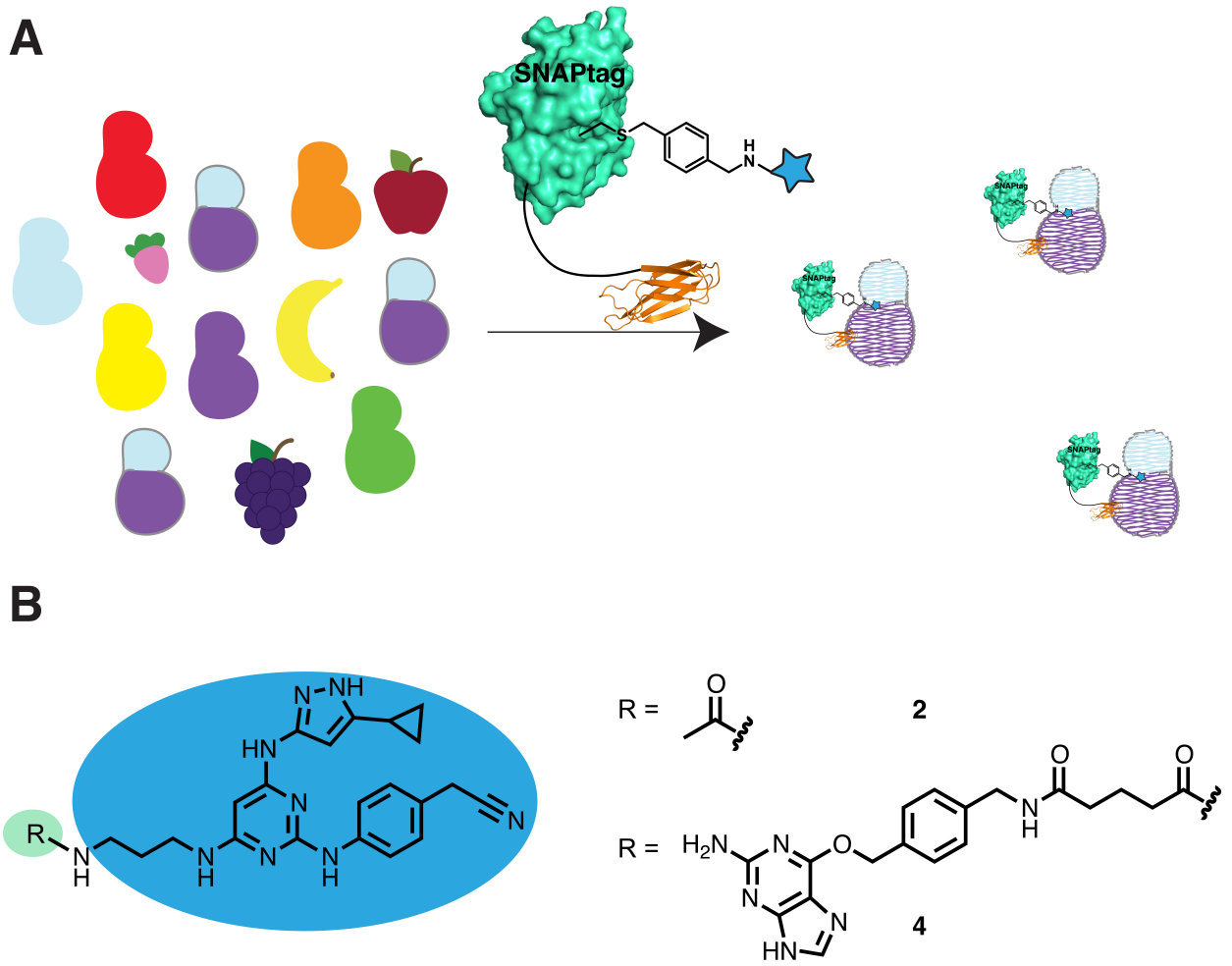

Figure 3-1. Intracellular antibodies as specificity elements of SNAPtag-based bivalent inhibitors. (A) General strategy for use of intracellular antibodies as specificity elements of SNAPtag-based bivalent kinase inhibitors. A bivalent inhibitor containing a non-selective ATP-competitive inhibitor and an intracellular antibody-SNAPtag fusion selectively interacts with its kinase target and blocks catalytic activity. (B) Reagents based on a promiscuous 5-cyclopropyl-3-aminopyrazolo-based inhibitor.

Here, we further investigate the role that intracellular antibodies play in selective bivalent inhibition of kinases. First, two bivalent inhibitors bearing the pan-kinase pharmacophore **4** were compared; one that utilizes a monobody as the secondary binding ligand and another that uses an Abl SH3-binding peptide. With this comparison, the selectivity gained from an intracellular antibody was explored. We found that the monobody-based bivalent inhibitor displaying the pan-kinase inhibitor was more potent than the peptide-based inhibitor and exhibited greater selectivity in K562 lysate. It was

then of interest to gauge the breadth of kinases that could be targeted with this approach. Intracellular antibodies of the kinases p38, Src and Fyn were incorporated into bivalent inhibitors and examined for their ability to impose potency and selectivity.

II. Results and Discussion

We have previously described bivalent inhibitors of the protein kinases Abl and ERK that utilize intracellular antibodies to direct a selective bivalent interaction when tethered to a promiscuous 5-cyclopropyl-3-aminopyrazolo-based inhibitor (compound **2**) (Figure 3-1 B). These bivalent inhibitors were generated by fusing intracellular antibodies selective for either Abl or ERK to the self-labeling protein SNAPtag and subsequent labeling with a derivative of **2** linked to the SNAPtag-labeling moiety benzylguanine (compound **4**). The purified bivalent inhibitors were assayed for potency *in vitro* and profiled for selectivity against mammalian kinases in lysate using the quantitative competition-based chemical proteomics method described in Chapter 2. The Abl bivalent inhibitor (SNAP(HA4)-**4**) met our criteria for a successful intracellular antibody-containing bivalent inhibitor. The inhibitor was highly potent (IC_{50} = 8.3 nM) against Abl3D activity *in vitro* and was found to bind BCR-Abl with high specificity in K562 lysate, exhibiting a 71-fold increase in potency relative to **2** in a dose-response experiment.

We were interested in comparing the ability of an intracellular antibody to increase bivalent selectivity for Abl versus a reagent that contains a consensus binding motif. To this end, we performed a comparison between SNAP(HA4)-**4** and a bivalent reagent that we have previously developed which contains a SH3 domain targeting polyproline motif peptide and a quinazoline-based kinase inhibitor, SNAP(PP)-**6**

(Figures 3-2 A and B) (8-10). The question we sought to answer was whether the same degree of selectivity could be achieved with the peptide-based bivalent inhibitor as had been obtained with SNAP(HA4)-**4**.

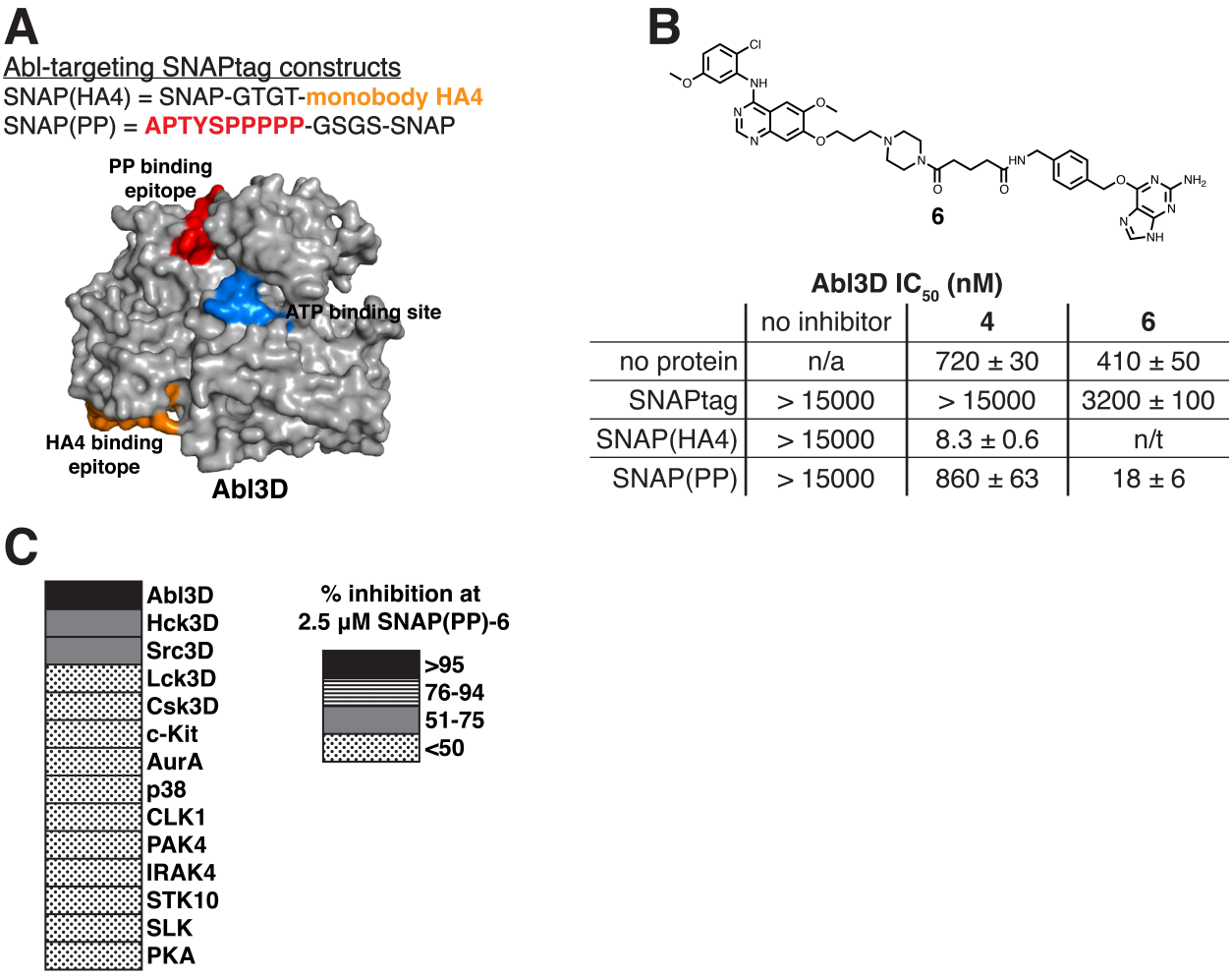

Figure 3-2. Bivalent inhibitors of Abl. (A) (Top panel) SNAPtag fusions that were used in this study. (Bottom panel) The binding sites for the ligands of the two different bivalent inhibitors are superimposed on a crystal structure of Abl3D, PDB ID 2FO0. (B) (Top panel) Structure of compound **6**. (Bottom panel) *In vitro* activities of bivalent inhibitors and various monovalent components against Abl3D. Abl3D contains the kinase, SH2 and SH3 domains. Values shown are the average of assays performed in triplicate ± SEM. (C) Percent inhibition of a panel of fourteen protein kinases treated with 2.5 μM SNAP(PP)-**6**. All assays were performed in triplicate and the SEM for all data points is <5%.

A comparison of previously described *in vitro* Abl kinase activity data highlighted that similar potency could be achieved with the monobody- and peptide-based bivalent inhibitors (Figure 3-2 B) (8). The bivalent inhibitors and various monovalent components

were assayed against an Abl construct containing the catalytic, SH2 and SH3 domains (Abl3D). Quinazoline **6** is a moderately potent (IC_{50} = 410 nM) inhibitor of Abl3D activity whose potency is diminished 7.8-fold upon conjugation to SNAPtag (IC_{50} = 3,200 nM). The peptide-based bivalent inhibitor, SNAP(PP)-**6**, inhibits Abl3D with an IC_{50} of 18 nM, a 23-fold increase in potency relative to unconjugated **6** and a 180-fold increase in potency compared to the monovalent SNAPtag-**6**. As was observed with the monovalent SNAP(HA4) construct, unconjugated SNAP(PP) does not affect Abl3D activity at the highest tested concentration (15,000 nM).

The two bivalent inhibitors, SNAP(HA4)-**4** and SNAP(PP)-**6**, utilize two different classes of secondary binding ligands; an intracellular antibody and a peptide, respectively. Yet the two constructs achieve similar potency against their target, Abl3D. We had previously examined the selectivity of a peptide-based Abl bivalent inhibitor against a small panel of kinases *in vitro*, and found it to be selective for its target (Figure 3-2 C) (8). At 2.5 μM bivalent inhibitor, only Abl3D was greater than 95% inhibited. The closely related Src family kinases Src3D and Hck3D were inhibited in the assay, but the bivalent inhibitor was 36-fold selective for Abl3D over Src3D. As was expected, screened kinases lacking a SH3-domain were not inhibited by the bivalent inhibitor.

While the bivalent reagent SNAP(PP)-**6** was selective for Abl *in vitro*, compound **6** is moderately selective for Abl, and we wanted to explore the selectivity of the polyproline peptide when conjugated to the pan-kinase inhibitor **4**. SNAP(PP) was conjugated to inhibitor **4** and the assembled bivalent inhibitor was analyzed for its ability to inhibit Abl activity *in vitro*. The construct was labeled with an excess of inhibitor **4**, purified, and labeling was confirmed with mass spectrometry (see Experimental

Procedures). Importantly, SNAP(PP)-**4** did not exhibit enhanced potency over the pharmacophore **4** alone (**4** IC_{50} = 720 nM, SNAP(PP)-**4** IC_{50} = 860 nM) (Figure 3-2 B). Next, the relative potency and selectivity of the bivalent inhibitor SNAP(PP)-**4** was assessed using the quantitative competition-based chemical proteomics method described in Chapter 2. Briefly, a single component kinase affinity matrix was generated by reacting an amine-containing version of **2** with NHS-activated sepharose. With this tool, the ability of the inhibitor to bind to a variety of full-length protein kinases in a complex cellular lysate was determined. K562 lysates pre-incubated with varying concentrations of the desired inhibitor or DMSO control were incubated with the affinity matrix, after which the resin was washed and proteins were eluted under denaturing conditions. Quantitative chemical proteomics were employed to assess the protein kinases enriched in the DMSO control and competed by the inhibitor at a single dose (1 μM). Experiments were performed with the bivalent inhibitor in K562 lysates, from which fold change values of kinases bound to the resin relative to DMSO were calculated. This profile was compared to that of the monobody-based bivalent inhibitor SNAP(HA4)-**4** and a monovalent SNAPtag-**4** control (Figure 3-3).

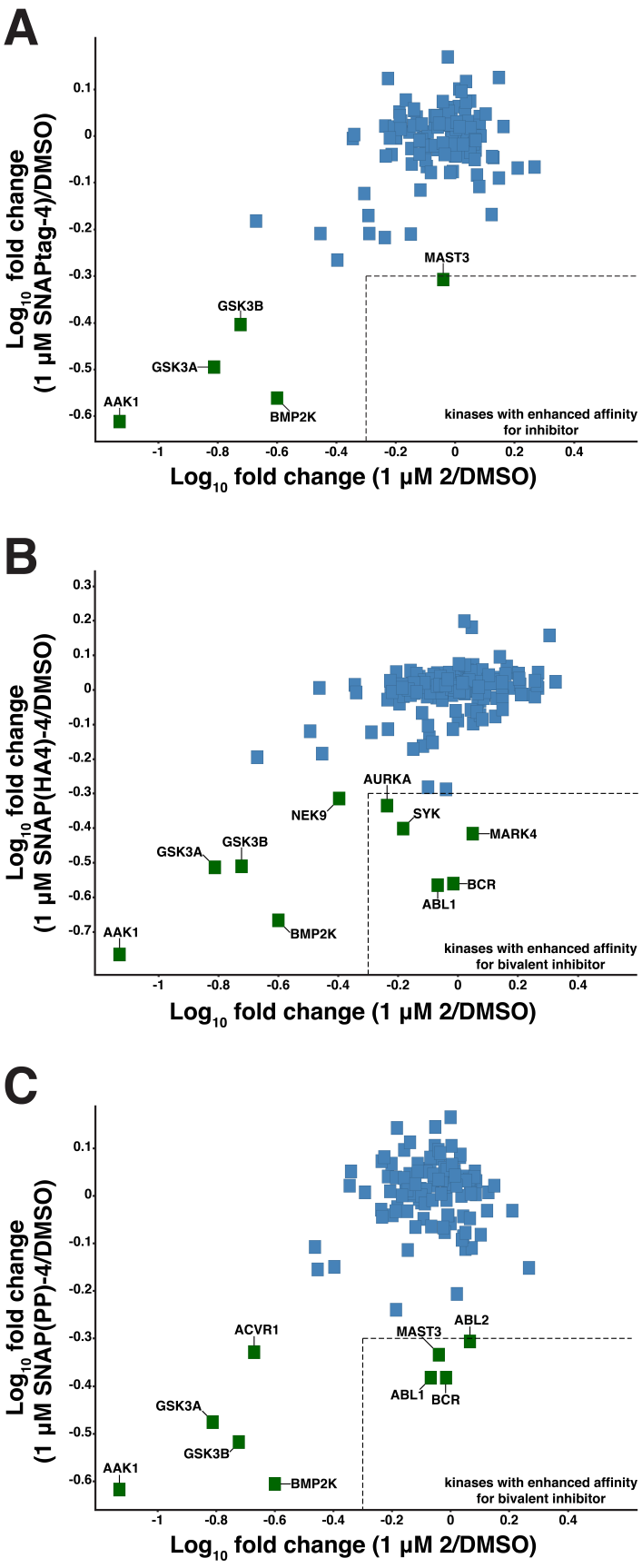

Figure 3-3. Quantitative competition-based chemical proteomics. In each case, the dotted region represents ≥2-fold increase in potency for the assembled bivalent inhibitor. (A) Fold change at 1 μM inhibitor relative to DMSO (average of 2 independent experiments) of kinases for SNAPtag-**4** compared to **2**. (B) Fold change at 1 μM inhibitor relative to DMSO (average of 2 independent experiments) of kinases for SNAP(HA4)-**4** compared to **2**. (C) Fold change at 1 μM inhibitor relative to DMSO (average of 2 independent experiments) of kinases for SNAP(PP)-**4** compared to **2**.

As described previously, comparison of the parent compound **2** versus SNAPtag-**4** shows that conjugation of this pharmacophore to SNAPtag generally decreases potency, consistent with the *in vitro* Abl3D activity assay data (Figure 3-2 B and Figure 3-3 B). Similarly, SNAP(HA4)-**4** exhibited a reduction in potency for the majority of protein kinases. BCR-Abl, however, exhibited an increase in potency relative to **2** alone (Figure 3-3 B). While enhancement of binding to BCR-Abl was observed for SNAP(PP)-**4** relative to the monovalent compound **2**, the amplitude of enhancement was dampened compared to bivalent SNAP(HA4)-**4** (Figure 3-3 C). SNAP(HA4)-**4** showed a 3.6-fold increase in potency for BCR-Abl at 1 μM, compared to a 2.4-fold increase with SNAP(PP)-**4**. The monobody-based bivalent demonstrated a 1.4-fold enhanced selectivity for BCR-Abl relative to the next most-competed kinase, MARK4, while SNAP(PP)-**4** was equipotent for BCR-Abl and MAST3, the next most-competed kinase at this dose of inhibitor. The peptide, when conjugated to an already-potent and moderately selective inhibitor of Abl can achieve similar levels of Abl activity *in vitro* compared to the monobody-based bivalent inhibitor. The peptide-based bivalent inhibitor conjugated to **4** demonstrates a moderately selective profile in K562 lysate with only one significant off-target, however, the peptide does not confer the same degree of selectivity within lysate that SNAP(HA4)-**4** accomplishes.

In an effort to develop more intracellular antibody-based bivalent inhibitors of protein kinases, we looked to the literature for previously described intracellular antibodies. The mitogen-activated protein kinase (MAPK) p38 consists of a single catalytic domain (11). It is involved in numerous cellular stress-response pathways, and a selective DARPin (p38p4) has been generated to bind to this kinase (2). Current

biochemical data for the p38p4/p38 interaction is rather limited, however, and we wanted to verify this binding interaction biochemically. In order to demonstrate the binding interaction between the kinase and the DARPin, p38p4 bearing a His6 affinity tag was expressed in *E. coli*. Through this tag the DARPin was immobilized on Ni-NTA resin and incubated with COS7 cell lysate transiently transfected with p38 and a closely related MAPK, ERK2. Upon washing and specific elution with imidazole, p38p4 and p38 were detected by immunoblot (Figure 3-4 A). ERK2, however, was not enriched from the lysate demonstrating that a binding interaction exists between p38 and p38p4, and that this interaction is selective for p38 over a closely related MAPK.

A

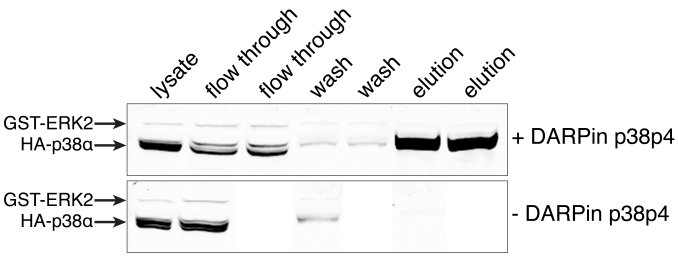

B

p38α-targeting SNAPtag constructs
SNAP(N10p38p4) = **p38p4**-$(SG)_5$-SNAP
SNAP(N15p38p4) = **p38p4**-$(GTGTG(SG)_5)$-SNAP
SNAP(C10p38p4) = SNAP-$(GS)_5$-**p38p4**
SNAP(C15p38p4) = SNAP-$(TGTGT(GS)_5)$-**p38p4**

C

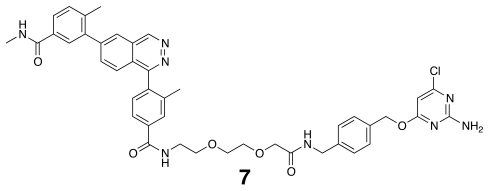

7

p38α IC_{50} (nM)

	no inhibitor	**7**
no protein	n/a	57 ± 17
SNAPtag	> 10000	180 ± 11
SNAP(N10p38p4)	> 10000	29 ± 3
SNAP(N15p38p4)	> 10000	64 ± 6
SNAP(C10p38p4)	> 10000	20 ± 2
SNAP(C15p38p4)	> 10000	36 ± 2

Figure 3-4. Bivalent inhibitors of p38α. (A) Immunoblots of COS7 lysates enriched onto DARPin p38p4-bound Ni-NTA resin. COS7 cells were transiently transfected with HA-p38α and GST-ERK2. Cells were lysed and cleared lysates subjected to Ni-NTA resin pre-conjugated to purified His6-p38p4 DARPin. After incubation at 4°C for one hour, resin was washed with lysis buffer and proteins were eluted with imidazole. The untreated lysate, flow through, wash and elution samples were analyzed by SDS-PAGE and immunoblotted with antibodies for p38 and ERK2. The pulldown was performed in duplicate. As a control, the pulldown was also performed with Ni-NTA in the absence of p38p4 DARPin. The control pulldown was performed in singlicate. (B) SNAPtag fusions that were used in this study. (C) (Top panel) Structure of compound **7**. (Bottom panel) *In vitro* activities of bivalent inhibitors and various monovalent components against activation loop-phosphorylated p38α. Values shown are the average of assays performed in triplicate ± SEM.

Upon verification that p38p4 was a viable ligand for p38, we needed to obtain the two components necessary for bivalent inhibitor assembly: a DARPin-containing fusion protein of SNAPtag and an ATP-competitive small molecule inhibitor linked to a benzylguanine derivative for SNAPtag-labeling. We designed SNAPtag fusion proteins containing the p38p4 DARPin linked to either the N-- or C-terminus of SNAPtag through flexible ten or fifteen amino acid linkers (Figure 3-4 B). We next turned to selecting a suitable ATP-competitive small molecule inhibitor that can be displayed from SNAPtag to form a bivalent inhibitor. Kinase inhibitors based on a phthalazine scaffold have been shown to be potent and selective inhibitors of p38 leading us to develop compound **7** for this purpose (12) (Figure 3-4 C). With the two modular components of our designed bivalent inhibitor in hand, we set forth to determine the potency of the assembled bivalent inhibitors. The bivalent inhibitors were prepared and purified prior to analysis. The abilities of the assembled bivalent inhibitors, and their constituent monovalent components, to block p38 function were assessed with an activity assay using an activation loop-phosphorylated form of this kinase. Unconjugated **7** is a potent inhibitor (IC_{50} = 57 nM) of p38 (Figure 3-4 C). Conjugation of the pharmacophore to SNAPtag leads to reduced inhibition of p38, with SNAPtag-**7** demonstrating 3-fold lower activity (IC_{50} = 180 nM). Disappointingly, the assembled bivalent inhibitors did not exhibit enhanced potency over unconjugated **7**. As a result, the p38 bivalent inhibitors were not analyzed further.

To explore further the generality of using intracellular antibodies as second site specificity ligands of bivalent inhibitors, we looked towards the Src family kinases (SFKs). Members of this protein kinase family have been identified as cellular

oncogenes with involvement in cell growth, differentiation, shape, migration and survival (13-15). The SFKs are multidomain, nonreceptor tyrosine kinases consisting of an N-terminal unique domain, regulatory SH3 and SH2 domains, a catalytic domain and a C-terminal tail (16). Recently, monobodies that bind to the polyproline-recognizing SH3 domains of several SFKs have been reported (3, 17). A moderately potent (K_d = 170 nM) monobody of the Fyn SH3 domain, termed monobody G9, was identified and found to be selective for the SH3 domain of Fyn over SH3 domains of other SFKs (17). SH3 domains of all eight members of the SrcA and SrcB subfamilies (Fyn, Src, Yes, Fgr and Hck, Lck, Blk, Lyn) were used in an ELISA, and phage displaying G9 bound exclusively to the Fyn SH3 domain with no cross-reactivity. Similarly, a monobody of the Src SH3 domain, 1E3, was reported via an enzyme-linked ligand binding assay (ELBA) to interact selectively with Src and did not recognize the SH3 domains of Yes, Fyn, Lyn or Lck (3). The affinity of this monobody for the Src SH3 domain was not reported. During the selection of the Src-selective monobody, the authors isolated clone 1F11, a moderately potent (K_d = 250 nM) binder of Src's SH3 domain which also binds to the SH3 domains of Fyn, Yes and Lyn. Monobody 1F11, which contains a proline-rich motif similar to the consensus sequence of SH3-binding peptides, was found to compete for binding to both the Src and Fyn SH3 domains with a proline-rich peptide in a dose-dependent manner, indicating that this monobody interacts with its targets via the shallow proline-binding groove of SFK SH3 domains (3, 17). Interestingly, the monobodies G9 and 1E3 do not contain a proline-rich motif. However, both monobodies show competitive binding for their target SH3 domains (Fyn and Src, respectively) with respect to 1F11. Heteronuclear NMR spectroscopy studies indicate that the binding

mode of 1E3 is distinctly different from that of the 1F11 monobody to the Src SH3 domain (3). The data indicate that 1E3 binds to a cleft that is slightly different from the 1F11 binding site, with partial overlap of the binding epitopes for the two monobodies; a potential explanation for the mutually exclusive binding of the two monobodies to the Src SH3 domain.

To test the suitability of the three SFK monobodies to serve as components of bivalent inhibitors, SNAPtag fusion proteins were generated (Figure 3-5 A). The Src-targeting monobody, 1E3, was displayed from the N-terminus of SNAPtag via a five amino acid linker (SNAP(1E3)). Constructs SNAP(G9) (Fyn-targeting) and SNAP(1F11) (SFK-targeting) display their respective monobodies from the C-terminus of SNAPtag using a five amino acid linker. The fusion proteins were expressed from *E. coli* and purified, and subsequently labeled with excess **4**, purified and analyzed by mass spectrometry (see Experimental Procedures). Examination of the assembled bivalent inhibitors using quantitative competition-based chemical proteomics yielded surprising profiles. The three SFK-targeting bivalent inhibitors failed to demonstrate competitive binding to any SFKs in lysate (Figure 3-5 B, C, D). Interestingly, the protein kinase MAST3 showed enhanced competition for each of the three bivalent inhibitors with respect to the monovalent compound **2** alone. SNAP(1E3) and SNAP(G9) (Src- and Fyn-targeting constructs, respectively) also exhibited enhanced affinity for the non-receptor protein tyrosine kinase TYK2. Confusingly, while TYK2 does have an atypical SH2 domain, neither TYK2 nor MAST3 possess an SH3 domain. From these data, it is difficult to speculate what factors are leading to the observed specificity profiles. Notably, the potencies of the SFK bivalent inhibitors were not analyzed *in vitro*, prior to

analysis in lysate. It is possible that the geometry of the assembled bivalent inhibitors is not optimal for potent binding to their target kinases. In this case, a loss of potency relative to the two monovalent portions is conceivable and would prevent target binding in complex lysate.

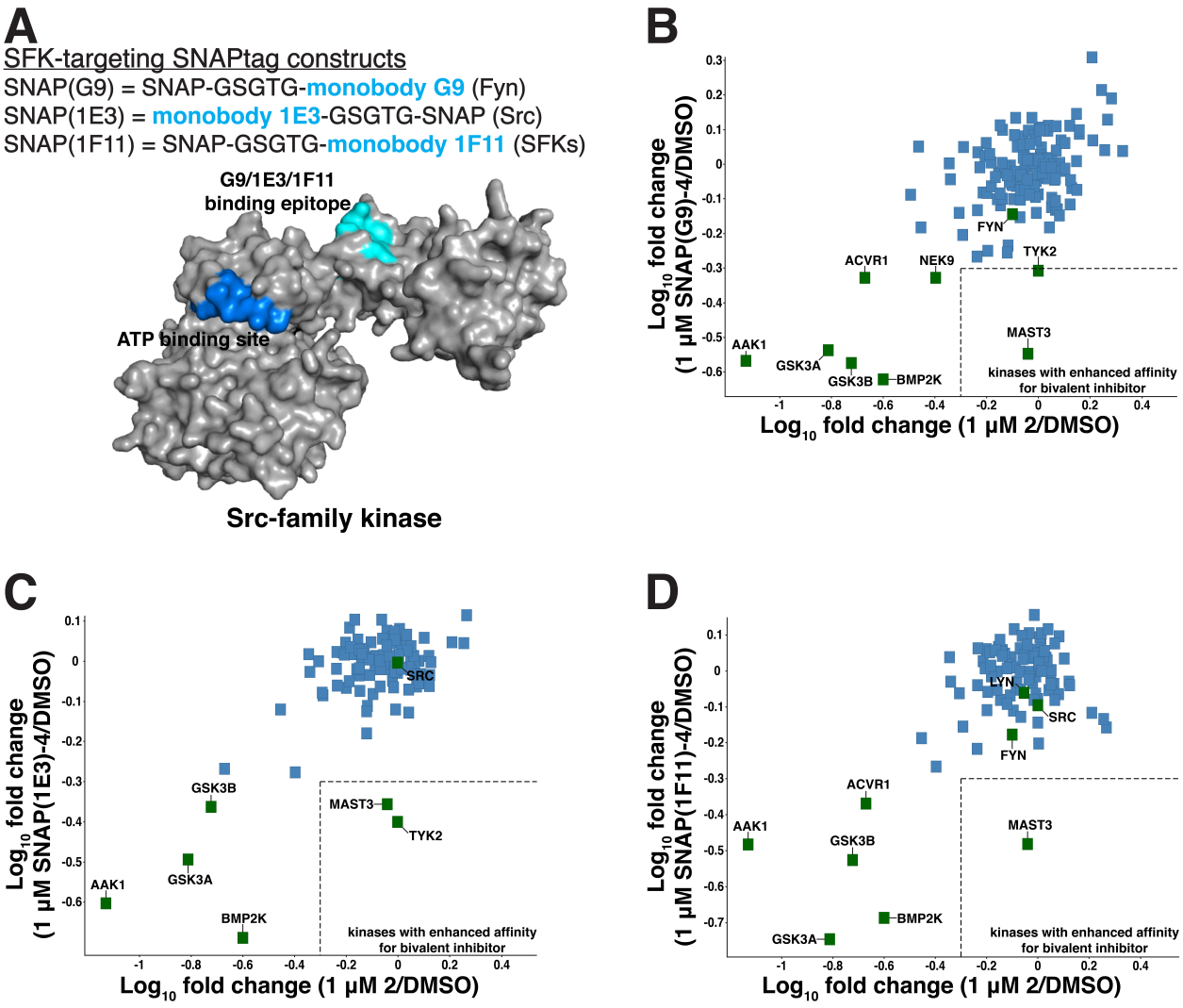

Figure 3-5. Bivalent inhibitors of Src family kinases (SFKs). (A) (Top panel) SNAPtag fusions that were used in this study. (Bottom panel) The binding sites for the ligands of the three different bivalent inhibitors are superimposed on a crystal structure of Src, PDB ID 1Y57. (B-D) Quantitative competition-based chemical proteomics. In each case, the dotted region represents ≥2-fold increase in potency for the assembled bivalent inhibitor. (B) Fold change at 1 μM inhibitor relative to DMSO (average of 2 independent experiments) of kinases for SNAP(G9)-**4** (Fyn-targeting) compared to **2**. (C) Fold change at 1 μM inhibitor relative to DMSO (average of 2 independent experiments) of kinases for SNAP(1E3)-**4** (Src-targeting) compared to **2**. (D) Fold change at 1 μM inhibitor relative to DMSO (average of 2 independent experiments) of kinases for SNAP(1F11)-**4** (SFK-targeting) compared to **2**.

III. Conclusion

With this study we sought to elucidate the role that intracellular antibodies play as secondary binding ligands in bivalent inhibitors and probe the modularity of bivalent inhibitor development utilizing these ligands. The efficiency of an Abl bivalent inhibitor was reduced when the monobody, HA4, was replaced with a SH3-targeting peptide. SNAP(HA4)-**4** is a highly potent inhibitor of Abl, capable of selecting its target from a lysate mixture of mammalian kinases. When a polyproline peptide was conjugated to the pan-kinase molecule **4**, two things occurred to ultimately affect the usefulness of the bivalent inhibitor. Firstly, the potency of inhibition decreased relative to either SNAP(HA4)-**4** or SNAP(PP)-**6**, a bivalent inhibitor displaying a more potent and selective small molecule. Additionally, the selectivity for BCR-Abl in K562 lysate decreased. Overall, these data suggest that the peptide is a less powerful directing group for bivalent inhibition of Abl.

Interested in exploring the generality of using intracellular antibodies in bivalent inhibitors, we incorporated previously published monobodies and a DARPin into various bivalent inhibitors of protein kinases. With a moderately potent inhibitor of p38 in hand (compound **7**, IC_{50} = 57 nM), the DARPin p38p4 was an interesting candidate for our study. However, biochemical characterization of the DARPin-p38 interaction was not available and the interaction needed to be verified. After confirming that the DARPin was capable of enriching p38 from the lysate of cells transiently expressing the kinase, enhanced inhibition of p38 activity did not result from bivalent inhibitor assembly. Various displays of the DARPin from SNAPtag were investigated but did not significantly affect the potency of the inhibitor. It is possible that p38p4 is not a potent

enough ligand of p38 to act as an effective secondary binding ligand. This result highlights the importance of carefully characterizing both envisioned ligands prior to bivalent assembly.

To further explore the use of intracellular antibodies as bivalent inhibitor ligands, constructs were generated to bind to Src and Fyn as well as a general SFK-targeting bivalent inhibitor. Regrettably, none of the three bivalent inhibitors showed impressive selectivity with our quantitative chemical proteomics platform. Without further study it is difficult to determine the cause of these failures. *In vitro* potency of the bivalent inhibitors was not measured in kinase activity assays prior to analysis in lysate. Information on how potently the assembled bivalent inhibitors bind their targets could give insight on the interactions in lysate. For instance, while previous studies have shown that the geometry of ligand display from SNAPtag has not had a significant effect on intracellular antibody-bivalent inhibitor potency, it is conceivable that the method of monobody display was suboptimal for kinase inhibition. Again, these results press the importance of carefully characterizing the secondary ligand prior to bivalent inhibitor assembly. Selecting a potent and highly selective ligand can result in great selectivity as evidenced by our Abl and ERK inhibitors. Prior to our use, the SFK-binding intracellular antibodies had only been characterized for selectivity against SFK SH3 domains. Furthermore, potency data for the Src ligand, 1E3, was not available. Moving forward, a more thorough characterization of ligands for use in bivalent inhibitors would be necessary.

IV. Experimental Procedures

A. Chemical synthesis

GENERAL METHODS. Syntheses of compounds **2**, **4** and **6** were described previously (Chapter 2 or (8)). Unless otherwise noted, all reagents were obtained from commercial suppliers and used without purification. ^{1}H-NMR spectra were obtained on a Bruker AV-300 or AV-301 instrument at room temperature. Chemical shifts are reported in ppm. ^{1}H resonances are referenced to Chloroform-d (7.26 ppm) or Methanol-d_4 (3.34). Mass spectrometry was performed on a Bruker Esquire Ion Trap MS instrument.

GENERAL HPLC PURIFICATION CONDITIONS. Preparatory reverse-phase C_{18} column (250 x 21 mm), Acetonitrile/Water – 0.1% CF_3CO_2H gradient: 1:99 to 100:0 over 70 min; 8 mL/min; 254 nm detection for 75 min or Methanol/Water – 0.1% CF_3CO_2H gradient: 1:99 to 100:0 over 70 min; 8 mL/min; 254 nm detection for 75 min.

GENERAL ANALYTICAL HPLC CONDITIONS. Analytical C_{18} column (250 x 4.6 mm), Acetonitrile/Water – 0.1% CF_3CO_2H gradient: 1:99 to 100:0 over 30 min. Methanol/Water – 0.1% CF_3CO_2H gradient: 1:99 to 100:0 over 30 min. Flow rate = 1mL/min; 220 and 254 nM detection for 35 min.

Synthetic scheme for 4-(benzyloxy)-6-chloropyrimidin-2-amine (CLP) synthesis

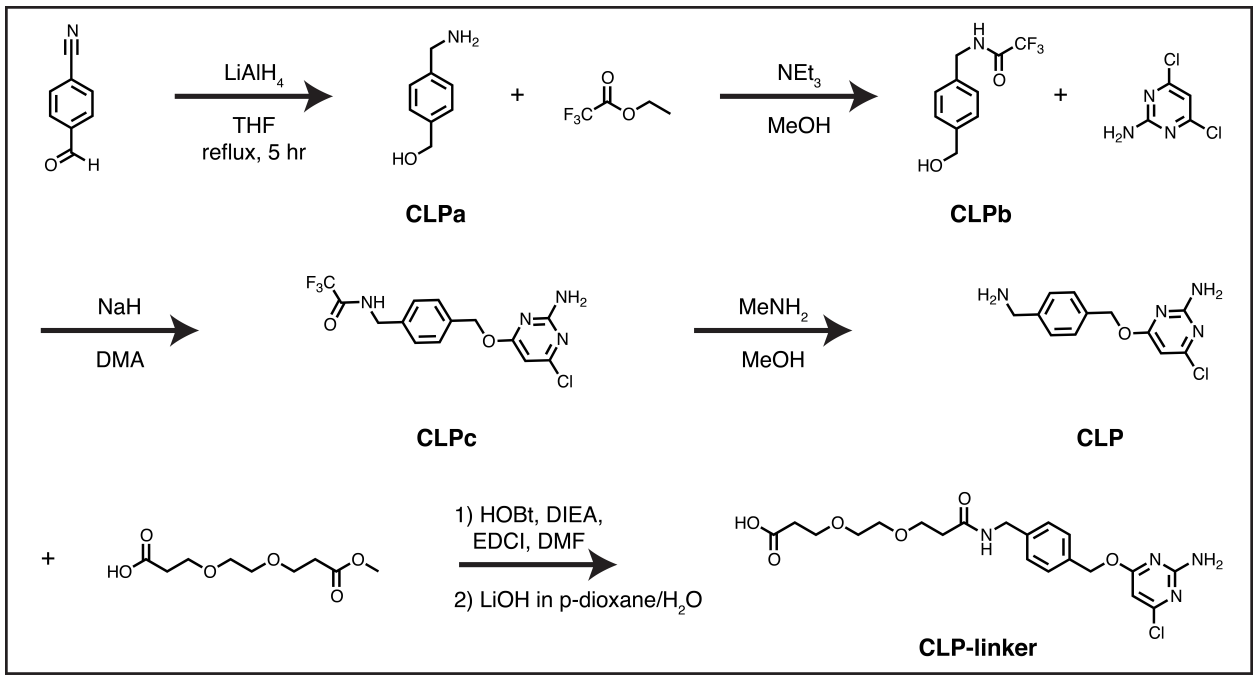

[CLPa]. A 1-L flask equipped with a stir bar and condenser was flame dried and cooled under N_2. The flask was charged with dry THF (200 mL) and cooled to 0 °C as $LiAlH_4$ (2.90 g, 76.4 mmol) was added. A solution of 4-cyanobenzaldehyde (2.50 g, 19.1 mmol) in dry THF (50 mL) was added dropwise to the cooled suspension and the reaction mixture was stirred at 66 °C for 6 h while monitoring by TLC (10% MeOH in $CHCl_3$). The reaction mixture was cooled to 0 °C as water (75 mL), 1M NaOH (15 mL) and another addition of water (100 mL) were added. The mixture was stirred at RT for 12 h and filtered on a fritted funnel. The filter cake was washed with CH_2Cl_2 (500 mL) and the resulting organic layer was washed with water (250 mL), saturated NaCl (250 mL), dried over anhydrous sodium sulfate and concentrated to yield **CLPa** as an off-white solid (0.743 g, 28%).

^{1}H-NMR ($CDCl_3$) 3.85, (s, 2H), 4.67 (s, 2H), 7.33 (m, 4H).

[CLPb]. To a stirred solution of **CLPa** (0.743 g, 5.42 mmol) in MeOH (6.8 mL) was added triethylamine (0.755 mL, 5.42 mmol) followed by ethyl trifluoroacetate (0.775 mL, 6.50 mmol). The reaction mixture was stirred at RT for 12 h while monitoring by TLC (10% MeOH in $CHCl_3$). The mixture was diluted in water (10 mL) and extracted with EtOAc (2 × 20 mL). The combined extracts were washed with saturated NaCl (20 mL), dried over anhydrous sodium sulfate and concentrated to yield **CLPb** as a yellow solid (1.15 g, 91%).

Calculated for $C_{10}H_{10}F_3NO_2$ $(M + Na)^+$: 256.1; Found 256.3.

[CLPc]. To a stirred solution of **CLPb** (1.15 g, 4.93 mmol) in DMA (10 mL) at 0 °C was added NaH (0.237 g, 9.86 mmol) and the mixture was stirred for 5 min before addition of 2-amino-4,6-dichloropyrimidine (0.809 g, 4.93 mmol). The reaction mixture was stirred at 90 °C for 12 h while monitoring by TLC (50% EtOAc in hexanes). The reaction was quenched with ice water (10 mL) and neutralized with 1M HCl (4 mL). The aqueous solution was extracted with EtOAc (3 × 50 mL) and the combined extracts were washed with saturated NaCl (100 mL), dried over anhydrous sodium sulfate and concentrated to yield a yellow oil. The crude material was purified by gradient column chromatography on silica gel, eluted with EtOAc in hexanes (0% → 40%) to yield **CLPc** as an off-white solid (0.460 g, 26%).

^{1}H-NMR ($CDCl_3$) 4.54 (d, 2H), 5.04 (bs, 1H), 5.33 (s, 2H), 6.17 (s, 1H), 7.32 (dd, 2H), 7.40 (dd, 2H).

Calculated for $C_{14}H_{12}ClF_3N_4O_2$ $(M + H)^+$: 361.7; Found 361.2.

[CLP]. To a stirred solution of **CLPc** (0.460 g, 1.28 mmol) in MeOH (2 mL) was added methylamine (4.5 mL as a 40% solution in MeOH, 73 mmol). The reaction mixture was

stirred at RT for 24 h while monitoring by TLC (10% MeOH in $CHCl_3$). The solution was concentrated *in vacuo* to yield **CLP** as a crude white solid which was used without further purification (0.448 g, 130%).

^{1}H-NMR ($CDCl_3$) 3.88 (s, 2H), 5.04 (bs, 1H), 5.31 (s, 2H), 6.16 (s, 1H), 7.34 (m, 4H).

[CLP-linker]. Step 1. To a stirred solution of **CLP** (0.137 g, 0.517 mmol) and 3-[2-(2-ethoxycarbonyl-ethoxy)-ethoxy]-propionic acid (0.11 g, 0.47 mmol) in DMF (4.7 mL) was added hydroxybenzotriazole (0.094 g, 0.611 mmol), DIEA (0.25 mL, 1.41 mmol) and 1-ethyl-3-(3-dimethylaminopropyl) carbodiimide (0.117 g, 0.611 mmol). The reaction mixture was stirred at RT for 48 h while monitoring with TLC (5% MeOH in $CHCl_3$ – 1% AcOH). The crude mixture was diluted in EtOAc (50 mL) and washed with K_2CO_3 (3 × 200 mL). The organic layer was dried over anhydrous sodium sulfate and concentrated *in vacuo* to yield a yellow oil. The crude material was purified by gradient column chromatography on silica gel, eluting with EtOAc in hexanes (0% → 100%) to yield the desired product (0.16 g, 71%).

^{1}H NMR (300 MHz, $CDCl_3$) δ 8.01 (s, 1H), 7.32 (q, 4H), 6.15 (s, 1H), 5.30 (s, 2H), 4.46 (d, 2H), 4.11 (q, *J* = 7.1 Hz, 2H), 3.77 – 3.72 (t, 2H), 3.64 (t, J = 6.4 Hz, 2H), 3.61 - 3.54 (m, 4H), 2.52 (t, 2H), 2.46 (t, J = 6.4 Hz, 2H), 1.23 (t, J = 7.1 Hz, 3H).

[CLP-linker]. Step 2. To a stirred solution of the product from **Step 1** (0.160 g, 0.333 mmol) in *p*-dioxane (1.7 mL) was added LiOH • H_2O (0.0307 g, 0.733 mmol). Water was added dropwise until a clear solution was obtained (2 mL) and the reaction was stirred at RT for 4 h while monitoring by TLC (50% EtOAc in hexanes – 1% AcOH). The mixture was diluted in water (50 mL), extracted with EtOAc (50 mL) and made acidic to pH 1 with 1M HCl. The acidic solution was extracted with EtOAc (3 × 50 mL) and the

combined extracts were concentrated *in vacuo* to yield **CLP-linker** as a white solid (0.150 g, 100%).

Synthetic scheme for compound 7 synthesis

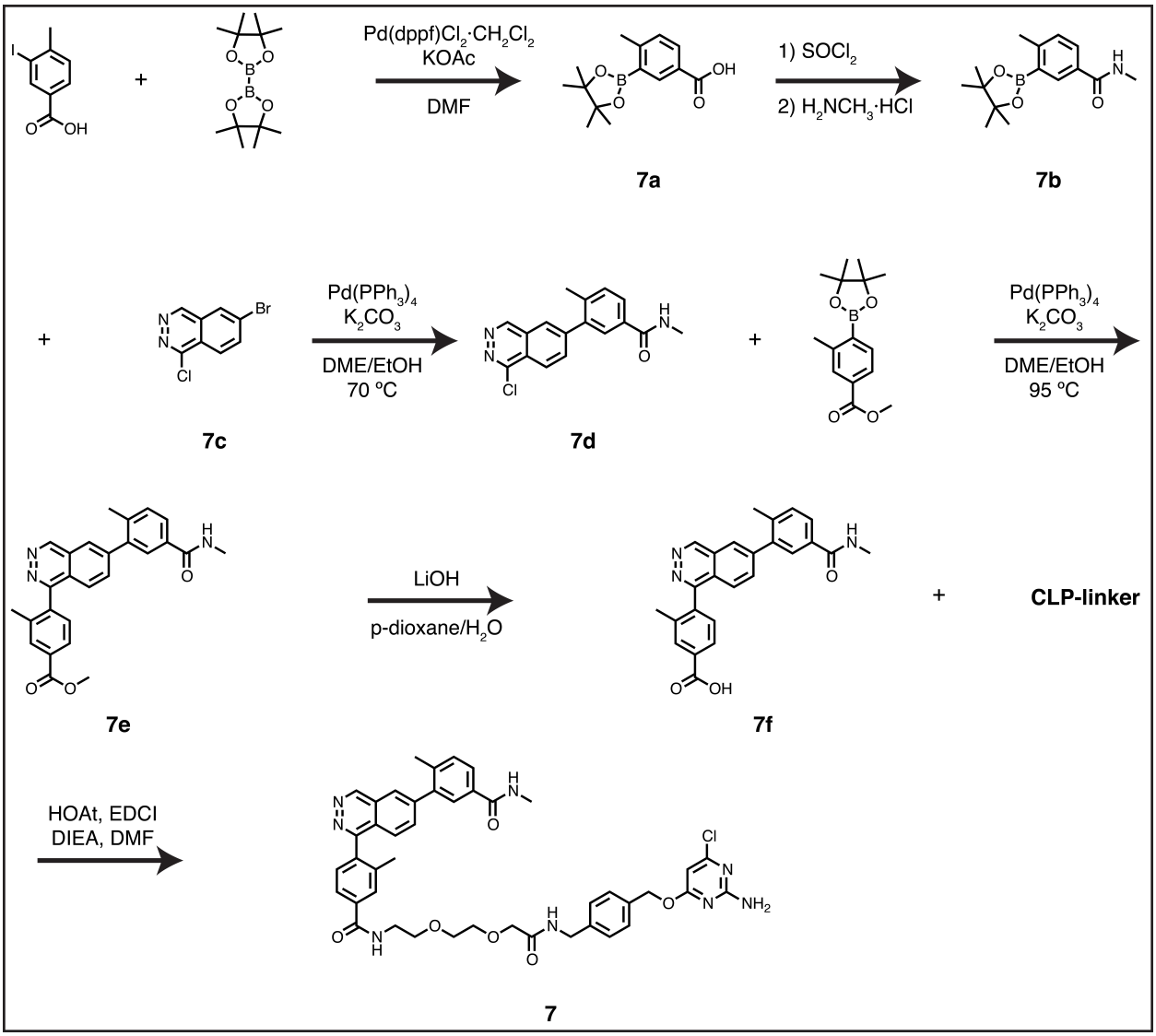

[7a]. To a stirred solution of 3-iodo-4-methylbenzoic acid (0.354 g, 1.35 mmol), bis(pinacolato)diboron (0.516 g, 2.03 mmol) and potassium acetate (0.663 g, 6.75 mmol) in DMF (7 mL) was added [1,1′-bis(diphenylphosphino)ferrocene] dichloropalladium(II), complex with dichloromethane (0.11 g, 0.135 mmol). The reaction mixture was stirred at 80 °C for 9 h while monitoring by TLC (5% MeOH in CH_2Cl_2). The

mixture was diluted in HCl (2 M) and extracted with EtOAc (3 × 20 mL). The combined extracts were washed with saturated NaCl (100 mL), dried over anhydrous sodium sulfate, filtered through Celite and concentrated. The resulting residue was taken up in EtOAc and was with NaOH (2 M, 3 × 20 mL). The solution was acidified with HCL (5 M), extracted with EtOAc (3 × 20 mL), dried over anhydrous sodium sulfate, and concentrated to yield **7a** as a brown solid (0.334 g, 94%).

^{1}H-NMR ($CDCl_3$) δ 8.49 (s, 1H), 8.03 (d, 2H), 2.60 (s, 3H), 1.36 (s, 8H).

[7b]. A resealable tube was oven-dried and cooled under N_2. The tube was charged with **7a** (0.039 g, 0.149 mmol) and thionyl chloride (0.31 mL, 4.17 mmol). The reaction mixture was heated at 60 °C for 4 h at which point toluene (1 mL) was added and the mixture was concentrated. To this residue was added methylamine hydrochloride (0.013 g, 0.179 mmol), triethylamine (0.035 mL, 0.224 mmol) and CH_2Cl_2 (0.72 mL). The reaction mixture was stirred at room temperature for 20 h while monitoring by TLC (5% MeOH in CH_2Cl_2 – 1% AcOH). The solvent was evaporated and the residue taken up in EtOAc (20 mL). The solution was washed with saturated K_2CO_3 (2 × 20 mL), saturated NH_4Cl (2 × 20 mL), saturated NaCl (2 × 20 mL), dried over anhydrous sodium sulfate and concentrated to yield a light brown solid. The crude material was purified by gradient column chromatography on silica gel, eluted with MeOH in CH_2Cl_2 (0% → 3%) to yield **7b** as a light brown solid (0.035 g, 85%).

^{1}H-NMR ($CDCl_3$) δ 8.02 (s, 1H), 7.83 (dd, J = 7.9, 2.3 Hz, 2H), 3.01 (d, 3H), 2.57 (s, 3H), 1.35 (s, 8H).

[7c] was prepared by Simeon Andrews using a previously published procedure (18).

[7d]. To a stirred solution of **7c** (0.03 g, 0.123 mmol), **7b** (0.031 g, 0.112 mmol) and potassium carbonate (0.17 mL of a 2 M aqueous solution, 0.336 mmol) in a DME/EtOH mixture (1:4, 0.86 mL) was added tetrakis(triphenylphosphine)palladium(0) (0.0065 g, 0.0056 mmol). The reaction mixture was stirred at 70 °C for 1.5 h while monitoring by TLC (5% MeOH in CH_2Cl_2). The mixture was concentrated. The crude mixture was dissolved in MeOH/water (10 mL) and purified using General HPLC conditions but found to contain triphenylphosphine oxide after chromatography. The crude solid **7d** was used without further purification (0.047 g).

^{1}H-NMR ($CDCl_3$) δ 9.77 (s, 1H), 8.27 – 8.09 (m, 2H), 7.76 – 7.59 (m, 2H), 7.53 (dd, *J* = 8.2, 3.2 Hz, 2H), 4.35 (s, 3H), 3.06 (d, 3H).

Calculated for $C_{17}H_{14}ClN_3O$ $(M + H)^+$: 312.1; Found 312.2.

[7e]. To a stirred solution of **7d** (0.047 g, 0.151 mmol), 3-methyl-4-methoxycarbonylphenylboronic acid pinacolate (0.046 g, 0.166 mmol) and potassium carbonate (0.23 mL of a 2 M aqueous solution, 0.453 mmol) in a DME/EtOH mixture (1:4, 1 mL) was added tetrakis(triphenylphosphine)palladium(0) (0.0088 g, 0.0076 mmol). The reaction mixture was stirred at 95 °C for 1 h while monitoring by TLC (50% EtOAc in hexanes). The mixture was concentrated. The crude mixture was dissolved in MeOH/water (10 mL) and purified using General HPLC conditions to yield **7e** (0.0184 g, 38%).

^{1}H-NMR ($CDCl_3$) δ 10.07 (s, 1H), 8.52 (d, *J* = 8.2 Hz, 2H), 8.35 (d, *J* = 8.1 Hz, 2H), 8.30 – 8.13 (m, 3H), 8.11 – 7.95 (m, 2H), 3.98 (s, 3H), 2.36 (d, 6H), 2.19 (s, 3H).

Calculated for $C_{26}H_{23}N_3O_3$ $(M + H)^+$: 426.2; Found 426.4.

[7f]. To a stirred solution of **7e** (0.0184 g, 0.0433 mmol) in p-dioxane (0.2 mL) was added LiOH • H_2O (0.004g, 0.0953 mmol). Water was added dropwise until a clear solution was obtained (approximately 0.5 mL) and the reaction was stirred at RT for 7 h while monitoring by TLC (5% MeOH in CH_2Cl_2 – 1% AcOH). The mixture was diluted in NaOH (1 M, 20 mL), extracted with EtOAc (3 × 30 mL) and made acidic to pH 1 with 2 M HCl. The acidic solution was extracted with EtOAc (3 × 50 mL) and the combined extracts were concentrated *in vacuo* to yield **7f** as a yellow residue (0.0073 g, 41%).

[7]. To a stirred solution of **7f** (0.008 g, 0.0195 mmol) and **CLP-Linker** (0.0088 g, 0.0215 mmol) in DMF (0.195 mL) was added 1-hydroxy-7-azabenzotriazole (0.0035 g, 0.0254 mmol), DIEA (0.015 mL, 0.0585 mmol) and 1-ethyl-3-(3-dimethylaminopropyl) carbodiimide (0.0049 g, 0.0254 mmol). The reaction mixture was stirred at RT for 8 h while monitoring with TLC (10% MeOH in CH_2Cl_2 – 1% AcOH). The crude mixture was dissolved in MeOH/water (10 mL) and purified using General HPLC conditions. The purity of **7** was determined to be >95% by analytical HPLC (3.5 mg, 22%).

Calculated for $C_{43}H_{43}ClN_8O_6$ $(M + H)^+$: 803.3; Found 803.5.

B. Design of fusion constructs, protein expression and purification

i. SNAPtag fusion protein design

GENE DESIGN OF ABL-RECOGNIZING FUSION CONSTRUCTS. Design of SNAP(HA4) is described in Chapter 2. Design of SNAP(PP) is described by Hill and et al (8).

GENE DESIGN OF P38-RECOGNIZING FUSION CONSTRUCTS. Fusion constructs were designed to display the p38p4 DARPin from the N- or C-terminus of SNAPtag. The primers used for the synthesis of the N-terminal construct are described in step N, and

the primers used for the synthesis of the C-terminal construct are described in step C. Linker lengths were varied using QuikChange Mutagenesis.

GENE DESIGN OF SRC-RECOGNIZING FUSION CONSTRUCT. A fusion construct was designed to display the 1E3 monobody from the N-terminus of SNAPtag.

GENE DESIGN OF FYN-RECOGNIZING FUSION CONSTRUCT. A fusion construct was designed to display the G9 monobody from the C-terminus of SNAPtag.

GENE DESIGN OF SFK-RECOGNIZING FUSION CONSTRUCT. A fusion construct was designed to display the 1F11 monobody from the C-terminus of SNAPtag.

GENE SYNTHESIS. GENERAL METHODS. The monobody or DARPin genes were amplified from the pUC57 plasmid (Genscript) using the primers listed for the monobody or DARPin fragments. A mutant form of the human gene O^6-alkylguanine-DNA-alkyltransferase was amplified from the pSS26(b) plasmid (Covalys) using primers listed for the SNAPtag fragment. To obtain the fusion constructs, overlap extension PCR of the two fragments was performed using the primers listed for the fusion steps.

CLONING. GENERAL METHODS. Linear PCR fragments were cloned into plasmid pMCSG7 using ligation independent cloning (19).

ii. Primers used for p38-recognizing constructs

SNAPTAG-FUSION CONSTRUCT SEQUENCES:

SNAP(N10p38p4) = His6-p38p4-GSGSGSGSGS-SNAPTAG

SNAP(N15p38p4) = His6-p38p4-TGTGTGSGSGSGSGS-SNAPTAG

SNAP(C10p38p4) = His6-SNAPTAG-GSGSGSGSGS-p38p4

SNAP(C15p38p4) = His6-SNAPTAG-TGTGTGSGSGSGSGS-p38p4

SNAPTAG SEQUENCE:

DKDCEMKRTTLDSPLGKLELSGCEQGLHEIKLLGKGTSAADAVEVPAPAAVLGGPEPL

MQATAWLNAYFHQPEAIEEFPVPALHHPVFQQESFTRQVLWKLLKVVKFGEVISYQQL

AALAGNPAATAAVKTALSGNPVPILIPCHRVVSSSGAVGGYEGGLAVKEWLLAHEGHR

LGKPGLG

P38P4 SEQUENCE:

DLGKKLLVAARAGQDDEVRILMANGADVNARDDYGTTPLHLAAIMGHLEIVEVLLKNGA

DVNAADKYGNTPLHLAAAACHLEIVEVLLKNGADVNAMDASGRTPLHLAALTGHLEIVE

VLLKYGADVSAQDKFGKTAFDISIDNGNEDLAEILQ

SEQUENCE ENCODED BY PMCSG7:

MHHHHHHSSGVDLGTENLYFQSN

P38P4 DARPIN FRAGMENT:

Step N1:

Fwd: 5’ - TAC TTC CAA TCC AAT GAT CTG GGC AAA AAA CTG CTG - 3’

Rev: 5’ - TTC GCA ATC TTT GTC ACC GCT GCC GCT ACC GCT GCC GCT ACC

GCT CTG CAG AAT TTC GGC CAG - 3’

Step C1:

Fwd: 5’ - AAA CCG GGT CTG GGA GGT AGC GGC AGC GGT AGC GGC AGC GGT

AGC GAT CTG GGC AAA AAA CTG CTG - 3’

Rev: 5’ - TTAT CCA CTT CCA ATG CTA CTG CAG AAT TTC GGC CAG ATC - 3’

SNAPTAG FRAGMENT:

Step N2:

Fwd: 5’ - GCC GAA ATT CTG CAG AGC GGT AGC GGC AGC GGT AGC GGC AGC

GGT GAC AAA GAT TGC GAA ATG AAA - 3’

Rev: 5’ - T TAT CCA CTT CCA ATG CTA TCC CAG ACC CGG TTT AC - 3’

Step C2:

Fwd: 5’ - TAC TTC CAA TCC AAT GAC AAA GAT TGC GAA ATG AAA C - 3’

Rev: 5’ - TTT GCC CAG ATC GCT ACC GCT GCC GCT ACC GCT GCC GCT ACC TCC CAG ACC CGG TTT ACC CAG - 3’

FUSION PCR:

Step N3:

Fwd: 5’ - TAC TTC CAA TCC AAT GAT CTG GGC AAA AAA CTG CTG - 3’

Rev: 5’ - T TAT CCA CTT CCA ATG CTA TCC CAG ACC CGG TTT AC - 3’

Step C3:

Fwd: 5’ - TAC TTC CAA TCC AAT GAC AAA GAT TGC GAA ATG AAA C - 3’

Rev: 5’ - TTAT CCA CTT CCA ATG CTA CTG CAG AAT TTC GGC CAG ATC - 3’

N15 QUIKCHANGE PRIMERS:

Fwd: 5’ - CC GAA ATT CTG CAG GGT ACT GGC ACC GGT AGC GGT AGC GGC AGC GG - 3’

Rev: 5’ - ACC CTG CAG AAT TTC GGC CAG ATC TTC GTT GCC GTT ATC - 3’

C15 QUIKCHANGE PRIMERS:

Fwd: 5’ - CCG GGT CTG GGA ACT GGT ACC GGC ACG GGT AGC GGC AGC GGT AGC - 3’

Rev: 5’ - AGT TCC CAG ACC CGG TTT ACC CAG ACG ATG ACC TTC ATG - 3’

iii. Primers used for Src-recognizing construct

SNAPTAG-FUSION CONSTRUCT SEQUENCE:

SNAP(1E3) = His6-1E3-GSGTG-SNAPTAG

SNAPTAG SEQUENCE:

DKDCEMKRTTLDSPLGKLELSGCEQGLHEIKLLGKGTSAADAVEVPAPAAVLGGPEPL

MQATAWLNAYFHQPEAIEEFPVPALHHPVFQQESFTRQVLWKLLKVVKFGEVISYQQL

AALAGNPAATAAVKTALSGNPVPILIPCHRVVSSSGAVGGYEGGLAVKEWLLAHEGHR

LGKPGLG

1E3 SEQUENCE:

AVSDVPRKLEVVAATPTSLLISWDAPFQTIQYYRITYGETGGNSPVQEFTVPGSKSTATI

SGLKPGVDYTITVYAVTLCARCSKPISINYRTS

SEQUENCE ENCODED BY PMCSG7:

MHHHHHHSSGVDLGTENLYFQSN

1E3 MONOBODY FRAGMENT:

Step 1:

Fwd: 5’ - TAC TTC CAA TCC AAT GCT GTG TCC GAT GTG CC - 3’

Rev: 5’ - GTT TCA TTT CGC AAT CTT TGT CGC CCG TAC CGC TGC CTG AGG TAC

GGT AGT TGA TGG - 3’

SNAPTAG FRAGMENT:

Step 2:

Fwd: 5’ - CCA TCA ACT ACC GTA CCT CAG GCA GCG GTA CGG GCG ACA AAG

ATT GCG AAA TGA AAC - 3’

Rev: 5’ - T TAT CCA CTT CCA ATG CTA TCC CAG ACC CGG TTT AC - 3’

FUSION PCR:

Step 3:

Fwd: 5’ - TAC TTC CAA TCC AAT GCT GTG TCC GAT GTG CC - 3’

Rev: 5’ - T TAT CCA CTT CCA ATG CTA TCC CAG ACC CGG TTT AC - 3’

iv. Primers used for Fyn-recognizing construct

SNAPTAG-FUSION CONSTRUCT SEQUENCE:

SNAP(G9) = His6-SNAPTAG-GSGTG-G9

SNAPTAG SEQUENCE:

DKDCEMKRTTLDSPLGKLELSGCEQGLHEIKLLGKGTSAADAVEVPAPAAVLGGPEPL

MQATAWLNAYFHQPEAIEEFPVPALHHPVFQQESFTRQVLWKLLKVVKFGEVISYQQL

AALAGNPAATAAVKTALSGNPVPILIPCHRVVSSSGAVGGYEGGLAVKEWLLAHEGHR

LGKPGLG

G9 SEQUENCE:

AVSDVPRKLEVVAATPTSLLISWDAPTMVTQYYRITYGETGGNSPVQEFTVPGSKSTA

TISGLKPGVDYTITVYAVTWRWRYSKPISINYRTS

SEQUENCE ENCODED BY PMCSG7:

MHHHHHHSSGVDLGTENLYFQSN

G9 MONOBODY FRAGMENT:

Step 1:

Fwd: 5’ - GGT AAA CCG GGT CTG GGA GGC AGC GGT ACG GGC GCC GTT TCT

GAT GTT CCG - 3’

Rev: 5’ - T TAT CCA CTT CCA ATG CTA GCT GGT ACG GTA GTT AAT CG - 3’

SNAPTAG FRAGMENT:

Step 2:

Fwd: 5’ - TAC TTC CAA TCC AAT GAC AAA GAT TGC GAA ATG AAA C - 3’

Rev: 5’ - CGG AAC ATC AGA AAC GGC GCC CGT ACC GCT GCC TCC CAG ACC CGG TTT ACC - 3’

FUSION PCR:

Step 3:

Fwd: 5’ - TAC TTC CAA TCC AAT GAC AAA GAT TGC GAA ATG AAA C - 3’

Rev: 5’ - T TAT CCA CTT CCA ATG CTA GCT GGT ACG GTA GTT AAT CG - 3’

v. Primers used for SFK-recognizing construct

SNAPTAG-FUSION CONSTRUCT SEQUENCE:

SNAP(1F11) = His6-SNAPTAG-GSGTG-1F11

SNAPTAG SEQUENCE:

DKDCEMKRTTLDSPLGKLELSGCEQGLHEIKLLGKGTSAADAVEVPAPAAVLGGPEPL MQATAWLNAYFHQPEAIEEFPVPALHHPVFQQESFTRQVLWKLLKVVKFGEVISYQQL AALAGNPAATAAVKTALSGNPVPILIPCHRVVSSSGAVGGYEGGLAVKEWLLAHEGHR LGKPGLG

1F11 SEQUENCE:

VSDVPRKLEVVAATPTSLLISWDAPGISQGYYRITYGETGGNSPVQEFTVPGSKSTATI SGLKPGVDYTITVYAYSRPLPSKPISINYRT

SEQUENCE ENCODED BY PMCSG7:

MHHHHHHSSGVDLGTENLYFQSN

1F11 MONOBODY FRAGMENT:

Step 1:

Fwd: 5’ - GGT AAA CCG GGT CTG GGA GGC AGC GGT ACG GGC GTC TCT GAT GTG CCG CG - 3’

Rev: 5’ - T TAT CCA CTT CCA ATG CTA GGT GCG GTA GTT GAT GCT A - 3’

SNAPTAG FRAGMENT:

Step 2:

Fwd: 5’ - TAC TTC CAA TCC AAT GAC AAA GAT TGC GAA ATG AAA C - 3’

Rev: 5’ - CG CGG CAC ATC AGA GAC GCC CGT ACC GCT GCC TCC CAG ACC CGG TTT ACC - 3’

FUSION PCR:

Step 3:

Fwd: 5’ - TAC TTC CAA TCC AAT GAC AAA GAT TGC GAA ATG AAA C - 3’

Rev: 5’ - T TAT CCA CTT CCA ATG CTA GGT GCG GTA GTT GAT GCT A - 3’

vi. Protein expression and purification

SNAPtag protein plasmids were transformed into BL21(DE3) *E. coli* cells and three colonies were used to inoculate 250 mL of LB broth with ampicillin (100 µg/mL). Cultures were grown at 37 °C to an OD_{600} of 1.0, cooled to 18 °C and induced with 0.5 mM IPTG. Proteins were expressed at 18 °C overnight. Cells were harvested by centrifugation, and the pellets were stored at -80 °C. For protein purification, the pellets were thawed at 0 °C and resuspended in 8 mL of His6 lysis buffer (50 mM HEPES pH 7.5, 100 mM NaCl, 20 mM imidazole) supplemented with PMSF (1 mM) and a Pierce™ Protease Inhibitor Mini Tablet (EDTA-free) (Pierce #88666). The cells were lysed using

sonication, and the lysate was cleared by centrifugation at 4 °C. The cleared lysate was added to 250 µL of 5 PRIME® PerfectPro Ni-NTA Agarose and rotated at 4 °C for 1 h. The resin was washed with His6 lysis buffer (15 × 1 mL) and eluted with His6 elution buffer (50 mM HEPES pH 7.5, 100 mM NaCl, 300 mM imidazole). The most concentrated fractions were pooled and exchanged into storage buffer (50 mM Tris, pH 7.5, 100 mM NaCl, 5 mM DTT). Proteins were analyzed by SDS-PAGE and found to be >95% pure by Coomassie stain. The proteins were separated into aliquots, snap-frozen and stored at -80 °C.

C. Bivalent inhibitor assembly and purification

(Protocol adapted from Mollwitz, *et al*.) (20) SNAPtag or the SNAPtag-intracellular antibody constructs were labeled with **4** using the following conditions. Purified SNAPtag protein (50 µM) was incubated with **4** (75 µM; 1.5-fold excess) in labeling buffer (20 mM Tris buffer, pH 8, 200 mM NaCl, and 4 mM DTT) for 2 h at 25 °C. The final reaction volume was 2.5 mL. The protein-small molecule conjugates were then purified using GE Healthcare PD-10 Desalting Columns equilibrated with 50 mM HEPES pH 7.5, 150 mM NaCl, 1.5 mM $MgCl_2$, 5% glycerol and 1 mM DTT. Labeling reactions were purified twice using two PD-10 Desalting Columns according to the manufacturer's procedure. The concentration of the eluted protein was determined using Coomassie® Plus Protein Assay Reagent Kit. Constructs were snap-frozen and stored at -80 °C.

Thawed inhibitors were analyzed by LC-MS on a Bruker Esquire Ion Trap MS instrument and deconvoluted species compared to verify quantitative labeling.

D. Mass spectra of bivalent inhibitors assembled using 4.

Raw ESI spectra are seen on the left and deconvoluted mass spectra on the right.

*Mass spectra were not acquired for p38-targeting constructs.

SNAPtag-4 Calculated for $C_{1015}H_{1566}N_{280}O_{285}S_6$: 22443 Da. Observed: 22473 Da. Unlabeled species not observed.

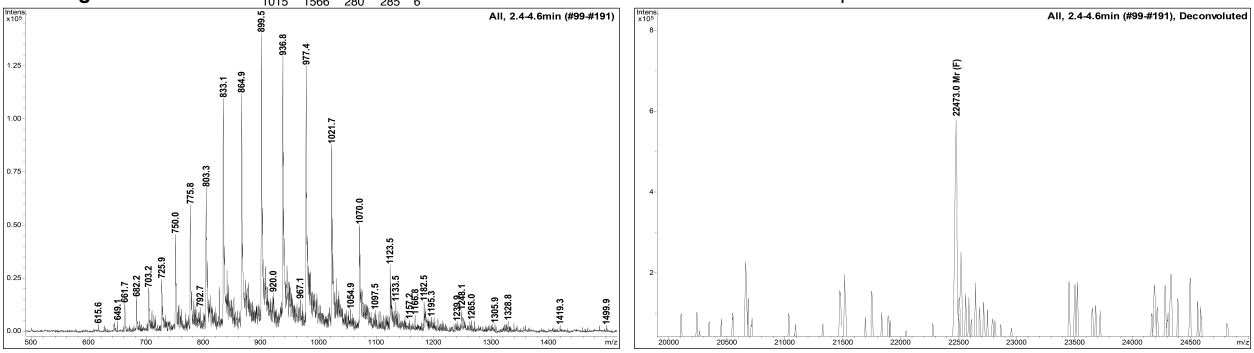

SNAP(HA4)-4 Calculated for $C_{1513}H_{2311}N_{397}O_{449}S_{10}$: 33566 Da. Observed: 33567 Da. Unlabeled species not observed.

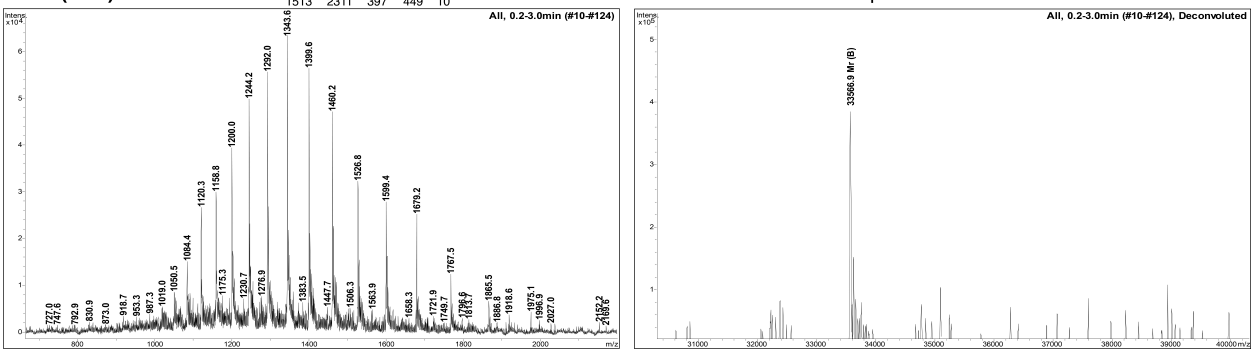

SNAP(PP)-4 Calculated for $C_{1079}H_{1669}N_{299}O_{300}S_6$: 23821 Da. Observed: 23835 Da. Unlabeled species not observed.

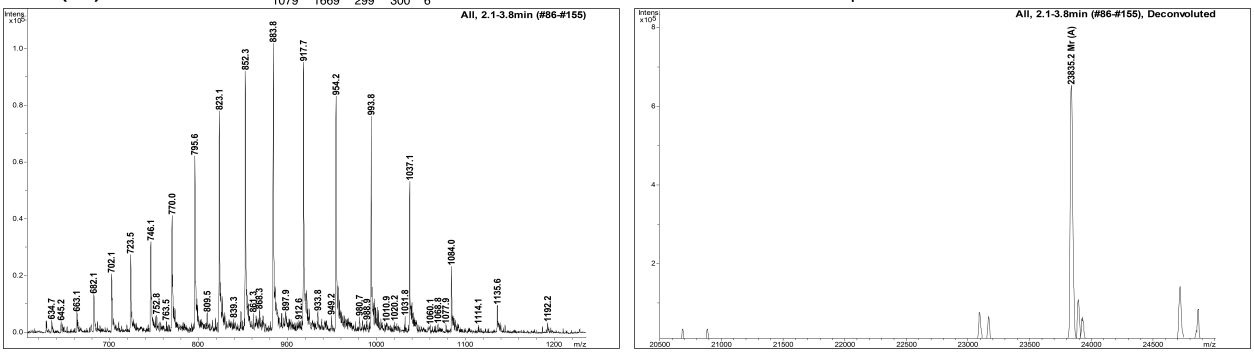

SNAP(G9)-4 Calculated for $C_{1494}H_{2308}N_{404}O_{431}S_7$: 33049 Da. Observed: 33067 Da. Unlabeled species not observed.

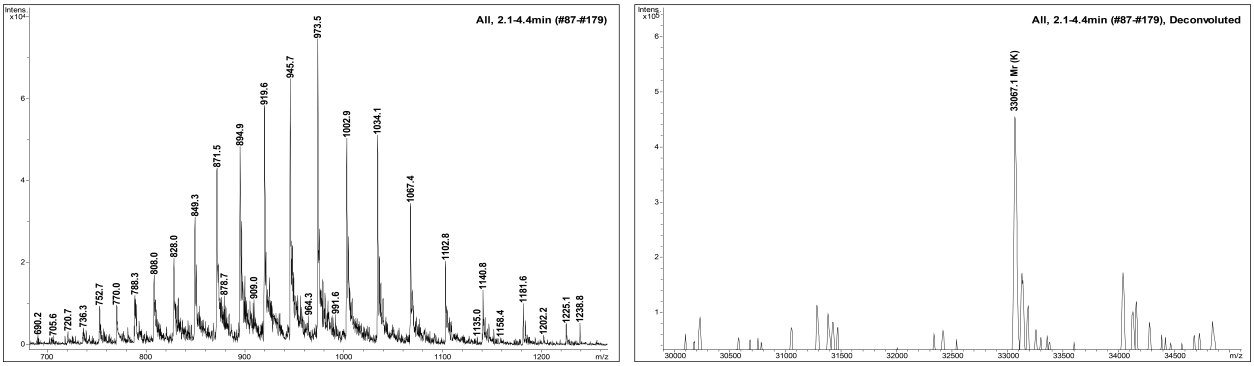

SNAP(1E3)-4 Calculated for $C_{1478}H_{2296}N_{400}O_{430}S_8$: 32805 Da. Observed: 32823 Da. Unlabeled species not observed.

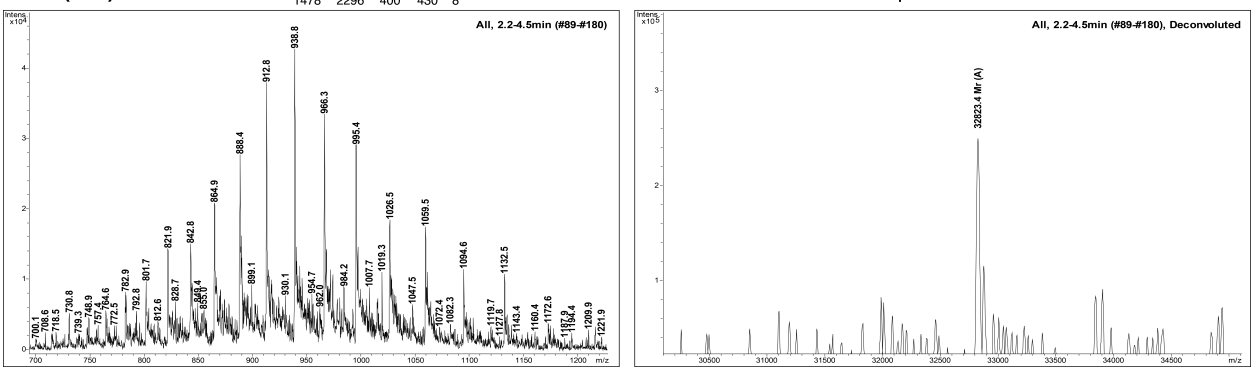

SNAP(1F11)-4 Calculated for $C_{1465}H_{2270}N_{396}O_{426}S_6$: 32438 Da. Observed: 32456 Da. Unlabeled species not observed.

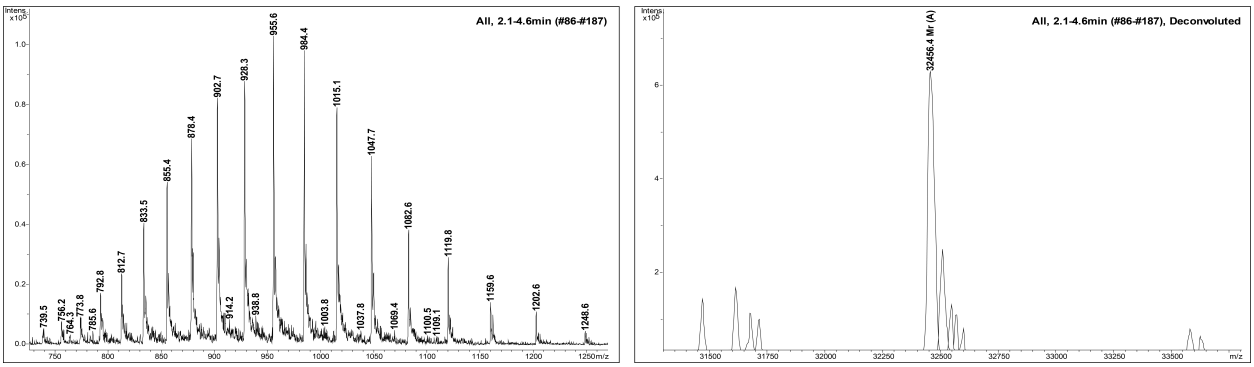

E. *In vitro* kinase activity assays

i. Assay conditions for Abl3D

ASSAY CONDITIONS FOR **4** AND **6** AGAINST ABL3D. **4** or **6** (initial concentration in DMSO = 12.5 μM, 3-fold serial dilutions, 10 data points) was assayed in triplicate against Abl3D (final concentration = 0.8 nM) in assay buffer containing 75 mM HEPES, pH = 7.5, 150 mM NaCl, 15 mM $MgCl_2$, 3.75 mM EGTA, 0.2 mg/mL BSA, 3.75 mM DTT,

0.75 mM Na_3VO_4, 5% DMSO, $\gamma^{32}P$ ATP (0.2 μCi/well) and an optimized Abl peptide substrate of the sequence Ac-EAIYAAPFAKKK (final concentration = 100 μM). The final volume of each assay well was 30 μL. The enzymatic reaction was run at room temperature for 2 hours and terminated by spotting 4.6 μL of the reaction mixture onto a phosphocellulose membrane. Membranes were washed with 0.5% phosphoric acid (4 × 10 minutes each wash), dried, and the radioactivity was determined by phosphorimaging with a GE Typhoon FLA 9000 phosphor scanner. The scanned membranes were quantified with ImageQuant software and converted to percent inhibition. Data was analyzed using Prism Graphpad software and IC_{50} values were determined using non-linear regression analysis.

ASSAY CONDITIONS FOR SNAPTAG, SNAP(HA4) AND **4** CONJUGATES AGAINST ABL3D. SNAPtag proteins (initial concentration = 15-30 μM, 3-fold serial dilutions, 10 data points) were assayed in triplicate against Abl3D (final concentration = 0.8 nM) in assay buffer containing 75 mM HEPES, pH = 7.5, 150 mM NaCl, 15 mM $MgCl_2$, 3.75 mM EGTA, 0.2 mg/mL BSA, 3.75 mM DTT, 0.75 mM Na_3VO_4, $\gamma^{32}P$ ATP (0.2 μCi/well) and an optimized Abl peptide substrate of the sequence Ac-EAIYAAPFAKKK (final concentration = 100 μM). The final volume of each assay well was 30 μL. The enzymatic reaction was run at room temperature for 2 hours and terminated by spotting 4.6 μL of the reaction mixture onto a phosphocellulose membrane. Membranes were washed with 0.5% phosphoric acid (4 × 10 minutes each wash), dried, and the radioactivity was determined by phosphorimaging with a GE Typhoon FLA 9000 phosphor scanner. The scanned membranes were quantified with ImageQuant software

and converted to percent inhibition. Data was analyzed using Prism Graphpad software and IC_{50} values were determined using non-linear regression analysis.

ii. Assay conditions for p38α

ASSAY CONDITIONS FOR **7** AGAINST P38A. **7** (initial concentration in DMSO = 12.5 μM, 3-fold serial dilutions, 10 data points) was assayed in triplicate against activated p38α (final concentration = 1 nM) in assay buffer containing 37.5 mM Tris, pH = 7.5, 15 mM $MgCl_2$, 0.75 mM EGTA, 0.75 mM Na_3VO_4, 0.015% Triton X-100, 3.75 mM DTT, 0.2 mg/mL BSA, $\gamma^{32}P$ ATP (0.2 μCi/well) and Myelin Basic Protein substrate (final concentration = 0.2 mg/mL). The final volume of each assay well was 30 μL. The enzymatic reaction was run at room temperature for 2 hours and terminated by spotting 4.6 μL of the reaction mixture onto a phosphocellulose membrane. Membranes were washed with 0.5% phosphoric acid (4 × 10 minutes each wash), dried, and the radioactivity was determined by phosphorimaging with a GE Typhoon FLA 9000 phosphor scanner. The scanned membranes were quantified with ImageQuant software and converted to percent inhibition. Data was analyzed using Prism Graphpad software and IC_{50} values were determined using non-linear regression analysis.

ASSAY CONDITIONS FOR SNAPTAG, SNAP(N10P38P4), SNAP(N15P38P4), SNAP(C10P38P4), SNAP(C15P38P4) AND **7** CONJUGATES AGAINST P38A. SNAPtag proteins (initial concentration = 15-30 μM, 3-fold serial dilutions, 10 data points) was assayed in triplicate against activated p38α (final concentration = 1 nM) in assay buffer containing 37.5 mM Tris, pH = 7.5, 15 mM $MgCl_2$, 0.75 mM EGTA, 0.75 mM Na_3VO_4, 0.015% Triton X-100, 3.75 mM DTT, 0.2 mg/mL BSA, $\gamma^{32}P$ ATP (0.2 μCi/well) and Myelin Basic Protein substrate (final concentration = 0.2 mg/mL). The final

volume of each assay well was 30 µL. The enzymatic reaction was run at room temperature for 2 hours and terminated by spotting 4.6 µL of the reaction mixture onto a phosphocellulose membrane. Membranes were washed with 0.5% phosphoric acid (4 × 10 minutes each wash), dried, and the radioactivity was determined by phosphorimaging with a GE Typhoon FLA 9000 phosphor scanner. The scanned membranes were quantified with ImageQuant software and converted to percent inhibition. Data was analyzed using Prism Graphpad software and IC_{50} values were determined using non-linear regression analysis.

F. DARPin p38p4 pull-down assay

COS7 cells were cultured at 37 °C in a humidified atmosphere containing 5% CO_2. COS7 cells were plated 12 h before transfection at a density of 2×10^6 cells per plate of two 10-cm plates in 10 mL of complete growth medium (high glucose DMEM + 10% Fetal Bovine Serum). The transfection complex was prepared by combining p38 in the pDEST26HA plasmid (final concentration = 1 µg DNA/plate) and ERK2 in the pCeGFPLIC plasmid (final concentration = 1 µg DNA/plate) with 4 µL FuGENE® HD reagent (Promega) in a final volume of 1 mL in OptiMEM and incubating at RT for 15 min. Prior to transfection, cells were washed with serum-free DMEM (3 × 2 mL) and OptiMEM (2 mL). Transfection mixture (1 mL) was added to cells in 9 mL OptiMEM and the medium was replaced with complete growth medium (10 mL) after 15 h. The proteins were expressed for a total of 18 h. The cells were lysed by sonication in lysis buffer containing 50 mM HEPES pH 7.5, 300 mM NaCl, 20 mM imidazole and 1x Roche© EDTA-free Complete Protease Inhibitor Cocktail. The lysate (1.6 mL, combined from two 10-cm plates) was cleared by centrifugation and 500 µL applied directly to

His6-p38p4 DARPin immobilized on 5 PRIME® PerfectPro Ni-NTA Agarose. The DARPin was previously diluted in lysis buffer containing 50 mM HEPES pH 7.5, 300 mM NaCl, 20 mM imidazole and 0.1 mg/mL BSA such that 1 mL of 10 μM DARPin was added to 20 μL Ni-NTA resin. Additionally, Ni-NTA resin was prepared as described in the absence of DARPin as a control. Pull downs were rotated at 4 °C for 1.5 h and washed with lysis buffer (500 μL) before addition of mammalian lysate. The Ni-NTA pull-downs were incubated with the mammalian lysate for 1 hr at 4 °C and washed with lysis buffer (6 × 500 μL) before eluting with buffer containing 50 mM HEPES pH 7.5, 300 mM NaCl and 600 mM imidazole (50 μL). Eluted samples were subjected to SDS-PAGE, transferred to nitrocellulose and probed with anti-p38 MAPK Antibody (Rabbit, Cell Signaling #9212L) and anti-ERK1/2 MAPK Antibody (Rabbit, Cell Signaling #4695). Secondary detection was achieved using IRDye secondary antibodies (Li-Cor #926-32211 and #926-68070). The scanned blots were processed with Li-Cor Odyssey software.

G. Quantitative competition-based chemical proteomics

Quantitative competition-base chemical proteomics studies were performed as described in Chapter 2.

H. Gene sequences

Affinity tag/vector sequence = red
SNAPtag = orange
Flexible linker = green
Intracellular antibody = blue

SNAP(HA4)
ATGCACCATCATCATCATCATTCTTCTGGTGTAGATCTGGGTACCGAGAACCTGTA
CTTCCAATCCAATGACAAAGATTGCGAAATGAAACGTACCACCCTGGATAGCCCGC
TGGGCAAACTGGAACTGAGCGGCTGCGAACAGGGCCTGCATGAAATTAAACTGCT
GGGTAAAGGCACCAGCGCGGCCGATGCGGTTGAAGTTCCGGCCCCGGCCGCCGT

GCTGGGTGGTCCGGAACCGCTGATGCAGGCGACCGCGTGGCTGAACGCGTATTT
TCATCAGCCGGAAGCGATTGAAGAATTTCCGGTTCCGGCGCTGCATCATCCGGTG
TTTCAGCAGGAGAGCTTTACCCGTCAGGTGCTGTGGAAACTGCTGAAAGTGGTTAA
ATTTGGCGAAGTGATTAGCTATCAGCAGCTGGCGGCCCTGGCGGGTAATCCGGCG
GCCACCGCCGCCGTTAAAACCGCGCTGAGCGGTAACCCGGTGCCGATTCTGATTC
CGTGCCATCGTGTGGTTAGCTCTAGCGGTGCGGTTGGCGGTTATGAAGGTGGTCT
GGCGGTGAAAGAGTGGCTGCTGGCCCATGAAGGTCATCGTCTGGGTAAACCGGG
TCTGGGAGGTACGGGCACCGGCTCTTCTGTTTCAAGCGTTCCGACCAAGCTGGAG
GTTGTTGCTGCCACACCGACAAGTCTGCTGATTTCATGGGATGCCCCGATGAGCT
CCTCTAGTGTTTATTACTATCGCATTACATACGGCGAAACCGGCGGTAACAGCCCG
GTGCAGGAGTTTACCGTTCCCTATTCAAGCTCCACCGCCACAATTTCTGGGCTGAG
CCCGGGAGTCGATTACACTATCACCGTGTATGCGTGGGGTGAAGACTCAGCAGGG
TATATGTTTATGTATTCTCCCATCTCCATCAACTATCGCACTTGCTAG

SNAP(N10p38p4)
ATGCACCATCATCATCATCATTCTTCTGGTGTAGATCTGGGTACCGAGAACCTGTA
CTTCCAATCCAATGATCTGGGCAAAAAACTGCTGGTGGCCGCCCGCGCCGGCCAG
GATGATGAAGTGCGCATTCTGATGGCCAACGGCGCCGATGTGAACGCCCGCGAT
GATTATGGCACCACCCCGCTGCATCTGGCCGCCATTATGGGCCATCTGGAAATTG
TGGAAGTGCTGCTGAAAAACGGCGCCGATGTGAACGCCGCCGATAAATATGGCAA
CACCCCGCTGCATCTGGCCGCCGCCGCCTGCCATCTGGAAATTGTGGAAGTGCTG
CTGAAAAACGGCGCCGATGTGAACGCCATGGATGCCAGCGGCCGCACCCCGCTG
CATCTGGCCGCCCTGACCGGCCATCTGGAAATTGTGGAAGTGCTGCTGAAATATG
GCGCCGATGTGAGCGCCCAGGATAAATTTGGCAAAACCGCCTTTGATATTAGCATT
GATAACGGCAACGAAGATCTGGCCGAAATTCTGCAGAGCGGTAGCGGCAGCGGT
AGCGGCAGCGGTGACAAAGATTGCGAAATGAAACGTACCACCCTGGATAGCCCGC
TGGGCAAACTGGAACTGAGCGGCTGCGAACAGGGCCTGCATGAAATTAAACTGCT
GGGTAAAGGCACCAGCGCGGCCGATGCGGTTGAAGTTCCGGCCCCGGCCGCCGT
GCTGGGTGGTCCGGAACCGCTGATGCAGGCGACCGCGTGGCTGAACGCGTATTT
TCATCAGCCGGAAGCGATTGAAGAATTTCCGGTTCCGGCGCTGCATCATCCGGTG
TTTCAGCAGGAGAGCTTTACCCGTCAGGTGCTGTGGAAACTGCTGAAAGTGGTTAA
ATTTGGCGAAGTGATTAGCTATCAGCAGCTGGCGGCCCTGGCGGGTAATCCGGCG
GCCACCGCCGCCGTTAAAACCGCGCTGAGCGGTAACCCGGTGCCGATTCTGATTC
CGTGCCATCGTGTGGTTAGCTCTAGCGGTGCGGTTGGCGGTTATGAAGGTGGTCT
GGCGGTGAAAGAGTGGCTGCTGGCCCATGAAGGTCATCGTCTGGGTAAACCGGG
TCTGGGATAG

SNAP(N15p38p4)
ATGCACCATCATCATCATCATTCTTCTGGTGTAGATCTGGGTACCGAGAACCTGTA
CTTCCAATCCAATGATCTGGGCAAAAAACTGCTGGTGGCCGCCCGCGCCGGCCAG
GATGATGAAGTGCGCATTCTGATGGCCAACGGCGCCGATGTGAACGCCCGCGAT
GATTATGGCACCACCCCGCTGCATCTGGCCGCCATTATGGGCCATCTGGAAATTG
TGGAAGTGCTGCTGAAAAACGGCGCCGATGTGAACGCCGCCGATAAATATGGCAA
CACCCCGCTGCATCTGGCCGCCGCCGCCTGCCATCTGGAAATTGTGGAAGTGCTG
CTGAAAAACGGCGCCGATGTGAACGCCATGGATGCCAGCGGCCGCACCCCGCTG
CATCTGGCCGCCCTGACCGGCCATCTGGAAATTGTGGAAGTGCTGCTGAAATATG

GCGCCGATGTGAGCGCCCAGGATAAATTTGGCAAAACCGCCTTTGATATTAGCATT
GATAACGGCAACGAAGATCTGGCCGAAATTCTGCAGGGTACTGGCACCGGTAGCG
GTAGCGGCAGCGGTAGCGGCAGCGGTGACAAAGATTGCGAAATGAAACGTACCA
CCCTGGATAGCCCGCTGGGCAAACTGGAACTGAGCGGCTGCGAACAGGGCCTGC
ATGAAATTAAACTGCTGGGTAAAGGCACCAGCGCGGCCGATGCGGTTGAAGTTCC
GGCCCCGGCCGCCGTGCTGGGTGGTCCGGAACCGCTGATGCAGGCGACCGCGT
GGCTGAACGCGTATTTTCATCAGCCGGAAGCGATTGAAGAATTTCCGGTTCCGGC
GCTGCATCATCCGGTGTTTCAGCAGGAGAGCTTTACCCGTCAGGTGCTGTGGAAA
CTGCTGAAAGTGGTTAAATTTGGCGAAGTGATTAGCTATCAGCAGCTGGCGGCCC
TGGCGGGTAATCCGGCGGCCACCGCCGCCGTTAAAACCGCGCTGAGCGGTAACC
CGGTGCCGATTCTGATTCCGTGCCATCGTGTGGTTAGCTCTAGCGGTGCGGTTGG
CGGTTATGAAGGTGGTCTGGCGGTGAAAGAGTGGCTGCTGGCCCATGAAGGTCAT
CGTCTGGGTAAACCGGGTCTGGGATAG

SNAP(C10p38p4)
ATGCACCATCATCATCATCATTCTTCTGGTGTAGATCTGGGTACCGAGAACCTGTA
CTTCCAATCCAATGACAAAGATTGCGAAATGAAACGTACCACCCTGGATAGCCCGC
TGGGCAAACTGGAACTGAGCGGCTGCGAACAGGGCCTGCATGAAATTAAACTGCT
GGGTAAAGGCACCAGCGCGGCCGATGCGGTTGAAGTTCCGGCCCCGGCCGCCGT
GCTGGGTGGTCCGGAACCGCTGATGCAGGCGACCGCGTGGCTGAACGCGTATTT
TCATCAGCCGGAAGCGATTGAAGAATTTCCGGTTCCGGCGCTGCATCATCCGGTG
TTTCAGCAGGAGAGCTTTACCCGTCAGGTGCTGTGGAAACTGCTGAAAGTGGTTAA
ATTTGGCGAAGTGATTAGCTATCAGCAGCTGGCGGCCCTGGCGGGTAATCCGGCG
GCCACCGCCGCCGTTAAAACCGCGCTGAGCGGTAACCCGGTGCCGATTCTGATTC
CGTGCCATCGTGTGGTTAGCTCTAGCGGTGCGGTTGGCGGTTATGAAGGTGGTCT
GGCGGTGAAAGAGTGGCTGCTGGCCCATGAAGGTCATCGTCTGGGTAAACCGGG
TCTGGGAGGTAGCGGCAGCGGTAGCGGCAGCGGTAGCGATCTGGGCAAAAAACT
GCTGGTGGCCGCCCGCGCCGGCCAGGATGATGAAGTGCGCATTCTGATGGCCAA
CGGCGCCGATGTGAACGCCCGCGATGATTATGGCACCACCCCGCTGCATCTGGC
CGCCATTATGGGCCATCTGGAAATTGTGGAAGTGCTGCTGAAAAACGGCGCCGAT
GTGAACGCCGCCGATAAATATGGCAACACCCCGCTGCATCTGGCCGCCGCCGCC
TGCCATCTGGAAATTGTGGAAGTGCTGCTGAAAAACGGCGCCGATGTGAACGCCA
TGGATGCCAGCGGCCGCACCCCGCTGCATCTGGCCGCCCTGACCGGCCATCTGG
AAATTGTGGAAGTGCTGCTGAAATATGGCGCCGATGTGAGCGCCCAGGATAAATTT
GGCAAAACCGCCTTTGATATTAGCATTGATAACGGCAACGAAGATCTGGCCGAAAT
TCTGCAGTAG

SNAP(C15p38p4)
ATGCACCATCATCATCATCATTCTTCTGGTGTAGATCTGGGTACCGAGAACCTGTA
CTTCCAATCCAATGACAAAGATTGCGAAATGAAACGTACCACCCTGGATAGCCCGC
TGGGCAAACTGGAACTGAGCGGCTGCGAACAGGGCCTGCATGAAATTAAACTGCT
GGGTAAAGGCACCAGCGCGGCCGATGCGGTTGAAGTTCCGGCCCCGGCCGCCGT
GCTGGGTGGTCCGGAACCGCTGATGCAGGCGACCGCGTGGCTGAACGCGTATTT
TCATCAGCCGGAAGCGATTGAAGAATTTCCGGTTCCGGCGCTGCATCATCCGGTG
TTTCAGCAGGAGAGCTTTACCCGTCAGGTGCTGTGGAAACTGCTGAAAGTGGTTAA
ATTTGGCGAAGTGATTAGCTATCAGCAGCTGGCGGCCCTGGCGGGTAATCCGGCG

GCCACCGCCGCCGTTAAAACCGCGCTGAGCGGTAACCCGGTGCCGATTCTGATTC
CGTGCCATCGTGTGGTTAGCTCTAGCGGTGCGGTTGGCGGTTATGAAGGTGGTCT
GGCGGTGAAAGAGTGGCTGCTGGCCCATGAAGGTCATCGTCTGGGTAAACCGGG
TCTGGGAACTGGTACCGGCACGGGTAGCGGCAGCGGTAGCGGCAGCGGTAGCG
ATCTGGGCAAAAAACTGCTGGTGGCCGCCCGCGCCGGCCAGGATGATGAAGTGC
GCATTCTGATGGCCAACGGCGCCGATGTGAACGCCCGCGATGATTATGGCACCAC
CCCGCTGCATCTGGCCGCCATTATGGGCCATCTGGAAATTGTGGAAGTGCTGCTG
AAAAACGGCGCCGATGTGAACGCCGCCGATAAATATGGCAACACCCCGCTGCATC
TGGCCGCCGCCGCCTGCCATCTGGAAATTGTGGAAGTGCTGCTGAAAAACGGCG
CCGATGTGAACGCCATGGATGCCAGCGGCCGCACCCCGCTGCATCTGGCCGCCC
TGACCGGCCATCTGGAAATTGTGGAAGTGCTGCTGAAATATGGCGCCGATGTGAG
CGCCCAGGATAAATTTGGCAAAACCGCCTTTGATATTAGCATTGATAACGGCAACG
AAGATCTGGCCGAAATTCTGCAGTAG

SNAP(1E3)
ATGCACCATCATCATCATCATTCTTCTGGTGTAGATCTGGGTACCGAGAACCTGTA
CTTCCAATCCAATGCTGTGTCCGATGTGCCGCGTAAGCTGGAAGTGGTTGCTGCG
ACCCCGACGAGCCTGCTGATCTCATGGGATGCGCCGTTTCAGACCATTCAGTATTA
CCGTATCACCTATGGCGAAACGGGCGGTAACAGTCCGGTGCAAGAATTTACCGTT
CCGGGTAGCAAATCTACCGCGACGATTAGCGGCCTGAAGCCGGGTGTCGATTACA
CCATCACGGTTTATGCCGTCACGCTGTGCGCCCGCTGTTCAAAGCCGATTTCCATC
AACTACCGTACCTCAGGCAGCGGTACGGGCGACAAAGATTGCGAAATGAAACGTA
CCACCCTGGATAGCCCGCTGGGCAAACTGGAACTGAGCGGCTGCGAACAGGGCC
TGCATGAAATTAAACTGCTGGGTAAAGGCACCAGCGCGGCCGATGCGGTTGAAGT
TCCGGCCCCGGCCGCCGTGCTGGGTGGTCCGGAACCGCTGATGCAGGCGACCG
CGTGGCTGAACGCGTATTTTCATCAGCCGGAAGCGATTGAAGAATTTCCGGTTCCG
GCGCTGCATCATCCGGTGTTTCAGCAGGAGAGCTTTACCCGTCAGGTGCTGTGGA
AACTGCTGAAAGTGGTTAAATTTGGCGAAGTGATTAGCTATCAGCAGCTGGCGGC
CCTGGCGGGTAATCCGGCGGCCACCGCCGCCGTTAAAACCGCGCTGAGCGGTAA
CCCGGTGCCGATTCTGATTCCGTGCCATCGTGTGGTTAGCTCTAGCGGTGCGGTT
GGCGGTTATGAAGGTGGTCTGGCGGTGAAAGAGTGGCTGCTGGCCCATGAAGGT
CATCGTCTGGGTAAACCGGGTCTGGGATAG

SNAP(G9)
ATGCACCATCATCATCATCATTCTTCTGGTGTAGATCTGGGTACCGAGAACCTGTA
CTTCCAATCCAATGACAAAGATTGCGAAATGAAACGTACCACCCTGGATAGCCCGC
TGGGCAAACTGGAACTGAGCGGCTGCGAACAGGGCCTGCATGAAATTAAACTGCT
GGGTAAAGGCACCAGCGCGGCCGATGCGGTTGAAGTTCCGGCCCCGGCCGCCGT
GCTGGGTGGTCCGGAACCGCTGATGCAGGCGACCGCGTGGCTGAACGCGTATTT
TCATCAGCCGGAAGCGATTGAAGAATTTCCGGTTCCGGCGCTGCATCATCCGGTG
TTTCAGCAGGAGAGCTTTACCCGTCAGGTGCTGTGGAAACTGCTGAAAGTGGTTAA
ATTTGGCGAAGTGATTAGCTATCAGCAGCTGGCGGCCCTGGCGGGTAATCCGGCG
GCCACCGCCGCCGTTAAAACCGCGCTGAGCGGTAACCCGGTGCCGATTCTGATTC
CGTGCCATCGTGTGGTTAGCTCTAGCGGTGCGGTTGGCGGTTATGAAGGTGGTCT
GGCGGTGAAAGAGTGGCTGCTGGCCCATGAAGGTCATCGTCTGGGTAAACCGGG
TCTGGGAGGCAGCGGTACGGGCGCCGTTTCTGATGTTCCGCGTAAGCTGGAAGTT

GTTGCTGCGACCCCGACTAGCCTGCTGATCAGCTGGGATGCTCCTACTATGGTTA
CGCAGTATTACCGTATCACGTACGGTGAAACCGGTGGTAACTCCCCGGTTCAGGA
GTTCACTGTACCTGGTTCCAAGTCTACTGCTACCATCAGCGGCCTGAAACCGGGT
GTTGACTATACCATCACTGTATACGCTGTTACTTGGCGGTGGCGGTATAGCAAGCC
AATCTCGATTAACTACCGTACCAGCTAG

SNAP(1F11)
ATGCACCATCATCATCATCATTCTTCTGGTGTAGATCTGGGTACCGAGAACCTGTA
CTTCCAATCCAATGACAAAGATTGCGAAATGAAACGTACCACCCTGGATAGCCCGC
TGGGCAAACTGGAACTGAGCGGCTGCGAACAGGGCCTGCATGAAATTAAACTGCT
GGGTAAAGGCACCAGCGCGGCCGATGCGGTTGAAGTTCCGGCCCCGGCCGCCGT
GCTGGGTGGTCCGGAACCGCTGATGCAGGCGACCGCGTGGCTGAACGCGTATTT
TCATCAGCCGGAAGCGATTGAAGAATTTCCGGTTCCGGCGCTGCATCATCCGGTG
TTTCAGCAGGAGAGCTTTACCCGTCAGGTGCTGTGGAAACTGCTGAAAGTGGTTAA
ATTTGGCGAAGTGATTAGCTATCAGCAGCTGGCGGCCCTGGCGGGTAATCCGGCG
GCCACCGCCGCCGTTAAAACCGCGCTGAGCGGTAACCCGGTGCCGATTCTGATTC
CGTGCCATCGTGTGGTTAGCTCTAGCGGTGCGGTTGGCGGTTATGAAGGTGGTCT
GGCGGTGAAAGAGTGGCTGCTGGCCCATGAAGGTCATCGTCTGGGTAAACCGGG
TCTGGGAGGCAGCGGTACGGGCGTCTCTGATGTGCCGCGCAAACTGGAAGTGGT
GGCCGCAACGCCGACCTCGCTGCTGATTTCGTGGGATGCTCCGGGTATCTCGCAA
GGCTATTACCGTATTACCTATGGTGAAACGGGCGGTAACAGTCCGGTGCAGGAAT
TTACCGTTCCGGGCAGCAAATCTACCGCGACGATTAGCGGCCTGAAGCCGGGTGT
CGATTACACGATCACCGTCTACGCCTATTCACGCCCGCTGCCGTCAAAGCCGATTA
GCATCAACTACCGCACCTAG

V. References

1. Wojcik J et al. (2010) A potent and highly specific FN3 monobody inhibitor of the Abl SH2 domain. *Nature Structural & Molecular Biology* 17:519–527.

2. Amstutz P, Koch H, Binz HK, Deuber SA, Plückthun A (2006) Rapid selection of specific MAP kinase-binders from designed ankyrin repeat protein libraries. *Protein engineering, design & selection : PEDS* 19:219–229.

3. Karatan E et al. (2004) Molecular recognition properties of FN3 monobodies that bind the Src SH3 domain. *Chem Biol* 11:835–844.

4. Kummer L et al. (2012) Structural and functional analysis of phosphorylation-specific binders of the kinase ERK from designed ankyrin repeat protein libraries. *Proceedings of the National Academy of Sciences* 109:E2248–57.

5. Bandeiras TM et al. (2008) Structure of wild-type Plk-1 kinase domain in complex with a selective DARPin. *Acta crystallographica Section D, Biological crystallography* 64:339–353.

6. Gronemeyer T, Chidley C, Juillerat A, Heinis C, Johnsson K (2006) Directed evolution of O6-alkylguanine-DNA alkyltransferase for applications in protein labeling. *Protein engineering, design & selection : PEDS* 19:309–316.

7. Juillerat A et al. (2003) Directed evolution of O^6-alkylguanine-DNA alkyltransferase for efficient labeling of fusion proteins with small molecules in vivo. *Chem Biol* 10:313–317.

8. Hill ZB, Perera BGK, Maly DJ (2009) A Chemical Genetic Method for Generating Bivalent Inhibitors of Protein Kinases. *J Am Chem Soc* 131:6686–6688.

9. Hill ZB, Perera BGK, Maly DJ (2011) Bivalent inhibitors of the tyrosine kinases ABL and SRC: determinants of potency and selectivity. *Mol BioSyst* 7:447.

10. Pisabarro MT, Serrano L (1996) Rational design of specific high-affinity peptide ligands for the Abl-SH3 domain. *Biochemistry* 35:10634–10640.

11. Zheng C et al. (2006) MAPK-activated protein kinase-2 (MK2)-mediated formation and phosphorylation-regulated dissociation of the signal complex consisting of p38, MK2, Akt, and Hsp27. *J Biol Chem* 281:37215–37226.

12. Herberich B et al. (2008) Discovery of highly selective and potent p38 inhibitors based on a phthalazine scaffold. *J Med Chem* 51:6271–6279.

13. Parsons SJ, Parsons JT (2004) Src family kinases, key regulators of signal transduction. *Oncogene* 23:7906–7909.

14. Blume-Jensen P, Hunter T (2001) Oncogenic kinase signalling. *Nature* 411:355–365.

15. Gulyani A et al. (2011) A biosensor generated via high-throughput screening quantifies cell edge Src dynamics. *Nat Chem Biol* 7:437–444.

16. Register AC, Leonard SE, Maly DJ (2014) SH2-Catalytic Domain Linker Heterogeneity Influences Allosteric Coupling across the SFK Family. *Biochemistry* 53:6910–6923.

17. Huang R, Fang P, Kay BK (2012) Isolation of monobodies that bind specifically to the SH3 domain of the Fyn tyrosine protein kinase. *New Biotechnology* 29:526–533.

18. Hill ZB, Perera BGK, Andrews SS, Maly DJ (2012) Targeting Diverse Signaling Interaction Sites Allows the Rapid Generation of Bivalent Kinase Inhibitors. *ACS Chem Biol* 7:487–495.

19. Stols L et al. (2002) A new vector for high-throughput, ligation-independent cloning encoding a tobacco etch virus protease cleavage site. *Protein Expr Purif* 25:8–15.

20. Mollwitz B et al. (2012) Directed evolution of the suicide protein O^6-alkylguanine-DNA alkyltransferase for increased reactivity results in an alkylated protein with exceptional stability. *Biochemistry* 51:986–994.